HYDRODYNAMIC PERFORMANCE OF MECHANICAL AND BIOLOGICAL PROSTHETIC HEART VALVES

Winona F. Bishop

B.A.Sc., University of British Columbia, 1987

A THESIS SUBMITTED IN PARTIAL FULFILLMENT OF
THE REQUIREMENT FOR THE DEGREE OF

MASTER OF APPLIED SCIENCE

in

The Faculty of Graduate Studies
Department of Mechanical Engineering

We accept this thesis as conforming
to the required standard

THE UNIVERSITY OF BRITISH COLUMBIA

April 1990

In presenting this thesis in partial fulfilment of the requirements for an advanced degree at the University of British Columbia, I agree that the Library shall make it freely available for reference and study. I further agree that permission for extensive copying of this thesis for scholarly purposes may be granted by the head of my department or by his or her representatives. It is understood that copying or publication of this thesis for financial gain shall not be allowed without my written permission.

Department of Mechanical Engineering

The University of British Columbia
Vancouver, Canada

Date April 27, 1990

ABSTRACT

One of the major achievements in cardiac surgery over the past 30 years has been the ability to replace severely diseased heart valves with prosthetic ones. The option of using prosthetic heart valves for the treatment of valvular diseases has improved and prolonged many lives. This is reflected in around 120,000 heart valve replacement operations carried out every year in North America alone to correct the cardiovascular problems of stenosis, insufficiency, regurgitation, etc.

The development of artificial heart valves depends on reliable knowledge of the hemodynamic performance and physiology of the cardiovascular system in addition to a sound understanding, at the fundamental level, of the associated fluid mechanics. It is evident from the literature review that noninvasive measurements in a confined area of complex transient geometry, providing critical information relating to valve performance, are indeed scarce.

This thesis presents results of an extensive test program aimed at measuring turbulence stresses, steady and transient velocity profiles and their decay downstream of the mitral valve. Three mechanical tilting disc-type heart valves (Björk-Shiley convexo- concave, Björk-Shiley monostrut, and Bicer-Val) and two biological tissue valves (Hancock II and Carpentier-Edwards supraannular) are studied. The investigation was carried out using a sophisticated and versatile cardiac simulator in conjunction with a highly sensitive, noninvasive, two-component three-beam laser doppler anemometer system. The study covers both the steady (valve fully open) and pulsatile (resting heart rate) flow conditions. The continuous monitoring of the parametric time histories revealed useful details of the complex flow as well as helped establish location and timing of the peak parameter values. In addition,

orientation experiments are conducted on the mechanical valves in an attempt to reduce stresses by altering the position of the major orifice. The experiments suggest correlation between high stresses and orientation.

Based on the the data, the following general conclusions can be made:

(i) Hemodynamic test results should be presented in nondimensional form to render them independent of test facilities, flow velocities, size of models, etc. This would facilitate comparison of results by different investigators, using different facilities and test conditions.

(ii) The valves tested showed very disturbed flow fields which generated high turbulent stresses presenting a possibility of thromboembolism and, perhaps, haemolysis.

(iii) Implantation orientation of the valve significantly affect the mechanical prostheses flow field. The single vortex formation in the posterior orientation results in a reduction in stresses compared to the anterior configuration.

(iv) The present results together with the earlier information on pressure drop and regurgitation provide a comprehensive and organized picture of the valve performance.

(v) The information is fundamental to the improvement in valve design, and development of guidelines for test methodology and acceptable performance criteria for marketing of the valves.

TABLE OF CONTENTS

LIST OF TABLES

LIST OF FIGURES

LIST OF SYMBOLS

D – upstream inside tube diameter

N – number of cycles for averaging

t – time or instant of measurement in each cycle measured from the beginning of the diastolic cycle

T – time measured from the onset of mitral flow

$U(t)$ – instantaneous velocity where $U(t) = \overline{U}(t) + U'(t)$

$\overline{U}(t)$ – 9-point forward averaged mean velocity component

$U'(t)$ – fluctuating velocity component

$u(t)$ – instantaneous velocity component +45° to the axial direction where $U(t) = iu(t) + jv(t)$

$\overline{u}(t)$ – mean velocity component +45° to the axial direction

$u'(t)$ – fluctuating velocity component +45° to the axial direction

U_{V_0} – nondimensional velocity, U/V_0

$v(t)$ – instantaneous velocity component -45° to the axial direction where $U(t) = iu(t) + jv(t)$

$\overline{v}(t)$ – mean velocity component -45° to the axial direction

$v'(t)$ – fluctuating velocity component -45° to the axial direction

V_0 – average velocity based on the annulus area

X, Y, Z – axes as defined in Figure 2-5

Y_0 – radial distance measured from the central axis ($Y = 0$) at $Z = 0.4D$

ρ – density

τ_R – Reynolds stress

τ_u – normal stress in the u velocity direction

τ_v – normal stress in the v velocity direction

$<>$ – average over N cycles

DEFINITIONS

anterior orientation:	(in reference to tilting disc prostheses), the major orifice anteriorly located, i.e. towards the aorta
calcification:	hardening of the leaflets in tissue prostheses due to the deposits of calcium
diastole:	period of relaxation of the heart muscle during which blood flows into the ventricles
endocarditis:	inflammation of the endocardium, and most commonly involving a heart valve
hemolysis:	destruction of red blood cells
heterograft:	prostheses constructed from tissue of animals (usually bovine or porcine)
homograft:	tissue prostheses constructed from human tissue
insufficiency:	inadequate function of the heart valves resulting in regurgitation (flow of blood in the wrong direction)
in vitro:	in an artificial environment
in vivo:	within the living body
peak average stresses:	the highest stress at each downstream location after the stresses, at each measuring point, are averaged over the entire time averaged cycle or a phase of the cycle
peak stresses:	the highest stress measured over the time averaged cycle or a phase of the cycle at each downstream location
posterior orientation:	(in reference to tilting disc prostheses), major orifice posteriorly located, i.e. away from the aorta
stenosis:	narrowing of the valve orifices
systole:	period in the heart cycle in which the heart contracts
thromboembolism:	coagulation of blood in the heart or blood vessels forming an obstruction to circulation
time average cycle:	the averaged values over N cycles

ACKNOWLEDGEMENT

I would like to take this opportunity to express my gratitude and sincere thanks to Professor V.J. Modi for the enthusiastic guidance given throughout the research program. His help and encouragement have been invaluable.

I would also like to acknowledge the time and assistance given by Dr. W.R.E. Jamieson. His assistance in obtaining the tissue valves and providing clinical expertise was most appreciated. In addition, many thanks to Dr. Toshi Akutsu for his help and knowledge in this area of research.

Special thanks also to Bicer Medical Ltd. for supplying us with the Bicer prosthesis and Shiley Canada for supplying the Björk-Shiley Monostrut.

Finally, special appreciation is extended to my husband, Erik, for his patience, understanding and support during trying times.

The project was supported by the Natural Sciences and Engineering Research Council Grants A-2181 and STR-32682.

1. INTRODUCTION

1.1 Preliminary Remarks

One of the major achievements in cardiac surgery over the past 30 years has been the ability to replace severely diseased heart valves with prosthetic ones. The option of using prosthetic heart valves for the treatment of valvular heart disease has improved and prolonged many lives.

Although heart valve replacement has become a standard procedure worldwide, the ideal valve substitute remains to be designed. Even after 30 years, problems associated with heart valve prostheses have not been totally eliminated.

Patients opting for artificial heart valves continue to face a substantial risk of serious complications during and after their replacement surgery. It is important to remember that valve replacement is not a cure, but rather a substitute, of a lesser problem for a greater one, in an attempt to improve the quality and duration of life.

Valve related complications for patients with an artificial heart valve include: thromboembolism, haemolysis, calcification, tissue overgrowth, bioincompatibility, suture tears, valve-leakage, and mechanical failure. The first three complications are the most prevalent and have been attributed to fluid dynamic disturbances[1,2]. This has created an area in medicine where engineering principles can be applied in order to improve heart valve performance. The objective of this thesis is to study the flow disturbances downstream of mechanical and biological prosthetic heart valves in the mitral position. This will necessitate a thorough velocity and turbulence evaluation of the valves using a two-component Laser Doppler Anemometer.

1.2 The Heart and Mitral Valve Disease

The human heart is a four chambered muscular organ which is shaped and sized roughly like a man's closed fist. The heart lies in the mediastinum just behind the body of the sternum between the points of attachment of the second through the sixth ribs. The heart weighs approximately 300 g and contracts about 70 times a minute at rest expelling about 75 ml of blood with each beat. Almost 3 million litres of blood per year is pumped through the heart, during which the heart valves open and close approximately forty million times.

The vital role of the heart in maintaining homeostasis depends on the continuous and controlled movement of blood through the thousands of miles of capillaries that spread through every tissue and cell in the body.

The heart acts as a double pump with two pumping chambers (ventricles) and two collecting chambers (atria). The left ventricle pumps oxygenated blood around the body and back to the right atrium. The right atrium discharges to the right ventricle which pumps the deoxygenated blood to the lungs and back to the left ventricle. Figure 1-1 shows the frontal section of the heart.

Each ventricle has an inlet and an outlet valve which permit the flow of blood in only one direction. The moving parts of these valves are thin, flexible membranes called cusps. The inflow valves (tricuspid, mitral) separate the atria from the ventricles. The outflow valves (pulmonary, aortic) isolate the ventricles from the two main arterial trunks. The inflow valves, also called the atrio-ventricular (A-V) valves, prevent blood from backing into the atria (reversed flow called regurgitation) during ventricular contraction. The purpose of the outflow valves is to prevent the backward flow of blood from the aorta and the pulmonary artery during ventricular relaxation. The two outflow valves, also known as the semilunar

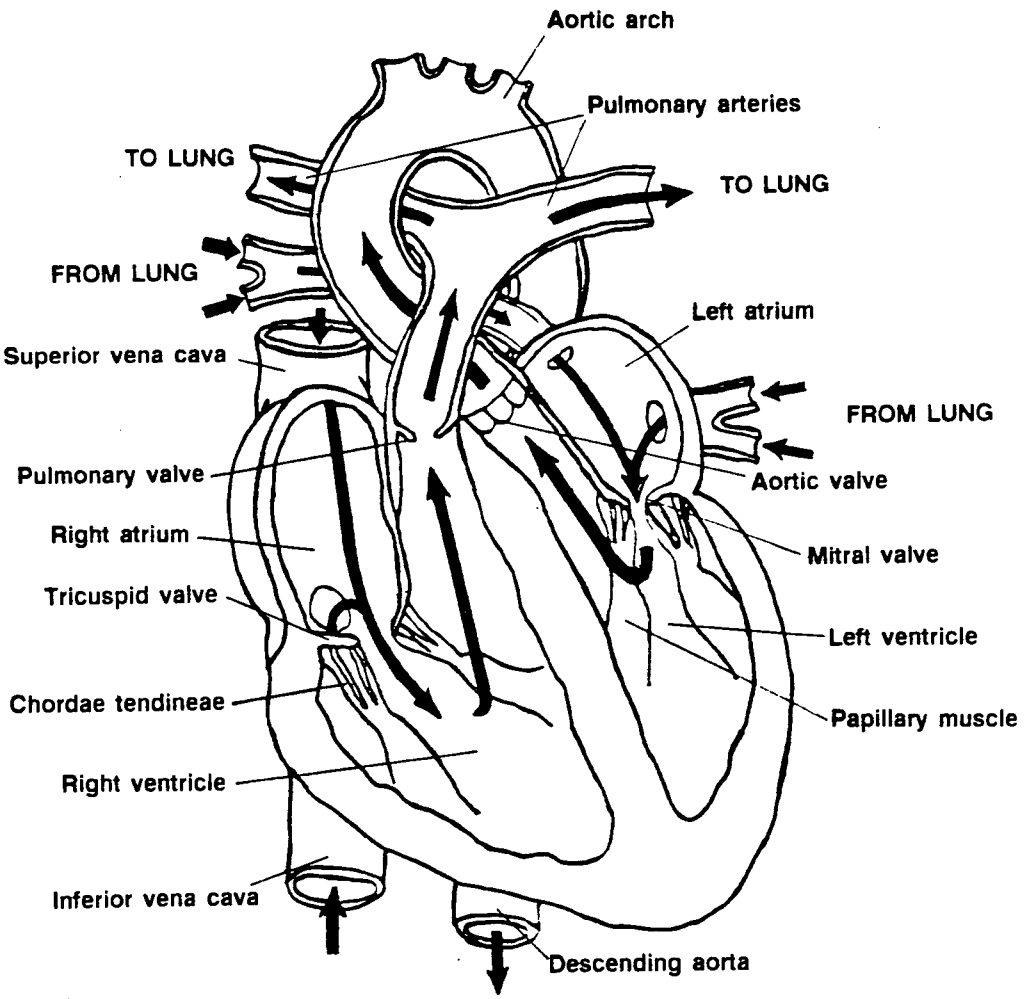

Figure 1-1 Frontal section of the heart showing the four chambers, valves and major vessels. Arrows indicate direction of blood flow.

valves, consist of 3 cusps each. Similarly, the tricuspid valve has 3 cusps while the mitral valve has only two.

The design and function of the mitral valve, although analogous to the tricuspid valve, differs markedly from those of the aortic and pulmonary valves.

The mitral valve consists of an annulus, a pair of cusps, the chordae tendineae and the papillary muscles as shown in Figure 1-2. The vital function of the mitral valve is to act as a check valve, preventing blood from regurgitating back into the lungs. In an healthy heart, the mitral valve closes rapidly, allowing little, if any, blood to regurgitate into the left atrium. The cusps are prevented from extending into the left atrium by the chordae tendineae attached to their edges. Similarly, the mitral valve opens rapidly, exposing a large orifice through which the blood can flow into the left ventricle from the left atrium with almost no resistance. The pressure difference necessary to propel blood through the valve is negligible as long as it is healthy.

During ventricular systole, when the A-V valves are closed, the mitral valve is called upon to withstand the greatest peak load of pressure among any of the valves during the cardiac cycle. The mitral valve has to resist back pressure as high as 120 mmHg when the ventricle pumps while the aortic valve experiences a high of 80 mmHg. The valves on the right side of the heart experience back pressures of only about 25 mmHg. Exposure to high pressure can lead to accelerated thickening of the valve cusps. For this reason, the 'left-sided' heart valves, particularly the mitral valve, are more susceptible to deterioration than the 'right-sided' heart valves.

Each of the four cardiac valves can deteriorate in two ways: they can become incapable of opening completely so that the effective orifice available for blood flow is narrowed (stenosis), or their function as valves may be impaired by incomplete

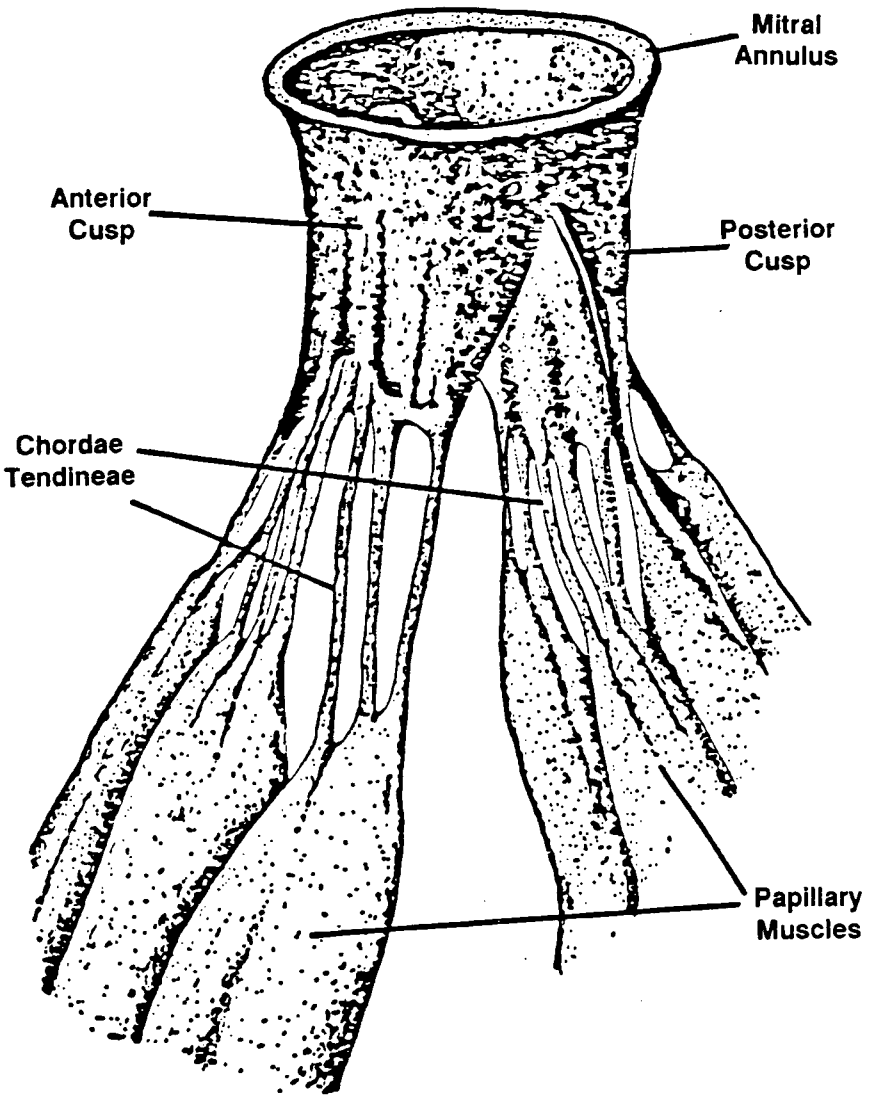

Figure 1-2 A schematic diagram of a natural mitral valve.

closure (insufficiency), through which the blood regurgitates.

The mitral valve is often affected by heart diseases, and may fail due to non-congenital reasons. Some of the diseases affecting the mitral valve are: annular calcification, rheumatic fever (on the decline in North America), endocarditis and ruptures of either the chordae tendineae or papillary muscles which maintain the position of the cusps. These heart diseases can lead to Mitral Stenosis or Mitral Regurgitation.

If nonsurgical correction or surgical reconstruction of the valve fails to improve the patient's condition, the valve may have to be replaced with a mechanical or biological prosthesis. To date, no valve has been designed which fully emulates any of the four natural valves.

1.3 Overview of Prosthetic Valve Development

The remarkable advances made in the design and application of mechanical and biological prosthetic heart valves has been an important chapter in medical history. The first defined period of valve development began in 1960 with the successful replacement of the aortic valve with the ball and cage device by Harken[3], and the subsequent modifications and application in the mitral position by Starr[4].

In many cases the early valves were the result of surgical innovation with little or no engineering input in their design. This led to a high incidence of valve thrombosis and mortality rate. However, the caged ball valve design seemed to yield promising results, and after the initial clinical success of Starr and Edwards[5], most surgeons used this type of prosthesis. Although the acceptance of the caged ball design was widespread, many problems remained to be solved[6]. The major undesirable feature of the ball valve is its occluding geometry with the ball in the centre of

the bloodstream causing a degree of obstruction. This led to intense laboratory investigations in an attempt to eliminate the risk and complications associated with previous models. Figure 1-3 shows the evolution of the cage ball valves.

Within a short time after the successful implantation of mechanical prostheses, biological prostheses were introduced in an attempt to imitate natural valves more closely, and thereby, improve hemodynamic functions and decrease thrombogenicity. However, many of the early tissue valve replacements failed[1,8-10]. The various reasons for failure included calcification of the leaflets leading to stenosis, shrinkage of the leaflets leading to insufficiency, infection and manufacturing problems. One particularly unsuccessful valve was structured from fascia lata[9] which suffered from poor durability and a high infection rate. However, with the improvement in design and manufacturing technique, biological valve performance improved at which time they became more widely accepted. The Hancock porcine bioprosthesis, commercially available in 1970, is representative of the "first generation" of successful biological valves.

The second period of valve development introduced the tilting or pivoting disc prostheses, as well as innovations in biological valves. The tilting or pivoting disc mechanical valve is distinguished by a single disc-shaped occluder that tilts during the opening phase.

With the realization that the lower-profile tilting or pivoting disk valves generally had lower thrombogenicity and, in small sizes, better hemodynamic efficiency than the ball and cage valves[11,12], further innovations with this design appeared. The first valve to appear in the market was the Wada-Cutter (W-C) valve in 1967. It consisted of a small hinged teflon disc. However, the fixed hinge was a drawback as accelerated wear was observed. Later, the same year, the Lillehei-Kaster tilting

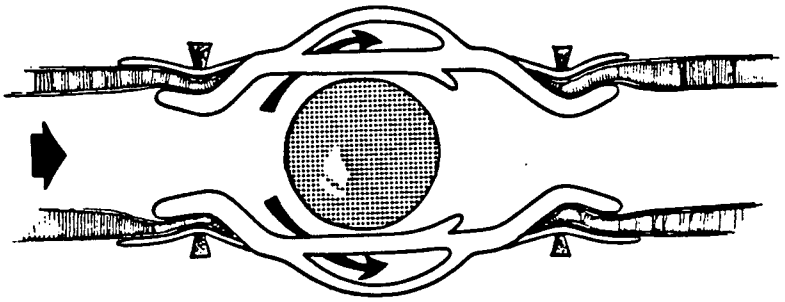

(a)

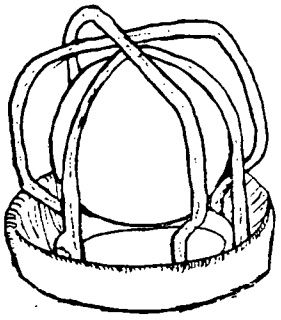

(b)

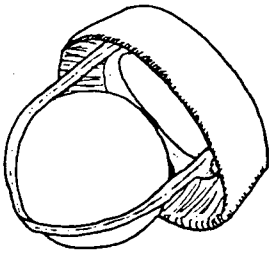

(c)

Figure 1-3 Evolution of caged ball valves: (a) Hufnagel[7](1952); (b) Harken (1960); (c) Starr Edwards (1962).

valve (L-K) was introduced. In 1969, Björk, in cooperation with Shiley developed the Björk-Shiley tilting disk valve (B-S). Both the L-K[13] and B-S[12,14] represented improvements in comparison with the W-C valve, which was soon withdrawn from the market. The drawbacks of the W-C valve were eliminated with the use of a free floating tilting disc made of Delrin, which had a seven times greater resistance to wear than Teflon. In addition, with a free floating disc, the wear was distributed evenly over the disc. However, in 1971, Delrin discs were replaced by pyrolite carbon discs, which were more durable, inert with respect to blood, and less susceptible to unacceptable levels of wear during a patients's lifetime. Both valves, however, showed a disturbing incidence of valve thrombosis. Further evolution of the L-K valve led to the Omniscience design. The B-S valve, following three further modifications, evolved into the monostrut model which has been on the market successfully for several years[12,14–17]. In 1977, the first implants of the Hall-Kaster tilting disc valve (later known as the Medtronic-Hall) were performed. The Bicer-Val tilting disc valve was first clinically tested in 1980, and limited numbers were implanted over the next three years under closely monitored conditions. Since 1983, several thousand have been successfully implanted worldwide. However, approval for use in Canada is still pending. Figure 1-4 shows schematic drawings of the Björk-Shiley c-c and the Bicer-Val prostheses.

In 1977, a bileaflet valve was introduced, the St. Jude cardiac valve[18,19](Figure 1-4). This model was an improvement over the previous bileaflet designs in terms of the hinge mechanism.

"Second generation" biological valves were introduced in the early 1970's with improved hemodynamic performance due to new developments in materials, design, preservation and mounting techniques. The most significant of these developments

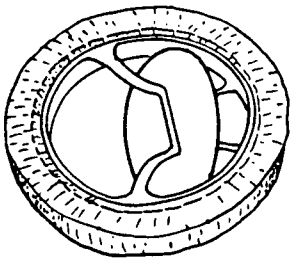

Björk-Shiley c-c

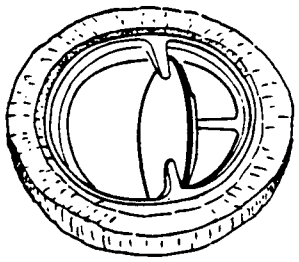

Bicer-Val

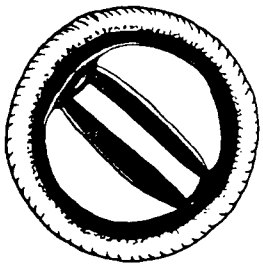

St. Jude bileaflet

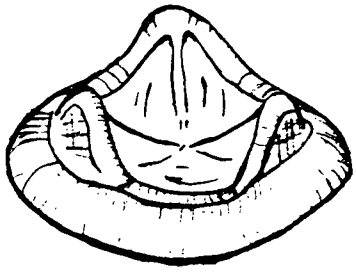

Carpentier-Edwards Supraannular

Figure 1-4 Schematic drawings of commonly used prostheses.

was the utilization of bovine pericardium by Ionescu in 1971[20]. The valve, however, was not tested clinically until 1976. In 1981, the Carpentier-Edwards supraannular porcine bioprosthesis (Figure 1-4) was released as an investigational prosthesis under the guidelines of the U.S. Food and Drug Administration (F.D.A.). Due to its superiority over the standard Carpentier-Edwards porcine valve (1975)[21], it quickly gained popularity. The Hancock porcine valve (Hancock II)[22] is an attempt to improve long term integrity and durability as well as meet surgical requirements. Enthusiasm for the biological valves fluctuates as cardiac surgeons are attracted to the perceived advantages of their in vivo flow characteristics and lack of thromboembolism, but at the same time they are deterred by their questionable durability.

The evolution of prosthetic valves has been one of constant change. Refinements in design have not only produced more durable valves but the incidence of thromboembolism has also been reduced. At present, there are only slight differences between the different types of mechanical or biological valves, and each type has advantages and disadvantages. The debate continues as to which group is superior. An evaluation of each group of valves is presented in a later section. At present, the types of valves can be divided as follows:

(a) Biological

  (i) the heterograft;

  (ii) the homograft;

(b) Mechanical

  (i) the tilting disc;

  (ii) the bileaflet;

  (iii) the caged ball.

The investigation presented here focuses on the first category of each type (the

heterograft and the tilting disc).

1.4 Overview of In Vivo and In Vitro Studies

The usual assessment of any heart valve replacement is achieved through long-term clinical implantation and follow up (in vivo performance) study . Clinical results are evaluated by actuarial patient survival analysis, relief of symptoms, and freedom from postoperative complications, particularly valve complications leading to reoperations, thromboembolism, and anticoagulant related haemorrhages. To evaluate the clinical performance of the Björk-Shiley monostrut prosthesis, five medical centres combined their early results from implantation in 486 patients[16]. The three year survival rate was 91% for aortic replacement (AVR), 92.3% for mitral replacement (MVR) and 76.2% for double valve replacement (DVR). No case of valve thrombosis or fatal thromboembolism was reported in anticoagulated patients. The degree of mechanical haemolysis was low and there was no instance of mechanical failure. Although the follow up period for the monostrut was short, the clinical results showed an improvement over previous Björk-Shiley models, particularly with regard to durability. Similar information has been reported on the monostrut valve and other models of the Björk-Shiley valve[11,12,14,16,17]. Several reports have also been presented on the incidents of mechanical failure of the early models of the Björk-Shiley valve[14,23,24]. Clinical information has also been reported for the Starr-Edwards aortic valve[25], the Lillehei-Kaster aortic valve[13], the St. Jude Medical valve[18,26]and the Medtronic Hall valve[27]. All show comparable results.

Similarly, clinical results for widely used biological valves are given by Miller[28] on the Hancock porcine valve, Ionescu[29] on the Ionescu-Shiley Pericardial Xenograft valve, Jamieson[21] on the Carpentier-Edward supraannular valve and by many others[30-34].

For instance, Jamieson and colleagues implanted 1,176 Supraannular valves between 1981 and 1985 in British Columbia, Canada. Actuarial survival at 3 years was 86% for AVR, 80% for MVR and 81% for DVR. The major valve related complication was thromboembolism.

Comparisons of the clinical performances of different heart valves are hampered by differences in patient/prosthesis selection, regimens of anticoagulation, definitions used for the classification of valve related complications, surgical techniques, and extent of patient follow-up by various centres. Therefore, most comparisons of prosthetic heart valves have been made using models where standardized testing conditions are available.

The objective of in vitro testing is to assess the performance of valves prior to implantation in the in vivo environment. This data is necessary to predict clinical performance and to interpret the clinical observations and areas of failure. In vitro tests include:

(i) steady state and pulsatile hydrodynamic testing;

(ii) accelerated fatigue testing;

(iii) material property testing.

To achieve comparative evaluation of the hydrodynamic performance of prosthetic heart valves, in vitro studies must be conducted under carefully controlled conditions and the relevance to the clinical situation must be clear. Hydrodynamic tests under steady and pulsatile conditions include measurements of:

(a) pressure drop and recovery;

(b) flow rate;

(c) energy loss;

(d) velocity profiles and their decay;

(e) viscous and turbulent shear stresses.

Steady flow investigations are useful during the developmental stages of a prosthesis as an indication of acceptability. However, the results of steady flow tests are not always accurate in predicting in vivo pressure gradients and can sometimes be misleading. Therefore, tests in pulsatile flow are essential for the simulation of the natural heart.

Most of the early studies were confined to pressure measurements across the valve for different flow rates and valve sizes[1,35]. Since many problems and complications associated with valve prostheses are related to the dynamic behaviour of the valves and the unsteady flow patterns, it is necessary to obtain more detailed flow information. Studies of flow disturbances downstream of prosthetic heart valves are essential to reveal mechanisms of haemolysis, endothelial damage, and thrombus formation. Studies using flow visualization[2,35] usually give only qualitative information on the location of the main flow, stagnation and vortex field.

Hot film anemometry was an improvement over flow visualization as it facilitated the measurement of local velocity fields around prosthetic heart valves. Flow disturbances have been studied in steady and pulsatile flow models of varying complexities using hot film anemometry as discussed by Hasenkam et al.[36,37] However, the major limitation of this procedure is the presence of probes in the flow field. The laser doppler anemometer (LDA) is a further improvement as it makes it possible to measure velocity components without disturbing the flow field. Because of this feature, it represents an unique tool for surveying downstream flow fields of heart valve prostheses. Reul and associates[38,39]developed a mock circulatory system for pulsatile flow studies and used a two-beam LDA for one-dimensional

velocity measurements of valves in the aortic position. They utilized the velocity distribution profiles to determine areas of recirculation in order to indicate where thrombus formation and deposition would occur. The drawback to using the two beam LDA was the inability to measure the turbulent shear stress directly as two components of velocity are necessary for the calculation. Since the Reynolds stress plays a vital role in the design and evaluation of prosthetic heart valves, a three beam LDA was used later[40].

Yoganathan and associates first used a LDA to measure both steady flow fields as well as turbulent intensities downstream of various prosthetic aortic heart valves[41]. They found disturbed flow fields and stagnation zones in the vicinity of all the valves under study. To better simulate the natural condition, a left heart pulse duplicator system was designed and built to conduct pulsatile experiments using a three-beam (two-dimensional) LDA[40,42–46]. The prosthetic valves studied were the Starr-Edwards caged ball valve, Björk-Shiley tilting disc valve, Medtronic-Hall tilting disc valve, and St. Jude bileaflet valve. Their results indicated that all four prosthetic valve designs created large intensity turbulent flow fields with regions of flow separation, stagnation and elevated turbulent shear stress. The maximum values of the mean turbulent shear stresses measured during peak systole were 1200 dynes/cm^2 for the Starr-Edwards, 1600 dynes/cm^2 for the B-S, 1000 dynes/cm^2 for the Medtronic-Hall, and 1050 dynes/cm^2 for the St. Jude. The corresponding values during the deceleration phase were about 800, 600, 450, and 800 dynes/cm^2, respectively.

Such high levels of turbulent shear stresses could cause damage to blood elements as indicated by Nevaril and associates[47], who concluded that platelets are susceptible to damage at stresses in the order of 1500 dynes/cm^2. Other experiments[48,49]

have shown that platelets are susceptible to damage by shear stresses as low as 100 to 500 dynes/cm^2. Also, the danger of thrombus formation and tissue overgrowth on the valve structure in regions of flow separation and stagnation was discovered. In studies with three newer mechanical valves (Björk-Shiley monostrut, Omni-Carbon, Duromedics), Yoganathan and Associates[46] still found relatively high turbulent shear stress, with peak values in the range of 1000 to 2000 dynes/cm^2. In overall analysis, Yoganathan found that these second generation low-profile mechanical valves are haemodynamically comparable to the Medtronic Hall and St. Jude Medical mechanical valves and superior to the first generation valves. However, it is unlikely that these valve designs will eliminate the problems of thrombosis, thromboembolic complications, and haemolysis. Yoganathan and Associates[42,44] also conducted fluid dynamic characteristics of a variety of first and second generation porcine and pericardial aortic bioprostheses under pulsatile conditions. The older designs created minimum turbulent shear stress of about 1500 dynes/cm^2 while the new designs led to turbulent shear stress as little as 750 dynes/cm^2. Similar results were also reported by Walburn and Associates[50].

To date, most of the in vitro investigations of pulsatile flow have concentrated on studying the flow field downstream of the aortic valves[36,37,39,42-44,46,50-54]. Although the general character of the velocity profiles produced by mitral prostheses may be expected to be qualitatively similar to those obtained with aortic prostheses of the same type, the magnitudes of the velocities and turbulent shear stresses, as well as the changes in the flow field as it progresses downstream, may be expected to be quite different as the vessel geometry is quite different. To conduct experiments on mitral valve prostheses, Woo and Yoganathan[45] developed a flow system that duplicated the pressure and flow characteristics of the left side of the human heart, although the system did not anatomically mimic the human "left" heart. The

results indicate that the four prosthetic valve designs studied (Beall caged-disc, Björk-Shiley tilting disc, Medtronic-Hall tilting disc, and St, Jude Bileaflet) create strong unsteady flow fields with high levels of turbulent shear stress as well as regions of flow separation and stagnation. The maximum turbulent shear stress of 1900 dynes/cm^2 was experienced by both the Beall valve and Medtronic-Hall valve.

Akutsu[55] and Modi assembled a complex duplicator which closely simulates the physiological function as well as the anatomical shape of the natural left side of the heart and its circulation system. As suggested by them, fluid dynamic data should be presented in terms of nondimensional similarity parameters as this eliminates the dependency on individual valve size, test fluid viscosity and density. Unfortunately, considerable amount of information recorded in literature is presented in dimensional form and therefore is valid only for specific situations and fails to evolve general conclusions. They concluded that prosthetic heart valves can raise turbulence intensity by as much as an order of magnitude which increases the possibility of thromboembolism and perhaps haemolysis. Based on the same annulus diameter, the Starr-Edwards prosthesis has a considerable lower turbulence intensity as well as peak velocity compared to the Bjõrk-Shiley and St. Jude valves. They also concluded that velocity and turbulence intensity profiles are essentially independent of the valve size, for a given configuration, when the results are nondimensionalized with reference to the velocity at the annulus.

As previously mentioned, the fluid dynamic disturbances past valve prostheses of various geometries and the stresses associated with these disturbances have been linked to the problems with the clinical use of prostheses. Chandran[56] and associates found that flow disturbances could be further compounded by the orientation of the prostheses with respect to the mitral valve annulus. This was especially evident

for tilting disc and bileaflet valves. For tilting disc valves, the flow condition at the mitral orifice is asymmetric. Therefore, the relative orientation of the disc to the aortic orifice may have a significant influence on the flow field forming in the ventricle. Chandran found that a posterior orientation (major orifice away from the aorta orifice) provided a smooth washout with minimal disturbance of flow compared with an anterior orientation (major orifice towards aortic orifice). Björk[57] also reported that a posterior orientation was optimal for the Björk-Shiley tilting disc valves.

A heart valve prosthesis must be capable of continuously regulating blood flow in an hostile physiological environment for a patient. Ritchie and Lubock[58] suggest that the useful (fatigue) life of a prosthetic cardiac valve can be estimated using both classical stress-strain/life and damage-tolerant fatigue analyses described under peak physiological loading conditions. The valve under study was the Björk-Shiley monostrut. They concluded that the monostrut had an acceptable lifespan provided that flaws larger than 500 μm are not present.

Because a prosthetic heart valve is required to operate for many years, in a hostile environment without maintenance, it is essential to conduct careful reliability tests on the materials used in the construction of valves, especially in regards to mechanical valves, before clinical application. Many analyses aimed at causes of wear and breakdown of elements in prosthetic heart valves have been conducted[32,59–61]. As a result, mechanical valve materials have evolved from teflon to delrin and finally pyrolite for the occluder and a cobalt alloy (Haynes 25) or titanium for the valve ring.

1.5. Mechanical vs Biological Valves

The field of valvular heart replacement has advanced during the last two and a half decades to a level where valve substitutes are considered quite reliable. It has branched into two areas of development: mechanical valves and biological valves. The ultimate goal of a heart valve substitute is to mimic the function of a natural human heart valve. This would entail durability, nonthrombogenicity and near normal hemodynamic performance. Both areas of development have progressed toward this final goal of the "ideal" valve substitute. However, there is still considerable room for improvement. In a search for the "ideal valve", cardiac surgeons and cardiologists are looking for a prosthesis that will give a satisfactory quality of life and expectation for survival. This has led to competing claims between the categories and different designs in the same category as to the superior performance.

The major advantage of mechanical heart valves is their durability. The problems some mechanical valves had with broken struts[23,30] has now been virtually eliminated by the choice of material and manufacturing techniques. The strength of mechanical valves is the weakness of currently used biological valves. Many authors have reported their failure[1,32,44,59,62] due to tissue degeneration and leaflet calcification, especially in children and young adults. However, this does not imply limited survival of the patient, since progressive valve deterioration allows reoperation of the patient before the onset of serious complications. Of course, it does introduce a further risk to the patient. It is unclear whether some of the newer biological valves being treated by slightly different preservation methods and manufacturing techniques will have a similar failure rate. Only time will tell.

The implantation of foreign objects in the circulatory system promotes thrombus formation and subsequent valve obstruction. Although biological valves are not free

from embolic complications, they appear to have an advantage over the mechanical designs in that the risk is lower in the former even when anticoagulants are not used. Since biological valves exhibit a relatively low rate of thromboembolic complications, anticoagulation therapy is less frequently needed. However, anticoagulants are a necessity with mechanical valves, and are associated with risks due to thromboembolism and haemorrhagic complications, which could prove to be fatal.

From the hemodynamic point of view, mechanical and the newer generation biological valves used at present are not always satisfactory. Problems with high pressure drops and the creation of jet-type flows still exist[44]. This could lead to haemolysis and/or damage to the endothelial tissue lining of the heart wall. Therefore, understanding and careful evaluation of the hemodynamics of valve prostheses is necessary before implantation.

In the end, it is the survival of the patient that is of paramount importance. It is not always clear whether the risks of reoperation due to a tissue valve's failure or the risk of thromboembolic complications associated with mechanical prostheses can lead to a satisfactory quality of life.

Based on the available literature, it is not possible to conclude superior performance of one valve design over others. Both Rabago et al.[63] and Hammermeister et al.[30], after extensive use of both mechanical and biological valves, can not establish which type is clinically superior. It is therefore, almost impossible to recommend the use of either mechanical or biological valves. A decision as to the choice of a valve is dependent on a variety of preoperative factors such as age, sex, and mental, geographic, and social conditions, as well as contraindications for anticoagulation, life expectancy and associated diseases.

1.6 Purpose and Scope of the Investigation

As pointed out previously, the analysis of in vivo and in vitro data on heart valve prostheses show that the optimum valve has still not been developed. It is apparent from the literature survey that there is considerable room for improvement of both mechanical and biological valves. Several authors have emphasized the connection between fluid dynamic disturbances and thrombus formation, haemolysis and endothelial injury when prosthetic heart valves are implanted.

Since all prosthetic valves present more of an obstruction to blood flow than a normal heart valve, it is not surprising that turbulent flow fields are created in the vicinity of prosthetic valves. The specific features of turbulent flow that are likely to be damaging to the blood constituents are the stresses which are intrinsic to turbulence, known as Reynolds stresses. In order to quantify the in vitro velocity and turbulent stress fields under pulsatile flow conditions, it is necessary to measure two components of velocity simultaneously. This is achieved with the use of a 3 beam Laser Doppler Anemometer.

The major objective of the current study is to gain a better quantitative understanding of the velocity and turbulent shear stress fields in the immediate vicinity of mechanical and biological prosthetic valves in the mitral position under simulated conditions of physiological pulsatile flow. The thesis presents velocity and turbulence maps as a method of comparison for 3 mechanical and 2 biological prosthetic valves. A further study conducted on the tilting disc mechanical valves includes results from a series of tests on the effect of valve orientation. These results together with data on pressure drop and regurgitation previously obtained in our laboratory, provide a comprehensive, detailed and organized picture of the fluid dynamic characteristics associated with various mitral valve designs. This type of indepth

study is necessary to improve prosthetic valve designs and develop guidelines for valve testing protocol.

2. EXPERIMENTAL APPARATUS AND METHODOLOGY

This chapter describes the test-models and the test-facility used in the experimental program. Some of the instrumentation used is standard equipment in most fluid mechanic laboratories and hence need no elaboration. First, the test-models are briefly described. This is followed by a brief description of the pulsatile flow cardiac simulator and associated equipment. Further details concerning their design and construction can be found elsewhere[55]. Finally, the Laser Doppler Anemometer (LDA) system and experiment methodology are discussed which provide reliable results, through a noninvasive approach, thus improving our understanding of the complex flow.

2.1 Test Models

Since the first artificial aortic valve implantation in 1960, many different configurations have been designed. However, few have made it to the final stage of implantation. The tilting disc prosthesis and the porcine biological prosthesis are two commonly used valvular designs that have survived years of rigorous testing. These two categories of valves will be the focus of this study.

The tilting disc valves are represented by the Björk-Shiley convexo-concave valve (B-S c-c), the Björk-Shiley monostrut (BS mono) and the Bicer-Val (Bicer). The selected porcine biological configurations are the Carpentier-Edwards supraannular valve (C-E) and the Hancock II (HK). The valves selected are all 27 mm mitral valves except for the C-E which is a 29 mm valve. The BS mono, BV, C-E, and HK represent new generation valves while the B-S c-c serves as a reference and represents the older generation valves. Table 2-1 lists the valves studied together

Table 2-1 Investigated prostheses showing dimensions of interest.

Valve	Position	Model	Size (Annulus Dia.) mm	Orifice Diameter mm	Ventricular Projection mm
Mechanical					
Bjork-Shiley c-c	mitral	MBRC	27	22	12.5
Bjork-Shiley Monostrut	mitral	XAMMB	27	21.9	13
Bicer-Val	mitral	300-05	27	21.5	13.5
Tissue					
Hancock II Porcine	mitral/ tricuspid	T510	27	21	14
Carpentier-Edwards SAV Porcine	mitral	6650	29	23	13

with their annulus diameter, orifice diameter and ventricular projection. Figure 2-1 shows photographs of each valve.

A Starr-Edwards (Model 2M6120) caged ball mechanical valve was used in the aortic position for all experiments. Among the mechanical valves, the caged ball valves have the lowest rate of regurgitation (3-7 percent) compared to tilting disc valves (10-13 percent) and bileaflet valves (10 percent)[64]. Therefore, for the purposes of this study, the Starr-Edwards valve was ideal in the aortic position as the small amount of regurgitation had a minimal effect on the flow development in the left ventricle chamber.

2.1.1 Tilting Mechanical Valves

The basic design of tilting disc valves creates two unequal regions of flow, namely the major and minor outflow regions (orifices) as shown in Figure 2-2. Stagnation in the minor outflow region has been the cause of thrombus formation and tissue overgrowth along the portion of the sewing ring adjacent to the minor outflow region. The geometry of the valve prostheses as well as the orientation of the prostheses with respect to the mitral valve annulus may significantly affect the flow development (vortex formation, regions of relative stasis and disturbed flow) in the human left ventricle.

Improvements in the fluid dynamics has been attempted through modifications in disc shape and increased opening angle. The three valves under study represent different disc shapes and opening angles (60°, 70°, 75°)

The Bjõrk-Shiley c-c valve consists of a free floating convexo-concave pyrolytic carbon disc suspended between two eccentrically situated stellite struts. The maximum opening angle from the mounting ring plane is 60°. The inflow strut is an

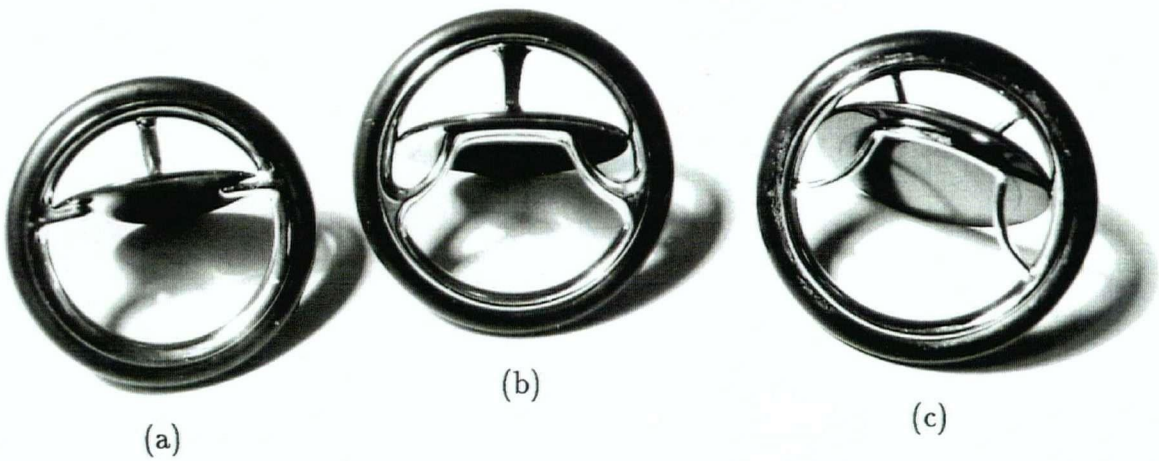

Figure 2-1 Photographs of the valves under study: (a) Bicer-Val; (b) Björk-Shiley Monostrut; (c) Björk-Shiley c-c.

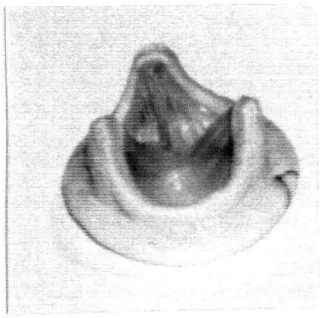

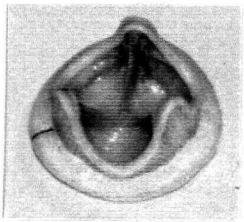

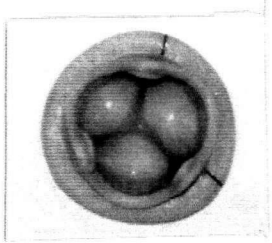

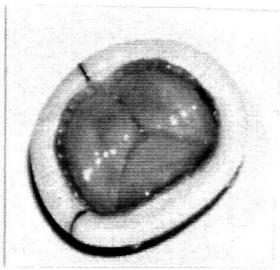

(d)

(e)

Figure 2-1 (cont.) Photographs of the valves under study: (d) Carpentier-Edwards Supraannular and (e) Hancock II.

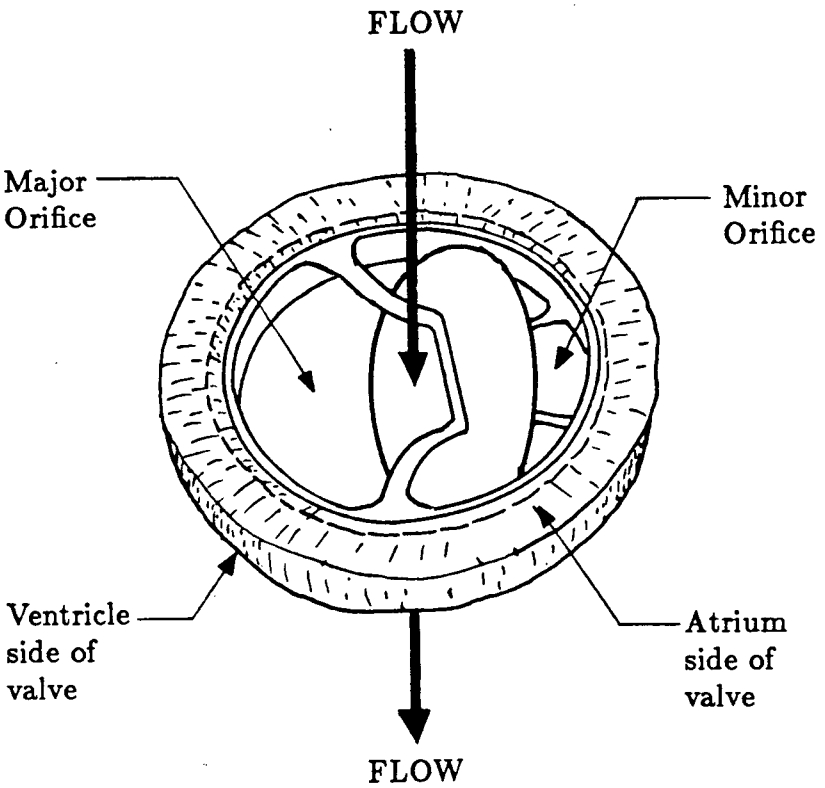

Figure 2-2 Schematic diagram of a tilting disc valve showing flow regions.

integral part of the valve ring while the outflow strut is welded to the ring. This valve was first introduced in 1976.

The Björk-Shiley monostrut valve is identical to the Björk-Shiley c-c with the free floating convexo-concave disc except for the presence of a single outflow strut perpendicular to the inflow strut. The pyrolytic disc tilts open to a maximum of 70°. The housing and struts are made from a single piece of Haynes 25, a cobalt alloy, thus avoiding any welding points which could be susceptible to mechanical failure. The design attempts to overcome the strut fracture complications of earlier models by making the struts an integral part of the valve ring.

The Bicer-Val valve consists of a free floating radiopacque pyrolytic carbon disc contained in an integral Haynes stellite housing. The low profile airfoil shaped disc is able to rotate about its vertical axis. A three point support mechanism allows a maximum disc opening angle of 75°. The first Bicer-Val clinical implant was performed in 1980.

In tilting disc valves, the disc does not seat against the ring when shut. It is suggested that this design allows some deliberate regurgitation to wash the valve ring in order to prevent thrombosis[65].

2.1.2 Porcine Biological Valves

The basic design of porcine biological valves, whose geometry is similar to the human aortic valve, can be expected to produce a more central jet-like flow than mechanical disc valves. If the jet shows high velocity components though, flow separation and areas of stagnation may occur. High stresses may also result at the boundary of the jet.

The Carpentier-Edwards supraannular prothesis is comprised of porcine aortic

valves that have been preserved in buffered glutaraldehyde and then mounted on a flexible frame. The frame is made of Elgiloy, a corrosion resistant alloy, chosen because of its superior spring efficiency and fatigue resistant characteristics. The lightweight frame is covered with a porous, knitted cloth to facilitate tissue ingrowth and encapsulation.

The Hancock II consists of porcine tissue attached to a stent machined from Delrin 500. Titanium radiopacque markers are placed close to the apex of the stent post to allow visualization of the relationship of the stent post to the ventricular wall. The stents are then covered with a Dacron knitted polyester fabric to facilitate tissue ingrowth. The Hancock II valves are chemically treated in T6 calcification retardant solution before sterilization and packaging.

2.2 Test Facility

In order to study mitral prosthetic heart valves, it is necessary to use a flow system that simulates the physiological function as well as the anatomical shape of the left side of the human heart. Steady and pulsatile flow experiments were conducted in a sophisticated and versatile cardiac simulator at the University of British Columbia. This facility was designed to permit hydrodynamic performance assessment of mitral and aortic prosthetic valves.

The test chamber consists of the atrium and aorta, a thin flexible transparent polyurethane ventricle, and a surrounding plexiglas box. This is all held in place by a support block as shown in Figure 2-3. The transparency of the ventricle and plexiglas box was essential for the LDA measurements. The "beating" of the heart is simulated by a computer controlled stepping motor which in turn drives a positive displacement pump. Through programming, any desired cardiac cycle can be obtained.

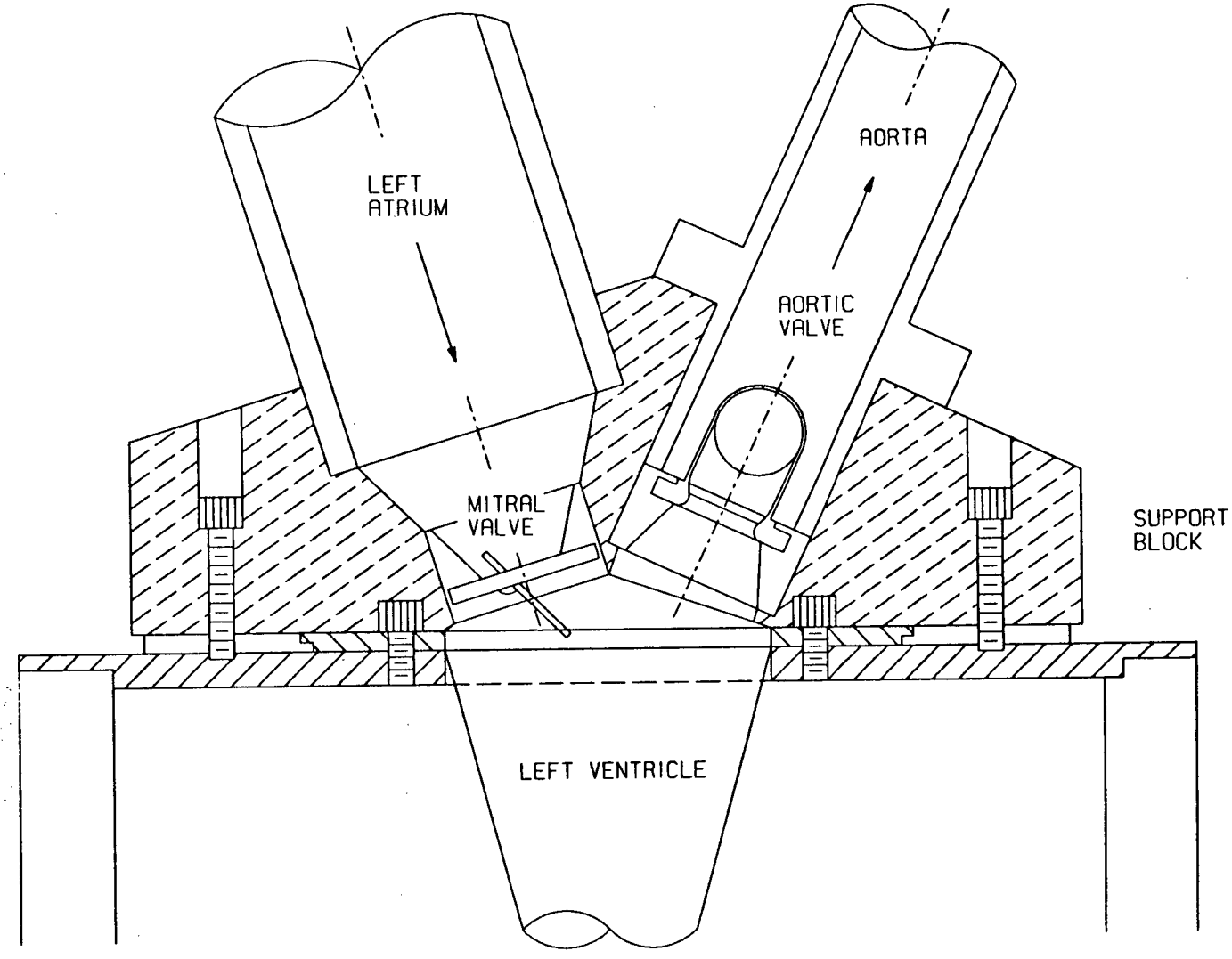

Figure 2-3 Details of the test chamber showing the left atrium, aorta, and a section of the left ventricle with the mitral and aortic valves in position.

The input and output impedances of the left side of the human circulatory system are simulated by means of a Windkessel which provides a desired characteristic resistance and compliance, and a water valve which adjusts the peripheral resistance.

The system is a closed loop. The drive unit sets the system in motion. The blood analogue fluid (water or saline solution) flows from the atrium through the mitral valve to the ventricle. The fluid continues through the aortic valve into the aorta and returns, via the mock circulatory system, to the atrium (the reserve tank).

The cardiac simulation system can also be used for steady flow experiments by using a bypass system with its own pump and orifice plate. A schematic diagram of the pulsatile and steady flow facility for velocity and turbulence measurements is shown in Figure 2-4.

2.3 Instrumentation

2.3.1 Laser Doppler Anemometry

As previously stated, many problems and complications associated with valve prostheses are related to the fluid dynamics. Therefore, detailed quantitative in vitro fluid dynamic studies should help to understand potential problems and complications that may arise with different designs of prosthetic heart valves. In order to quantify velocity and shear fields under pulsatile flow conditions, it is necessary to measure two components of velocity simultaneously. This may be achieved by the use of either hot film or Laser Doppler Anemometry(LDA). Hot film anemometers have several disadvantages such as the invasion of probes into the flow field which may cause disturbances, frequent need of calibration, and the inability to measure direction of the flow. The LDA, on the other hand, is a noninvasive optical measuring system which does not disturb the flow field. The only necessary conditions

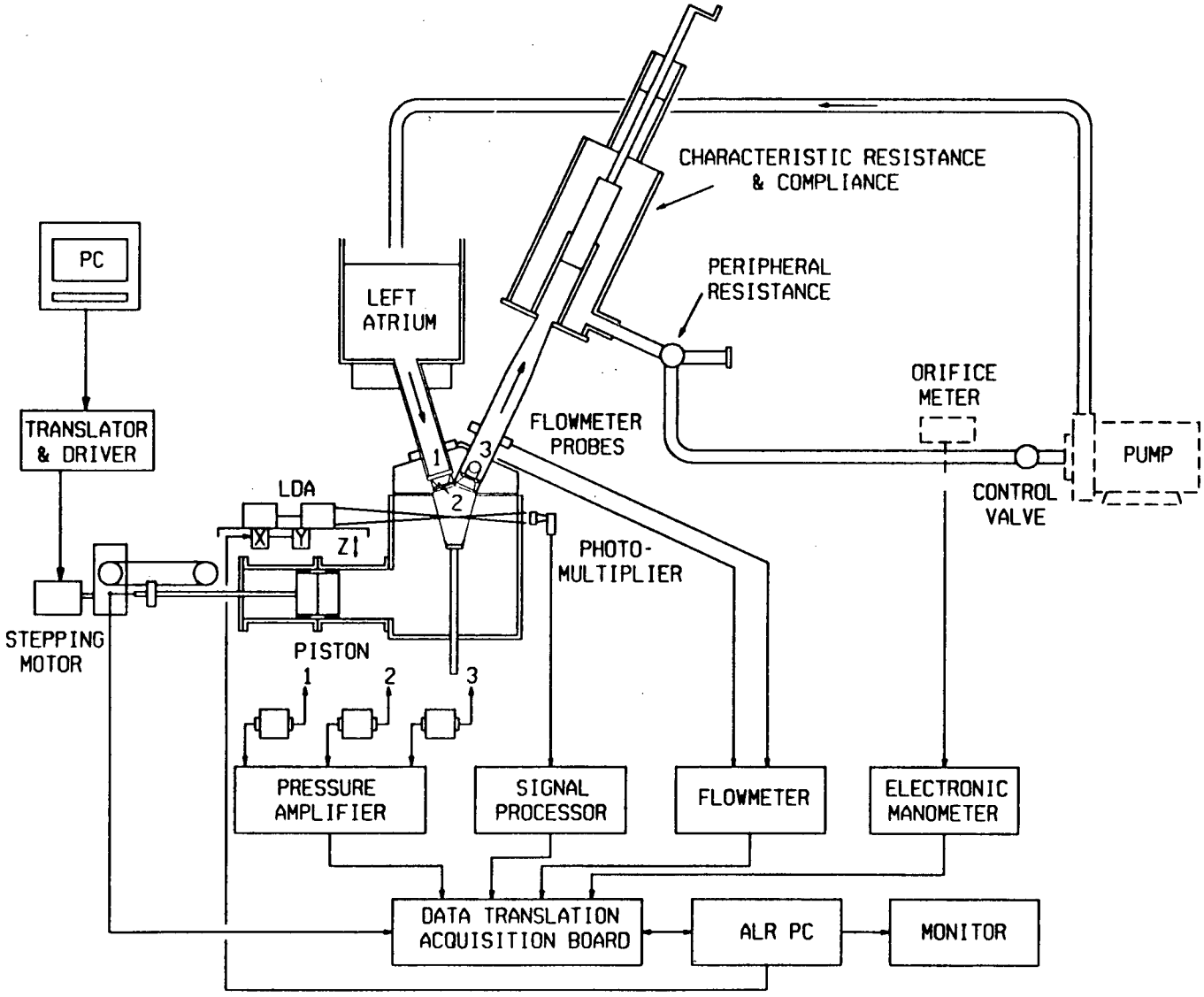

Figure 2-4 Schematic diagram of the pulsatile flow facility and associated instrumentation.

are a transparent medium with a suitable concentration of tracer particles and windows which allow optical access to the flow. Thus, it represents an ideal tool for measurement of the downstream flow field associated with a heart valve prosthesis.

In Laser Doppler Anemometry, laser light is scattered by particles suspended in the fluid. The light experiences a frequency shift (Doppler shift) and this is interpreted by electro-optics to obtain the velocity of the particles. The Laser Doppler Anemometer uses coherent incident beams, which form a system of interference fringes at the region of their intersection called the measuring volume. The distance between the fringes is fixed by the wavelength of the laser beam and the angle between the incident beams. The light scattered by the particle passing through the measuring volume is modulated with a frequency which is related to the velocity of the particle. A photomultiplier detects the Doppler-shifted signal scattered from the measuring volume.

Measurements of velocity and turbulence intensity in this study were carried out by a two component 3-beam ILT (Ion Laser Technology, Salt Lake City, Utah, USA) LDA system operating in the forward scatter mode. The LDA system consists of an Argon Ion laser (Model 5490ACWC), Dantec two-component 3-beam Argon-ion optics, and a Dantec Signal Processor Frequency Tracker (model 55N20). The air cooling of the ILT system was an attractive advantage over the water cooling of other similar systems. System accuracies are defined in Appendix I.

Separation of the two components of velocity is achieved by colour, using the green and the blue line of the Argon-ion spectrum. The two coloured beams, representing shifts in frequency, lie in the horizontal plane. Each of the shifted beams forms a fringe pattern with the main beam. Under this arrangement, the two sets of fringe patterns are perpendicular to each other permitting the detection

of two perpendicular velocity components simultaneously.

2.3.2 Traversing Mechanism

The laser and entire optical system were mounted on a three degree of freedom traverse mechanism that placed the measuring volume at almost any desired location in the ventricle. Two degrees of freedom (X,Y) were controlled by the main computer via two stepping motors (Sinano Electric Co. Ltd., Model 4H5618S-4) with an accuracy of 0.001 mm in the X direction and 0.005 in the Y direction. The third degree of freedom (z) was controlled through a scissor screw mechanism that raised and lowered the laser platform to any level in the ventricle. Fine adjustments in this direction were not possible (accuracy of 0.1 mm).

2.3.3 Computers

Two computers were responsible for the running of the cardiac pulse duplicator system. Data acquisition and processing was accomplished with an Advanced Logic Research (ALR) 386/220 personal computer. This computer also controlled the movement of the LDA system in the X and Y directions. The drive unit was controlled through a Nova Turbo PC XT.

2.4 Methodology

The amount of information that can be obtained by a planned variation of valve geometry and system variables is enormous. Therefore, with a limited number of valve geometries (5 in this study), more important fluid dynamic parameters were focused on.

Firstly, the test program for velocity and turbulence measurements were con-

ducted under two different flow conditions:

(i) separated flow past a fully open valve located in the mitral position (steady experiments);

(ii) pulsatile flow past a heart valve in the mitral position during a typical cardiac cycle (pulsatile experiments);

Secondly, for each condition, the only parameter altered was the valve orientation (mechanical valves only) for a fixed heart or flow rate.

Although measurements were taken throughout the ventricle, only data down the centreline is presented here. This is done for conciseness as the peak velocities and stresses were generally located in this plane.

2.4.1 Steady Flow Experiments

For steady experiments the control valve was adjusted to achieve a flow rate which roughly corresponded to the flow rate for the fully opened mitral valve during peak diastole in the pulsatile experiments. Measurements were carried out at 5 downstream locations to assess important features of the flow field. The downstream locations were 0.4D, 0.5D, 0.625D, 0.75D, 0.825D as shown in Figure 2-5. D represents the diameter of the upstream inlet tube just before the mitral valve. For the mechanical protheses, experiments were carried out using two different valve orientations: the anterior position (major orifice anteriorly located - towards the aortic orifice) and the posterior orientation (major orifice posteriorly located - away from the aortic orifice).

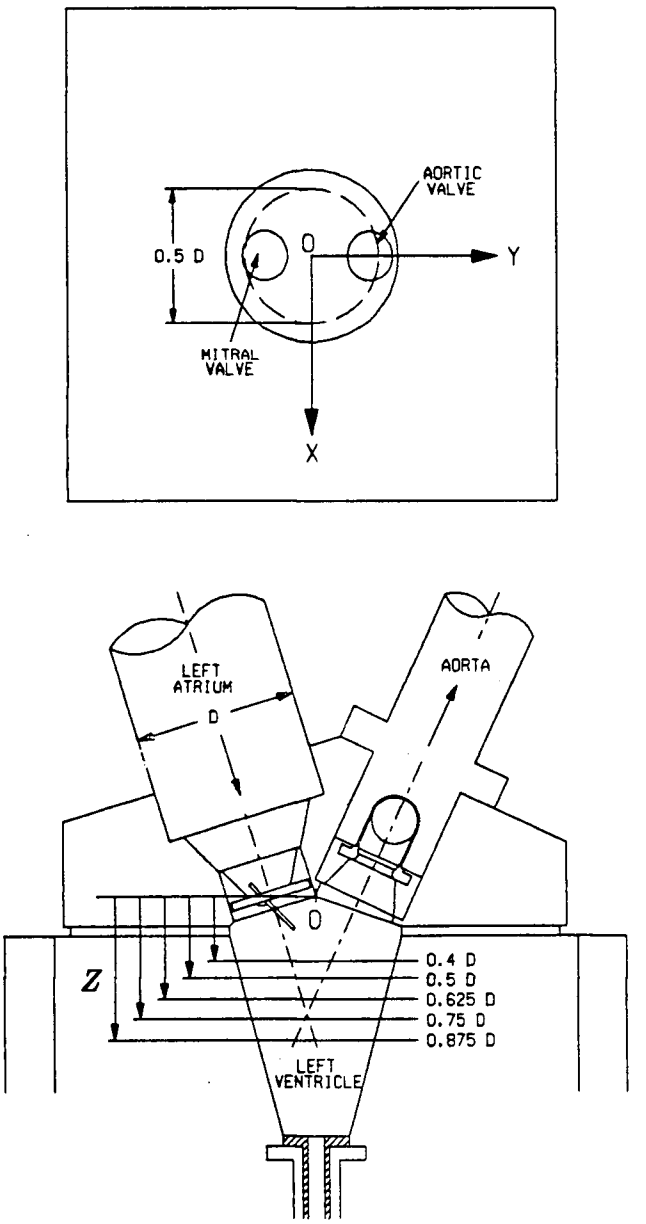

Figure 2-5 Plan and elevation view showing downstream measurement locations.

2.4.2 Pulsatile Flow Experiments

Experience of earlier researchers suggest that a large amount of repeated tests are needed to obtain statistically valid and reliable results. Therefore, the pulsatile flow velocity experiments were conducted at only one heart rate. For the average person at rest, a heart rate of about 62-72 beats per minute and a cardiac output of about 5 litres per minute is considered normal. Therefore, experiments were conducted at 70 beats/min, a blood pressure of approximately 120/80 and cardiac outputs in the range of about 4-5 l/min. The effective stroke volume used was around 60 ml/min. As in the steady experiments, data were collected downstream of the valves at 5 different locations for both normal and reversed orientations. In pulsatile flow, there are 3 distinct phases in each diastolic cycle: acceleration phase, peak phase, and deceleration phase. For each of these phases, the velocity profile, the Reynolds shear stress, and the turbulent normal stress may approach abnormal values. For this reason, data representing these 3 phases are emphasized, although a complete history (time and spatial) was documented.

Figure 2-6 shows a typical mitral flow rate vs. time chart to illustrate where in the diastolic cycle the 3 phases occur.

2.4.3 LDA Measurement Techniques

To facilitate comparison of data from different experiments, it was necessary to select a system of references in space. In the x-y plane, the centre of the ventricle was chosen to this end. In the z direction, the mid-point of the mitral valve orifice was the logical choice as all the experiments were centred around this valve. Figure 2-5 shows the origin and z locations at which measurements were carried out. The

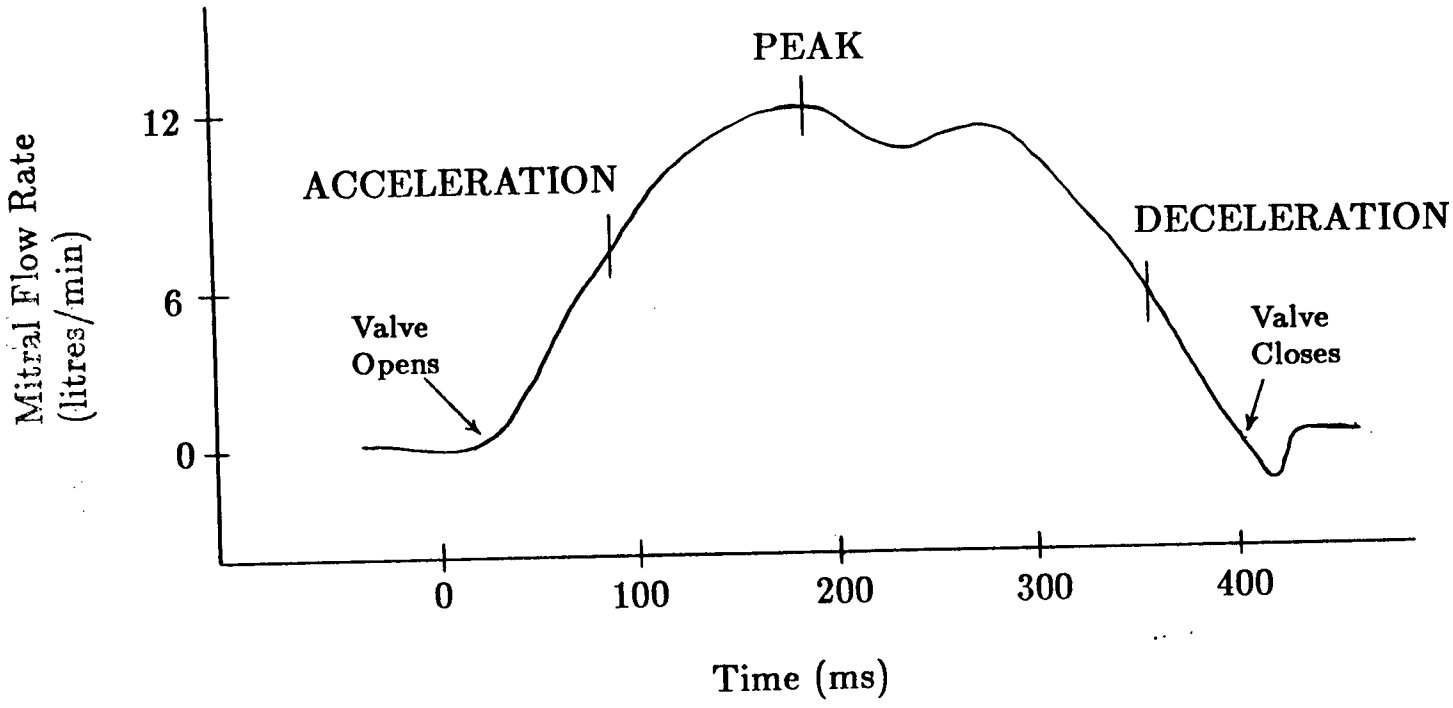

Figure 2-6 Instances in the cardiac cycle where measurements were emphasized.

highest level the laser could traverse was limited to 0.4D due to interference from the plexiglas box enclosing the ventricle. This limitation produced a gap in the velocity profiles and valuable information in close proximity to the valve was unobtainable.

The centre of the ventricle was located by first focusing the laser beams on the far wall of the ventricle in the y direction, then traversing to the near wall. The mid-point would then correspond to the centre location in the y direction. A similar procedure was followed for the x direction. However, because of the effects of the refractive indices, the movement of the traverse table in the x direction did not correspond to the movement of the measuring volume in the flow field. For this reason, measurements were made in the y direction at different x location. Even with this constraint, data had to be corrected to reflect the refractive index of water. The computer moved the laser in a sweep in the y direction collecting data every 2 mm at a specific x location. On completion, the computer would move the laser 4 mm in the x direction to conduct another y sweep. This continued for the desired range of data. If a complete range of data were taken, a 3-dimensional map could be constructed.

Data were collected at a rate of 500 points per second. This allowed a profile to be constructed every 2 msec. Each data point represents the average over 20 cardiac cycles.

2.4.4 LDA Data Reduction

The two velocity components measured by the LDA system are perpendicular to each other and make $\pm 45°$ angles to the axial direction. Figure 2-7 shows the orientation of the velocity components within the ventricle. The u component is oriented towards the aortic valve and the v component is 90° from u. U represents

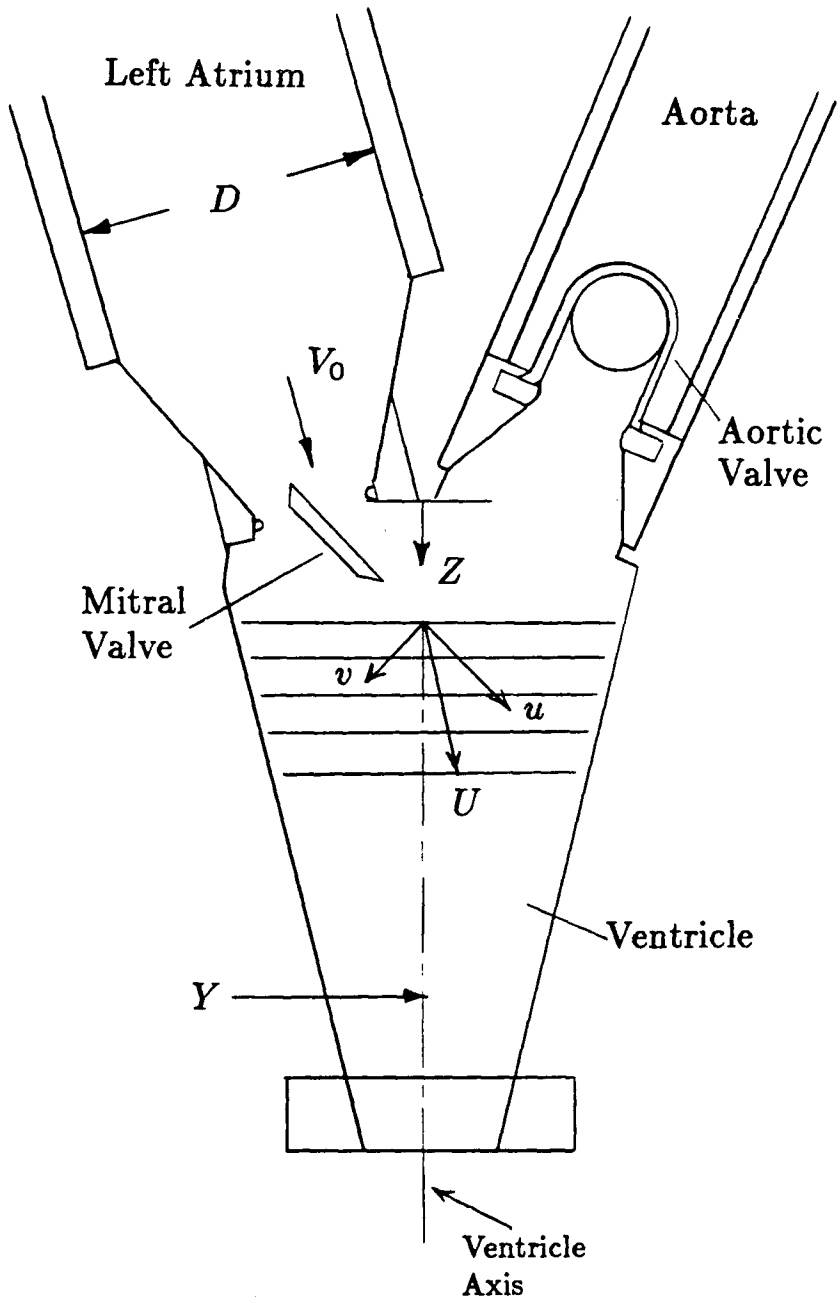

Figure 2-7 Orientation and definition of velocity components within the ventricle.

the resultant of u and v.

The instantaneous velocity $U(t)$ can be decomposed into a mean flow component $\overline{U}(t)$ and a fluctuating component $U'(t)$ such that

$$U(t) = \overline{U}(t) + U'(t).$$

The approach taken for the calculation of the mean flow involves measurement of the instantaneous velocity following the clock signal. The instantaneous velocity signal is then smoothed using a forward averaging technique involving nine neighbouring points. The process is repeated 10 times to provide an equivalent cut-off frequency of 25 Hz. This was sufficient to obtain a reasonable picture of the turbulence present. Since data were collected at a speed of 500 points per second, the 9-point forward averaging utilized a time window of 16 msec. The fluctuating velocity component is then obtained by subtracting the forward averaged data from the instantaneous velocity.

For each cycle:

$$u'(t) = u(t) - \overline{u}(t);$$

$$v'(t) = v(t) - \overline{v}(t);$$

where

$$U(t) = iu(t) + jv(t).$$

At each measuring point, a total of at least 20 measuring periods were averaged to obtain the final result for the Reynolds and normal stresses. The results now constitute the stresses over the time-averaged cycle as indicated below:

$$< \tau_{RN}(t) >= -\frac{\rho}{N}\sum_{c=1}^{N}[u'(t)v'(t)];$$

$$< \tau_u(t) >= \frac{\rho}{N} \sum_{c=1}^{N} u'(t)^2;$$

$$< \tau_v(t) >= \frac{\rho}{N} \sum_{c=1}^{N} v'(t)^2.$$

Where:

$<>$ = indicates average over N cycles;

N = number of cycles;

t = time or instant of measurement in each cycle;

$U(t)$ = instantaneous velocity;

$u'(t), v'(t)$ = fluctuating velocity components;

$\overline{u}(t), \overline{v}(t)$ = 9-point forward averaged mean velocity components;

The turbulence intensity, also a useful quantity, is proportional to the square root of the normal stresses. However, when presenting nondimensional results, the normal stress plot is better for displaying differences.

For velocity plots:

$$< u(t) >= \frac{1}{N} \sum_{c=1}^{N} u(t);$$

$$< v(t) >= \frac{1}{N} \sum_{c=1}^{N} v(t);$$

where:

$< u(t) >, < v(t) >$ = phase averaged velocity components (average over N cycles).

3. RESULTS AND DISCUSSION: STEADY STATE EXPERIMENTS

The purpose of steady state experiments is to help in the understanding of fluid dynamic characteristics of prosthetic heart valves under the fully open condition. These experiments are particularly useful during the developmental stages of a prosthesis as an indication of acceptability. However, the results correspond to only one phase of the cardiac cycle and hence should not be interpreted as revealing the overall valve performance. Since only one flow condition is simulated for steady state (fully open), results are time independent. In clinical situations, this would not be the case as flow conditions are time dependent.

Typically, the fluid flow in the ventricle passes through 3 distinct phases during each cardiac cycle: acceleration, peak, and deceleration. Whereas, steady state experiments may model the peak flow condition, they do not reveal information about the accelerating and decelerating phases of the heart cycle. For instance, tilting disc valves experience their highest stresses during the accelerating phase (Chapter 4), something steady state experiments cannot predict.

With an understanding of the limitations of the steady state experiments, the purpose of Chapter 3 is threefold. First, to study the effect of valve orientation on the heart chamber flow fields that develop when mechanical protheses are implanted. Second, to introduce results obtained for tissue protheses. And finally, to present the data for the steady state experiments to permit correlating these results to those obtained in Chapter 4 during the pulsatile flow simulation (for peak flow conditions).

In the accompanying figures, the velocity and stress profiles are nondimension-

alized using the annulus velocity V_0 (see Appendix II for values). These values are plotted against the nondimensionalized radial distance. This distance is calculated by dividing the radial distance (measured from the central axis of the ventricle) by the radial distance at $Z = 0.4D$.

In each figure, the nondimensionalized velocity is represented by solid lines, the Reynolds stress by crosses and the turbulent normal stresses by dotted lines. Turbulent normal stresses are shown rather than turbulent intensity because, in nondimensional form, the peaks and troughs are more visible. Recall that turbulent intensity is proportional to the square root of the normal stress. Each figure is accompanied by a schematic diagram which indicates the valve under study and its orientation.

Measurements were carried out at five downstream locations as defined in Chapter 2.

3.1 Mechanical Valves

Since the inlet condition at the mitral orifice created by the tilting disc prosthesis is asymmetric, steady state experiments are useful to determine the different type of flow patterns created when the valve orientation or disc opening angle are varied.

The flow patterns, a particular tilting disc valve develops, depend upon the alignment of the major and minor orifices relative to the ventricle. As the valve's disc does not open completely (i.e. the opening angle of the disc is less than 90°), the flow is deflected away from the perpendicular. The direction of these fluid flow jets therefore depend upon the orientation of the valve. The major and minor orifices create major and minor flows, respectively. The interaction of these flows with the geometry of the ventricle create different flow patterns - and as a result

different stress and velocity profiles. These profiles are analyzed for the two basic (opposite) configurations: first, the major orifice oriented anteriorly or facing the aortic valve (anterior orientation) and second, the major orifice oriented posteriorly or facing away from the aortic valve (posterior orientation).

The disc opening angle is also studied. The opening angles are a function of the valve design and cannot be altered. In effect, this analysis is a comparison between the three tilting disc valves. The Björk-Shiley c-c valve opens to 60°, the Björk-Shiley monostrut valve has an opening angle of 70° and the Bicer-Val valve opens the furthest – to 75°.

Figure 3-1 shows the velocity profiles for the anterior and posterior orientations of the B-S c-c prosthesis. Flow development is clearly different for the two orientations. In the anterior orientation, the flow field downstream is rather complex. The majority of fluid is directed to the opposite side of the ventricle and a separation region is created behind the disc. As the fluid strikes the ventricle wall, part of the flow is directed upward to form a counterclockwise vortex. Signs of this can be seen at the 0.4D station. However, the majority of the flow forms a clockwise vortex. The posterior orientation, on the other hand, appears to promote the formation of a single vortex. Flow through the valve strikes the near wall and is directed downstream towards the apex at which time it directed up the other side of the ventricle.

The complex interaction between the two counter-rotating vortices, seen with the anterior orientation, may result in higher stresses than for the posterior configuration.

Figures 3-2 and 3-3 show the velocity plots with the normal and Reynolds stresses added. For both configurations, high stresses are detected in the peak flow re-

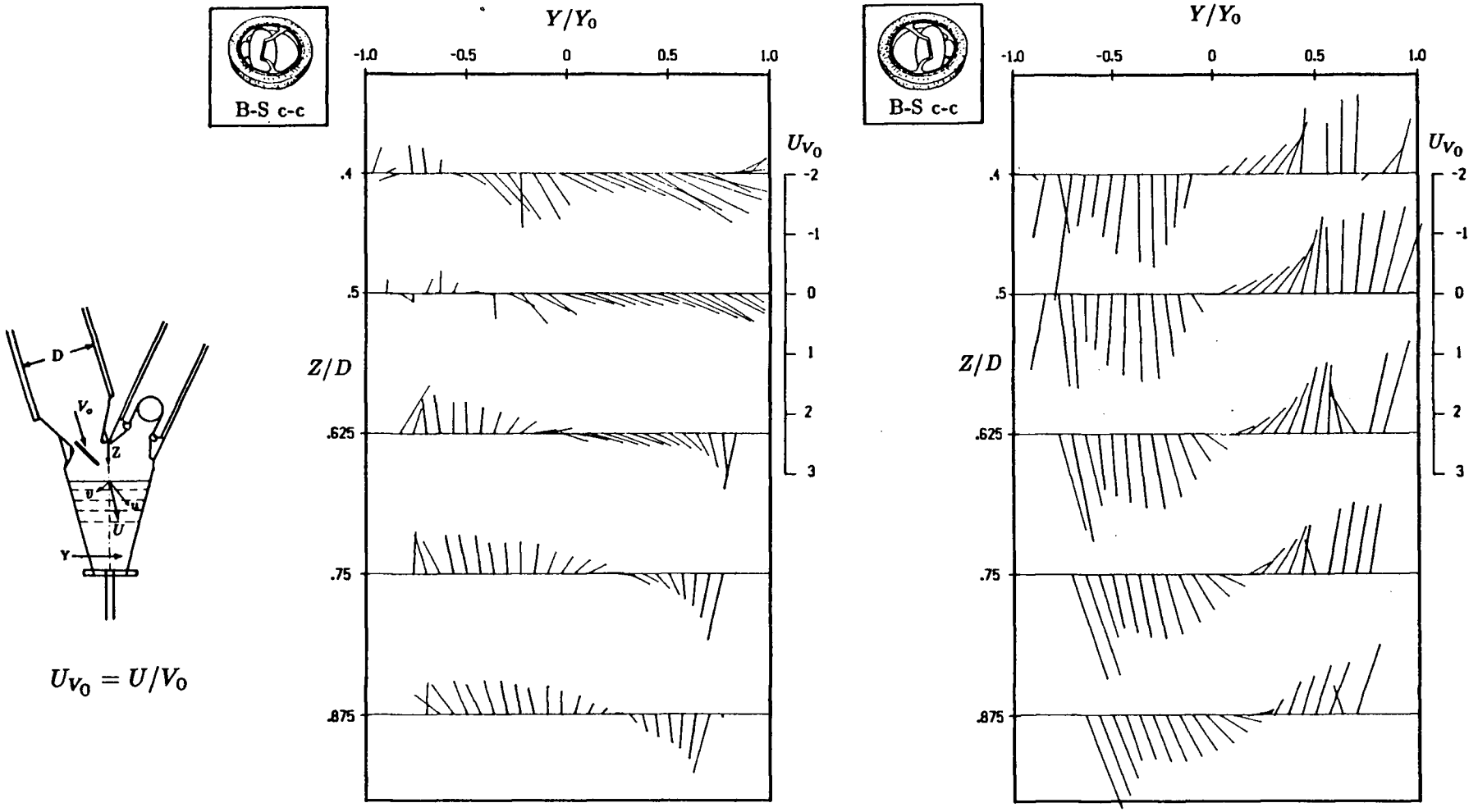

Figure 3-1 Nondimensional velocity profiles of the Björk-Shiley c-c prosthesis showing differences in the flow patterns between the anterior and posterior orientations for the steady state case.

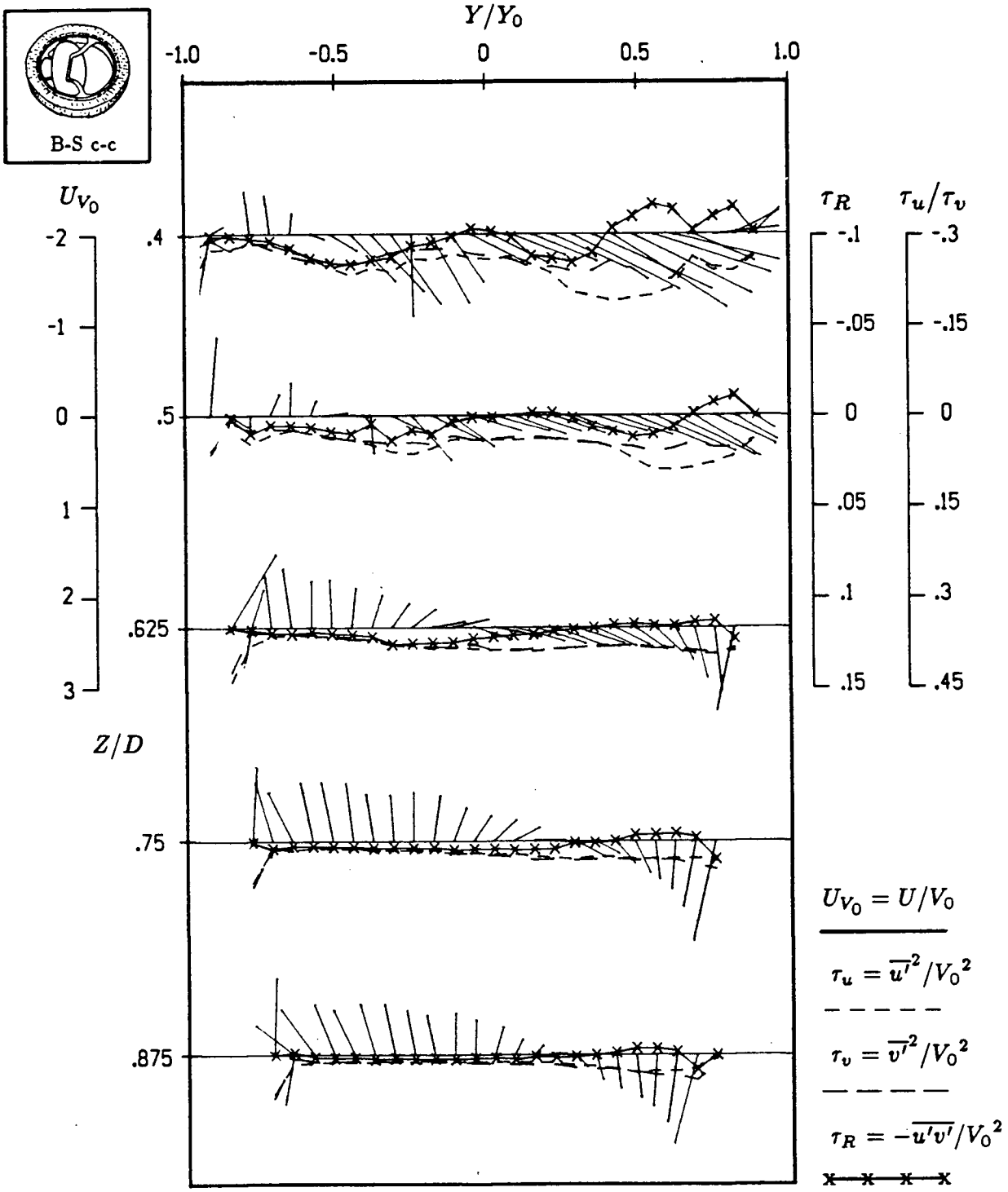

Figure 3-2 Steady state nondimensional velocity, Reynolds stress and normal stresses at five downstream stations for the anterior orientation of the B-S c-c prosthesis.

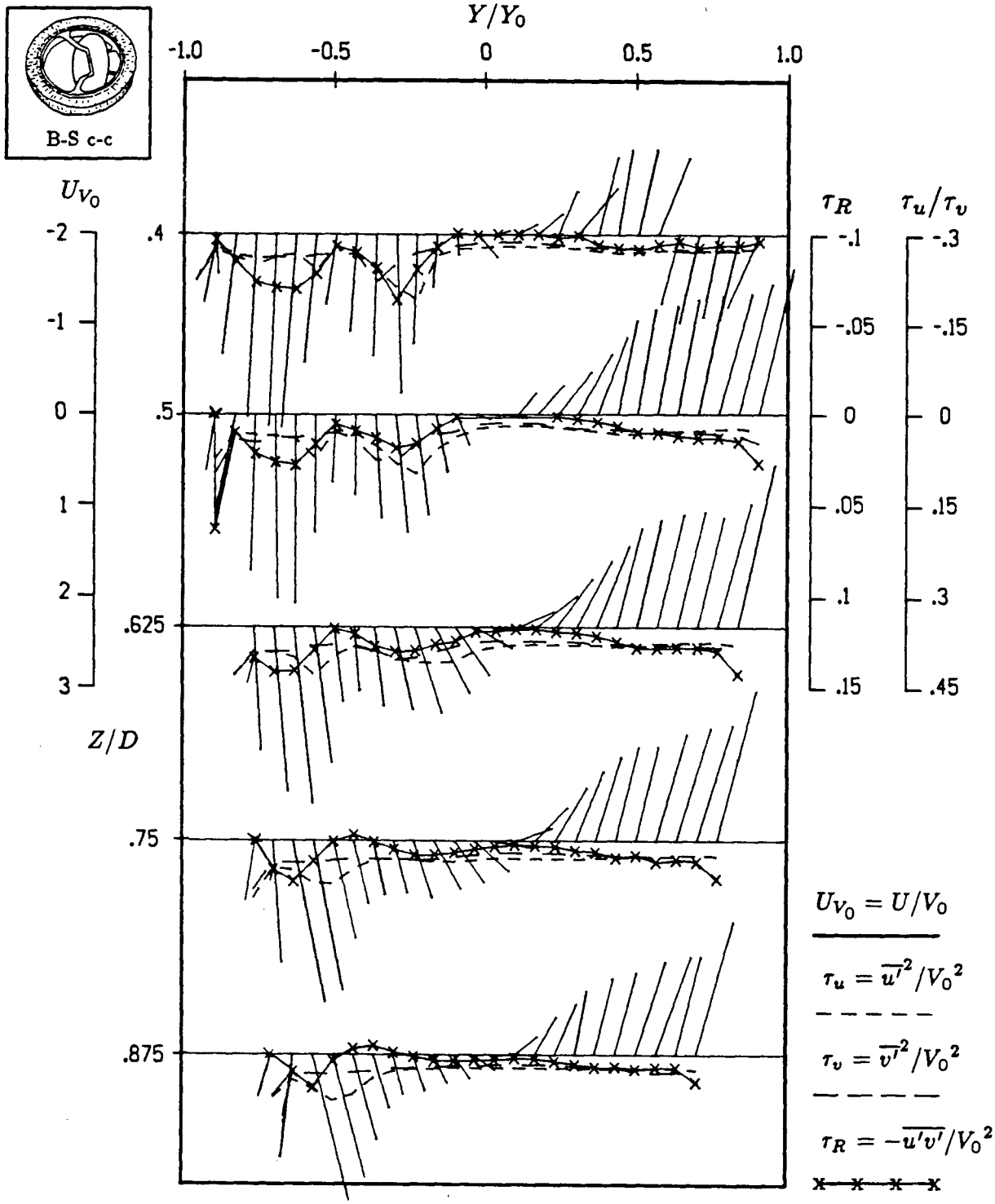

Figure 3-3 Steady state nondimensional velocity, Reynolds stress and normal stresses at five downstream stations for the posterior orientation of the B-S c-c prosthesis.

gion. The normal stresses are higher for the posterior orientation and the Reynolds stresses are higher for the anterior orientation. Elevated stresses are detected further downstream with the posterior configuration. This is due to the more pronounced jet formation, which penetrates further into the ventricle.

The flow pattern characteristics exhibited by the B-S c-c valve are typical to those found in the B-S mono and Bicer valves. The main differences between each valve's flow pattern can be attributed to each valve's opening angle. Figure 3-4 shows the effect of the disc opening a further 10 degrees (B-S mono prosthesis - anterior orientation). The jet through the major orifice is directed further into the ventricle, as the disc opening angle has increased. Large stresses are still apparent at 0.4D and 0.5D with a reduction further downstream.

When orienting the B-S mono valve into the posterior position, the flows through the two orifices are less distinct. As a result, the velocity gradients across the jet are lower than those exhibited by the B-S c-c valve. The resulting stresses are therefore also lower as can be seen in Figure 3-5. However, when comparing the stresses for the two orientations of this valve, two opposite behaviours are exhibited: at points closer to the valve, the stresses in the posterior position are lower while further downstream the stresses are greater than those in the anterior orientation. This may be due to the different vortex formations.

The tendencies developed by opening the disc further for the B-S valves continue for the Bicer valve as shown in Figures 3-6 and 3-7. By further increasing the opening angle by 5°, the flow through the two orifices is no longer distinct, and instead is represented by a single jet. The more aerodynamic shape of the disc as well as the design of the strut structure may account for the lower stresses this valve forms. The manufacturer claims the valve was designed to create laminar flow fields

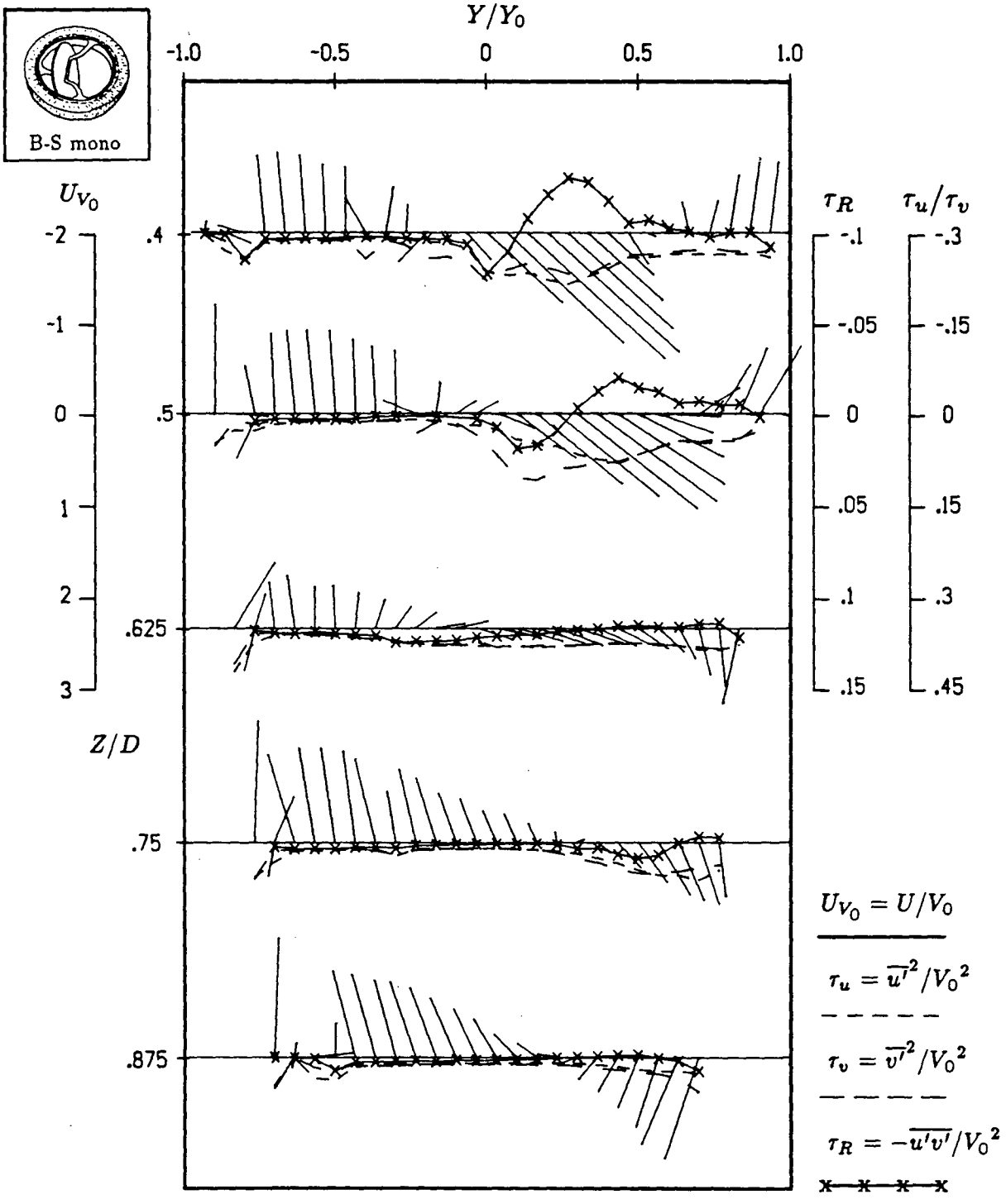

Figure 3-4 Steady state nondimensional velocity, Reynolds stress and normal stresses at five downstream stations for the anterior orientation of the B-S monostrut prosthesis.

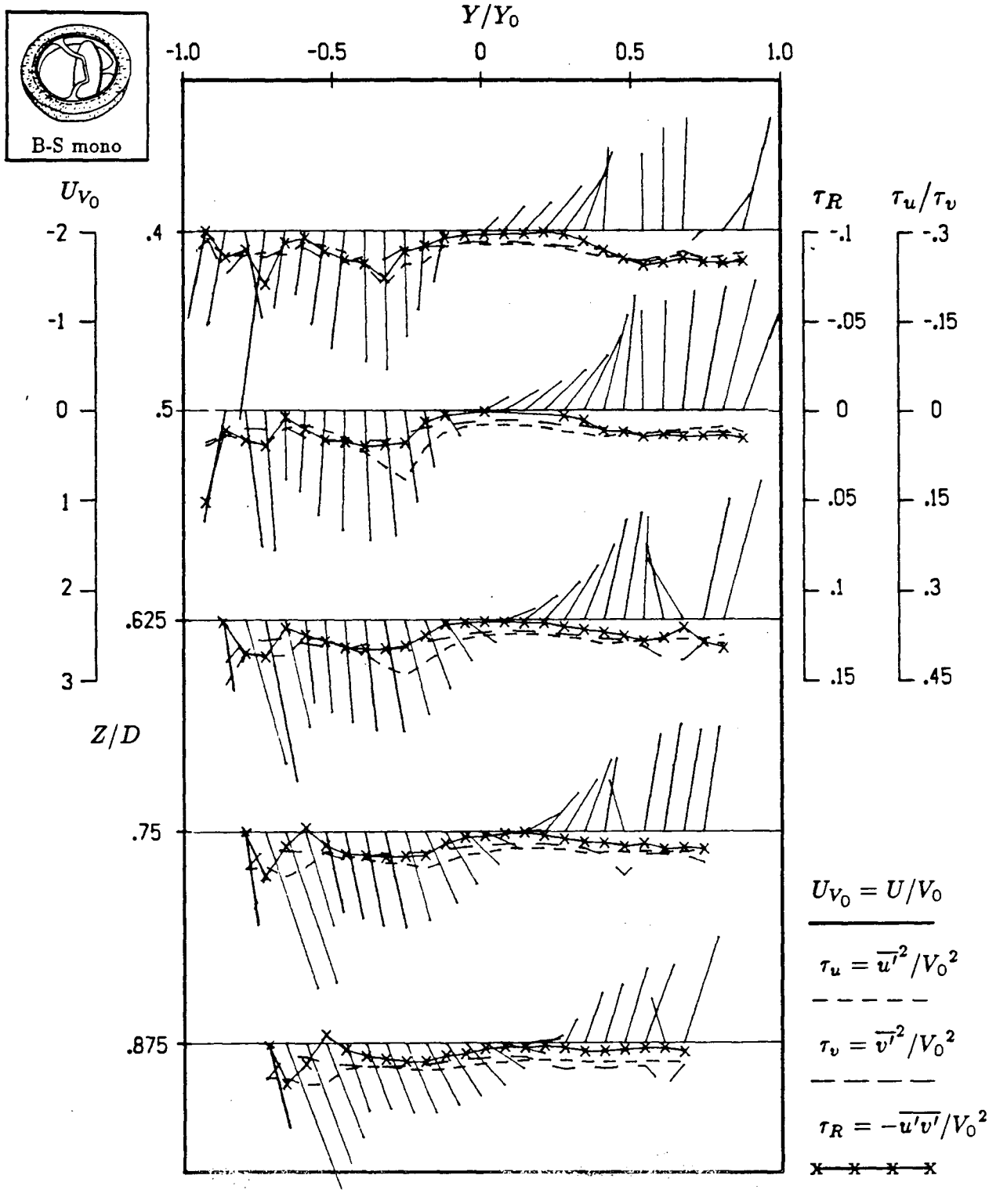

Figure 3-5 Steady state nondimensional velocity, Reynolds stress and normal stresses at five downstream stations for the posterior orientation of the B-S monostrut prosthesis.

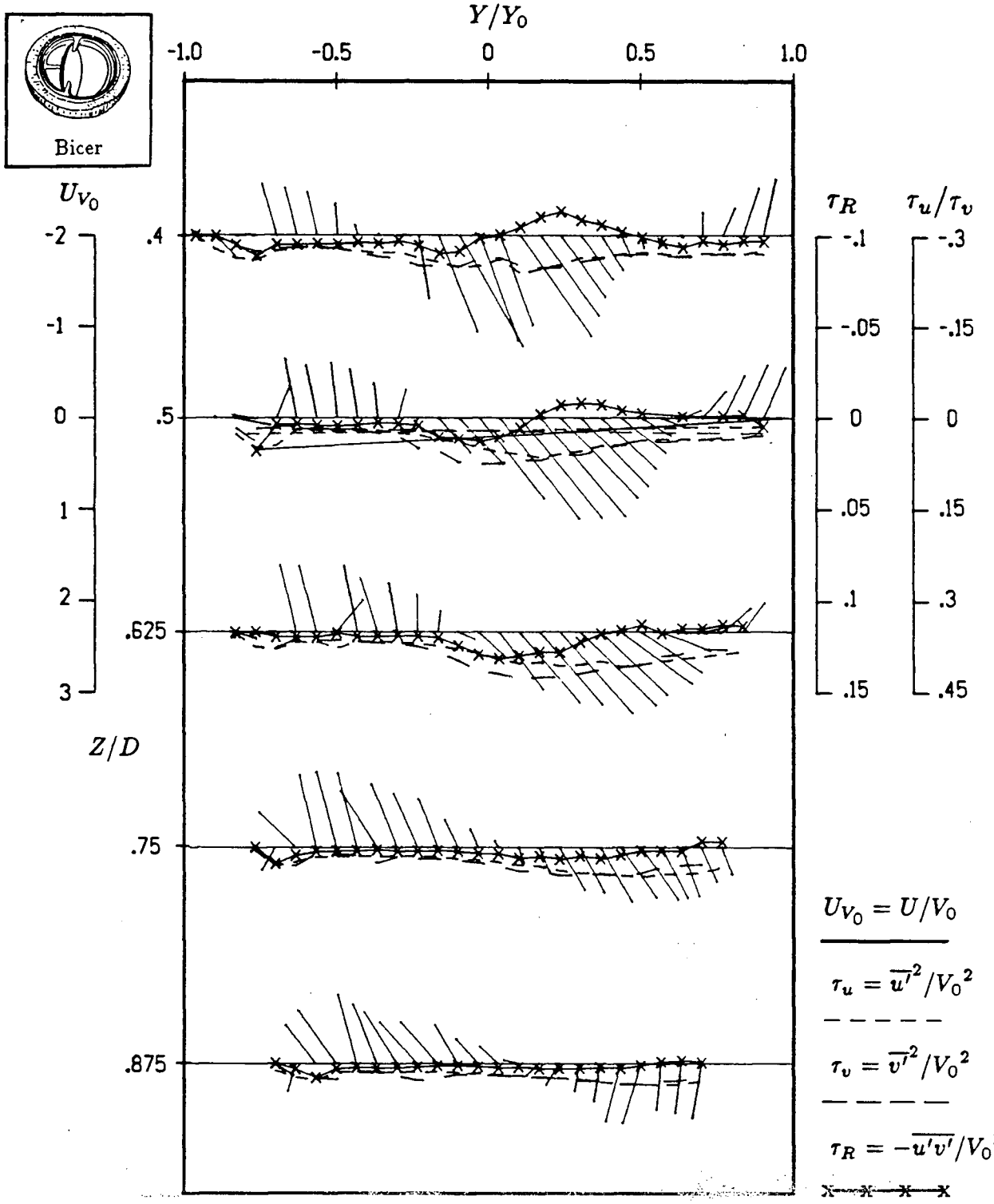

Figure 3-6 Steady state nondimensional velocity, Reynolds stress and normal stresses at five downstream stations for the anterior orientation of the Bicer-Val prosthesis.

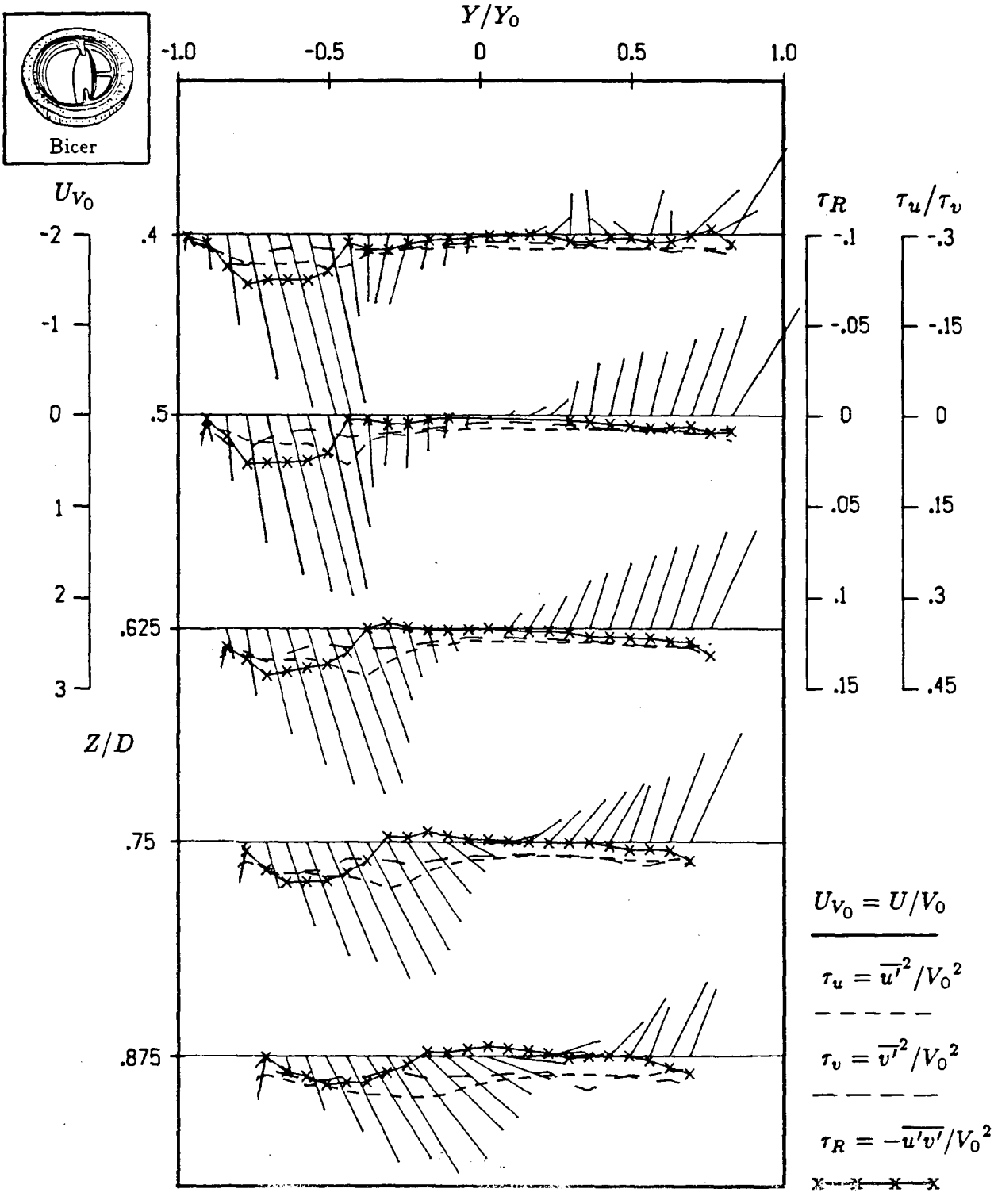

Figure 3-7 Steady state nondimensional velocity, Reynolds stress and normal stresses at five downstream stations for the posterior orientation of the Bicer-Val prosthesis.

where separation is minimized[66].

3.2 Biological Tissue Valves

The two prostheses chosen for this study are the Hancock II and Carpentier-Edwards supraannular. These two valves represent two of the newer generation biological tissue valves. The tests conducted on these protheses did not include orientation experiments, as this was the first time biological valves were used at this facility. The results obtained are presented here for completeness only.

Figure 3-8 shows the results obtained for the Hancock II prothesis. This valve produced a high-velocity, narrow jet-like flow down the axis of the ventricle. The flow reverses its direction at the apex of the ventricle and appears to flow upward along the wall toward the aortic orifice. The sharp velocity spike in the centre of the flow that is found at 0.4D quickly dissipates as the flow continues downstream. This spike may be explained by the greater frictional losses that the fluid experiences as it passes through the mitral orifice. The surface area to which the fluid is exposed is substantially greater for a biological valve (where the orifice forms a tube-like structure) than for a mechanical valve (where only the ring and disc impede the flow). As expected, the highest stresses (Reynolds and normal) were confined to a narrow region at the edge of the jet.

The results for the Carpentier-Edwards supraannular prothesis can be found on Figure 3-9. This valve's flow field is, unlike the Hancock II, deflected more towards the aortic side of the ventricle. This may in part be explained by the observed fibrillation of the leaflets. Also, unlike the Hancock valve, the jet formation is not nearly as pronounced at the locations near the valve and dissipates to a much greater extent downstream. This explains why the stresses are of a lower magnitude, especially further downstream. Only at 0.4D do the stresses formed

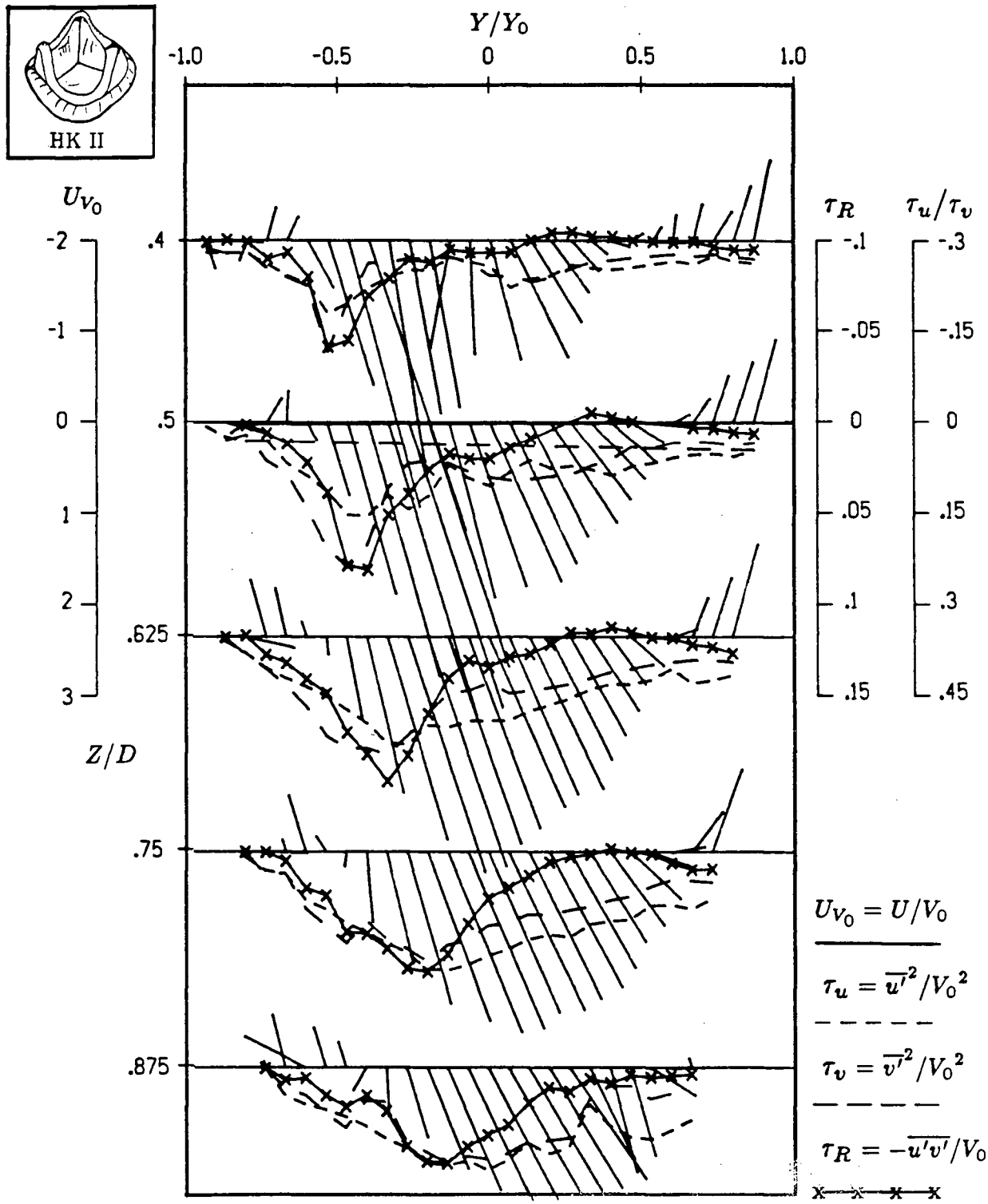

Figure 3-8 Steady state nondimensional velocity, Reynolds stress and normal stresses at five downstream stations for the anterior orientation of the Hancock II prosthesis.

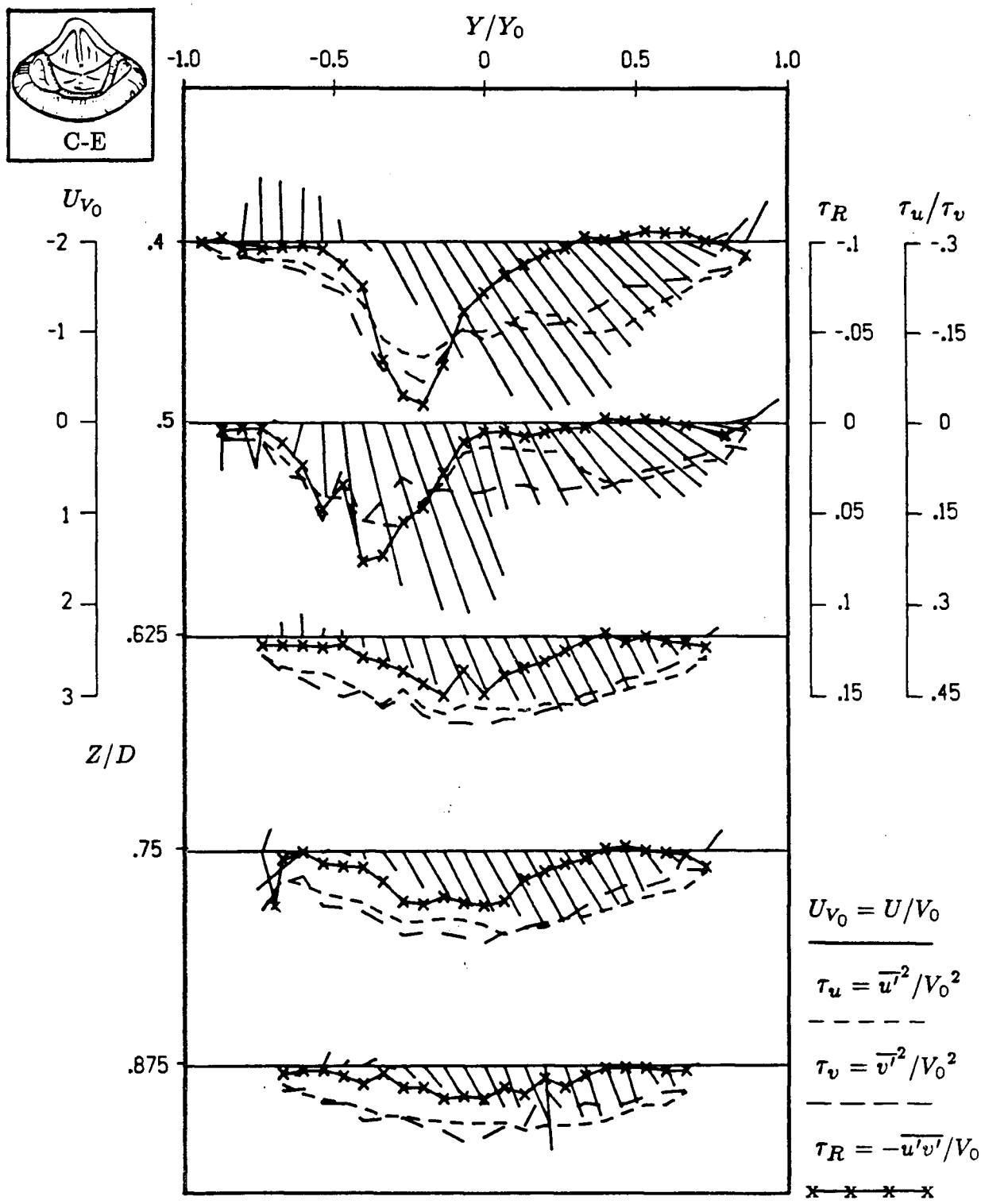

Figure 3-9 Steady state nondimensional velocity, Reynolds stress and normal stresses at five downstream stations for the posterior orientation of the Carpentier-Edwards Supraannular prosthesis.

by the Carpentier-Edwards rival those of the Hancock II. Predictably the stress maximums were again located along the edge of the jet formation.

As mentioned at the beginning of this chapter, steady state experiments are useful for comparing some of the different characteristics, such as orientation and opening angle, of various valves . In Chapter 4, it will be shown that the steady state results, stresses in particular, corrolate poorly with those observed for peak flow under unsteady conditions. However, the basic traits observed under steady state are valid. That is, the basic flow patterns (velocity profiles) due to valve orientation and disc opening angle can again be recognized in the pulsatile experiments.

4. RESULTS AND DISCUSSION: PULSATILE FLOW EXPERIMENTS

The pulsatile or unsteady state experiments aim at conducting realistic tests of prosthetic heart valves to assess their hemodynamic performance. Since in vivo clinical comparison of prosthetic valves is difficult to obtain, due to the difficulty of monitoring them in a living body, in vitro fluid dynamic investigations are essential. However, for the results to be of practical significance, in vitro experiments must accurately simulate the cardiovascular system. Even with complicated and sophisticated models, results can only be an approximation of the biological counterpart.

The purpose of this study is to determine influence of the mitral prosthetic heart valves on the downstream flow field in the left ventricle. For the tilting disc prostheses, this primarily involved looking at the effects due to the opening angle (60°, 70° and 75°) and the valve orientation (anterior or posterior). For the biological prostheses, effect of the valve geometry (similar to a natural tricuspid valve) on the flow field was the focus.

This chapter is divided into five sections. The first section presents results for the individual mechanical valves. This is followed in the second section with a comparative performance analysis performance of thes three mechanical valves. Similarly, the two biological valves are covered in sections three and four. Finally, section five discusses relative performance of the mechanical and tissue heart valve prostheses.

The test results are presented in the nondimensional form. Although this practice is quite routine in engineering, it is relatively new in this branch of medical science and has only recently found acceptance. Now the experiments need only be conducted at a single cardiac output (condition of rest for this study) due to

independence of the nondimensionalized parameters. The annulus diameter and velocity (V_0) at the annulus are used to this end. Values are given in Appendix 1.

The amount of information obtained through monitoring of important fluid dynamic parameters, spatially as well as temporally, is rather enormous. Furthermore, it is important to assess spatial distribution of the important parameters simultaneously at a given instant, and over the entire cardiac cycle, to appreciate the system behaviour. Hence concise yet meaningful procedures for presentation of results, helpful in establishing trends, presents a challenging task. The format adopted here was arrived at after considerable thought and serves the purpose quite well in the present situation.

4.1 Mechanical Valves

The Bjork-Shiley c-c (B-S c-c) valve serves as a reference to compare the newer generation models, the Bjork-Shiley monostrut and the Bicer Val. Hence, the B-S c-c is discussed first followed by the B-S mono and Bicer. For each valve, results for the anterior orientation are presented first followed by those for the posterior orientation and then a comparison of their relative performance.

4.1.1 Björk-Shiley Convexo-Concave (B-S c-c)

(a) Anterior Orientation

Figure 4-1 shows the time history of four nondimensional fluid dynamic parameters at station 0.4D. The period covers from just before the mitral valve opens until after the mitral valve closes and the aortic valve opens. The plots show how the velocity and stress fields change over an entire cardiac cycle at a given station in the ventricle.

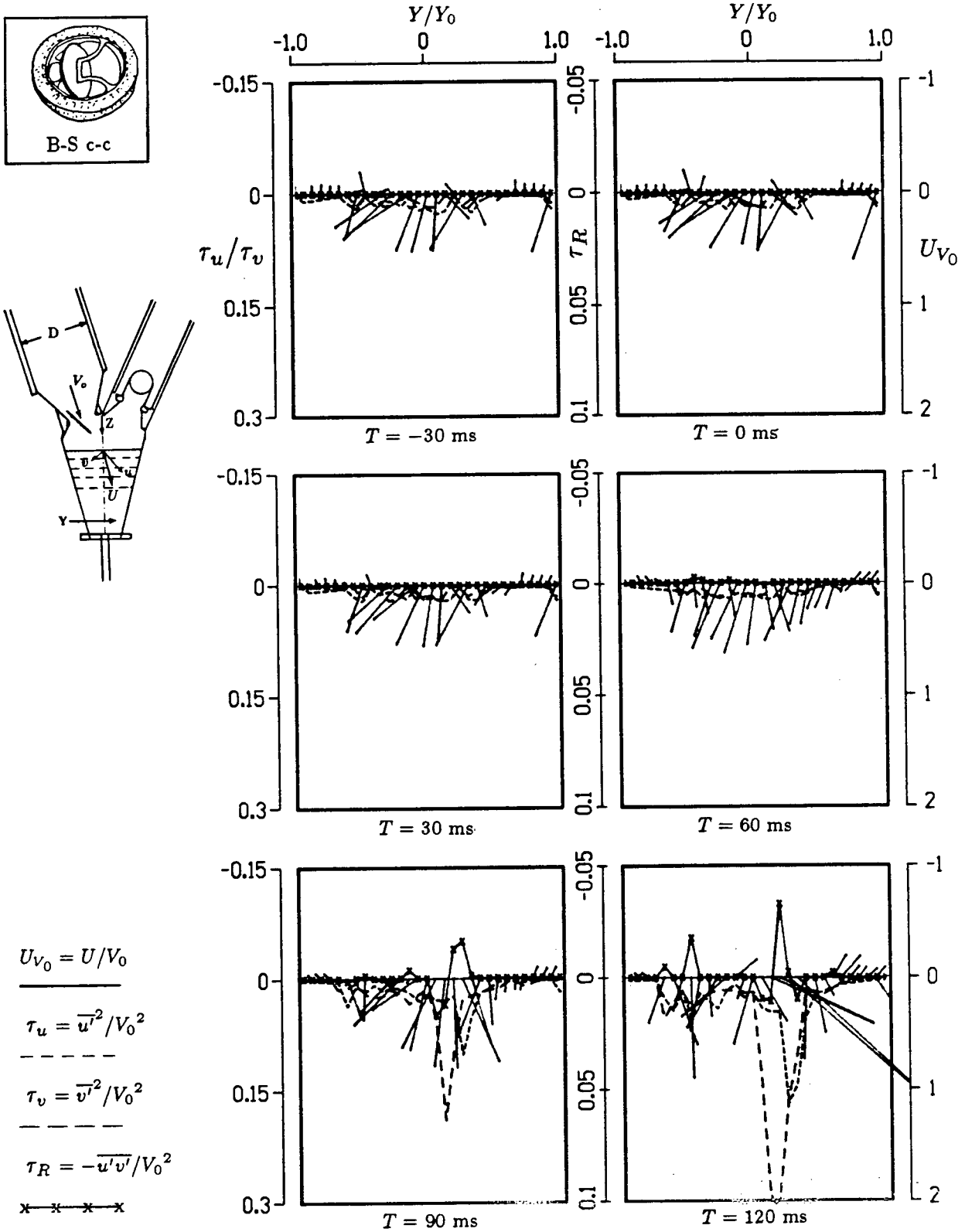

Figure 4-1 Time history of velocity and stress profiles for the Björk-Shiley c-c prosthesis in the anterior orientation at Z = 0.4D (-30 - 120 ms).

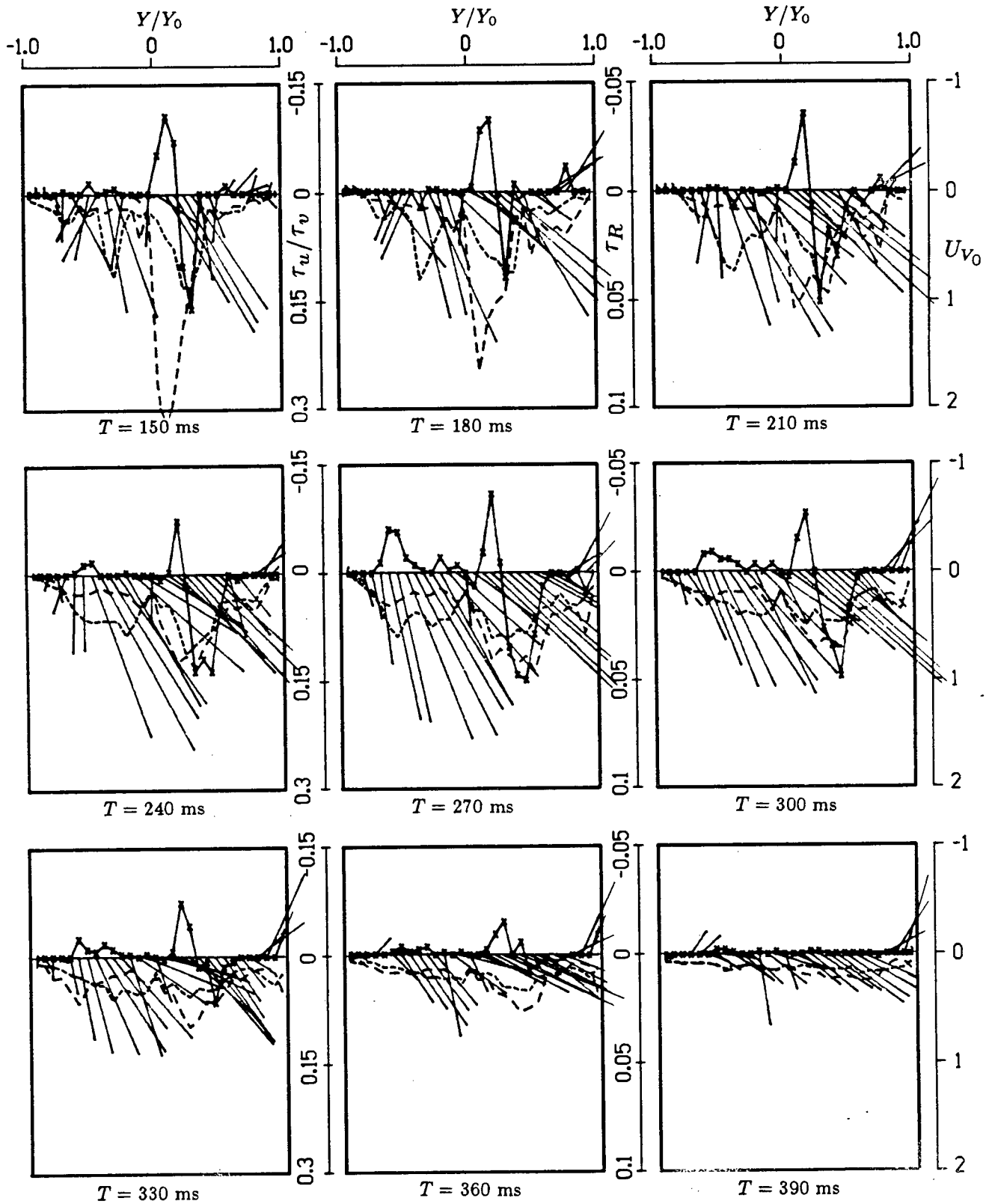

Figure 4-1 Time history of velocity and stress profiles for the Björk-Shiley c-c prosthesis in the anterior orientation at Z = 0.4D (150 - 390 ms).

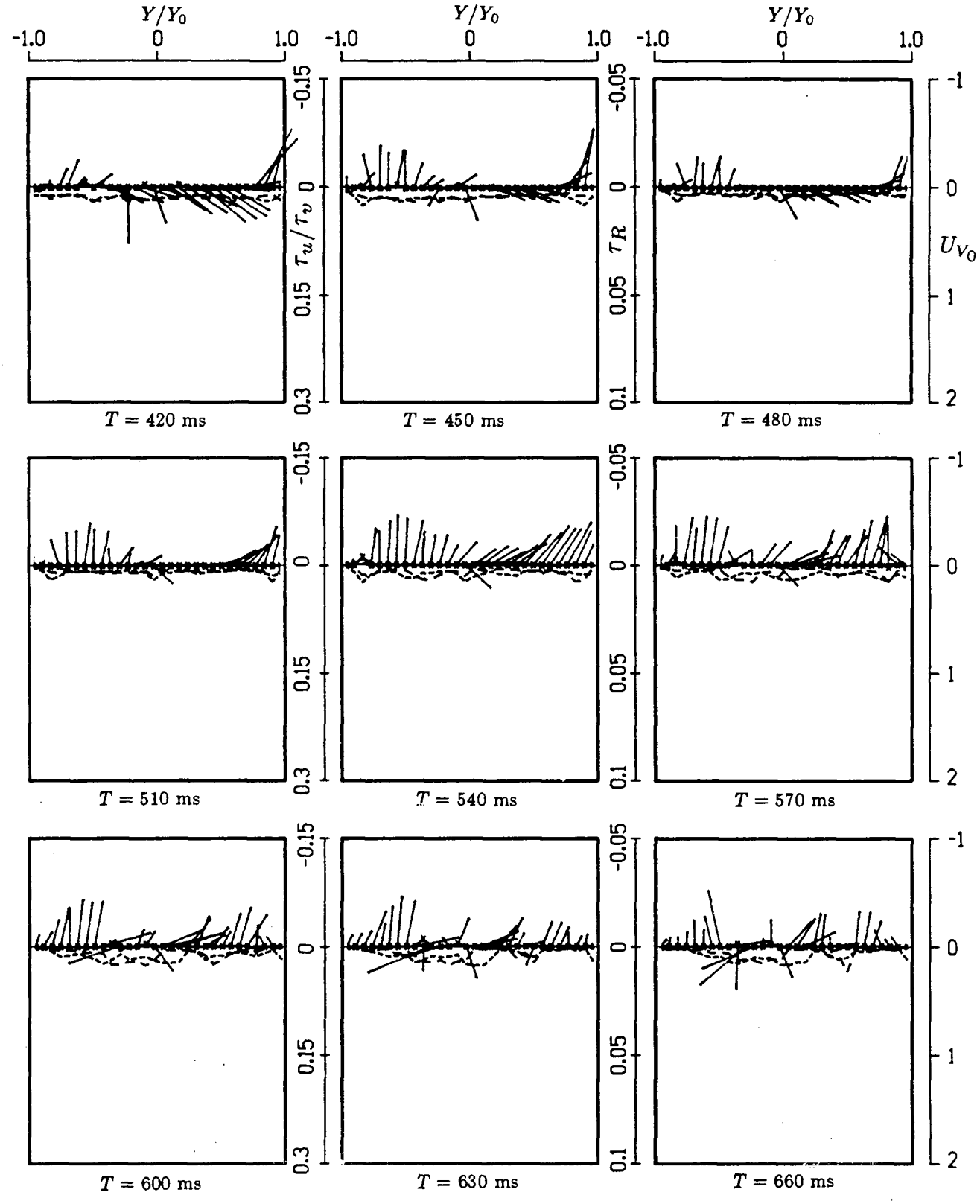

Figure 4-1 Time history of velocity and stress profiles for the Björk-Shiley c-c prosthesis in the anterior orientation at Z = 0.4D (420 - 660 ms).

There are two drawings accompanying the time history plot. The first is a schematic diagram identifying the valve as well as its orientation, and the second drawing shows the location (station) of measurements. It also shows several parameters such as D, V_0, U, u, v, etc.

At the early stage of diastole (0 - 60 msec), the flow field is primarily governed by the expansion of the ventricle. Note, there is little stress activity associated with this phase. However, at the initiation of flow through the mitral valve (between 60 and 80 msec), there is a sudden increase in both the Reynolds and normal stresses. The delay between the initiation of the flow and its detection at 0.4D location is attributed to the distance separating the two stations. Continuing on through the cycle, large disturbances are evident throughout the acceleration-phase (90 - 200 msec) and into the peak-phase (240 - 270 msec). As the flow field develops, two high velocity jet-like structures, developing from the major and minor orifices, can be identified. This is a basic feature of the tilting disc valves, although character of the two jets is dependent on the shape and opening angle of the disc, as well as the orientation of the valve as will be seen with the B-S mono and Bicer valves.

The flow fields created by the two jets and their interactions are quite complex. However, it is logical to expect that by mid-diastole flow through the orifices turn back upon reaching the ventricle apex and forms two counter-rotating vortices which are sustained throughout the remainder of the phase. Figure 4-2 shows a schematic drawing to illustrate this flow pattern. The sketch was composed from collected data as well as visual observations. The disruption of the two vortices induces flow disturbances particularly noticeable in the centre of the chamber (T= 115 - 180 ms).

During deceleration, beginning around 300 ms, the stresses are significantly re-

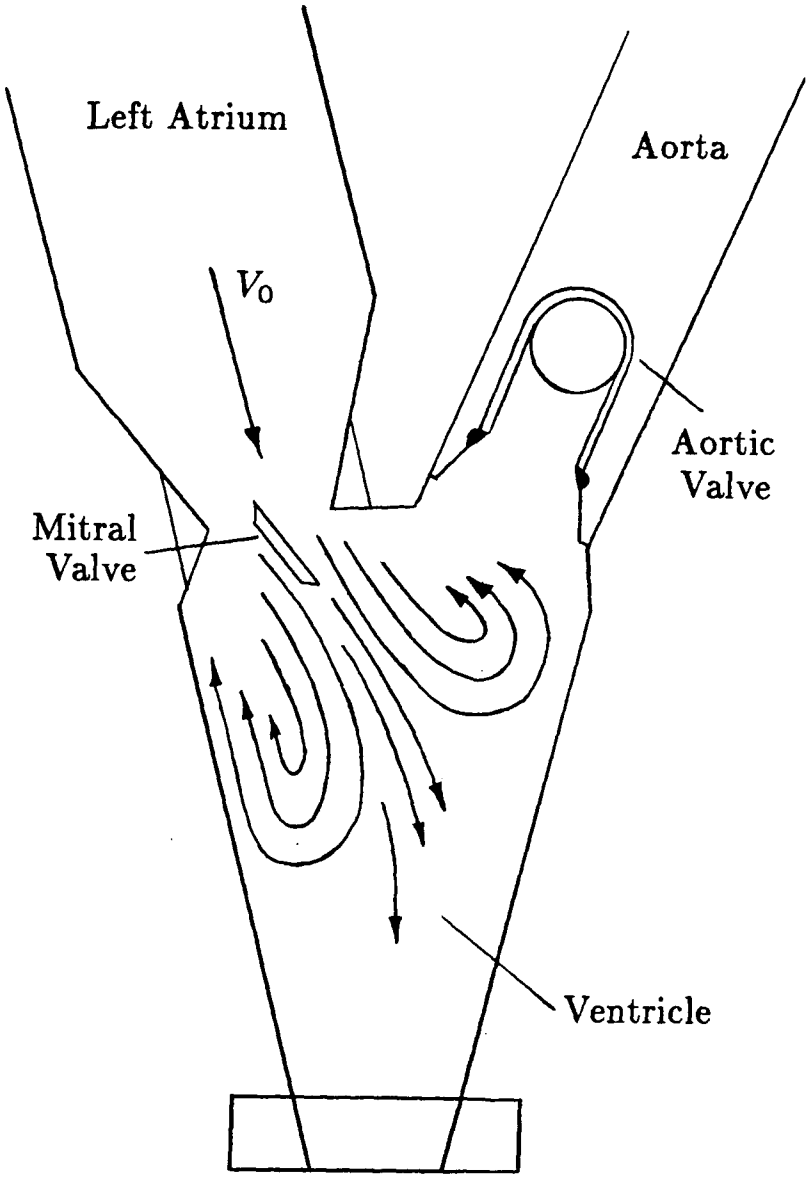

Figure 4-2 Schematic representation of the flow pattern in the left ventricle showing the two counter-rotating vortices formed for the anterior orientation of a tilting disc valve.

duced, and by the onset of systole (around 425 ms), the stresses drop to their lowest levels. Once the systolic cycle begins, flow is gradually directed towards the aortic valve.

This pattern was observed for all the three tilting disc valves in the anterior orientation. As the peak stresses of interest (i.e., high stresses that may promote thromboembolism or haemolysis) fell between the onset of diastole and the beginning of the deceleration phases, all future time history plots cover the period of 0 - 420 msec.

The following set of figures show changes in velocity and stresses downstream during the 3 distinct phases of accelerating, peak and decelerating flow. A schematic diagram of the valve is presented as before, as well as a figure showing the instance of measurement with respect to the mitral flow rate.

Figure 4-3 shows the early stage of diastole for the five downstream locations. Although the flow through the mitral valve has initiated, no flow pattern has been detected. The small positive flow seen at each downstream location is mainly due to the expansion of the ventricle walls at the onset of diastole.

Once the expected jet type of flow reaches the first measuring station (Figure 4-4), there is a sudden increase in the normal and Reynolds stresses. Figure 4-4 shows the initial increase in stresses at the 0.4D location. The disturbance can be seen to travel downstream as the flow continues to accelerate (Figure 4-5). The largest turbulent normal stress during the acceleration-phase was 1265 dynes/cm^2 (155 msec at 0.4D) while the highest Reynolds stress was 224 dynes/cm^2 (180 msec at 0.5D). Note that the highest stresses are located at the edges of the two jets.

As the flow accelerates towards the peak-phase, the velocity profile becomes more organized, resulting in reduction of the normal stresses. However, the Reynolds

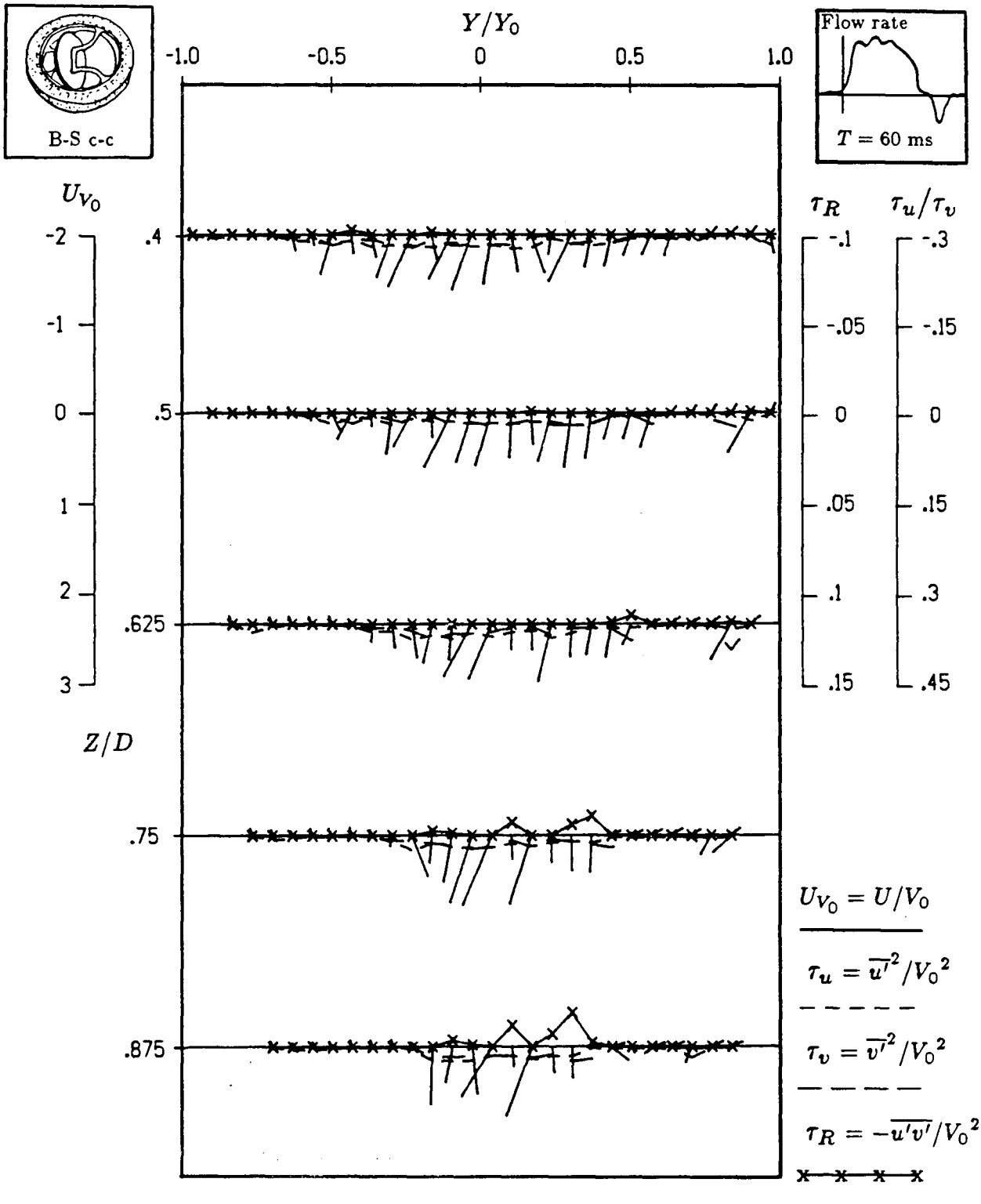

Figure 4-3 Variation of the nondimensional velocity, normal stresses, and the Reynolds stress at five downstream locations for the Björk-Shiley c-c prosthesis (27 mm) in the anterior orientation (T = 60 ms).

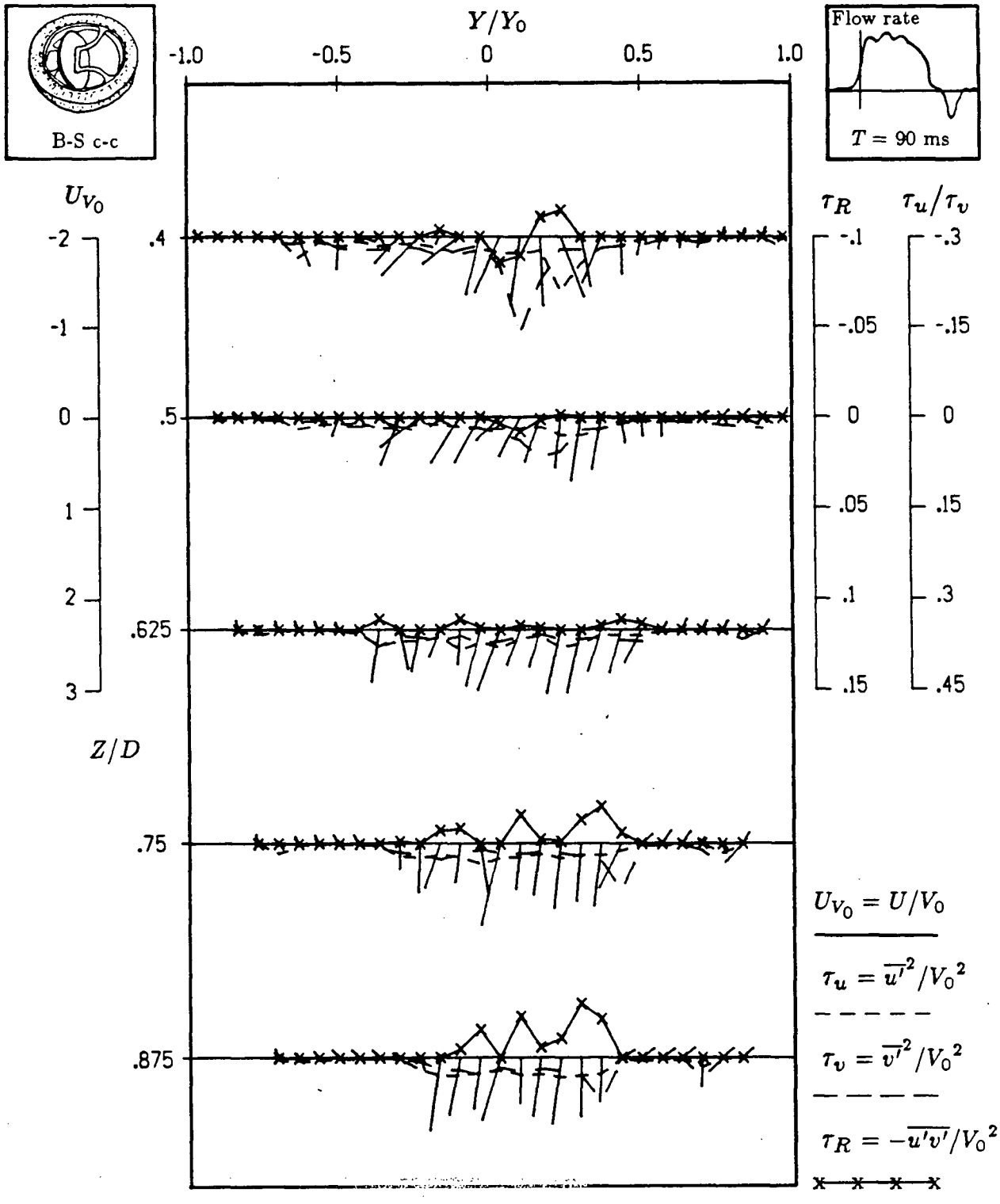

Figure 4-4 Variation of the nondimensional velocity, normal stresses, and the Reynolds stress at five downstream locations for the Björk-Shiley c-c prosthesis (27 mm) in the anterior orientation (T = 90 ms).

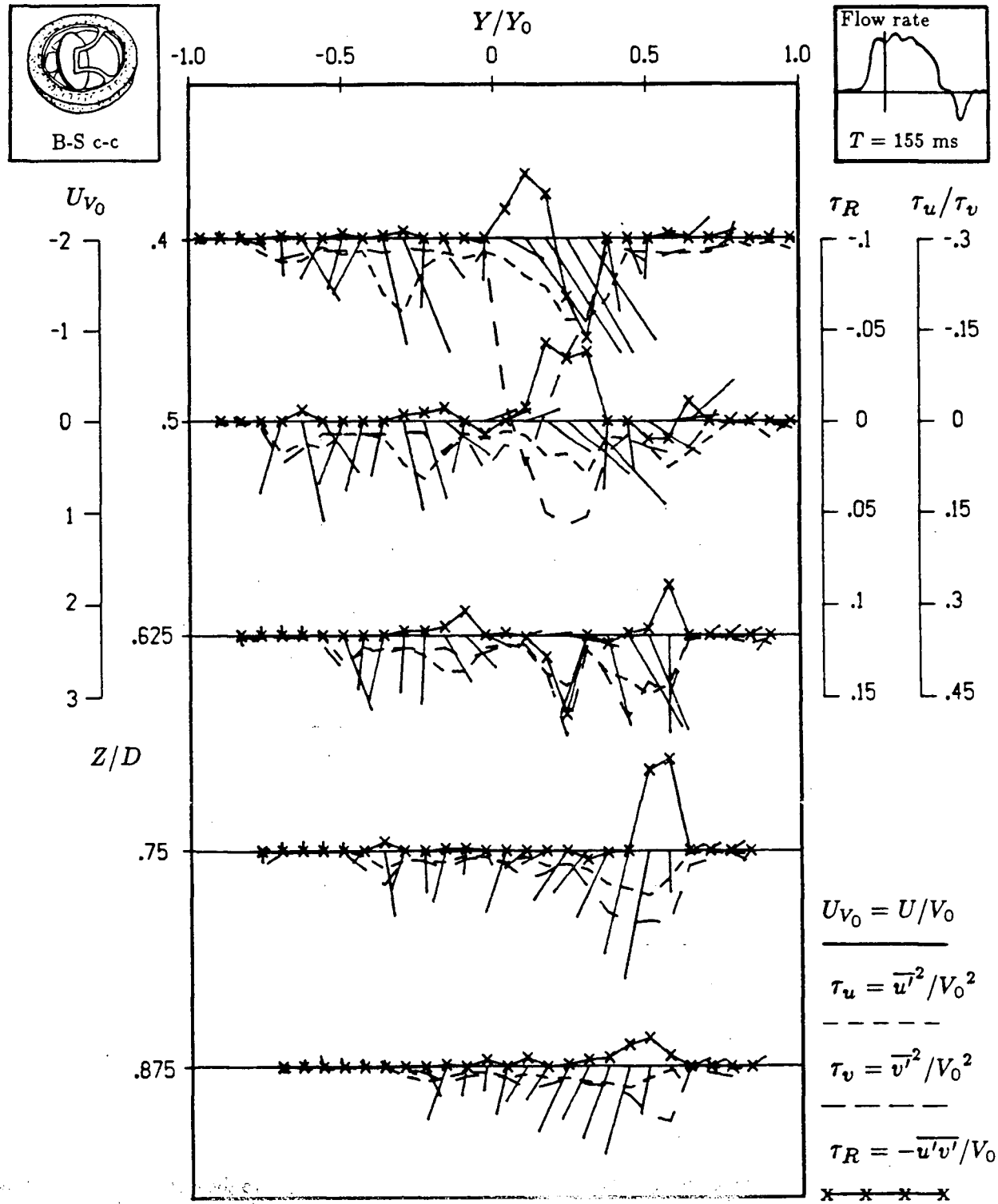

Figure 4-5 Variation of the nondimensional velocity, normal stresses, and the Reynolds stress at five downstream locations for the Björk-Shiley c-c prosthesis (27 mm) in the anterior orientation (T = 155 ms).

stress remains elevated through the peak flow phase (Figure 4-6). At the peak flow, the highest values of Reynolds and Normal stresses are 174 dynes/cm^2 (260 msec at 0.4D) and 605 dynes/cm^2 (255 msec at 0.5D), respectively, which are lower than those observed during the acceleration-phase.

It might be interesting at this point to recall Figure 3-2 (steady flow case) for comparison. There are definite similarities in the flow patterns. The main clockwise vortex is dominant in the ventricle for both the cases while the smaller counterclockwise vortex is slightly more noticeable in the unsteady phase. Note, in the steady case, the stresses are poorly predicted. Obviously, this is due to time independence of the steady state experiments. This clearly suggests the importance of simulation aimed at unsteady flows to obtain realistic results.

Getting back to the unsteady case, the deceleration-phase is characterized by a dramatic reduction in all the stresses (Figure 4-7). As well, a single vortex circulation pattern is formed and maintained until the mitral valve closes and the systole phase begins. On the onset of the systolic cycle, flow is gradually directed towards the aortic valve as seen in Figure 4-8.

To help establish periods of high stress level during diastole, the peak and peak average stresses for each of the three phases are compared in the following two diagrams. The peak stress is defined to be the highest stress measured over the time-averaged cycle (which is defined in Chapter 2) at each downstream location. The peak average stress, on the other hand, is defined to be the highest stress at each downstream location after the stresses, at each measuring point, are averaged over the entire time-averaged cycle. The boxed symbols represent the Reynolds stress and the open symbols the normal stress.

The peak normal and Reynolds stresses for the five downstream stations are

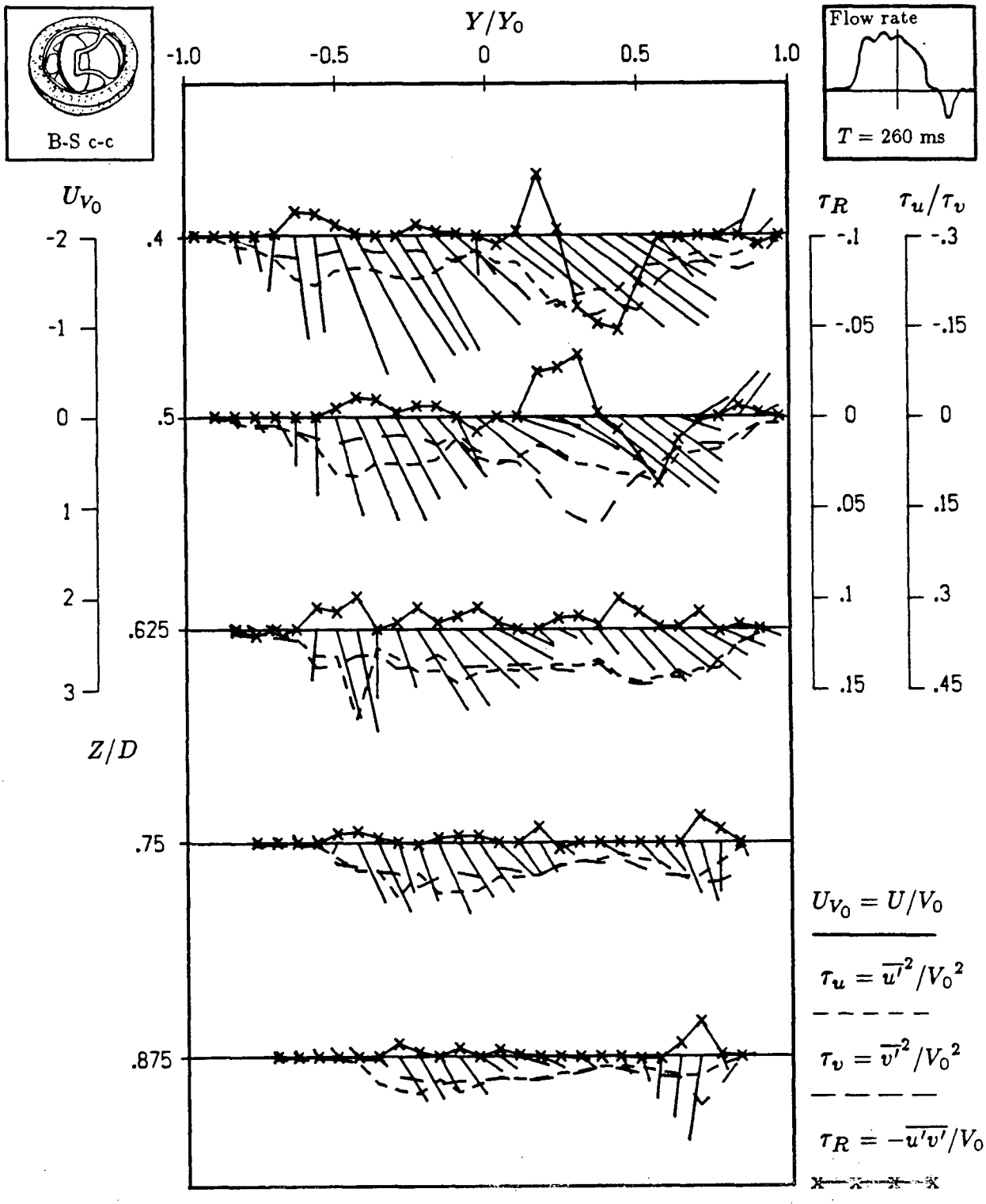

Figure 4-6 Variation of the nondimensional velocity, normal stresses, and the Reynolds stress at five downstream locations for the Björk-Shiley c-c prosthesis (27 mm) in the anterior orientation (T = 260 ms).

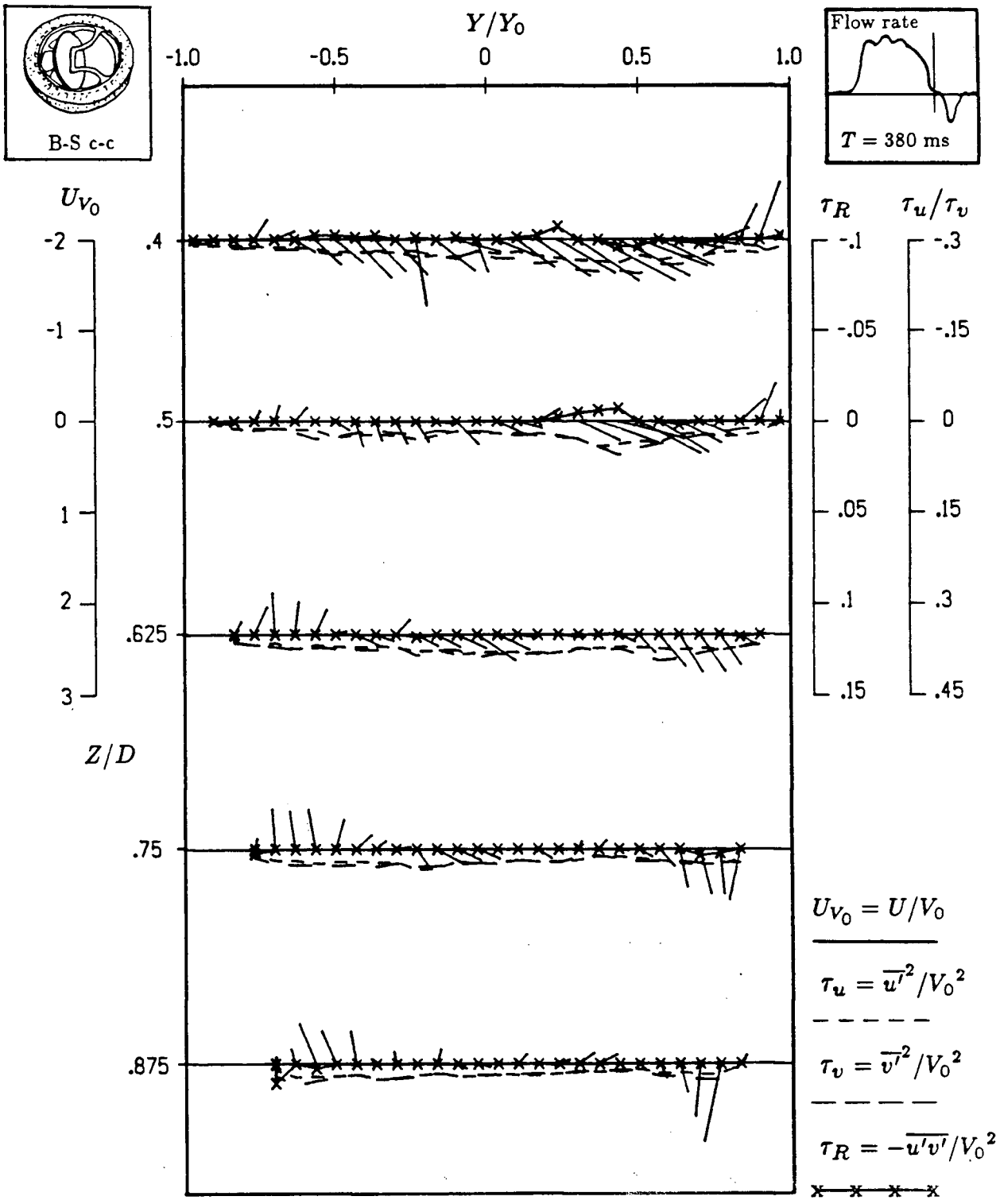

Figure 4-7 Variation of the nondimensional velocity, normal stresses, and the Reynolds stress at five downstream locations for the Björk-Shiley c-c prosthesis (27 mm) in the anterior orientation (T = 380 ms).

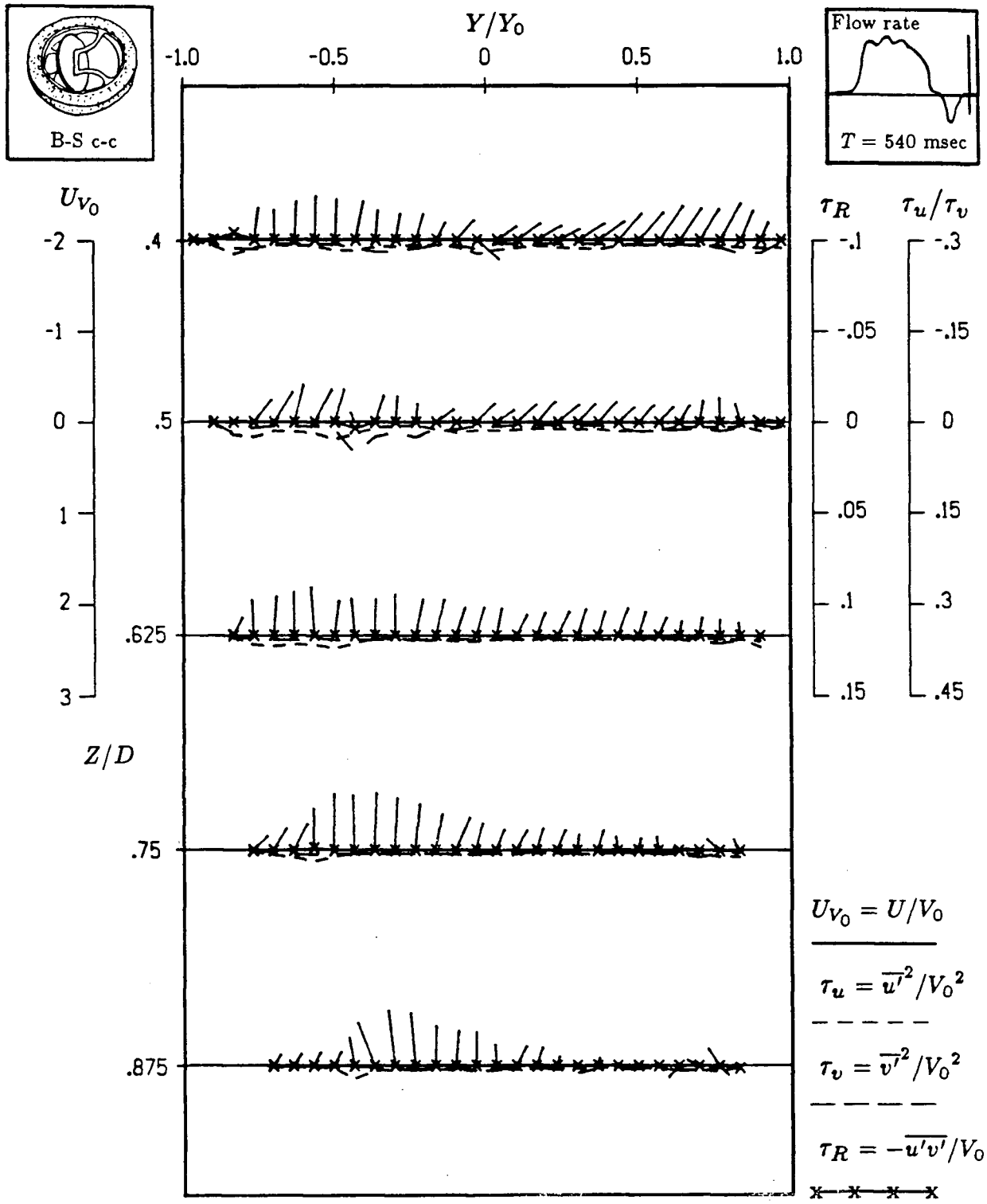

Figure 4-8 Variation of the nondimensional velocity, normal stresses, and the Reynolds stress at five downstream locations for the Björk-Shiley c-c prosthesis (27 mm) in the anterior orientation (T = 540 ms).

shown in Figure 4-9. The peak stress for each station in the ventricle is determined by the highest value during a phase of the cardiac cycle. The results show that for both the normal and Reynolds stresses, the accelerating-phase exhibited the highest stress levels while the decelerating-phase was relatively stress free. This confirms the earlier observation. However, it is not enough to consider just the peak stresses by themselves. Equally important is the duration of their existence at a sustained elevated stress level, though lower than the peak value, is more likely to cause the blood cell damage than a short term rise in stresses.

Figure 4-10 shows the peak averaged stresses over each phase of the cycle. The peak average stress is the maximum stress after averaging over each phase of the diastolic cycle. Although the results show similar trends, the gap between the accelerating and peak phases is less at certain stations. This suggests that the high stresses experienced during the accelerating-phase may be short-lived at some stations in the ventricle. The higher stresses at the 0.4D and 0.5D locations is due to the relatively small opening angle of the Björk-Shiley c-c valve.

(b) Posterior Orientation

Figure 4-11 shows the time history at the station 0.5D during the period 0 - 420 ms. As in the case of the anterior orientation, the expansion of the ventricle at the beginning of diastole generates the initial flow. However, once the flow begins to accelerate, a single vortex is created within the ventricle. Note that the two velocity jets seen in the anterior case are not so well defined in the posterior orientation. This is probably due to the disc opening towards the ventricle wall thus deflecting the flow towards the ventricle apex and then up towards the aortic valve.

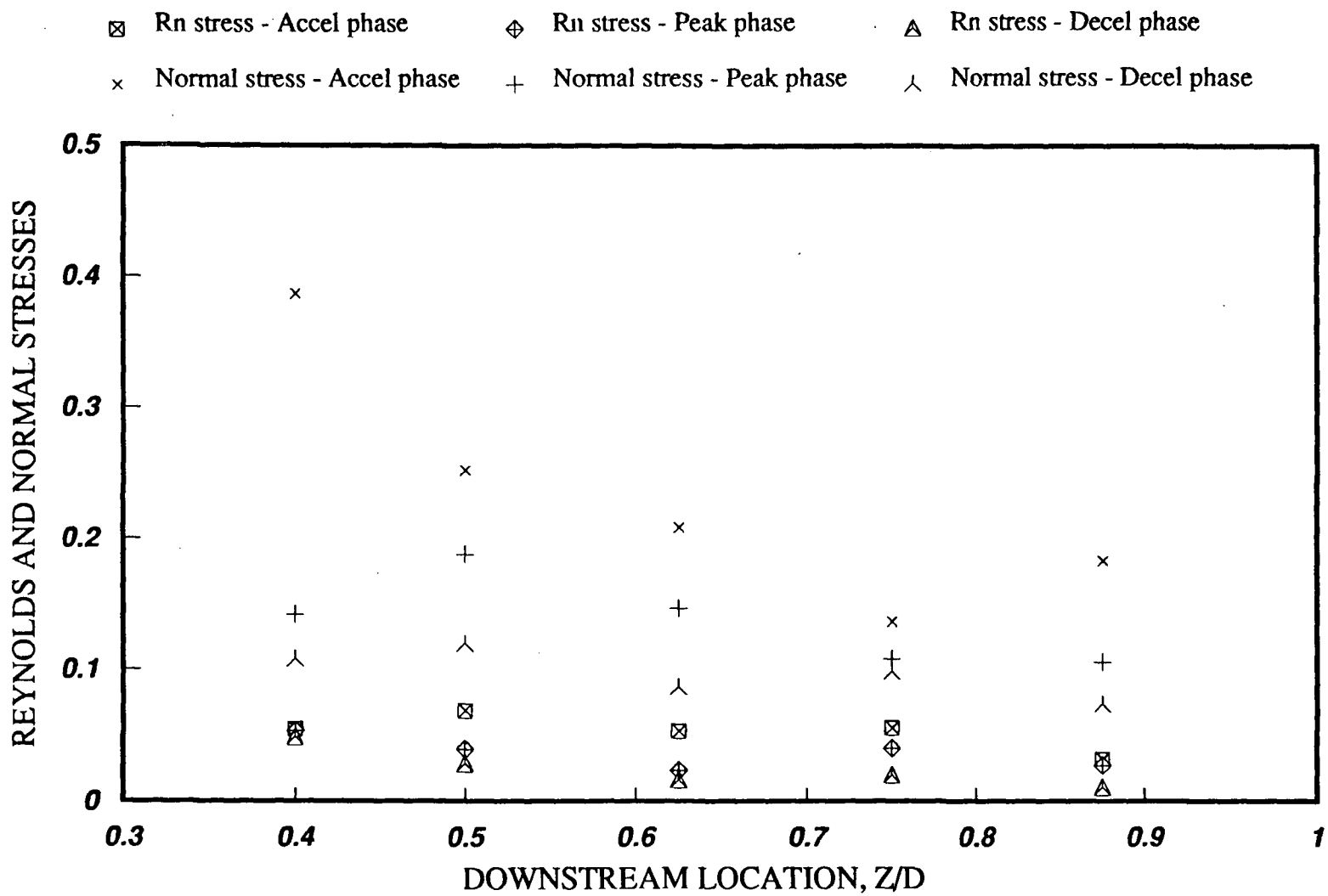

Figure 4-9 Variation of the nondimensional normal stresses and the Reynolds stress during the three phases of diastole at five downstream locations for the Björk-Shiley c-c prosthesis in the anterior orientation (27mm, Peak stresses).

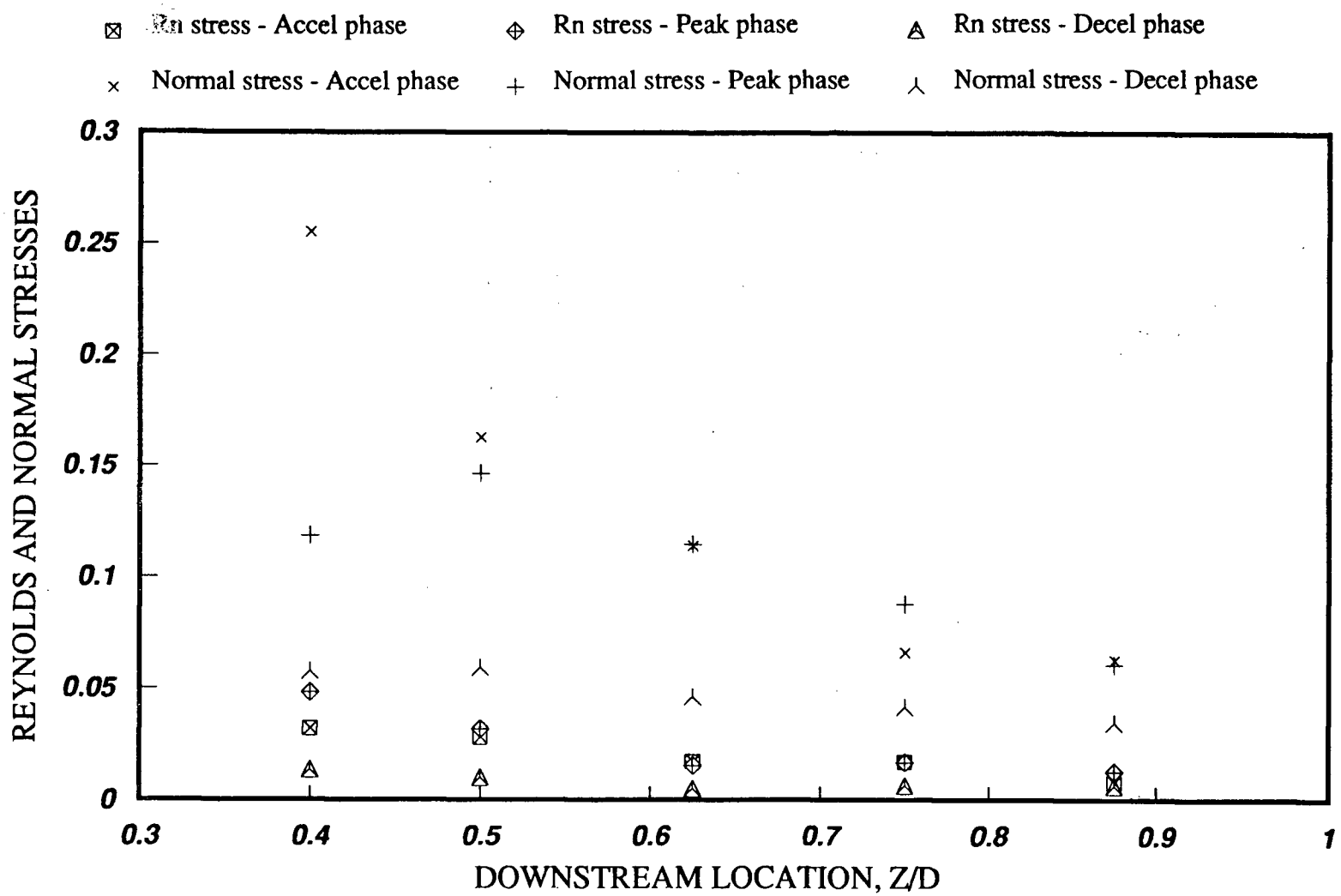

Figure 4-10 Variation of the nondimensional normal stresses and the Reynolds stress during the three phases of diastole at five downstream locations for the Björk-Shiley c-c prosthesis in the anterior orientation (27mm, Peak average stresses).

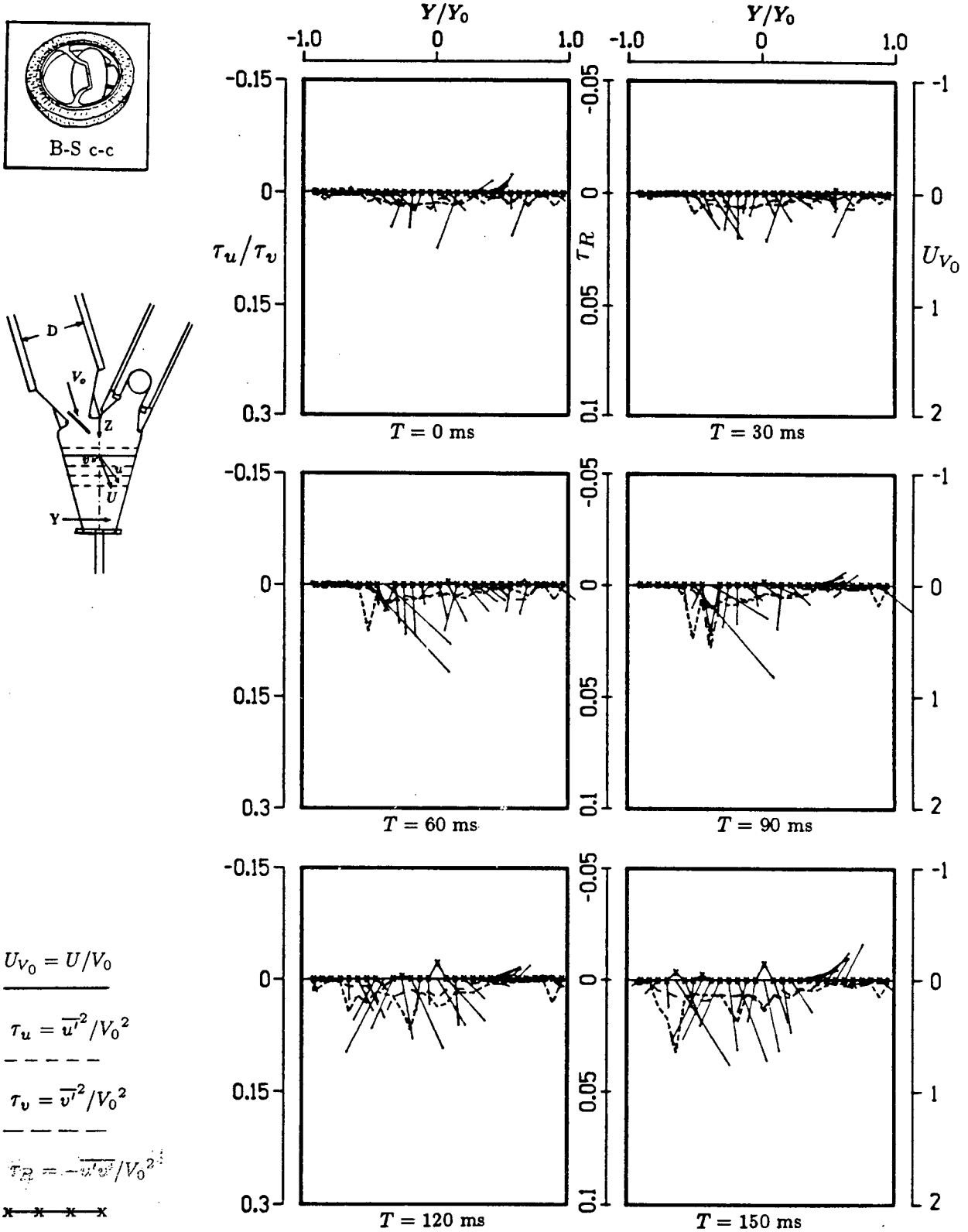

Figure 4-11 Time history of velocity and stress profiles for the Björk-Shiley c-c prosthesis in the posterior orientation at Z = 0.5D (0 - 150 ms).

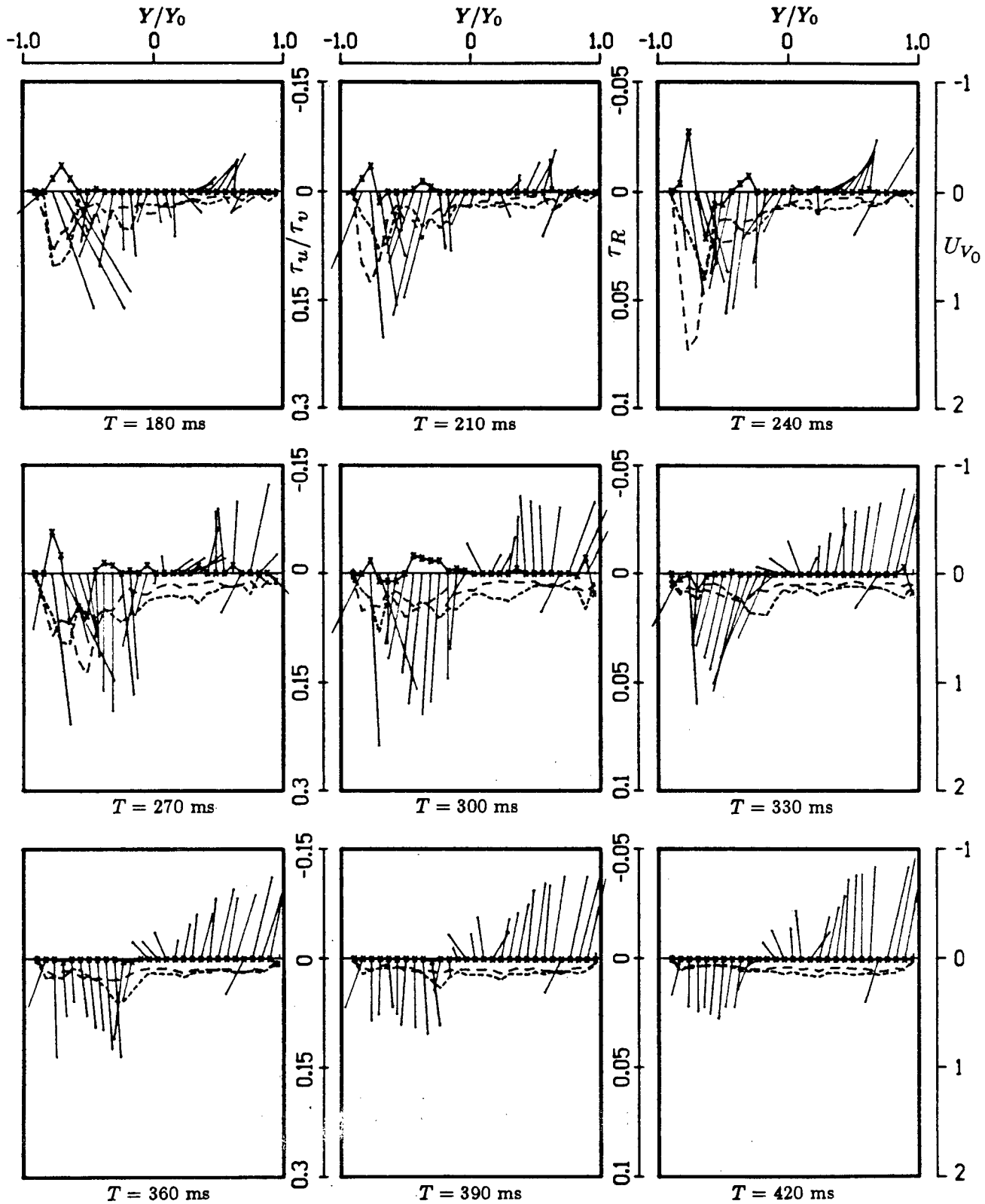

Figure 4-11 Time history of velocity and stress profiles for the Björk-Shiley c-c prosthesis in the posterior orientation at Z = 0.5D (180 - 420 ms).

Furthermore, the flow through the minor orifice augments that through the major orifice to create a single vortical circulation pattern. Figure 4-12 shows a schematic drawing to illustrate this flow pattern. In the anterior orientation, on the other hand, flow through the minor orifice was responsible for formation of the second vortex. Now, the rise in stresses occur primarily at the edge of the jet that forms as well as the region roughly corresponding to between the two orifices. Deceleration is easily detected by a reduction of stresses.

Figure 4-13 shows initial detection of the flow. Although the flow is in the process of adjustment, there is no sharp increase in the stresses as was found for the anterior orientation. With the acceleration of the flow (Figure 4-14), the normal and Reynolds stresses begin to increase but to levels considerably lower than those in the anterior case. The maximum normal stress during acceleration was observed to be 719 dynes/cm^2 (compared to 1265 dynes/cm^2) while the highest Reynolds stress was 81 dynes/cm^2 (compared to 224 dynes/cm^2).

At the peak flow (Figure 4-15), there appears to be no reduction in the Reynolds and normal stresses. Note, the high stresses are now further downstream than those for the anterior orientation. This is due to the jet being directed more towards the apex. As will be seen with the other two tilting disc valves, the posterior orientation causes larger disturbances further downstream than those in the anterior case.

As with the anterior case, a comparison of the steady flow results (Figure 3-3) with the pulsatile flow results at peak flow (Figure 4-15) would be of interest at this point. Once again, there are definite similarities in the flow patterns but the stresses are poorly predicted. As this was characteristic of all the prostheses studied, no further comparisons will be made.

Immediately after the deceleration-phase begins (Figure 4-16), all stresses are

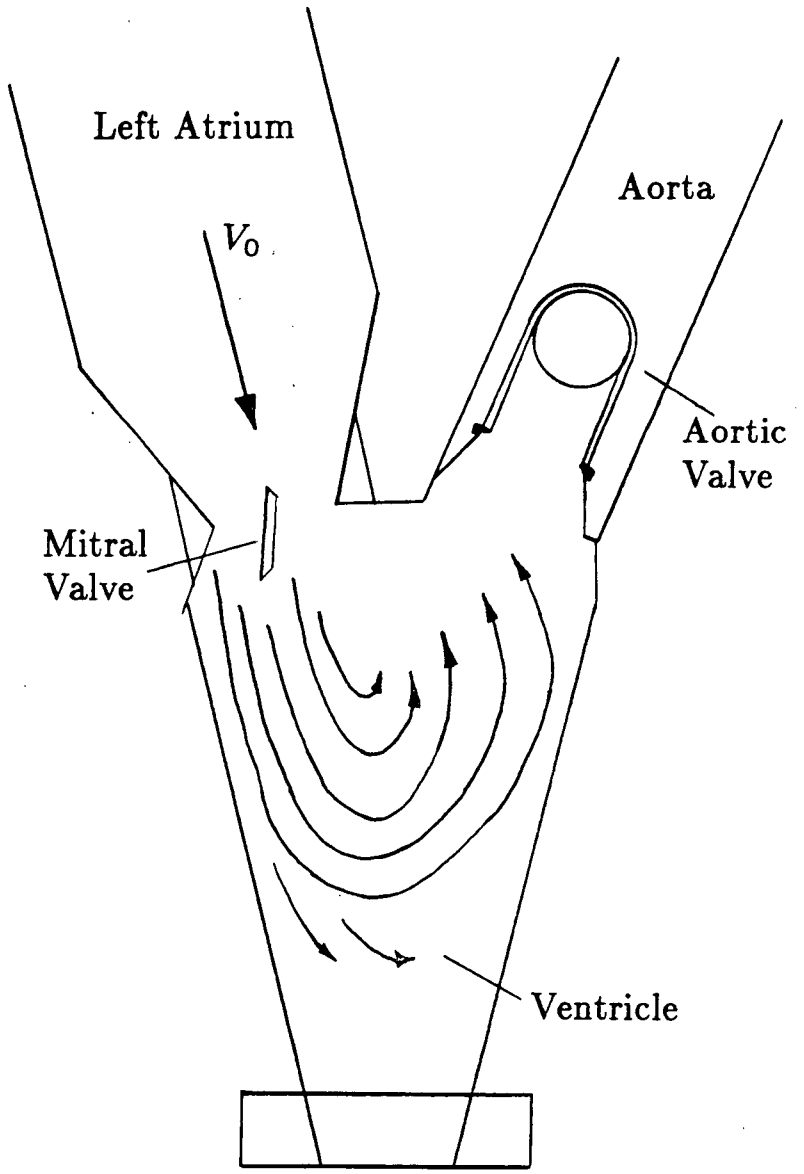

Figure 4-12 Schematic representation of the flow pattern in the left ventricle showing the single vortex formation for the posterior orientation of a tilting disc valve.

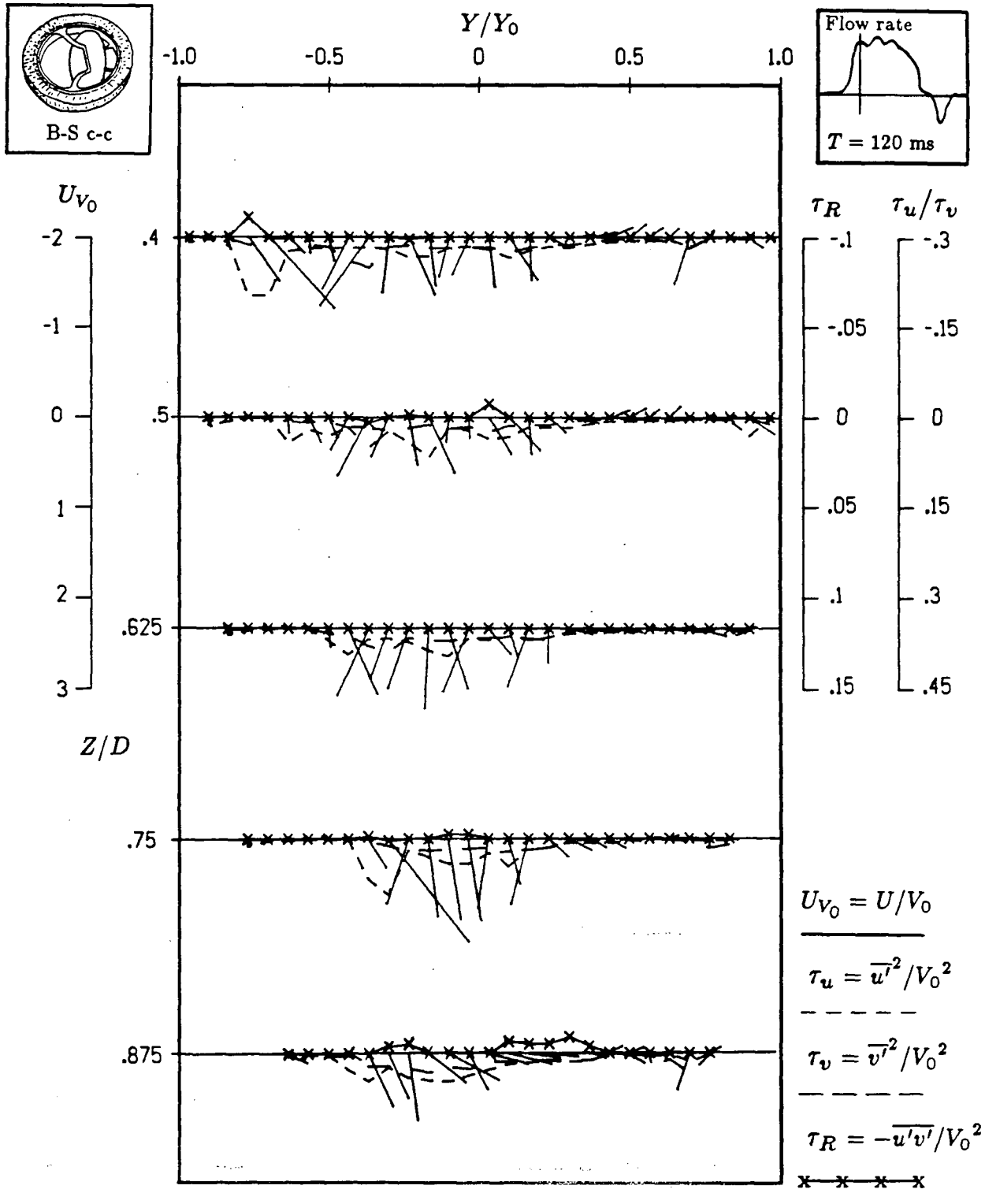

Figure 4-13 Variation of the nondimensional velocity, normal stresses, and the Reynolds stress at five downstream locations for the Björk-Shiley c-c prosthesis (27 mm) in the posterior orientation (T = 120 ms).

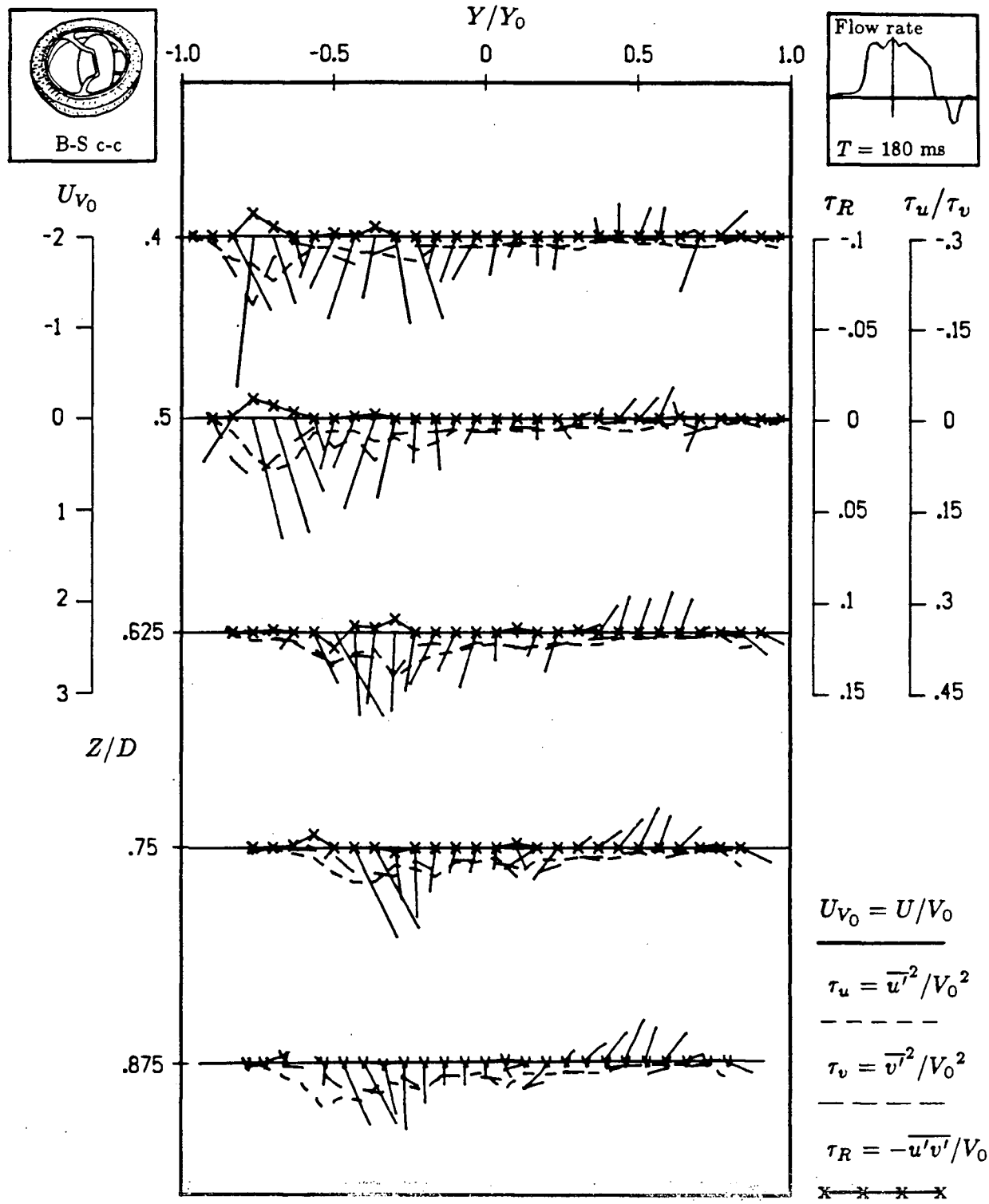

Figure 4-14 Variation of the nondimensional velocity, normal stresses, and the Reynolds stress at five downstream locations for the Björk-Shiley c-c prosthesis (27 mm) in the posterior orientation (T = 180 ms).

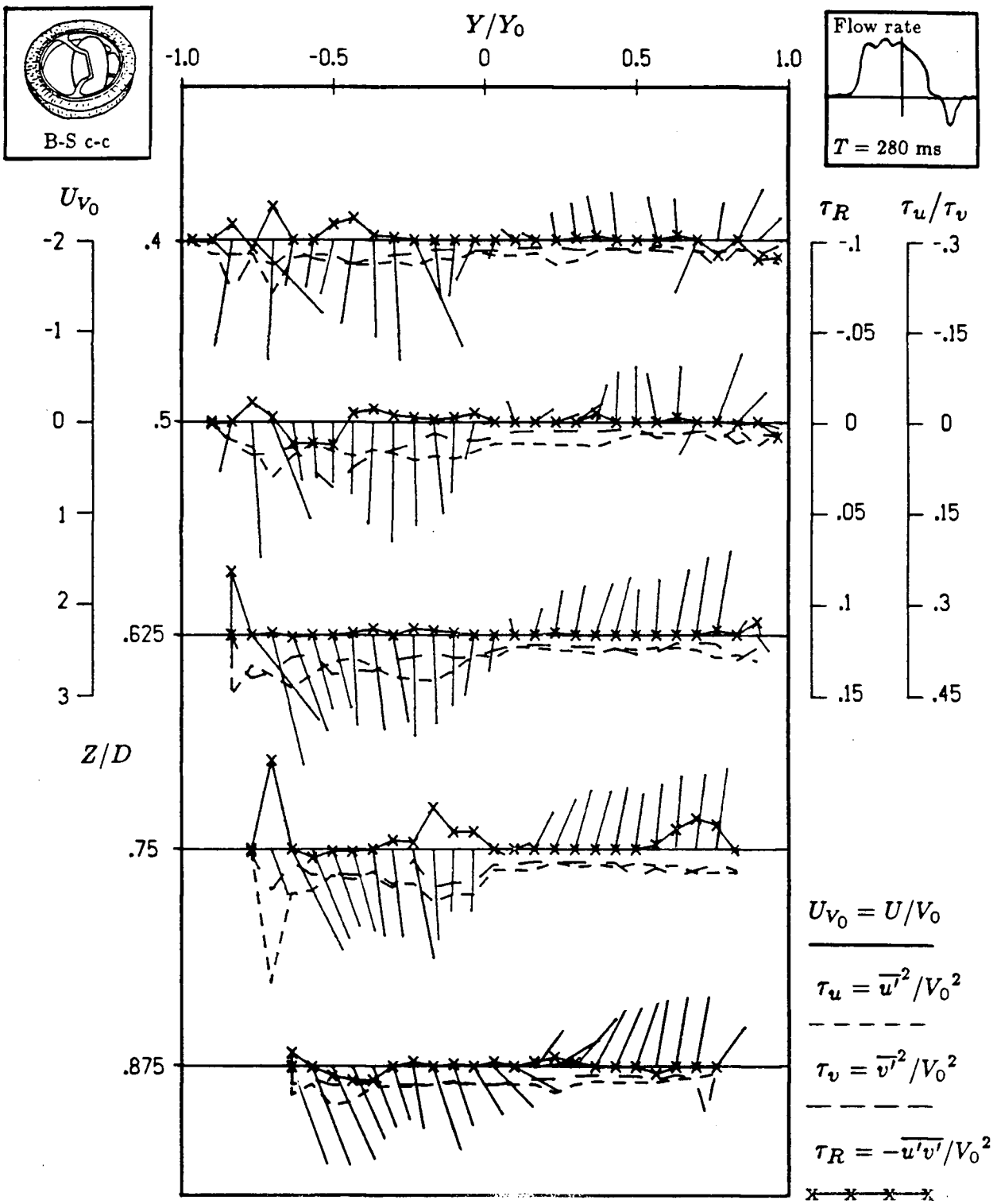

Figure 4-15 Variation of the nondimensional velocity, normal stresses, and the Reynolds stress at five downstream locations for the Björk-Shiley c-c prosthesis (27 mm) in the posterior orientation (T = 280 ms).

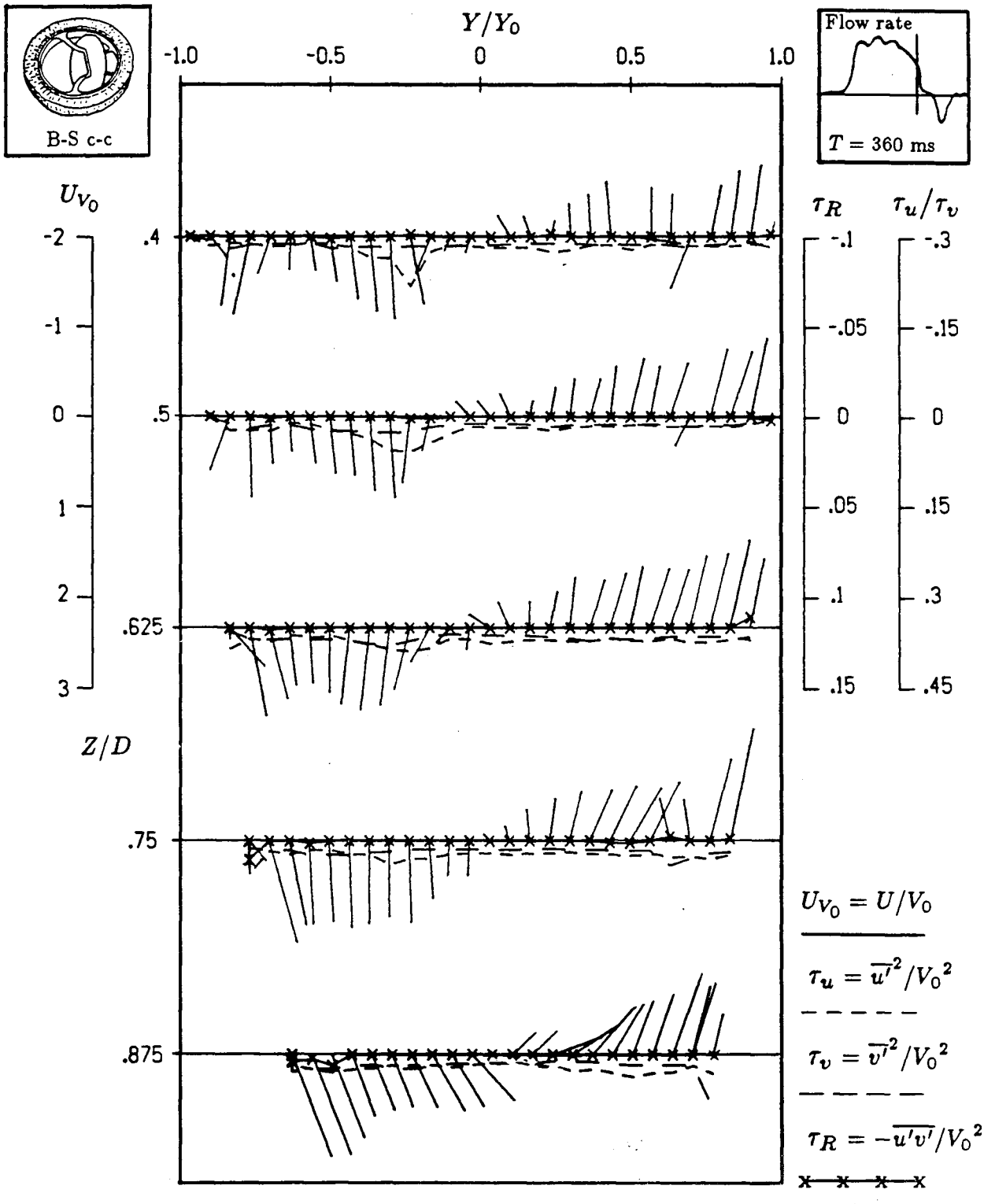

Figure 4-16 Variation of the nondimensional velocity, normal stresses, and the Reynolds stress at five downstream locations for the Björk-Shiley c-c prosthesis (27 mm) in the posterior orientation (T = 360 ms).

reduced as in the case of the anterior orientation.

Figure 4-17 shows the peak stresses during the three phases. The picture is quite different from that in the anterior case. The peak stresses during acceleration and peak phases are of the same magnitude, i.e., the acceleration-phase is no longer dominant. However, Figure 4-18 shows that when averaged over the phase, the acceleration stage is by far the dominant during the cycle. This suggests that any of the high stresses arising during the peak-phase are sustained only for a short period while the stresses in the acceleration-phase last longer.

(c) Anterior vs. Posterior Orientation

As previously mentioned, there appears to be a relationship between blood trauma and stress levels due to tilting disc valve orientation. Therefore, a comparison of valve orientations based on stress levels should aid in identifying a preferred in vivo orientation.

The following two figures present comparisons between the two orientations with reference to the Reynolds and normal stresses. Figure 4-19 shows the peak normal and Reynolds stresses at the five downstream locations. Except for the 0.75D station, the anterior orientation has the higher stresses. This is also true when the stresses are averaged over the diastolic phase as seen in Figure 4-20. In fact, here, the anterior orientation looks even worse indicating that the maximum stresses in an anterior orientation are sustained for a longer duration than those in a posterior configuration.

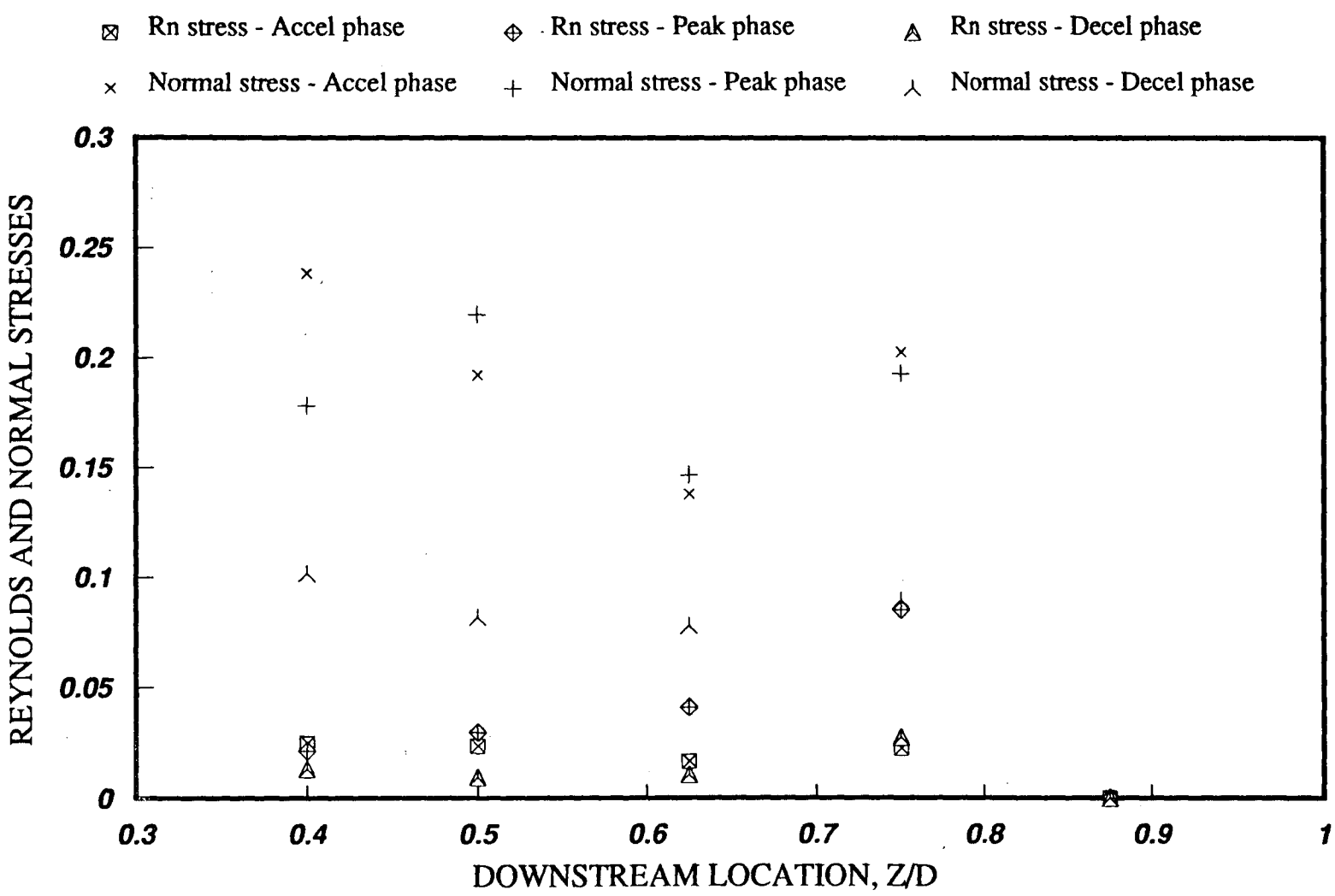

Figure 4-17 Variation of the nondimensional normal stresses and the Reynolds stress during the three phases of diastole at five downstream locations for the Björk-Shiley c-c prosthesis in the posterior orientation (27mm, Peak stresses).

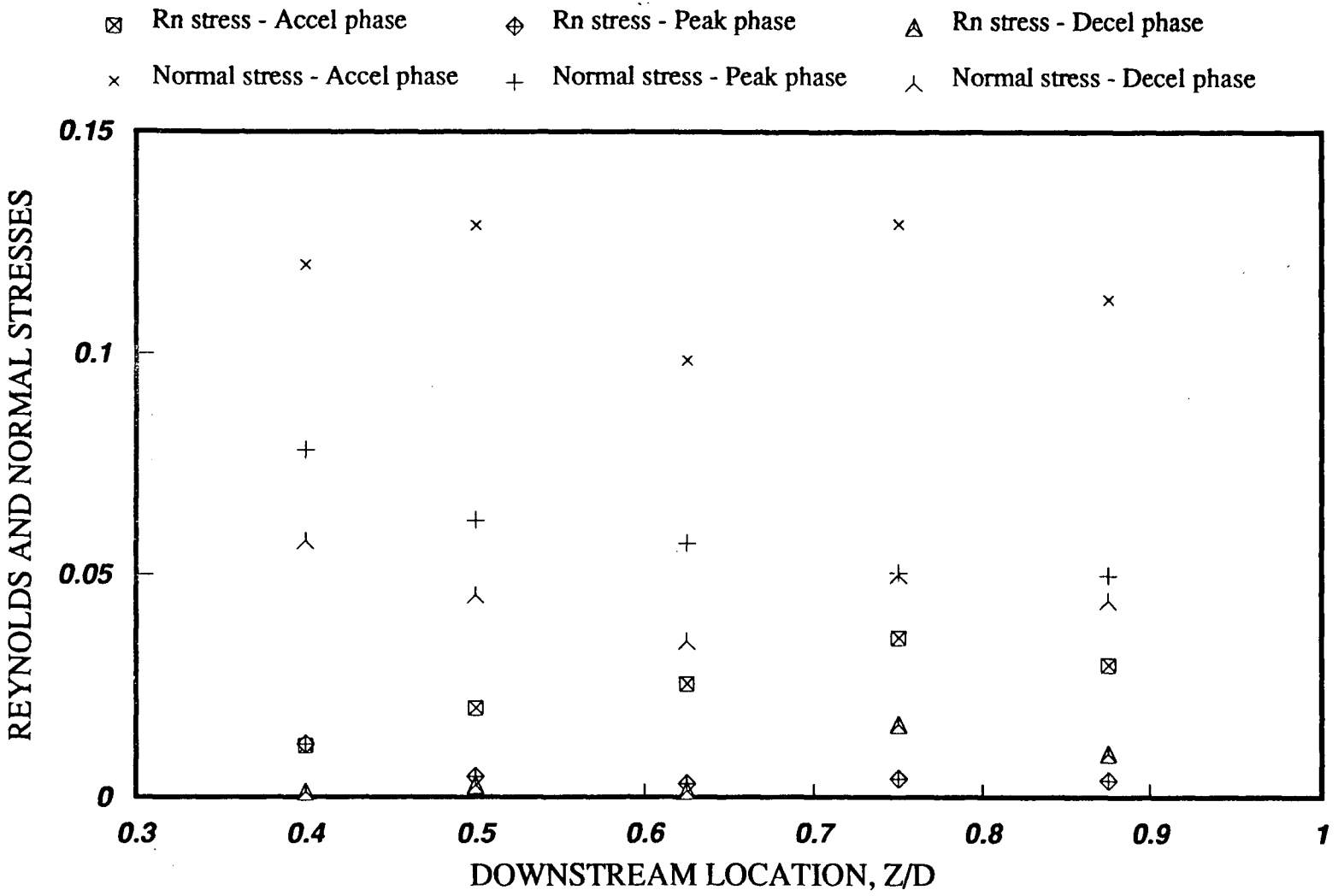

Figure 4-18 Variation of the nondimensional normal stresses and the Reynolds stress during the three phases of diastole at five downstream locations for the Björk-Shiley c-c prosthesis in the posterior orientation (27mm, Peak average stresses).

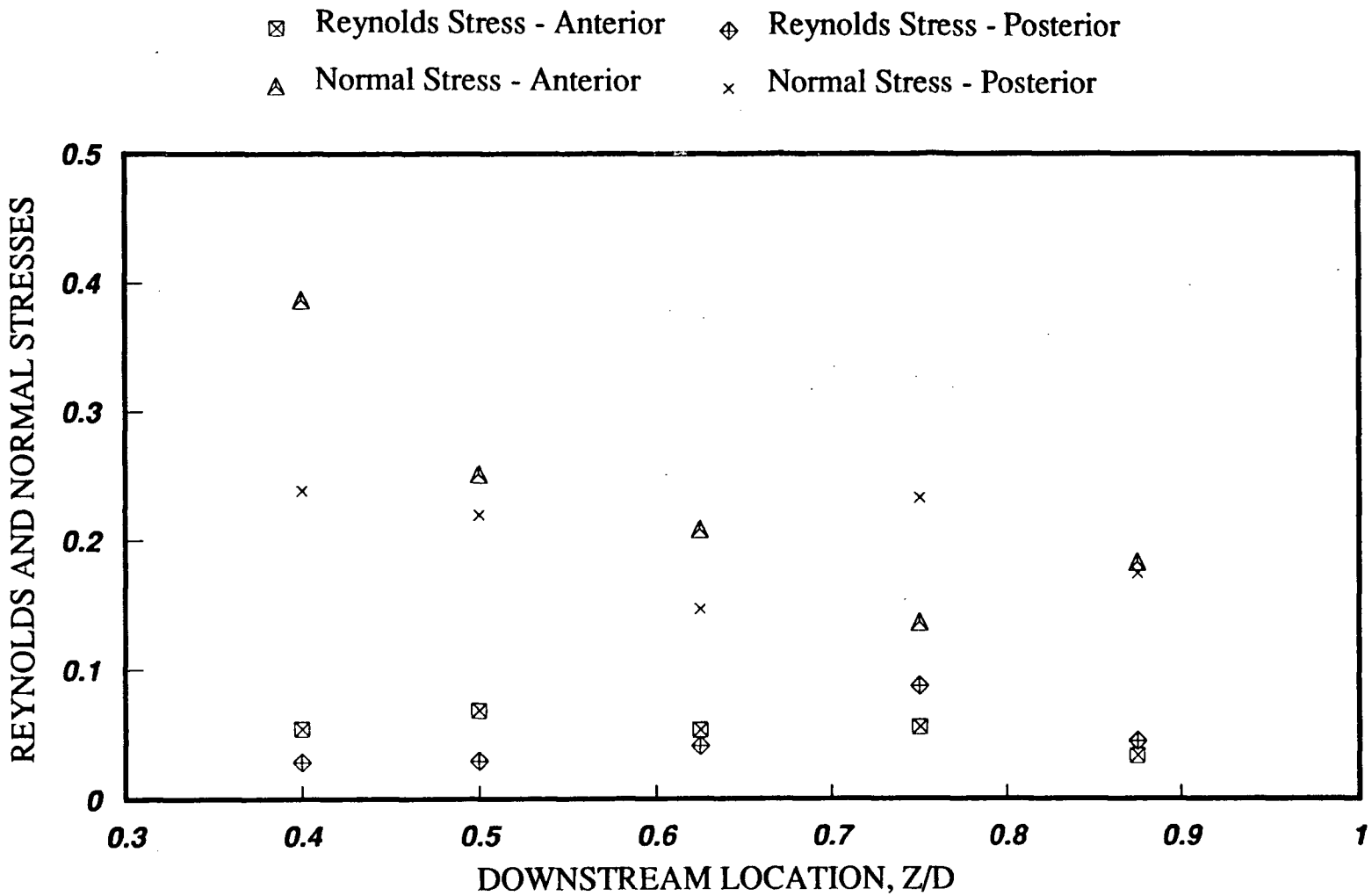

Figure 4-19 Variation of the nondimensional Reynolds and normal stresses at five downstream stations for the anterior and posterior orientations of the Björk-Shiley c-c prosthesis (27mm, Peak stresses).

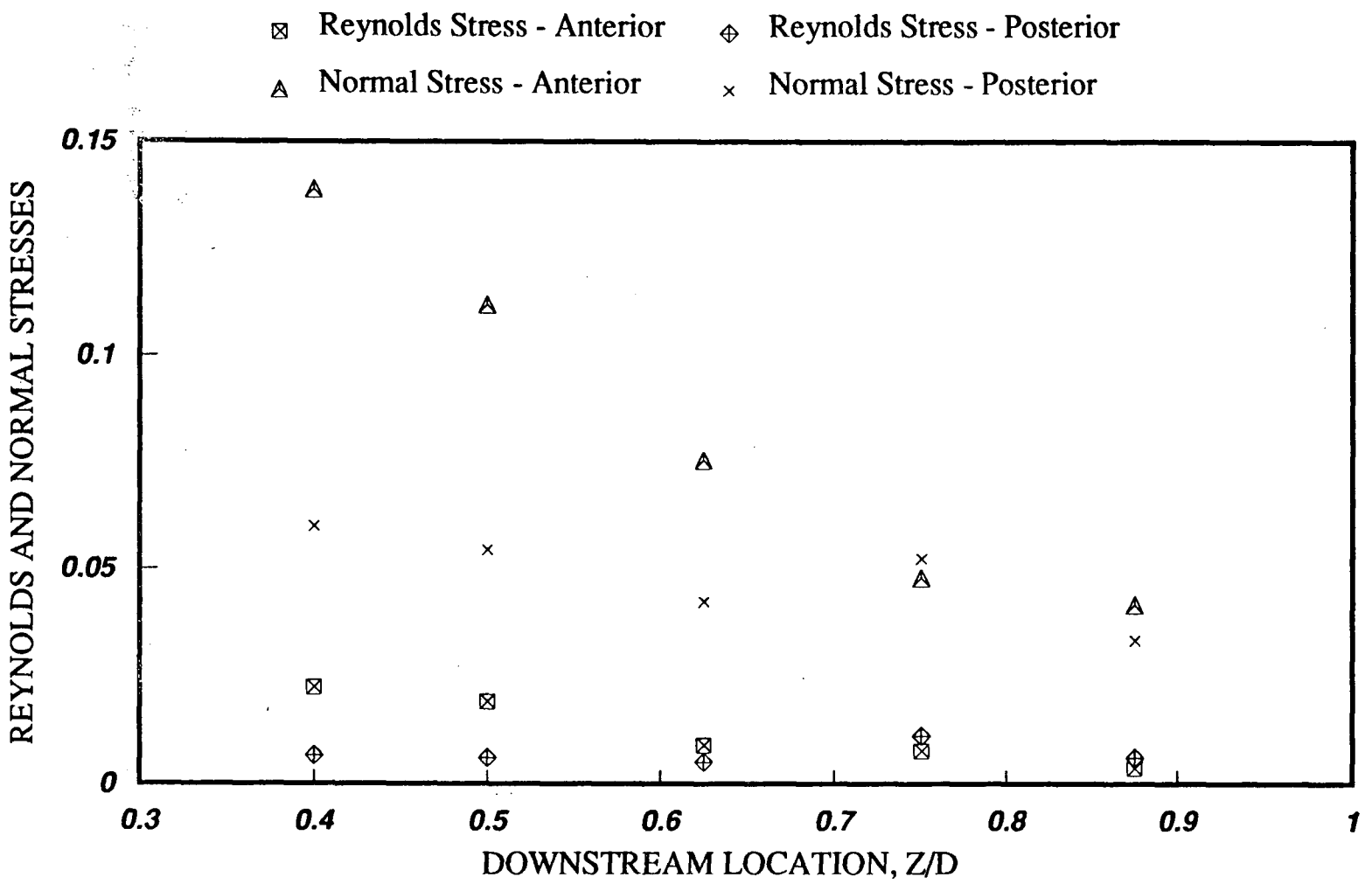

Figure 4-20 Variation of the nondimensional Reynolds and normal stresses at five downstream stations for the anterior and posterior orientations of the Björk-Shiley c-c prosthesis (27mm, Peak average stresses).

4.1.2 Björk-Shiley Monostrut

(a) Anterior Orientation

Figure 4-21 shows a series of time history plots, at the station 0.5D, for the B-S mono. This station was selected as the normal stresses were found to be the highest at that location, perhaps due to the opening angle geometry. The B-S mono opens a further 10 degrees compared to the B-S c-c, therefore, the jet through the major orifice is directed further downstream. For the Bicer valve, which opens a further 5 degrees, the highest stress levels were found to be even further downstream as discussed in Section 4.1.3.

As seen before, at the initiation of the flow, large disturbances appear which gradually decrease through the acceleration-phase. In the case of the B-S c-c, only the normal stresses reduced while the Reynolds stress remained virtually unchanged. However, with the B-S mono, it can clearly be seen that both the normal and Reynolds stresses decrease as the flow becomes more organized. Similar to the B-S c-c valve, two jet-like flow fields corresponding to flow through the two orifices can be detected.

Just after the initiation of the flow (Figure 4-22), the normal and Reynolds stresses rise to their highest level during the cardiac cycle. The normal stress rose to a high of 851 dynes/cm^2 (120 msec at 0.5D) while the Reynolds stress was 190 dynes/cm^2 (120 msec at 0.4D). The maximum Reynolds stress was of the same magnitude as that for the B-S c-c valve (224 dynes/cm^2) but the maximum normal stress showed a substantial reduction compared to the B-S c-c (1265 dynes/cm^2).

By the time the peak flow is established (Figure 4-23), the maximum normal

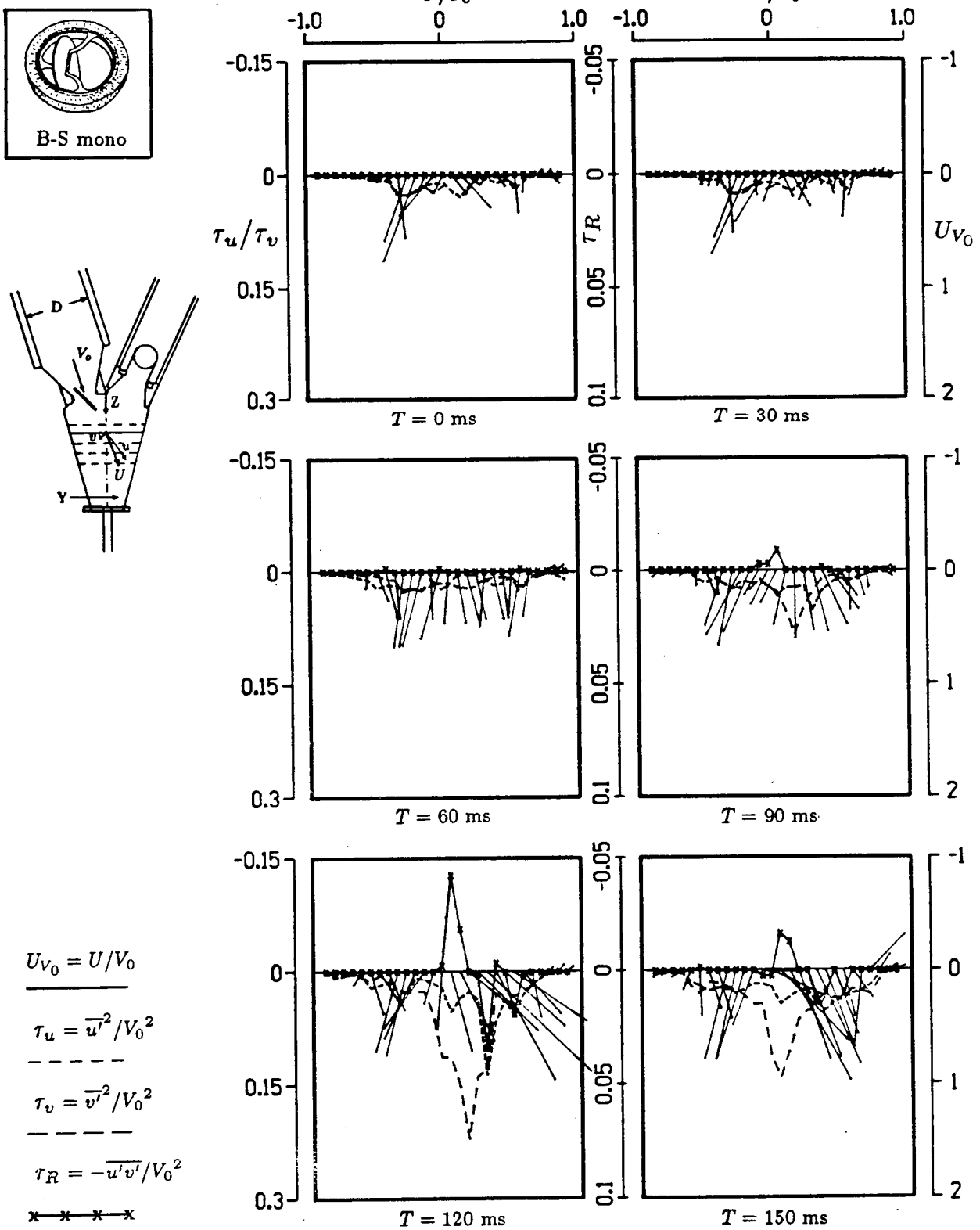

Figure 4-21 Time history of velocity and stress profiles for the Björk-Shiley monostrut prosthesis in the anterior orientation at Z = 0.5D (0 - 150 ms).

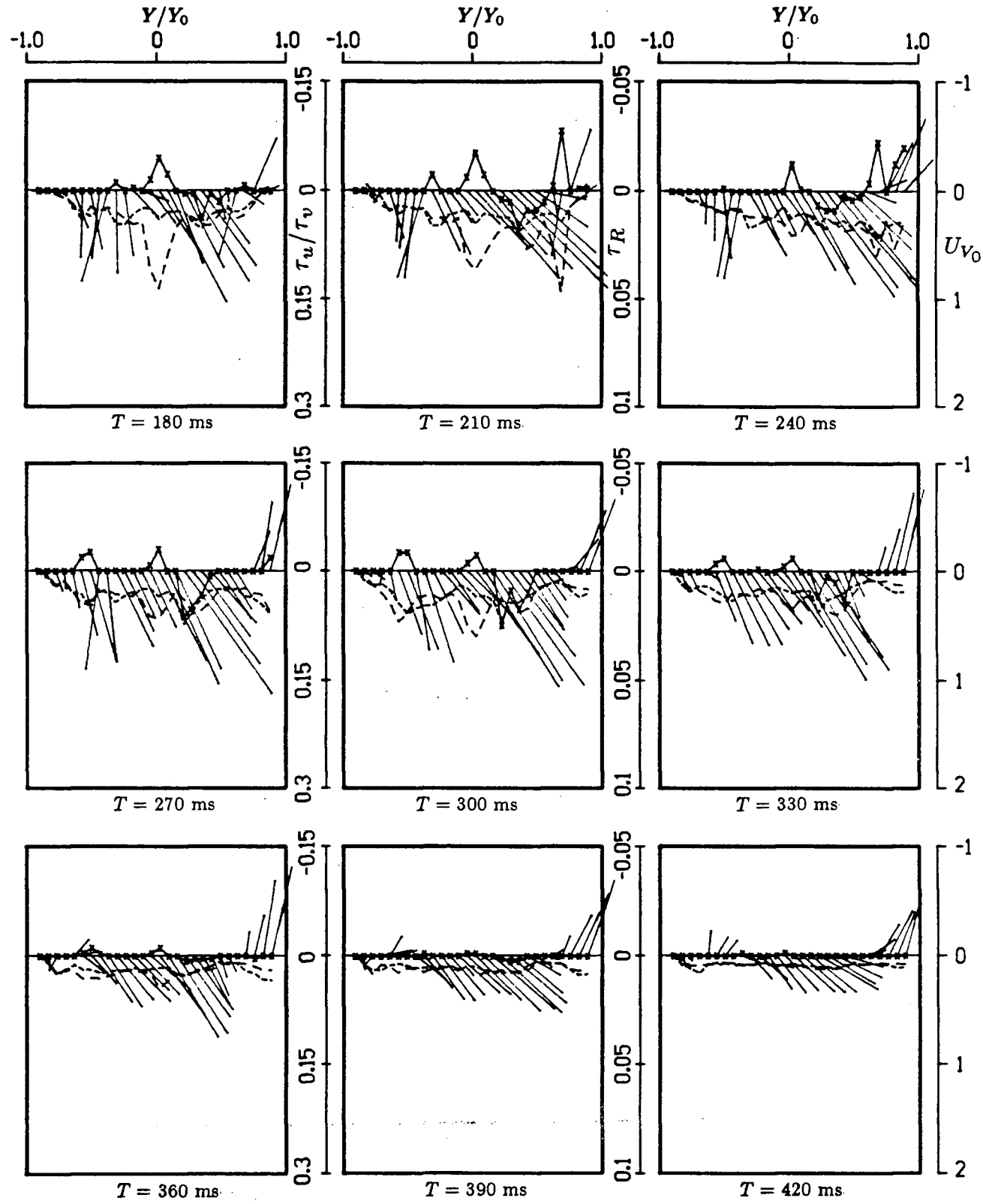

Figure 4-21 Time history of velocity and stress profiles for the Björk-Shiley monostrut prosthesis in the anterior orientation at Z = 0.4D (180 - 420 ms).

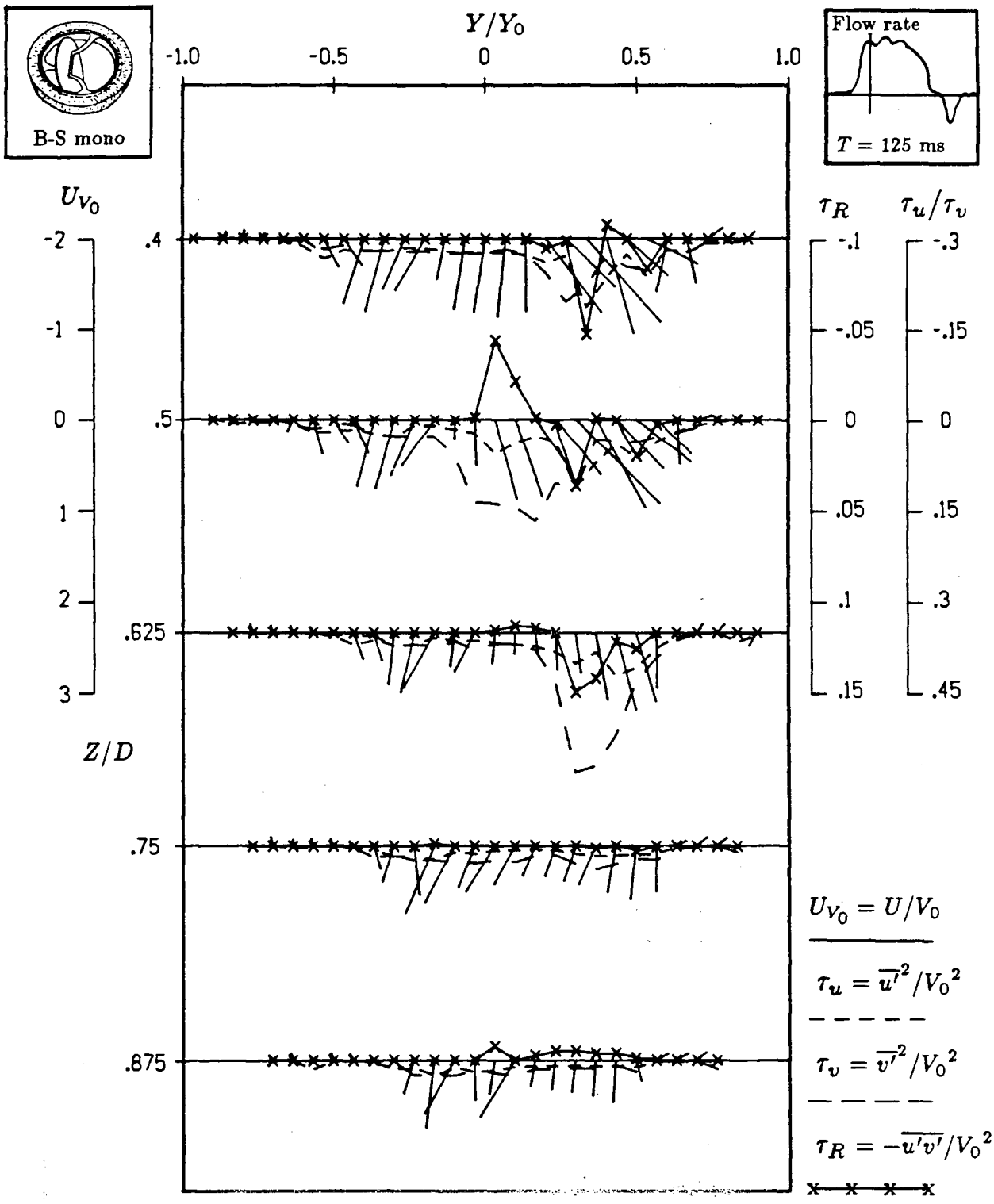

Figure 4-22 Variation of the nondimensional velocity, normal stresses, and the Reynolds stress at five downstream locations for the Björk-Shiley monostrut prosthesis (27 mm) in the anterior orientation (T = 125 ms).

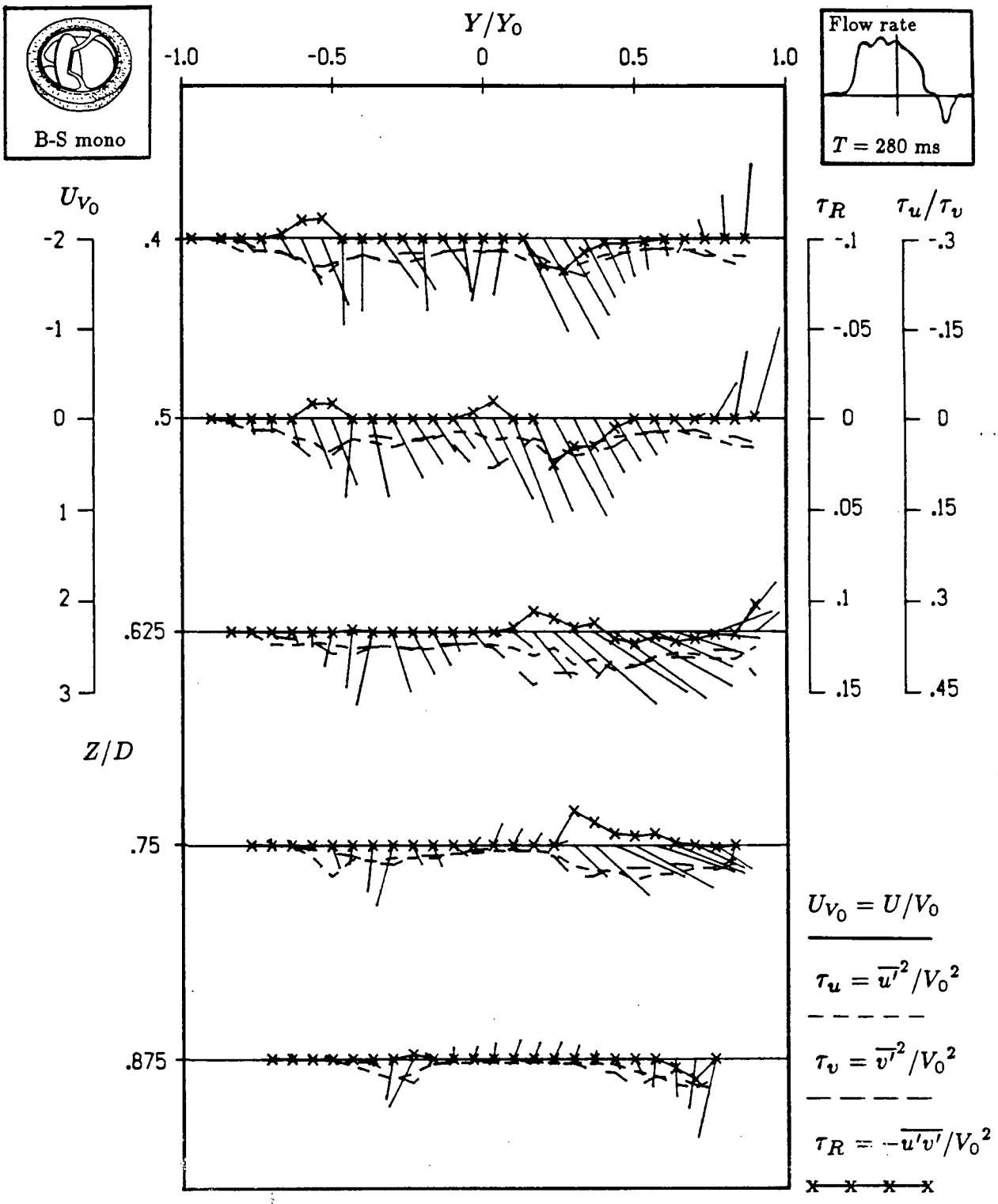

Figure 4-23 Variation of the nondimensional velocity, normal stresses, and the Reynolds stress at five downstream locations for the Björk-Shiley monostrut prosthesis (27 mm) in the anterior orientation (T = 280 ms).

stress has reduced to 277 dynes/cm^2 and the Reynolds stress to 77 dynes/cm^2. Note, the difference between the flow through the minor and major orifices. The jet from the major orifice is clearly more dominant. Because the monostrut divides the minor orifice into two sections, it would be logical to assume that two jets would result due to the sectioned orifice. In fact, Yoganathan et al.[46] reported that in the near vicinity of the monostrut valve in an aortic position, three high velocity jet type flow fields were produced (one from the major and two from the minor orifice). However, this was not detected in the present study probably due to the location of the first measuring station. By the time the flow reached 0.4D, only one jet from the minor orifice can be found; however, a rise in the turbulent stresses was detected at locations adjacent to the minor orifice.

The complex nature of the flow is again apparent with this valve. The two opposing vortices form with the counterclockwise one more dominant than that observed with the B-S c-c. This is probably due to the greater opening angle of the monostrut's disc.

Figure 4-24 shows the deceleration-phase when the stresses drop off. There appears to be a degree of similarity in flow characteristics for the prosthetic valves under study during the late diastolic phase.

Figures 4-25 and 4-26 show the peak as well as the peak average Reynolds and normal stresses during the three main phases of the diastolic phase. As in the case of the B-S c-c valve, both sets of data suggest that the acceleration-phase is the most turbulent one while the deceleration-phase is relatively quiescent. This implies that any damage that may occur to the blood cells due to the prosthetic device would most likely occur during the accelerating-phase as indicated by both the Reynolds and normal stresses. Also notice the locations of the highest stress levels in the

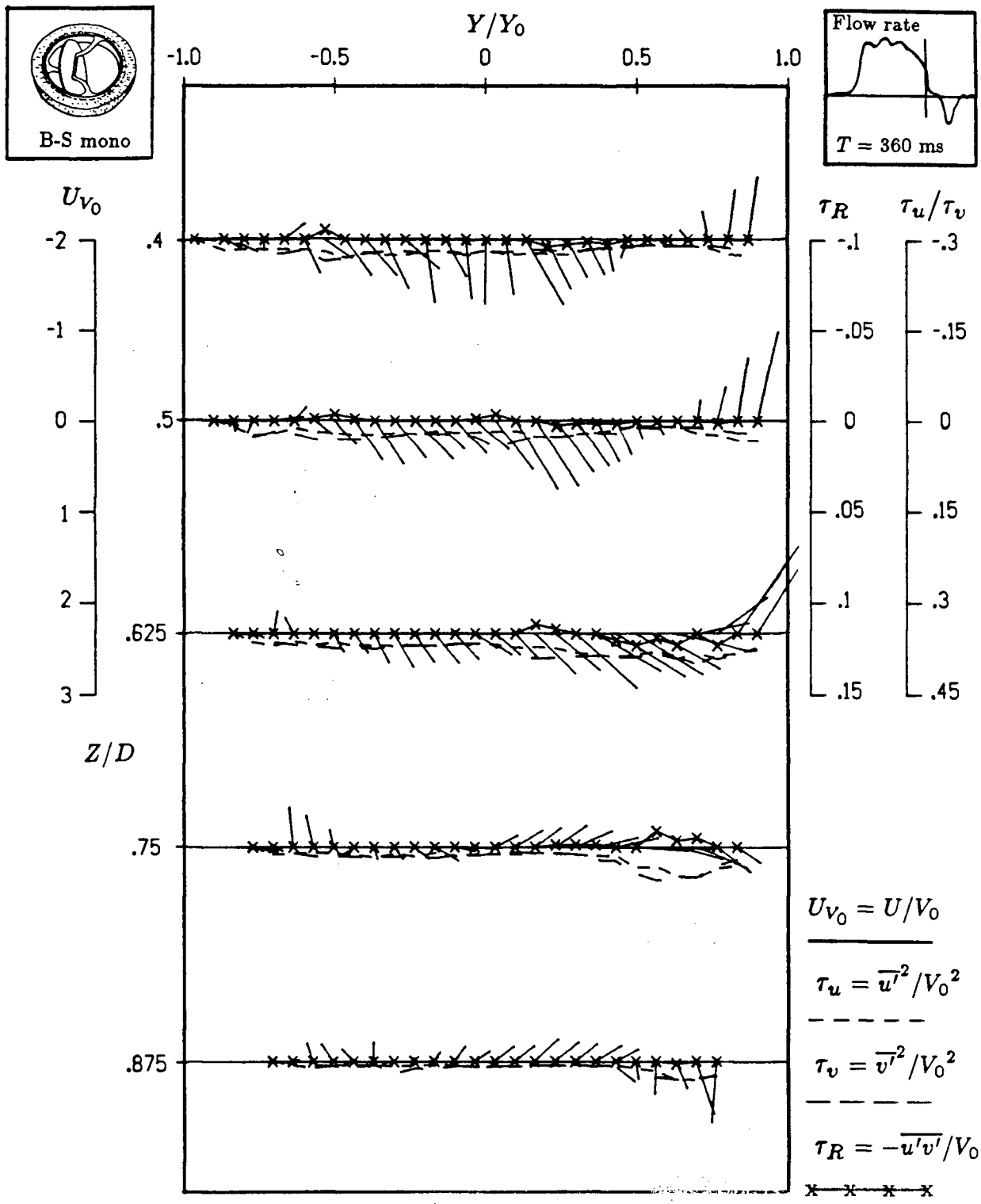

Figure 4-24 Variation of the nondimensional velocity, normal stresses, and the Reynolds stress at five downstream locations for the Björk-Shiley monostrut prosthesis (27 mm) in the anterior orientation (T = 360).

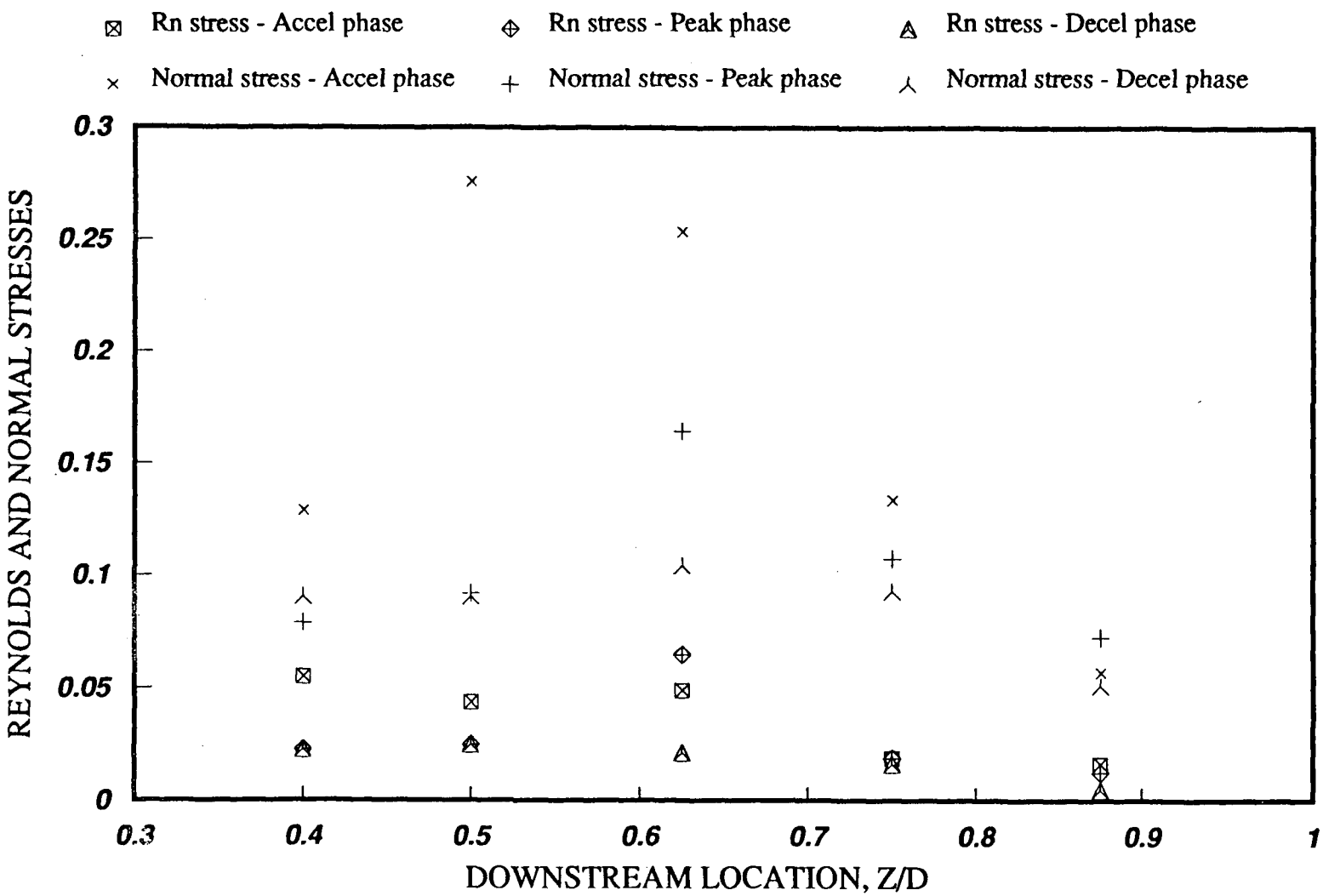

Figure 4-25 Variation of the nondimensional normal stresses and the Reynolds stress during the three phases of diastole at five downstream locations for the Björk-Shiley monostrut prosthesis in the anterior orientation (27mm, Peak stresses).

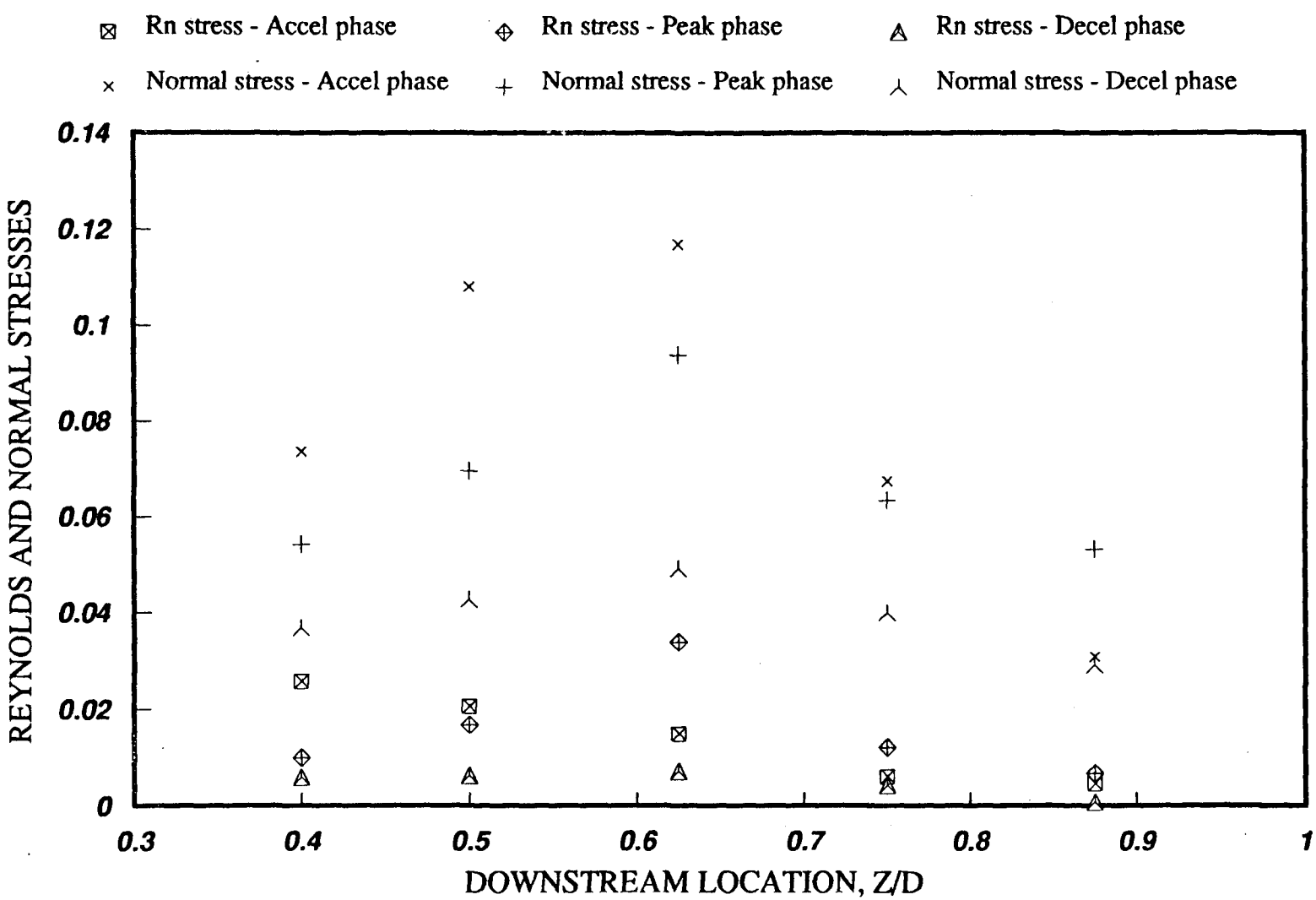

Figure 4-26 Variation of the nondimensional normal stresses and the Reynolds stress during the three phases of diastole at five downstream locations for the Björk-Shiley monostrut prosthesis in the anterior orientation (27mm, Peak average stresses).

ventricle. They compare with those observed for the B-S c-c. The stresses then drop off considerably at the two furthest measuring stations. This may be attributed to the direction of the jet-flow which is influenced by the opening angle of the disc. The larger the opening angle, the further downstream the jet-type of flow persists.

(b) Posterior Orientation

The time history profile for the posterior orientation (Figure 4-27) shows the familiar single counterclockwise vortex circulation as observed for the B-S c-c. However, velocities are considerably higher due to the larger opening angle. During acceleration, the two characteristic jets from the major and minor orifice form.

Just after the initiation of the flow (Figure 4-28), there is a sharp increase in the stresses at each of the five stations due to the high velocity jet. Unlike the B-S c-c, the B-S mono continues to experience high stresses throughout the acceleration phase. The maximum Reynolds stress reaches a value of 182 dynes/cm^2 at around 200 ms and the maximum normal stress level of 970 dynes/cm^2 at 120 ms. However, by the time the peak flow occurs (Figure 4-29), the Reynolds and normal stresses have reduced to 77 dynes/cm^2 and 396 dynes/cm^2, respectively. The effects of the strut structure are clearly apparent in the velocity profiles. Note the dips in the velocity profiles at locations corresponding to that of the struts in the major and minor orifices.

Figure 4-30 shows familiar fluid dynamic parameter profiles for the deceleration phase. However, there is one major difference. The velocity components are considerably higher in magnitude than for the B-S c-c valve, again due to the larger opening angle.

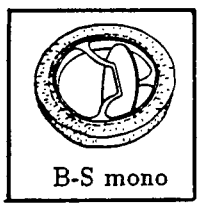

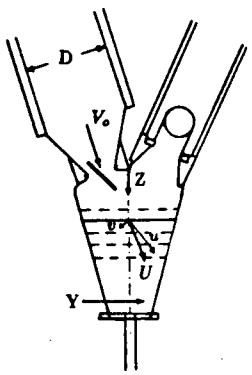

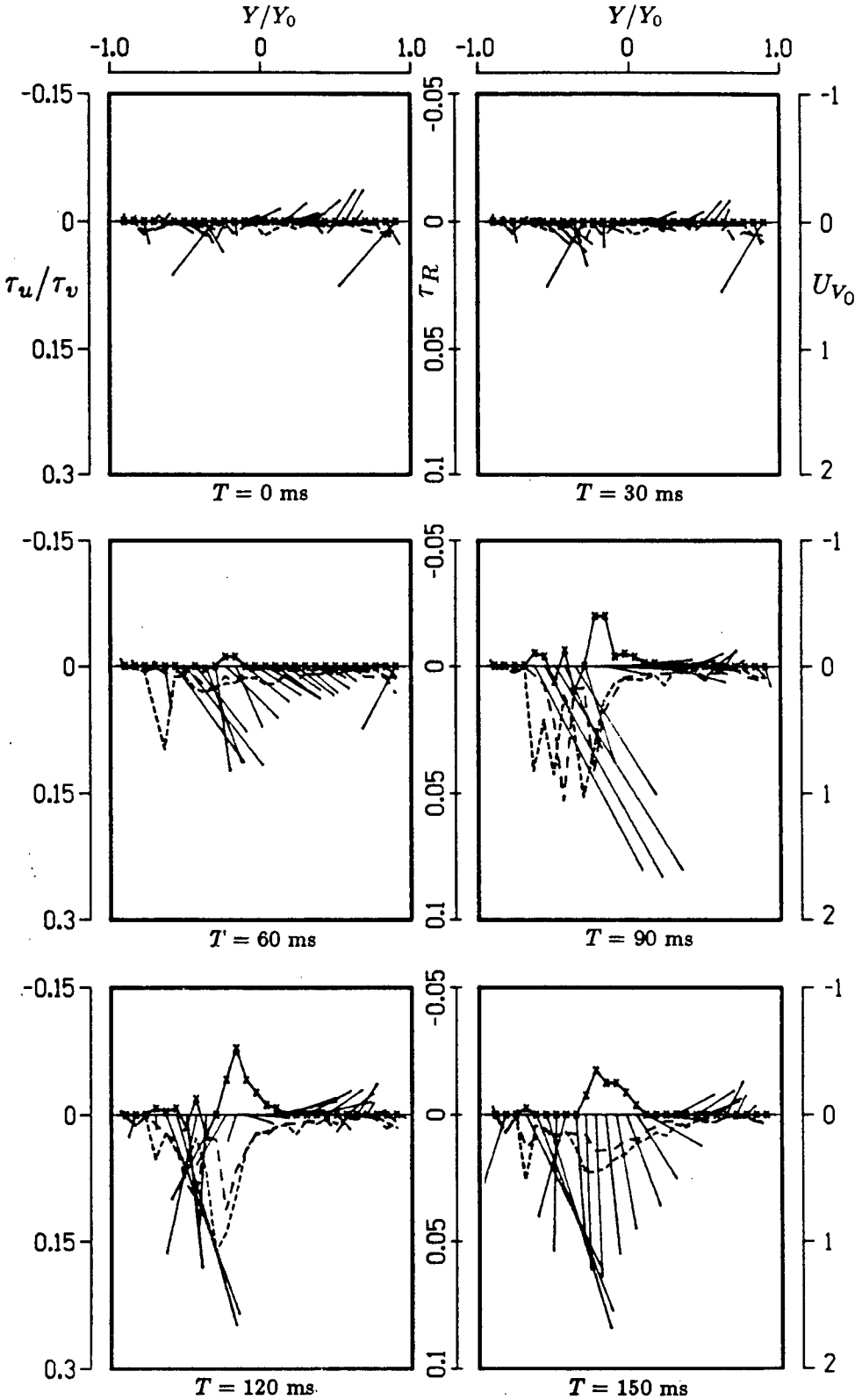

$U_{V_0} = U/V_0$

$\tau_u = \overline{u'}^2/V_0^2$

$\tau_v = \overline{v'}^2/V_0^2$

$\tau_R = -\overline{u'v'}/V_0^2$

Figure 4-27 Time history of velocity and stress profiles for the Björk-Shiley monostrut prosthesis in the posterior orientation at Z = 0.5D (0 - 150 ms).

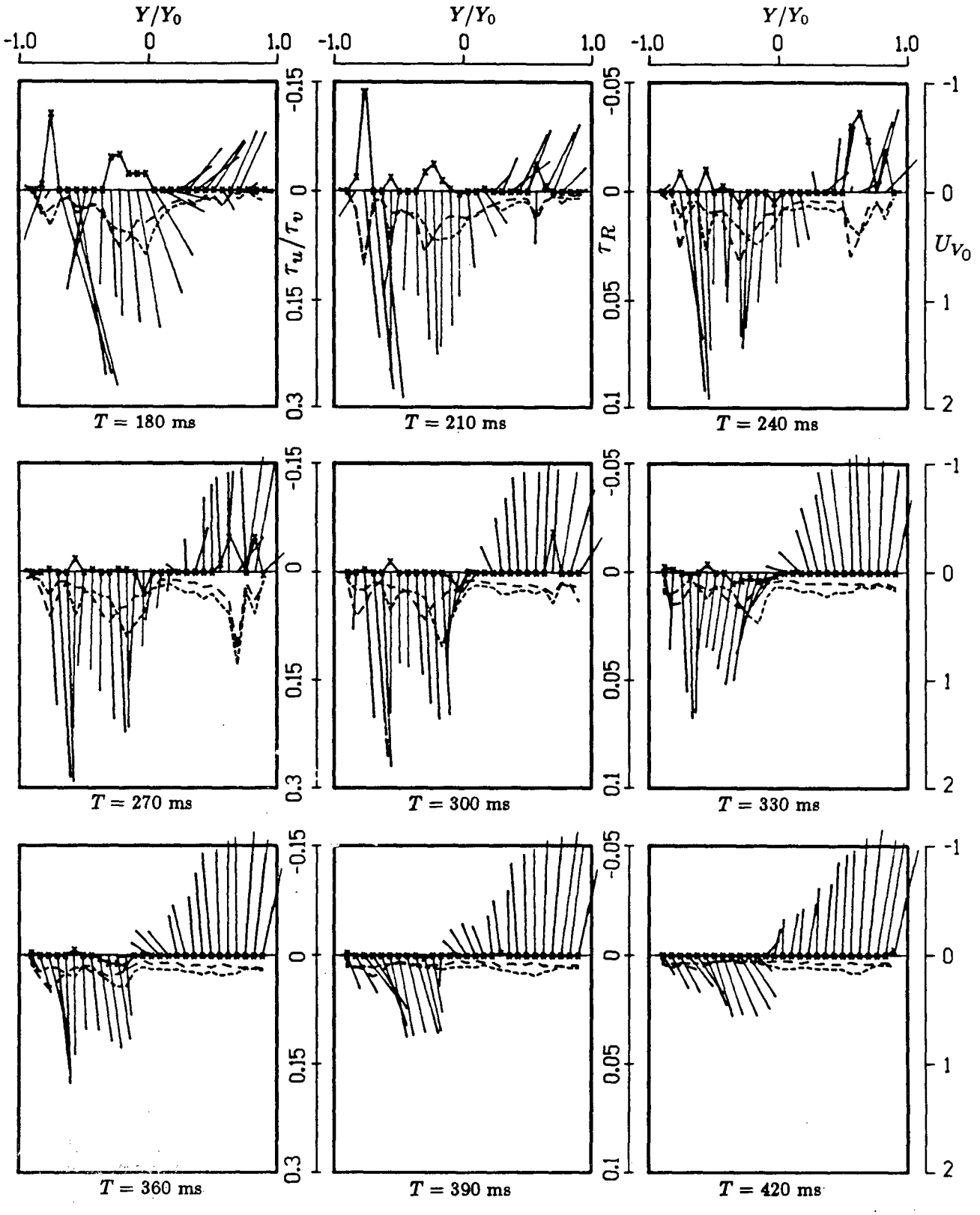

Figure 4-27 Time history of velocity and stress profiles for the Björk-Shiley monostrut prosthesis in the posterior orientation at Z = 0.5D (180 - 420 ms).

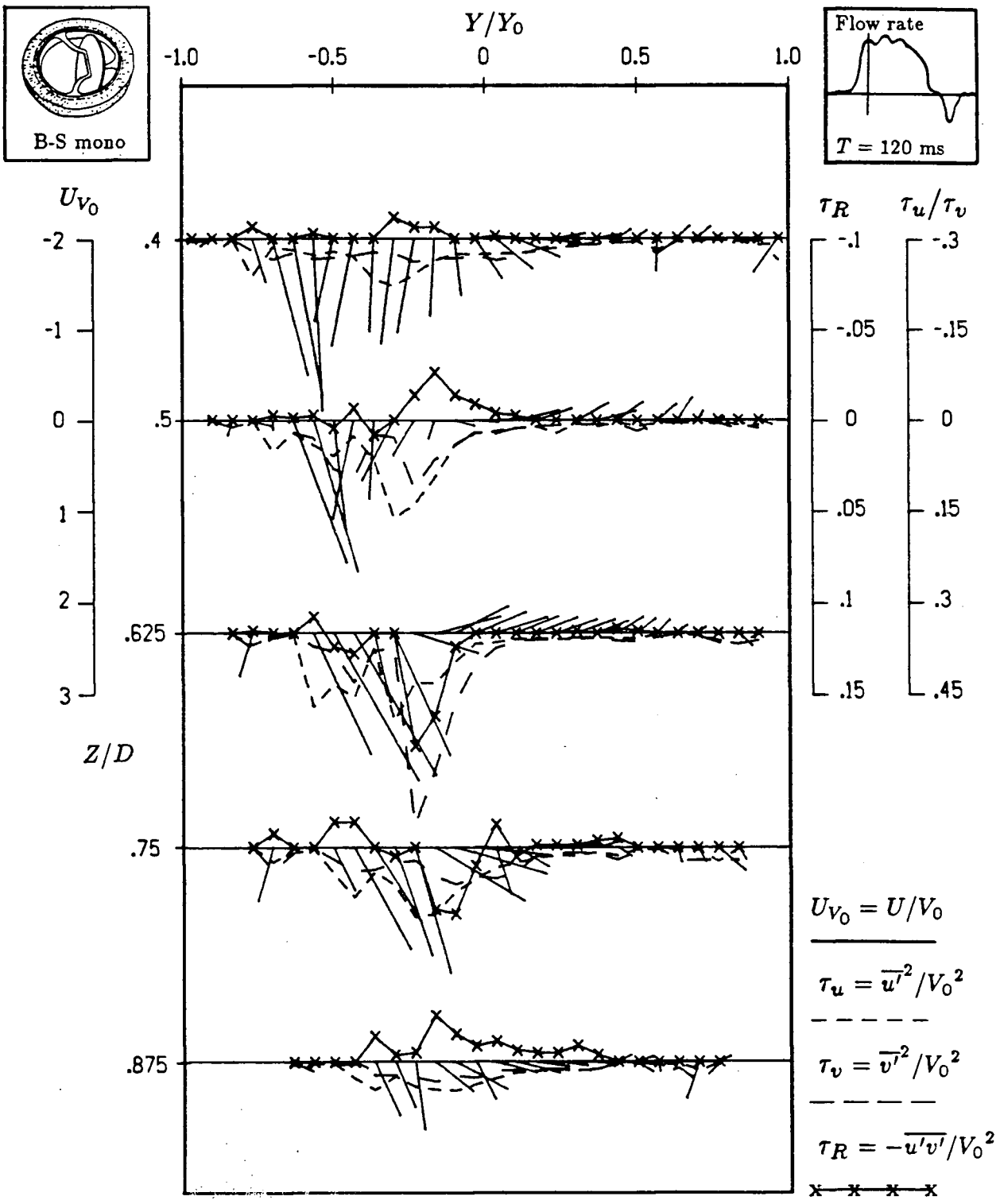

Figure 4-28 Variation of the nondimensional velocity, normal stresses, and the Reynolds stress at five downstream locations for the Björk-Shiley monostrut prosthesis (27 mm) in the posterior orientation (T = 120 ms).

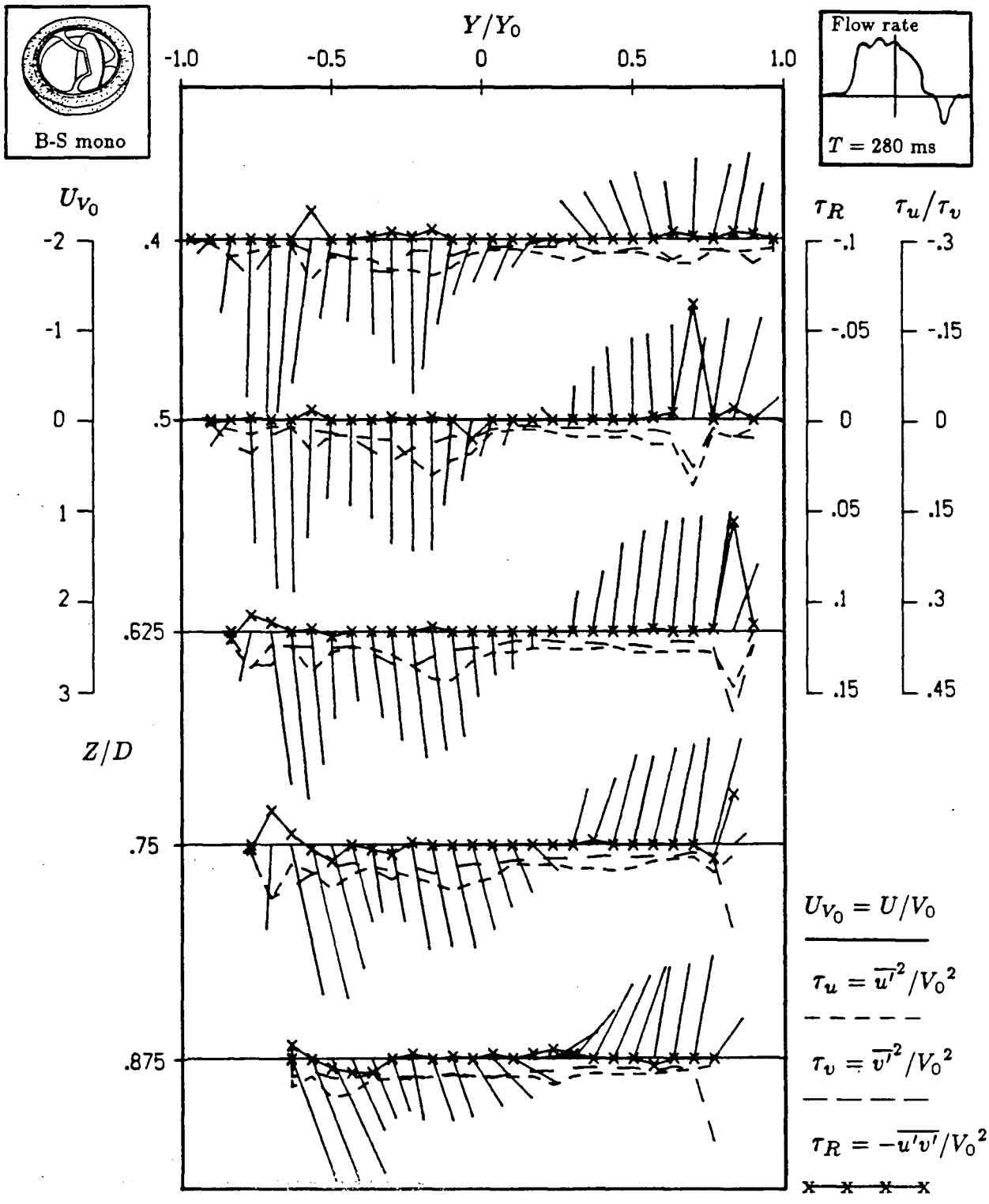

Figure 4-29 Variation of the nondimensional velocity, normal stresses, and the Reynolds stress at five downstream locations for the Björk-Shiley monostrut prosthesis (27 mm) in the posterior orientation (T = 280 ms).

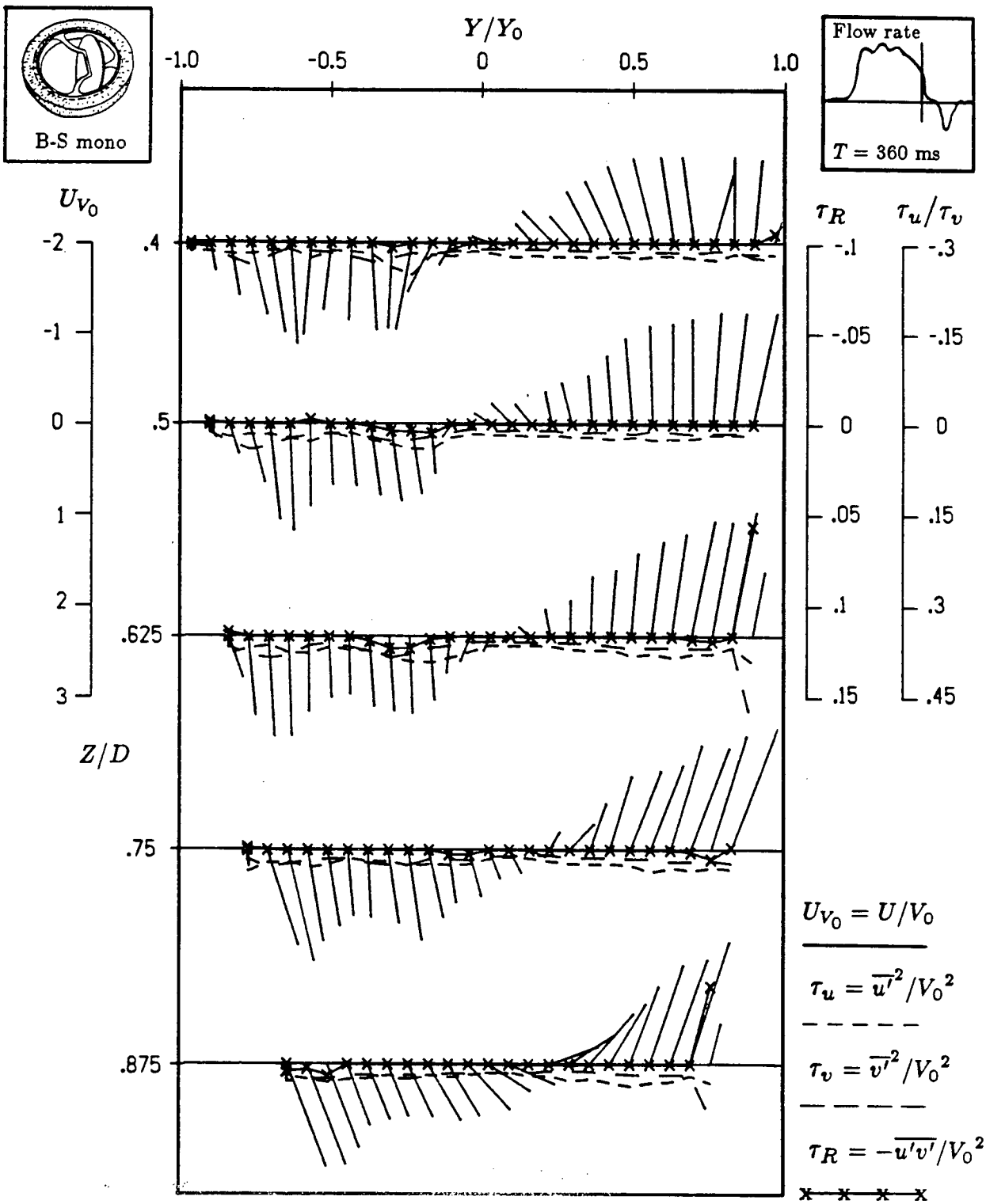

Figure 4-30 Variation of the nondimensional velocity, normal stresses, and the Reynolds stress at five downstream locations for the Björk-Shiley monostrut prosthesis (27 mm) in the posterior orientation (T = 360).

Both Figure 4-31 and Figure 4-32 show a dominance of the acceleration-phase in the region close to the annulus. In fact, for the peak stresses (Figure 4-31), the acceleration-phase dominates at all five stations with the highest levels at 0.625D for the normal stress and 0.5D for the Reynolds stress, respectively. However, the picture changes when the stresses are averaged over each phase (Figure 4-32). The accelerating-phase still dominates close to the annulus but then the peak phase dominates at the last two stations. This suggests that the high accelerating stresses are short-lived further downstream. Similar trends of high averaged stresses downstream were also observed for the posterior orientation of the B-S c-c. This is not surprising as both valves are similar in design and only differ in the opening angle and outflow strut configuration.

(c) Anterior vs Posterior Orientation

Based on the peak Reynolds and normal stresses (Figure 4-33), it is not clear which orientation is better as both the configurations show similar trends. It is noticeable that the highest stresses for an anterior orientation occur closer to the annulus while those for a posterior orientation manifest further downstream. This is also evident when the stresses are averaged over the diastolic cycle (Figure 4-34). However, the peak average results give a somewhat conflicting picture. Looking close to the annulus, the posterior orientation seems promising, while downstream the anterior orientation appears better. If the frequency spectrum of the turbulence is taken into account then the posterior orientation would appear to be better. This is because the turbulence closer to the annulus has a higher frequency component. As the fluid moves further downstream, it loses energy and therefore the turbulence

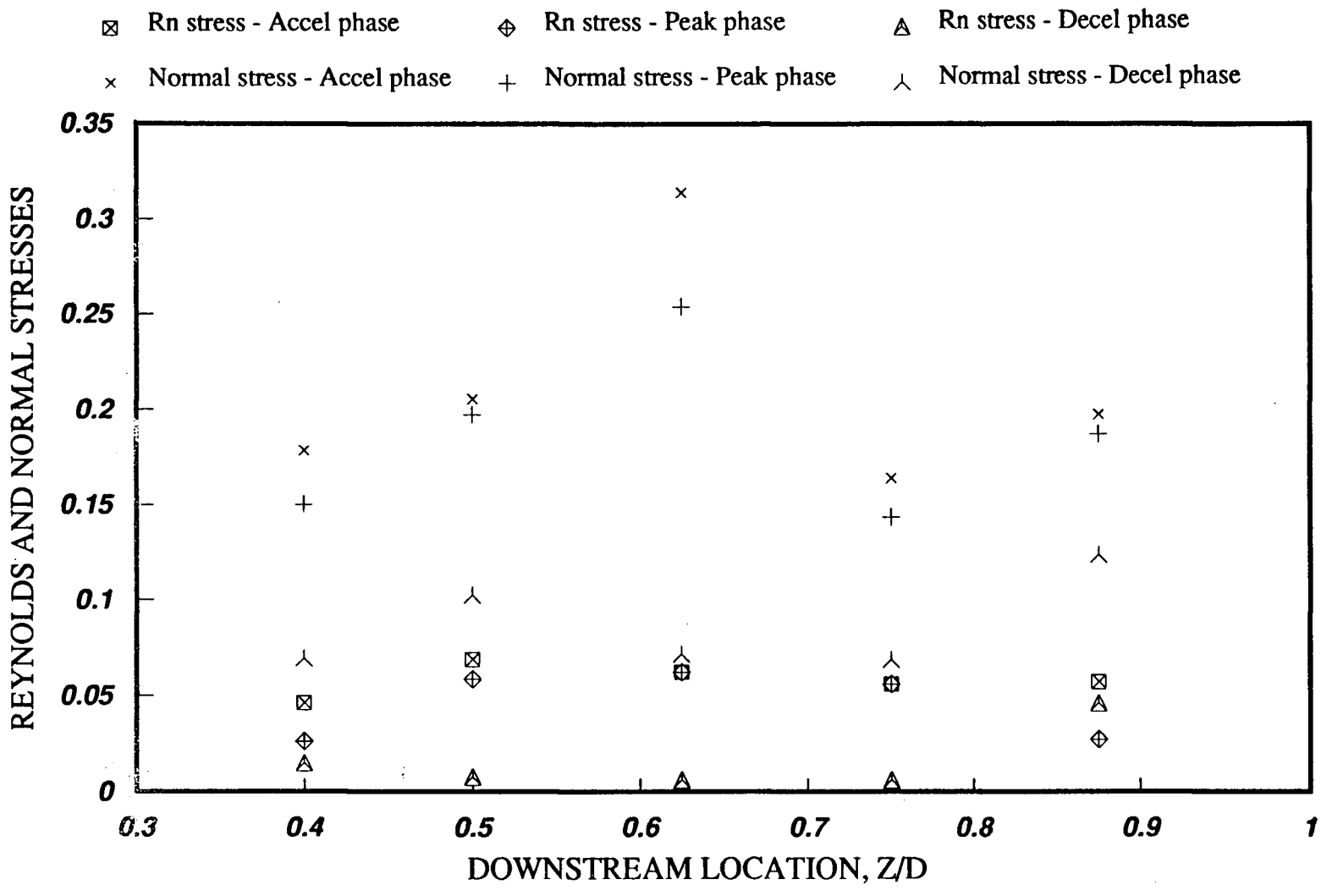

Figure 4-31 Variation of the nondimensional normal stresses and the Reynolds stress during the three phases of diastole at five downstream locations for the Björk-Shiley monostrut prosthesis in the posterior orientation (27mm, Peak stresses).

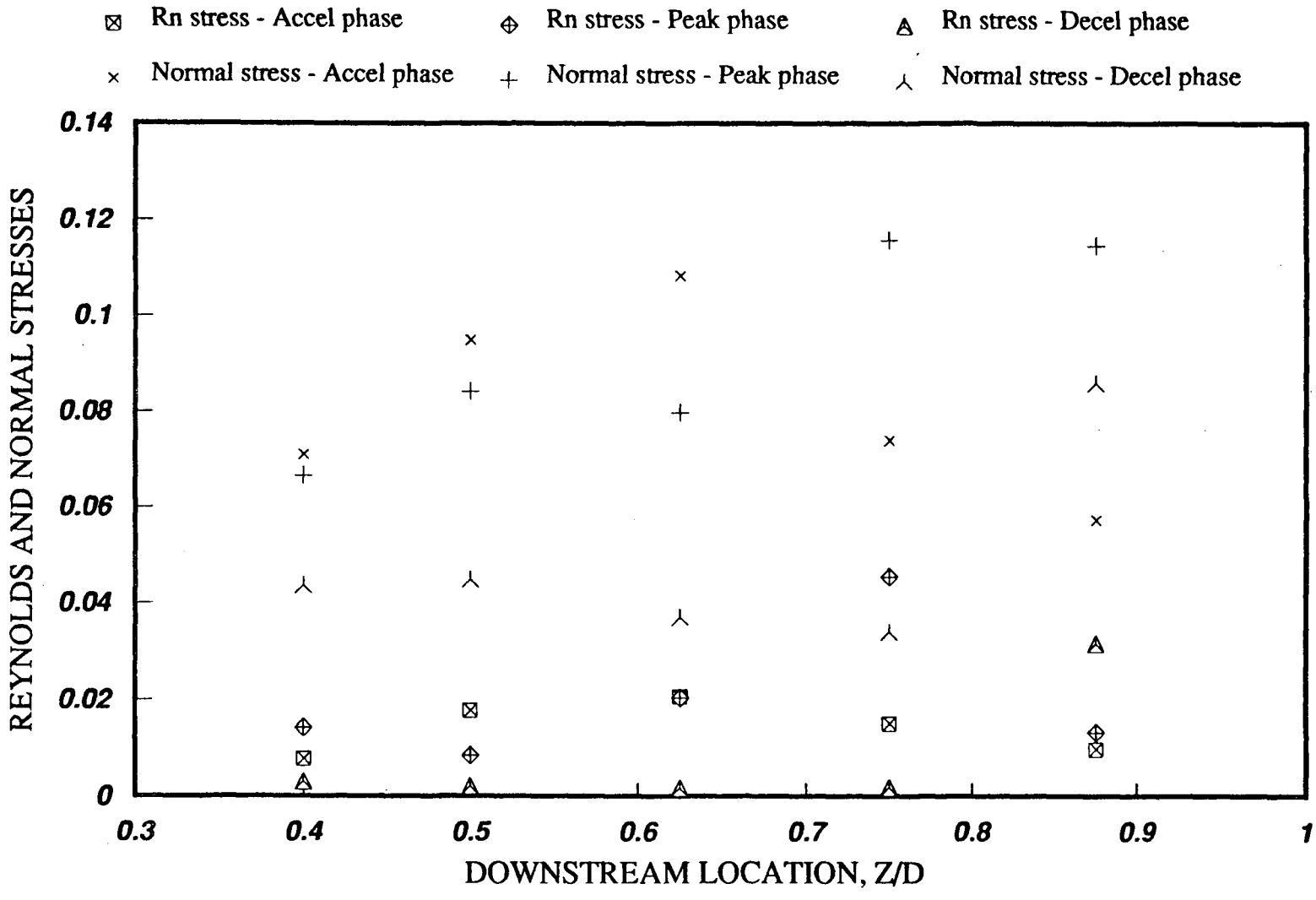

Figure 4-32 Variation of the nondimensional normal stresses and the Reynolds stress during the three phases of diastole at five downstream locations for the Björk-Shiley monostrut prosthesis in the posterior orientation (27mm, Peak average stresses).

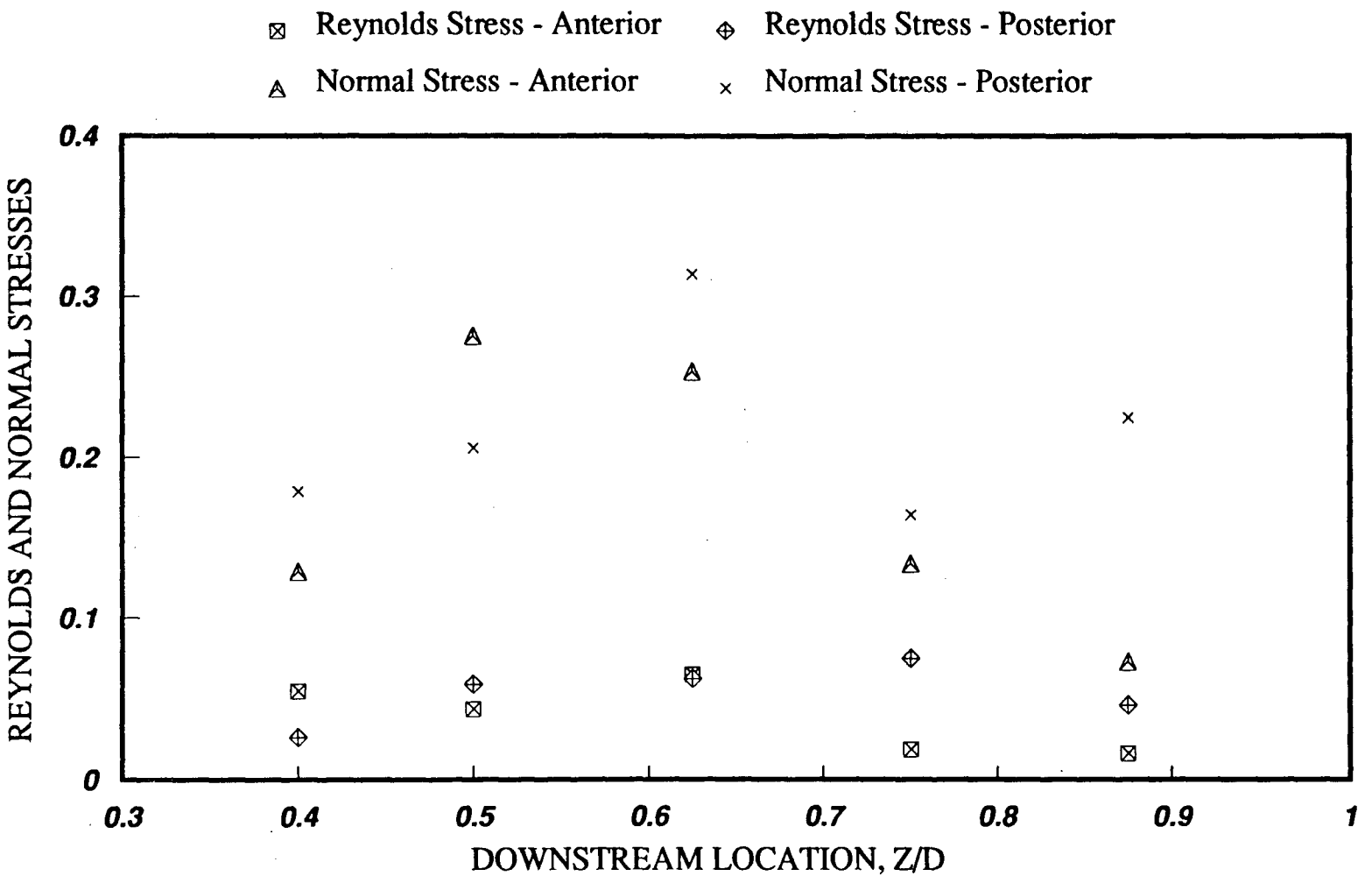

Figure 4-33 Variation of the nondimensional Reynolds and normal stresses at five downstream stations for the anterior and posterior orientations of the Björk-Shiley monostrut prosthesis (27mm, Peak stresses).

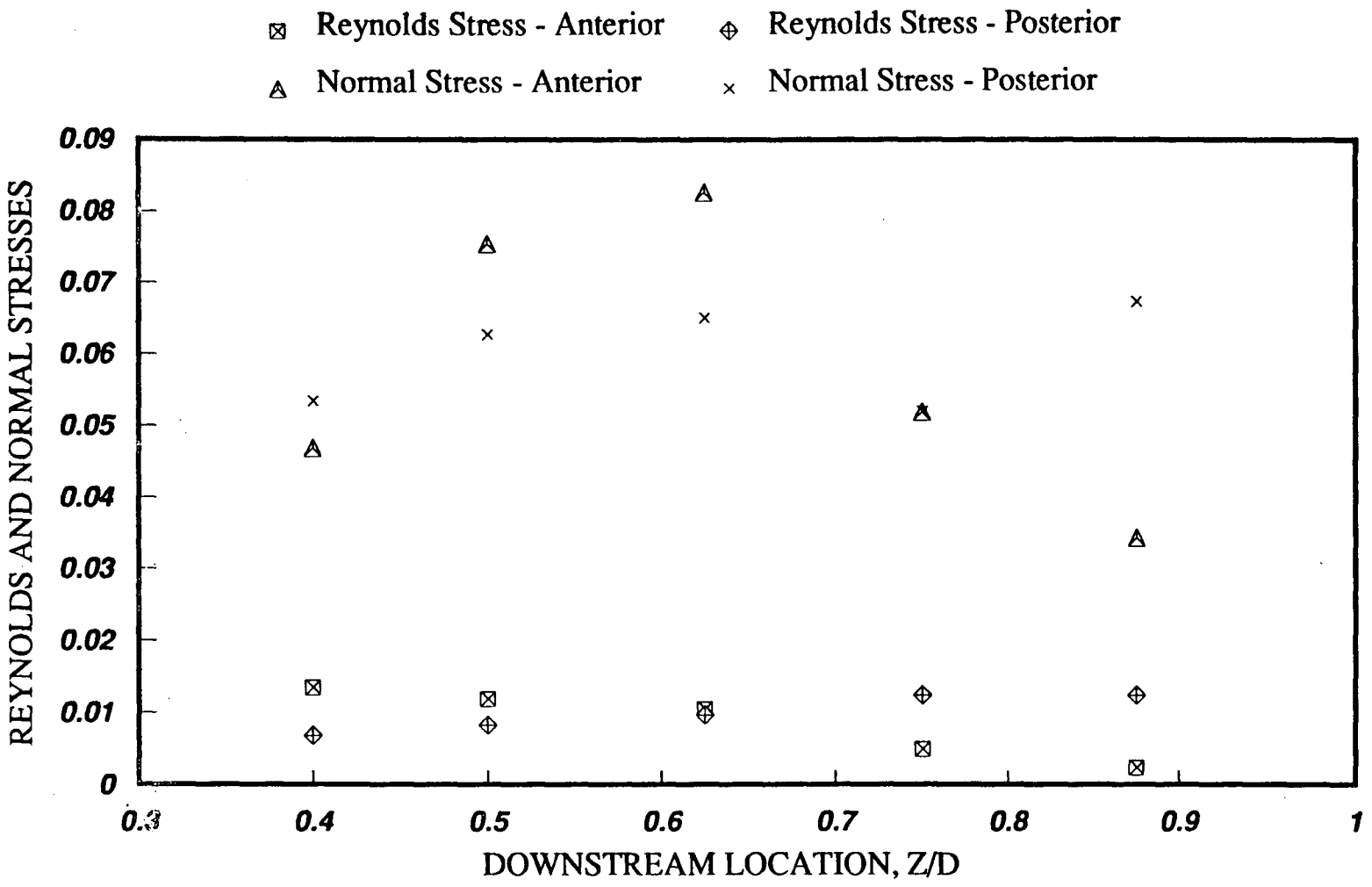

Figure 4-34 Variation of the nondimensional Reynolds and normal stresses at five downstream stations for the anterior and posterior orientations of the Björk-Shiley monostrut prosthesis (27mm, Peak average stresses).

is at a lower frequency. It is reasonable to expect that a higher frequency turbulence would inflict more damage, i.e., the posterior orientation would be desirable for the B-S mono valve.

4.1.3 Bicer Val

(a) Anterior Orientation

The flow character of the Bicer valve differs markedly from the other two configurations particularly close to the annulus. At 0.4D and 0.5D, there is only a single jet-flow rather than two as observed in the other configurations. This would suggest that there is little flow separation due to the valve geometry. This may be attributed to the aerofoil shaped disc, unobtruding inflow strut mechanism and wider opening angle thus deflecting the flow by a relatively smaller amount. This leads to all the fluid dynamic parameters to be smaller closer to the valve location. In fact, the maximum Reynolds stress and peak turbulent normal stress at the 0.4D location are substantially lower than those for either of the B-S valves. The same trend is observed at 0.5D; however, at 0.625D, sharp increases in both Reynolds and normal stresses are recorded in the time history profile at around 120 ms (Figure 4-35). Also, the single jet formation seen at 0.4D and 0.5D is no longer present. At this station, the flow starts to diverge with a part of the flow from the major orifice deflected upwards to form the counterclockwise vortex. The other part forms a clockwise vortex which interacts with the downward flow from the minor orifice producing a stagnant region in the centre of the ventricle.

Figure 4-36 shows the steep rise in stresses just after the initiation of the flow. Note that the highest stresses appear at the 0.625D location. As the trend has been,

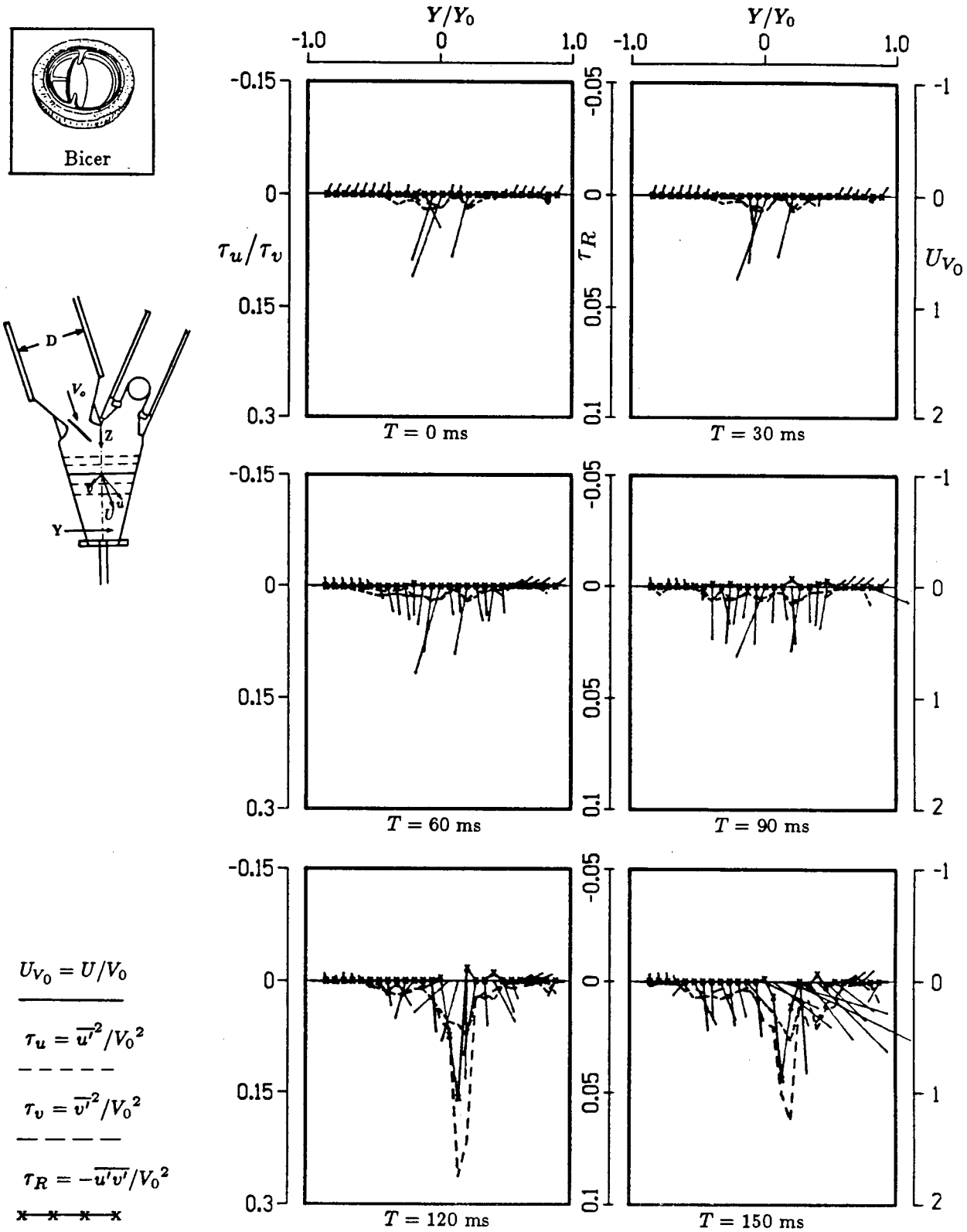

Figure 4-35 Time history of velocity and stress profiles for the Bicer-Val prosthesis in the anterior orientation at Z = 0.625D (0 - 150 ms).

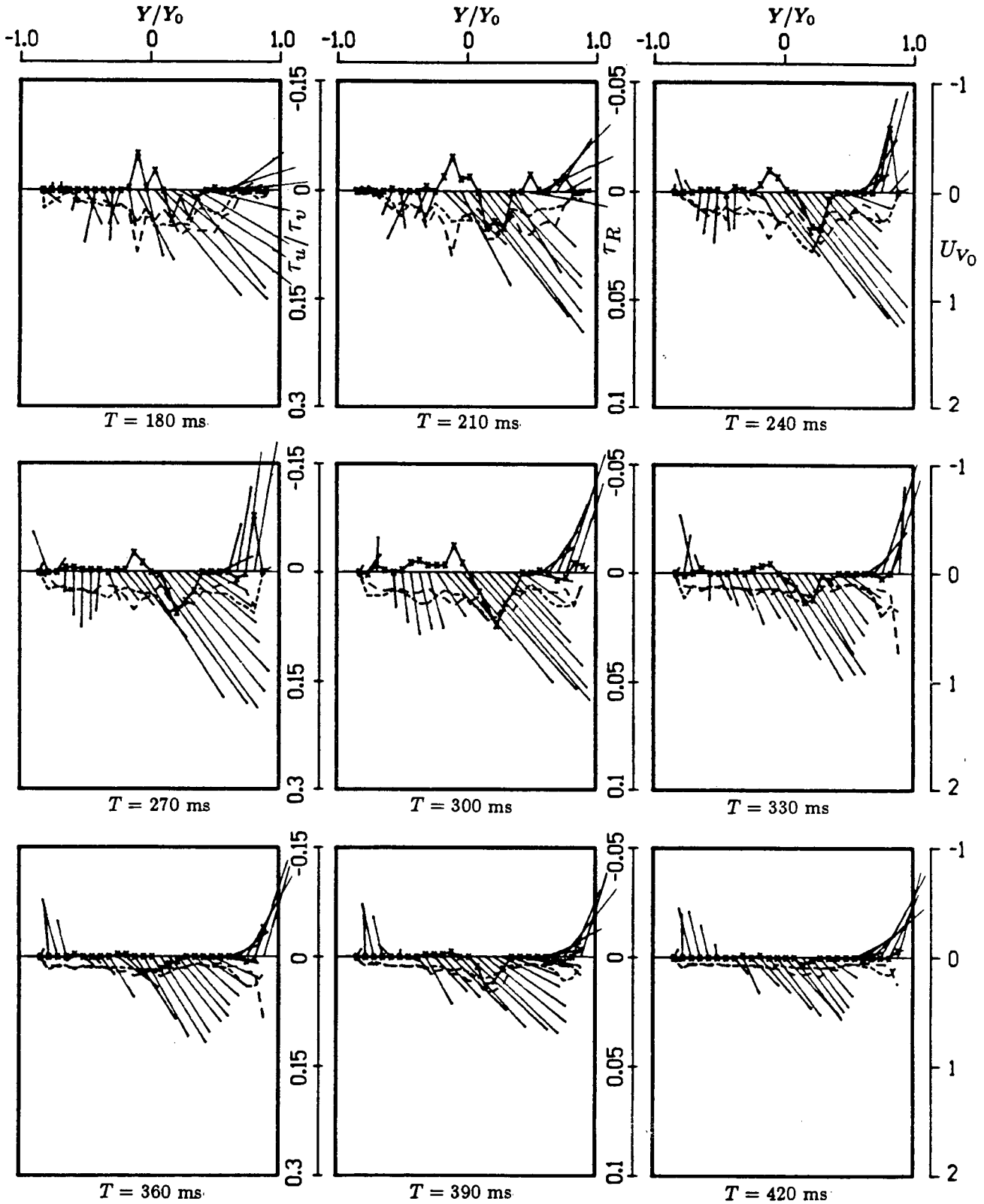

Figure 4-35 Time history of velocity and stress profiles for the Bicer-Val prosthesis in the anterior orientation at Z = 0.625D (180 - 420 ms).

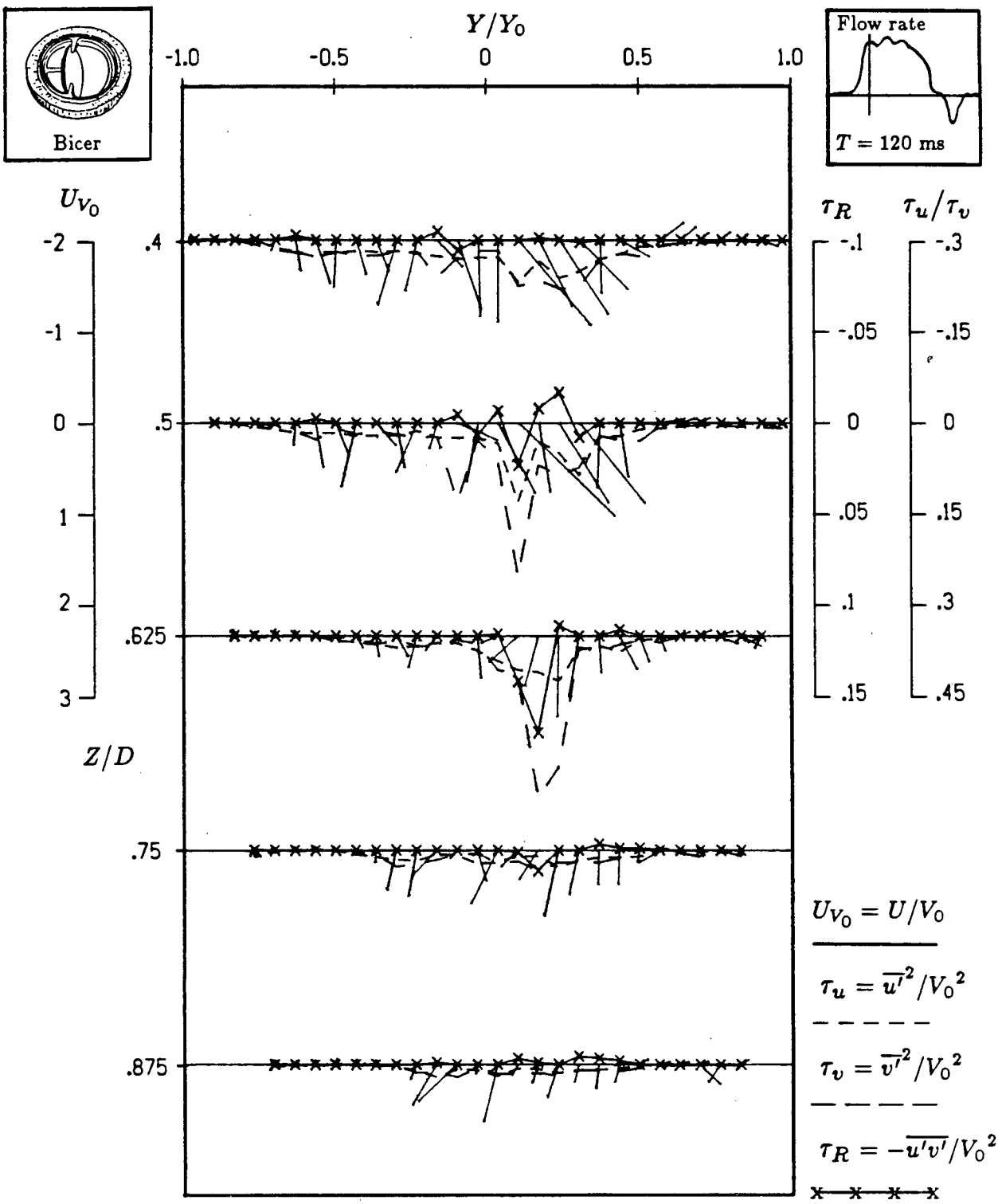

Figure 4-36 Variation of the nondimensional velocity, normal stresses, and the Reynolds stress at five downstream locations for the Bicer-Val prosthesis (27 mm) in the anterior orientation (T = 120 ms).

the larger the disc opening angle, the further downstream the highest stresses occur. The highest Reynolds and normals stresses at this station during the acceleration phase were 240 dynes/cm^2 and 1397 dynes/cm^2, respectively. However, by the time the peak flow phase is reached (Figure 4-37), there is a marked reduction in the stresses (114 dynes/cm^2 for the Reynolds stress and 309 dynes/cm^2 for the normal stress).

The deceleration-phase (Figure 4-38) is marked by a further reduction in stresses at all stations. This figure gives a good picture of the two counterrotating vortices present in the ventricle.

As observed before, Figures 4-39 and 4-40 confirm that the overall highest normal and Reynolds stresses occur at 0.625D during the acceleration-phase. The highest stresses at each downstream location also correspond to the accelerating-phase. Note, again the higher stresses occur close to the annulus for an anterior orientation. This is also the case for averaged stress fields (Figure 4-40). However, the highest stresses at the two furthest locations now occur during the peak phase suggesting that the accelerating peak stresses are short-lived, the conclusion arrived at earlier.

(b) Posterior Orientation

Figure 4-41 shows the time history of system parameter variations for the posterior orientation. As seen with the other two valves, a single vortex forms inside the ventricle. After the initial peaks, seen during the early acceleration-phase (Figure 4-42), stresses decrease in the later stages of the acceleration and peak phases (Figure 4-43). As for the anterior configuration, the maximum stresses during acceleration were experienced at 0.625D. The maximum Reynolds stress was found

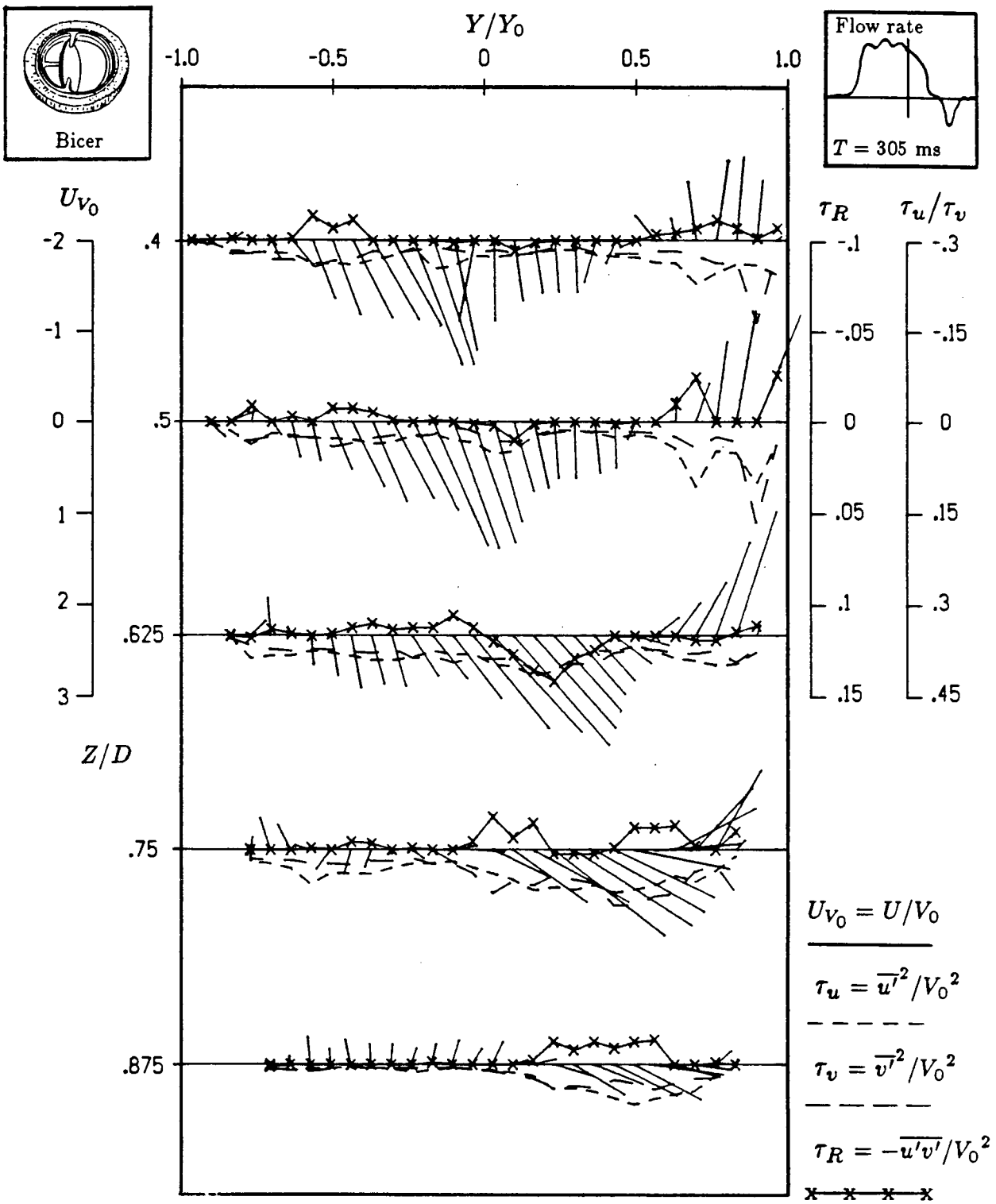

Figure 4-37 Variation of the nondimensional velocity, normal stresses, and the Reynolds stress at five downstream locations for the Bicer-Val prosthesis (27 mm) in the anterior orientation (T = 305 ms).

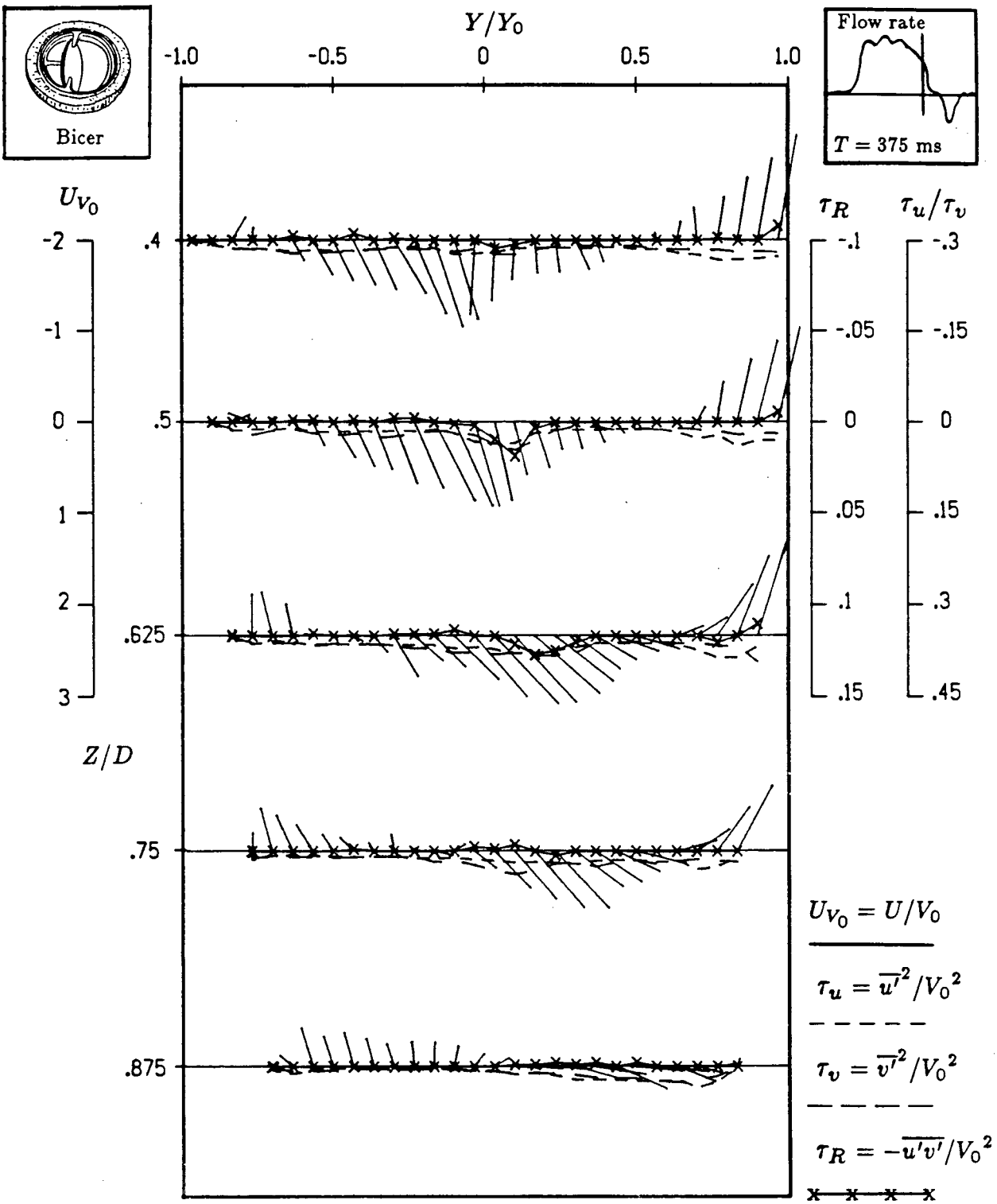

Figure 4-38 Variation of the nondimensional velocity, normal stresses, and the Reynolds stress at five downstream locations for the Bicer-Val prosthesis (27 mm) in the anterior orientation (T = 375 ms).

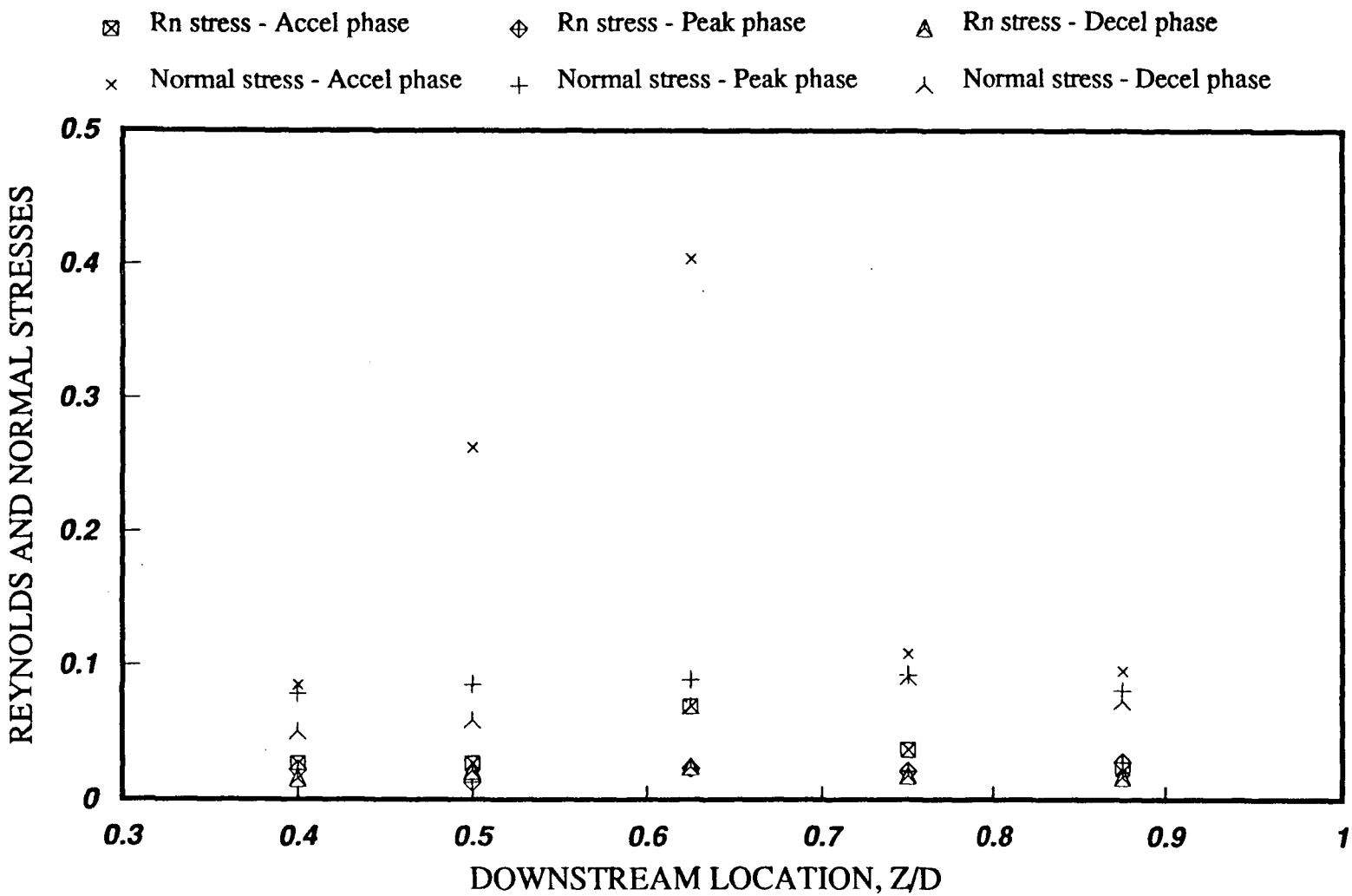

Figure 4-39 Variation of the nondimensional normal stresses and the Reynolds stress during the three phases of diastole at five downstream locations for the Bicer-Val prosthesis in the anterior orientation (27mm, Peak stresses).

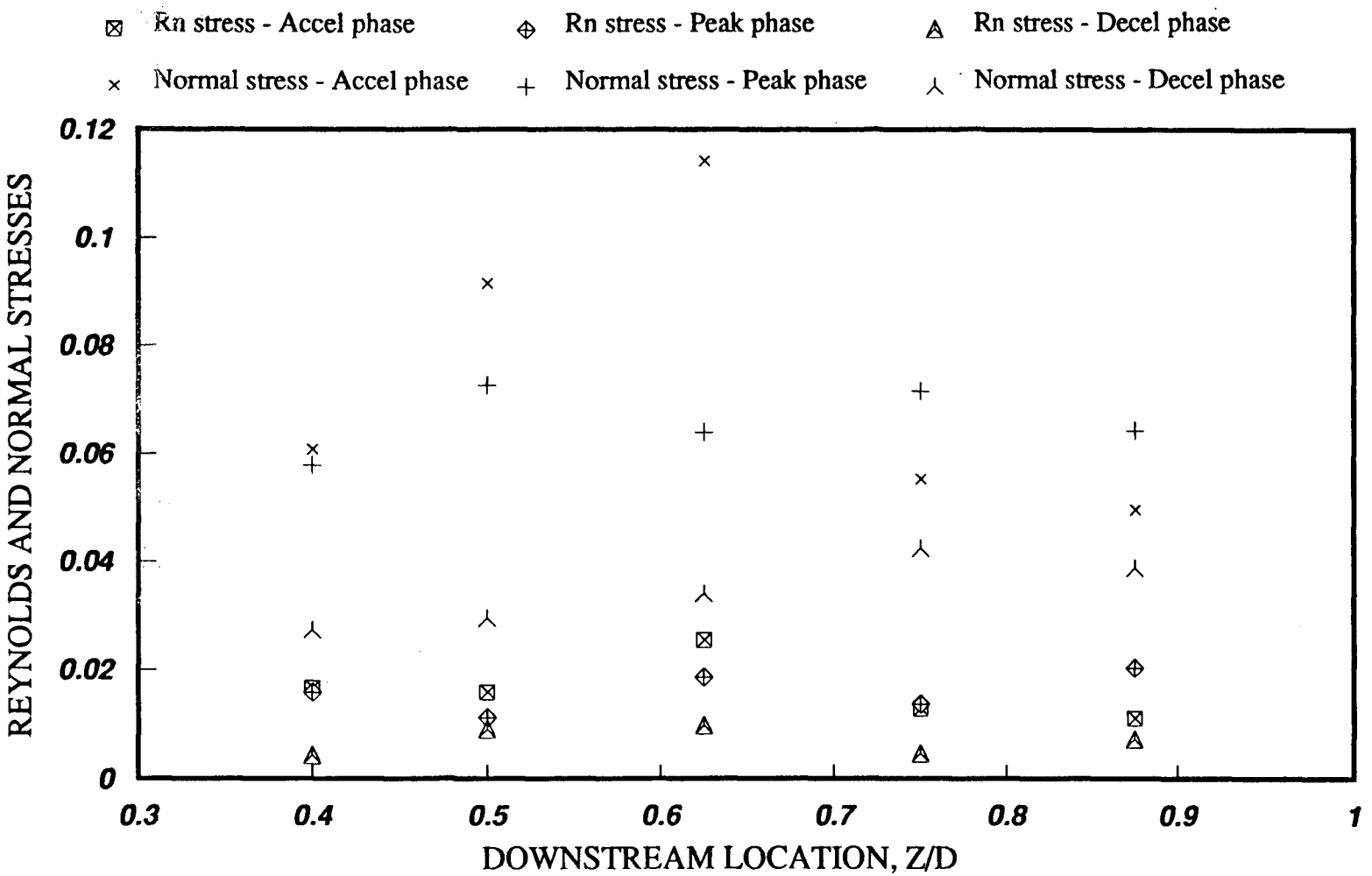

Figure 4-40 Variation of the nondimensional normal stresses and the Reynolds stress during the three phases of diastole at five downstream locations for the Bicer-Val prosthesis in the anterior orientation (27mm, Peak average stresses).

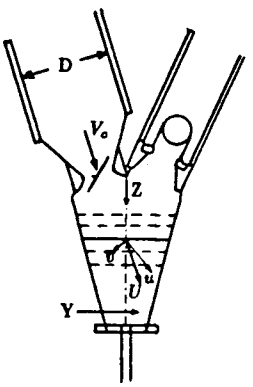

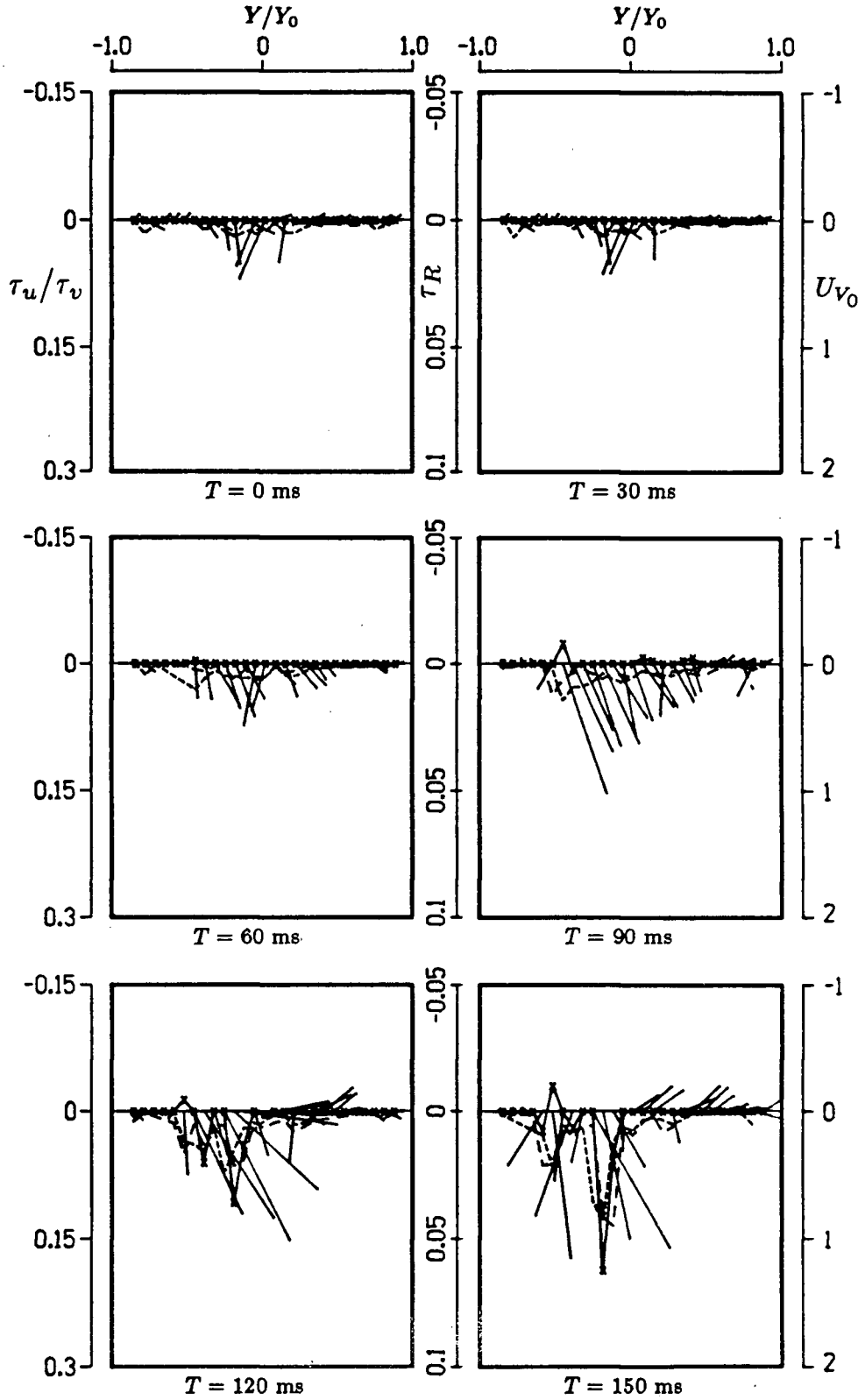

$U_{V_0} = U/V_0$

$\tau_u = \overline{u'}^2/{V_0}^2$

$\tau_v = \overline{v'}^2/{V_0}^2$

$\tau_R = -\overline{u'v'}/{V_0}^2$

Figure 4-41 Time history of velocity and stress profiles for the Bicer-Val prosthesis in the posterior orientation at Z = 0.625D (0 - 150 ms).

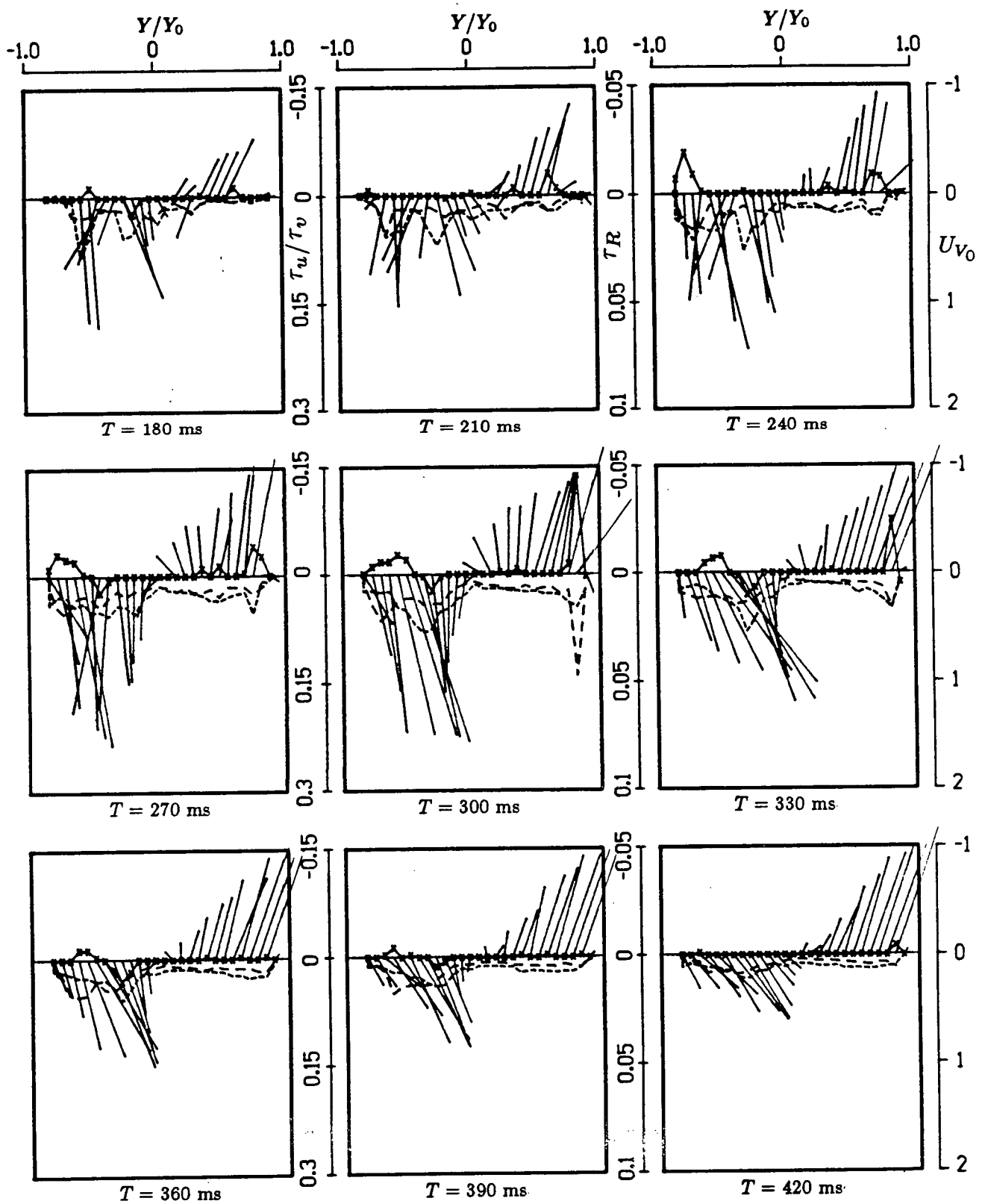

Figure 4-41 Time history of velocity and stress profiles for the Bicer-Val prosthesis in the posterior orientation at Z = 0.625D (180 - 420 ms).

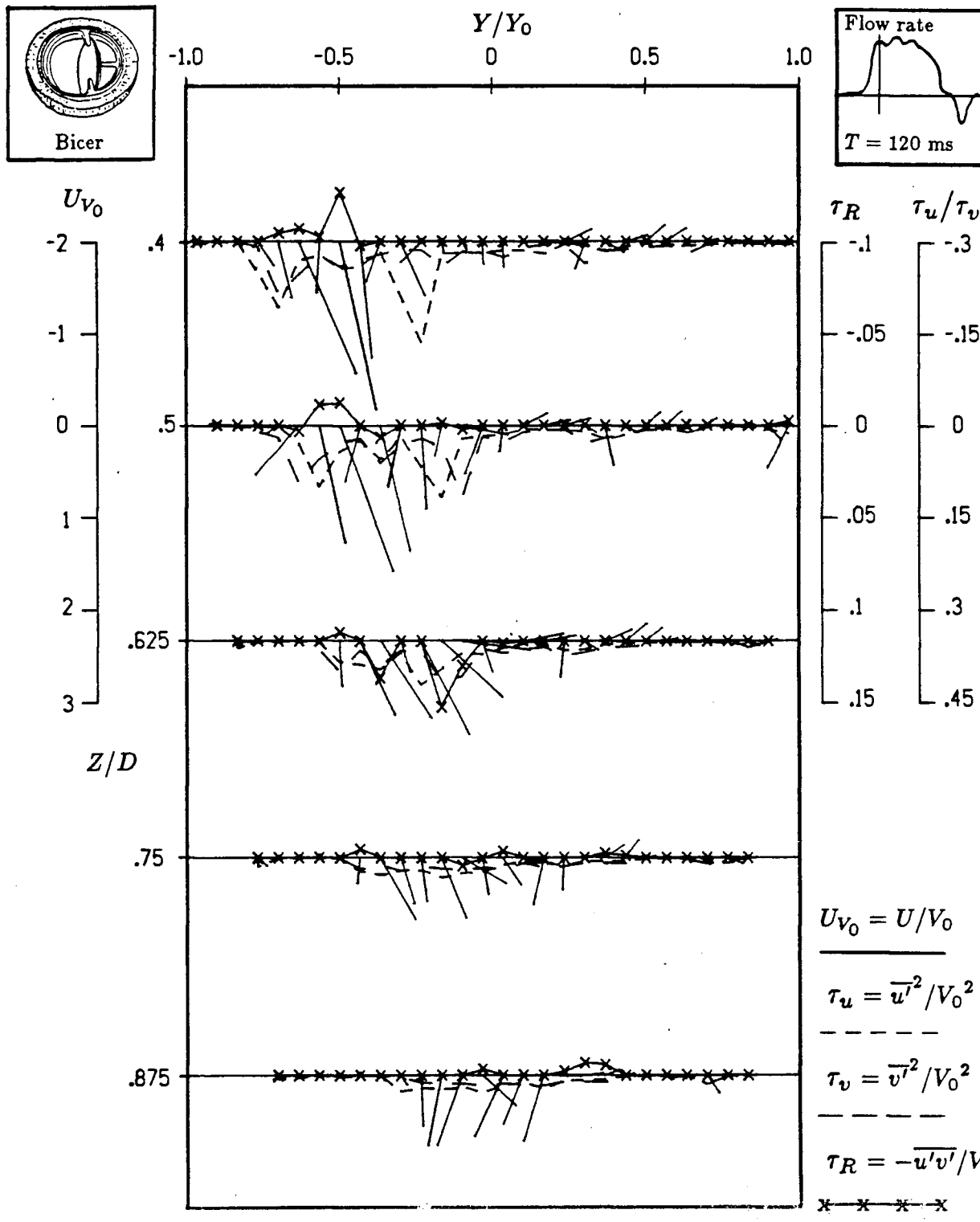

Figure 4-42 Variation of the nondimensional velocity, normal stresses, and the Reynolds stress at five downstream locations for the Bicer-Val prosthesis (27 mm) in the posterior orientation (T = 120 ms).

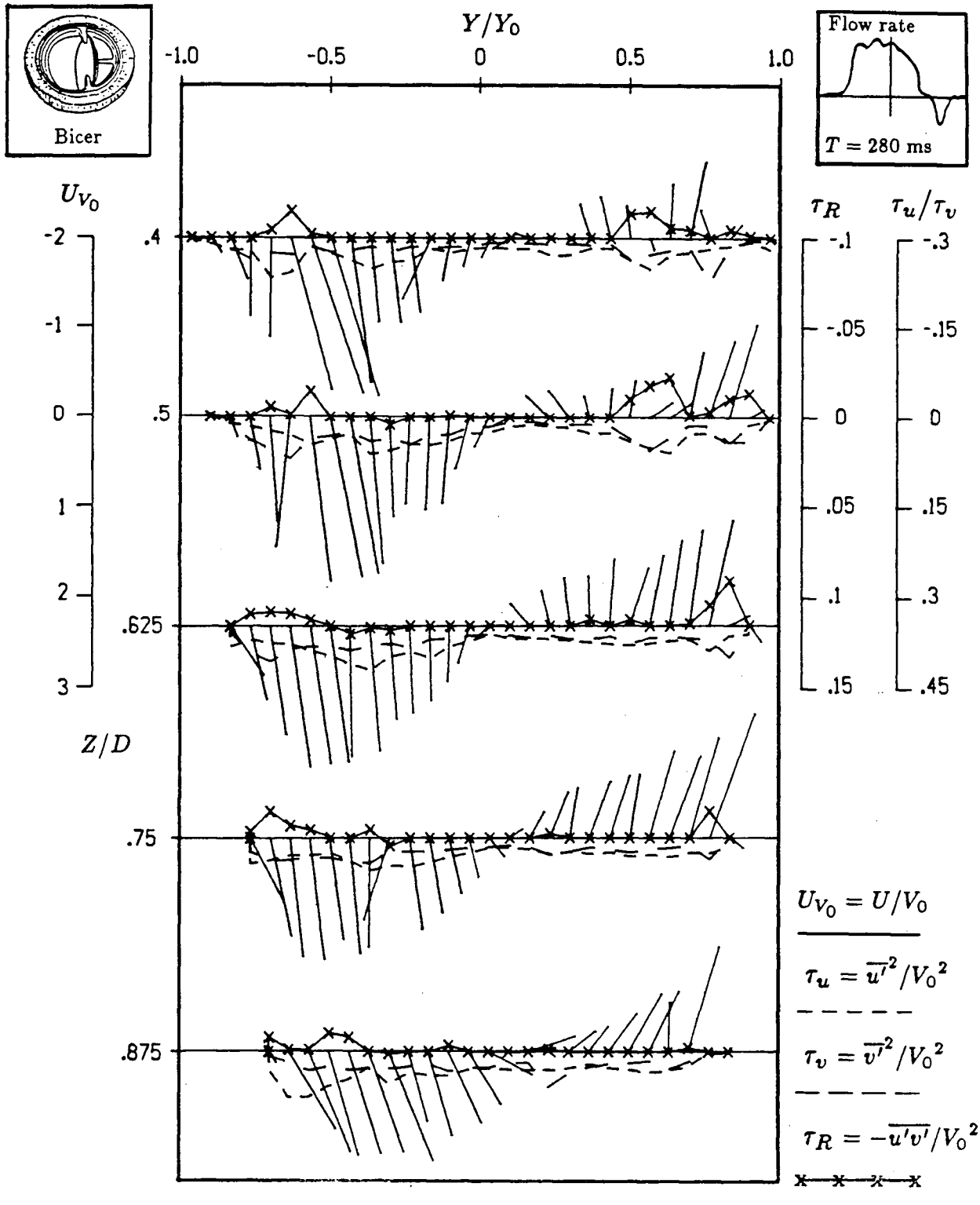

Figure 4-43 Variation of the nondimensional velocity, normal stresses, and the Reynolds stress at five downstream locations for the Bicer-Val prosthesis (27 mm) in the posterior orientation (T= 280 ms).

to be 236 dynes/cm^2 while the maximum normal stress was 545 dynes/cm^2. These are marked reductions from those observed for the anterior orientation. The flow character at the five downstream locations is worth noting. It did not show two peaks at any of the stations suggesting that there is little flow separation occurring at the annulus. As in the case of the anterior orientation, this can be attributed to the valve geometry.

Deceleration-phase (Figure 4-44) continues to be quiescent as before. This plot gives a good representation of the vortex circulation pattern typically observed for posterior orientations of the tilting disc valves.

Figure 4-45 shows the peak stresses developed during the three phases. The stresses are highest near the annulus during the acceleration phase and highest further downstream during the peak phase. However, overall, the acceleration phase is clearly the dominant phase as found for the other two valves. When averaged over the diastole phase (Figure 4-46), a similar trend can be observed for both the normal and Reynolds stresses with the acceleration phase still dominant. Note, however, that close to the annulus, the acceleration peak stresses are not that much higher than the maximum peak phase stresses. This suggests that the acceleration peak stresses are not dominant for the entire duration of the phase.

(c) Anterior vs. Posterior Orientation

As observed earlier, the peak Reynolds and normal stresses occur at the 0.625D station, regardless of the orientation. Figure 4-47, showing the peak stresses for both valves, confirms this observation. This can be attributed to the disc opening angle. However, the higher peaks were observed with an anterior orientation. The

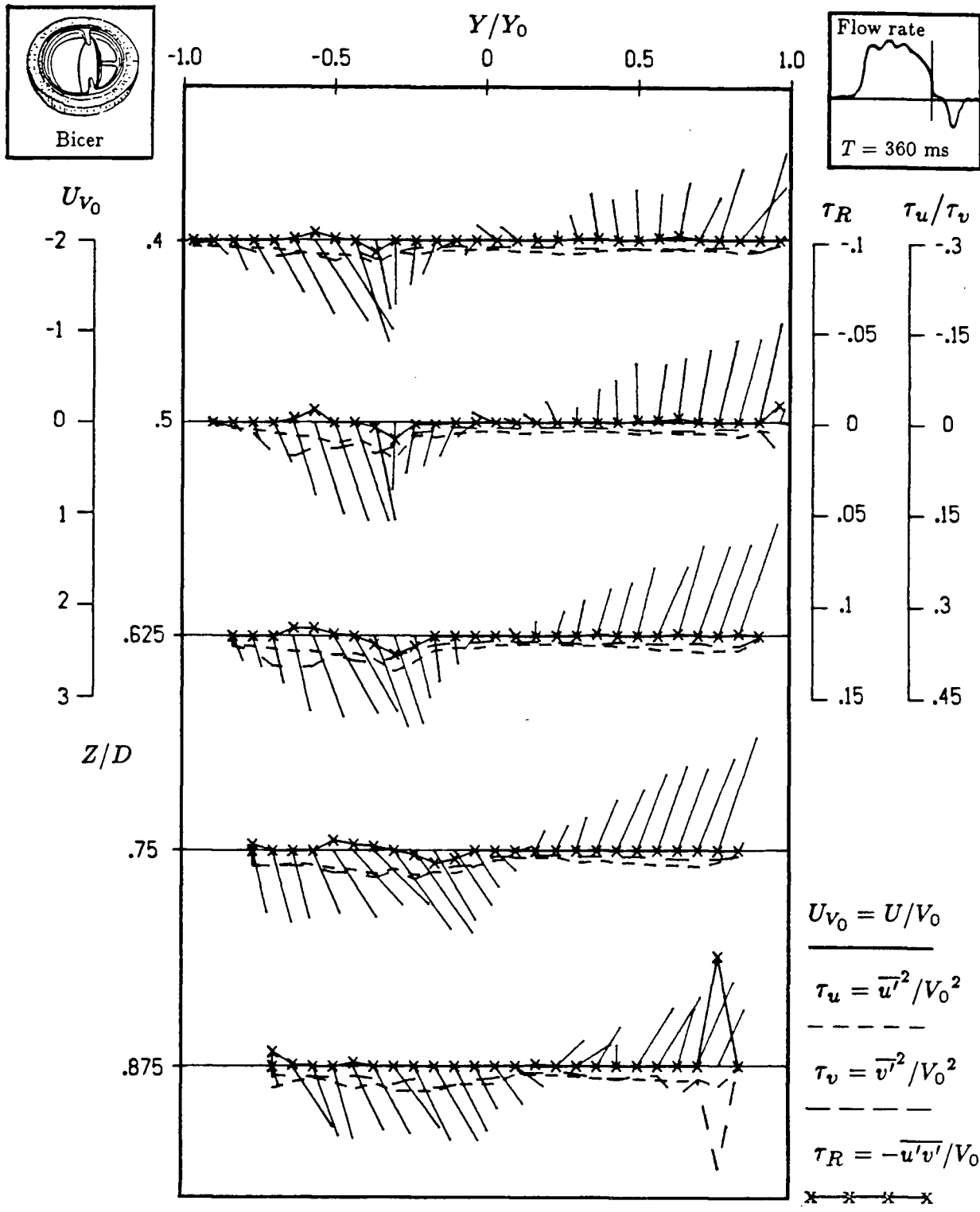

Figure 4-44 Variation of the nondimensional velocity, normal stresses, and the Reynolds stress at five downstream locations for the Bicer-Val prosthesis (27 mm) in the posterior orientation (T = 360 ms).

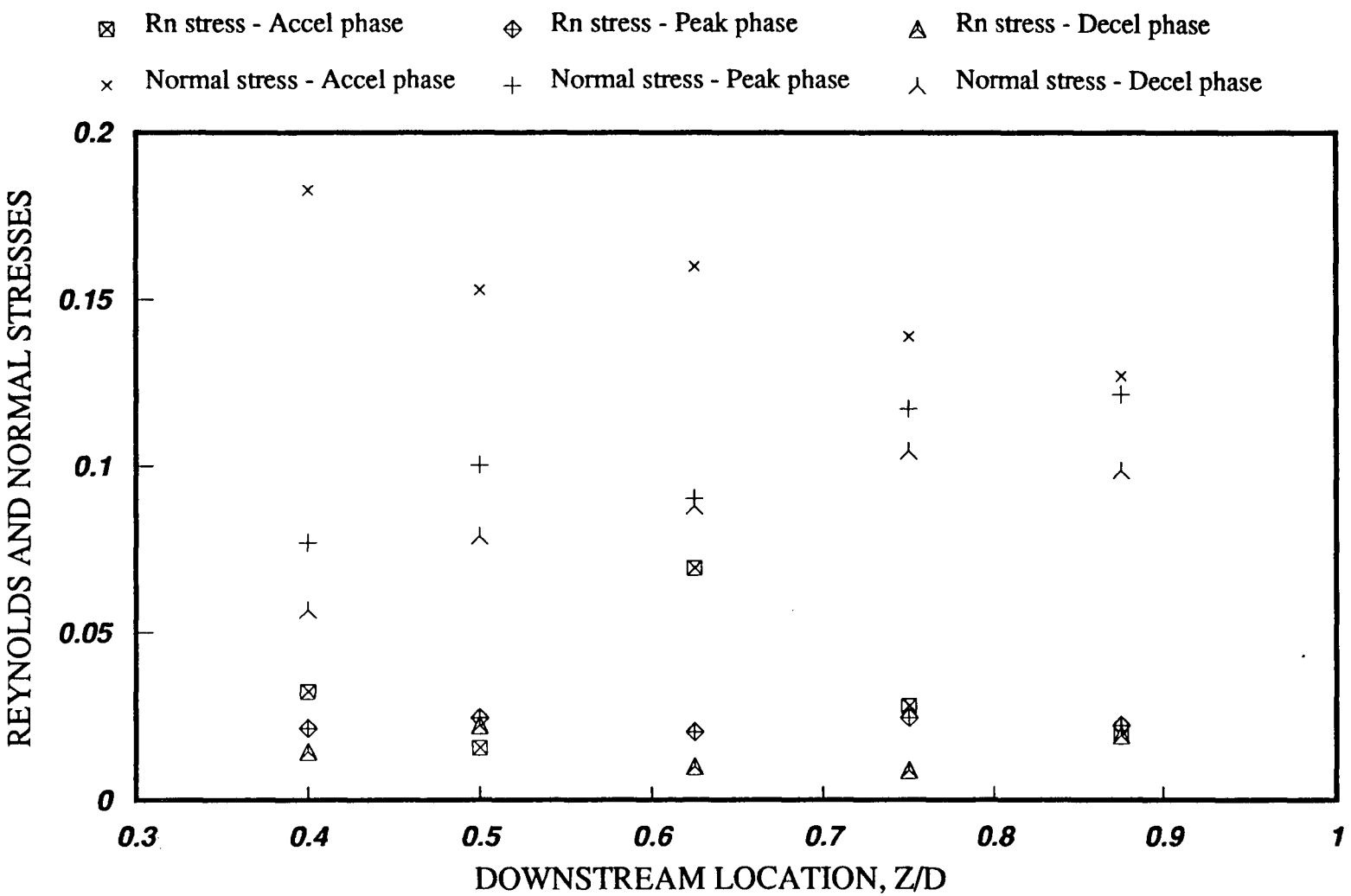

Figure 4-45 Variation of the nondimensional normal stresses and the Reynolds stress during the three phases of diastole at five downstream locations for the Bicer-Val prosthesis in the posterior orientation (27mm, Peak stresses).

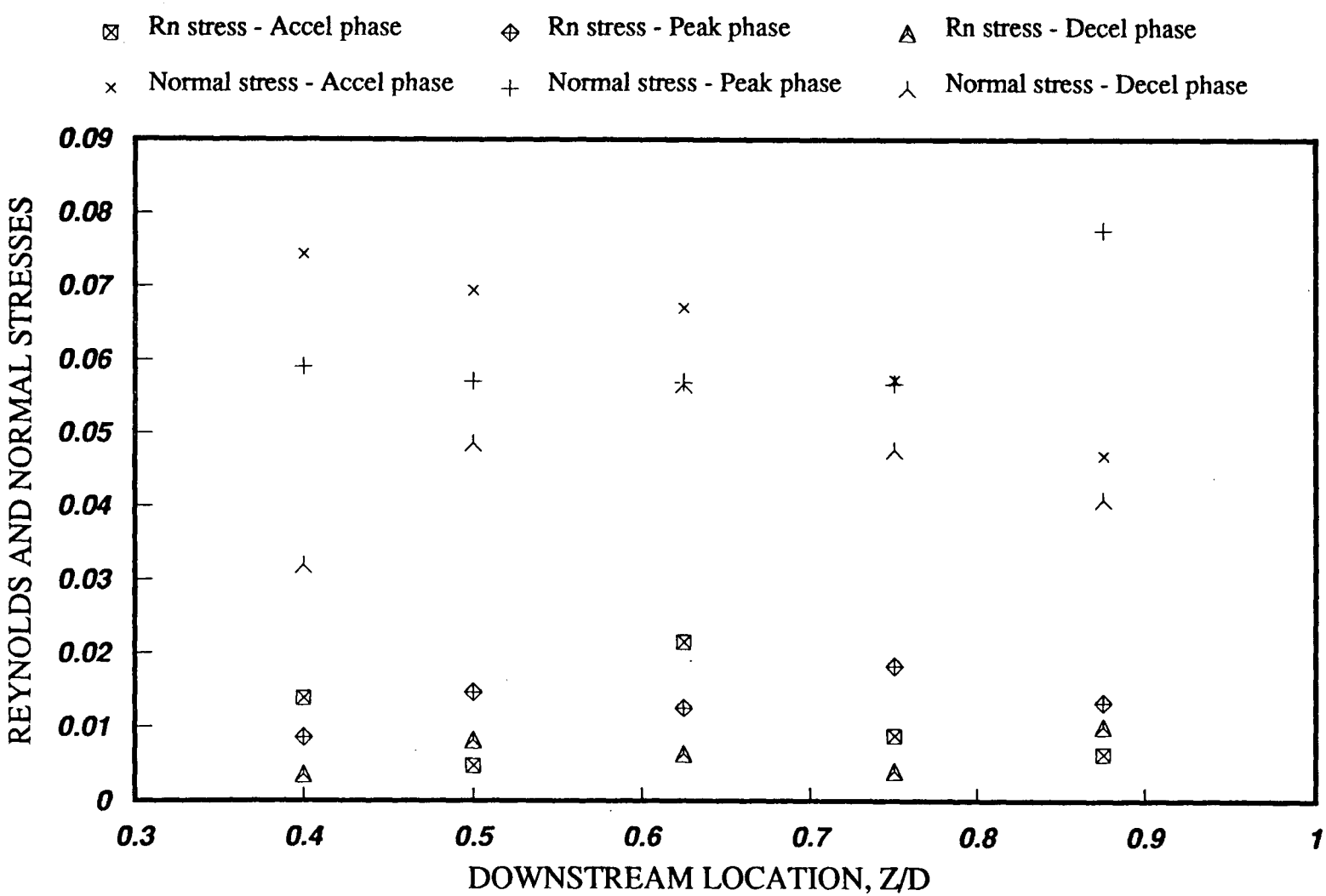

Figure 4-46 Variation of the nondimensional normal stresses and the Reynolds stress during the three phases of diastole at five downstream locations for the Bicer-Val prosthesis in the posterior orientation (27mm, Peak average stresses).

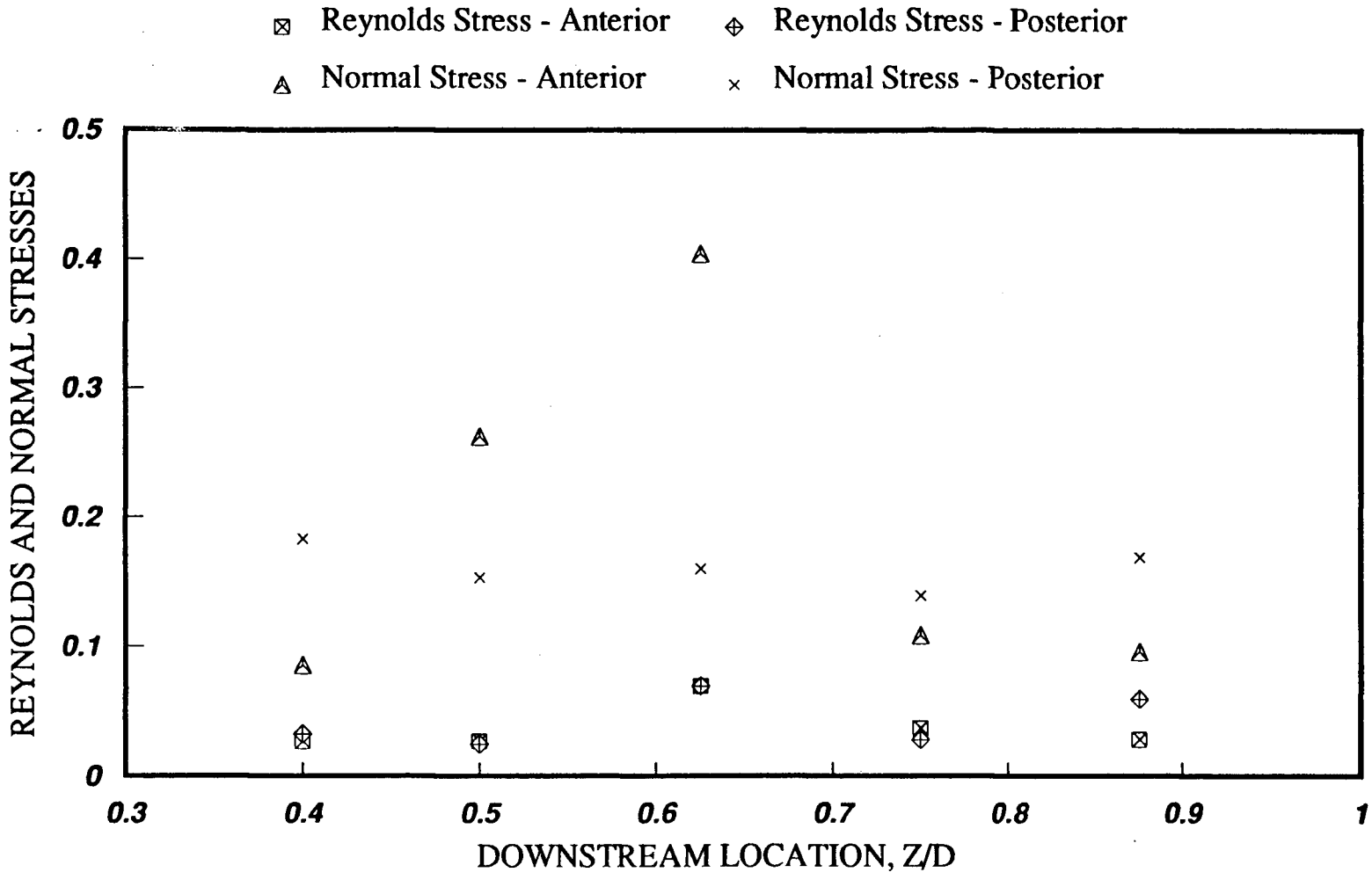

Figure 4-47 Variation of the nondimensional Reynolds and normal stresses at five downstream stations for the anterior and posterior orientations of the Bicer-Val prosthesis (27mm, Peak stresses).

posterior orientation had peaks at the 0.4D, 0.75D, and 0.825D stations; however, these peaks are relatively short-lived as seen in Figure 4-48. Here, both the Reynolds and normal stresses for the anterior orientation are generally worse. Note, that for an anterior orientation, the stresses rise to a peak at 0.625D then decrease further downstream while in a posterior orientation, the stresses remain at a relatively constant level at all downstream locations. This was generally true for all the three mechanical valves.

4.2 Summary of Comparative Performance (Mechanical Prostheses)

Tilting disc mechanical valves have been successfully used for twenty years. However, small changes in the design have been implemented over the years in an attempt to bring their function closer to that of the natural valve. As well, changes have been introduced to eliminate problems that have arisen over the years (e.g., one piece construction of the valve housing to eliminate strut fractures). The valves chosen in this study have undergone modifications as implemented by two manufacturers in an attempt to evolve more efficient configurations. The following summarizes essential configuration character of the three disc valves tested:

(a) Disc shape:

  (i) Björk-Shiley valves, convexoconcave;

  (ii) Bicer-Val, aerofoil shaped.

(b) Disc opening angle:

  (i) Björk-Shiley c-c, 60°;

  (ii) Björk-Shiley Monostrut, 70°;

  (iii) Bicer-Val, 75°.

(c) Strut configuration:

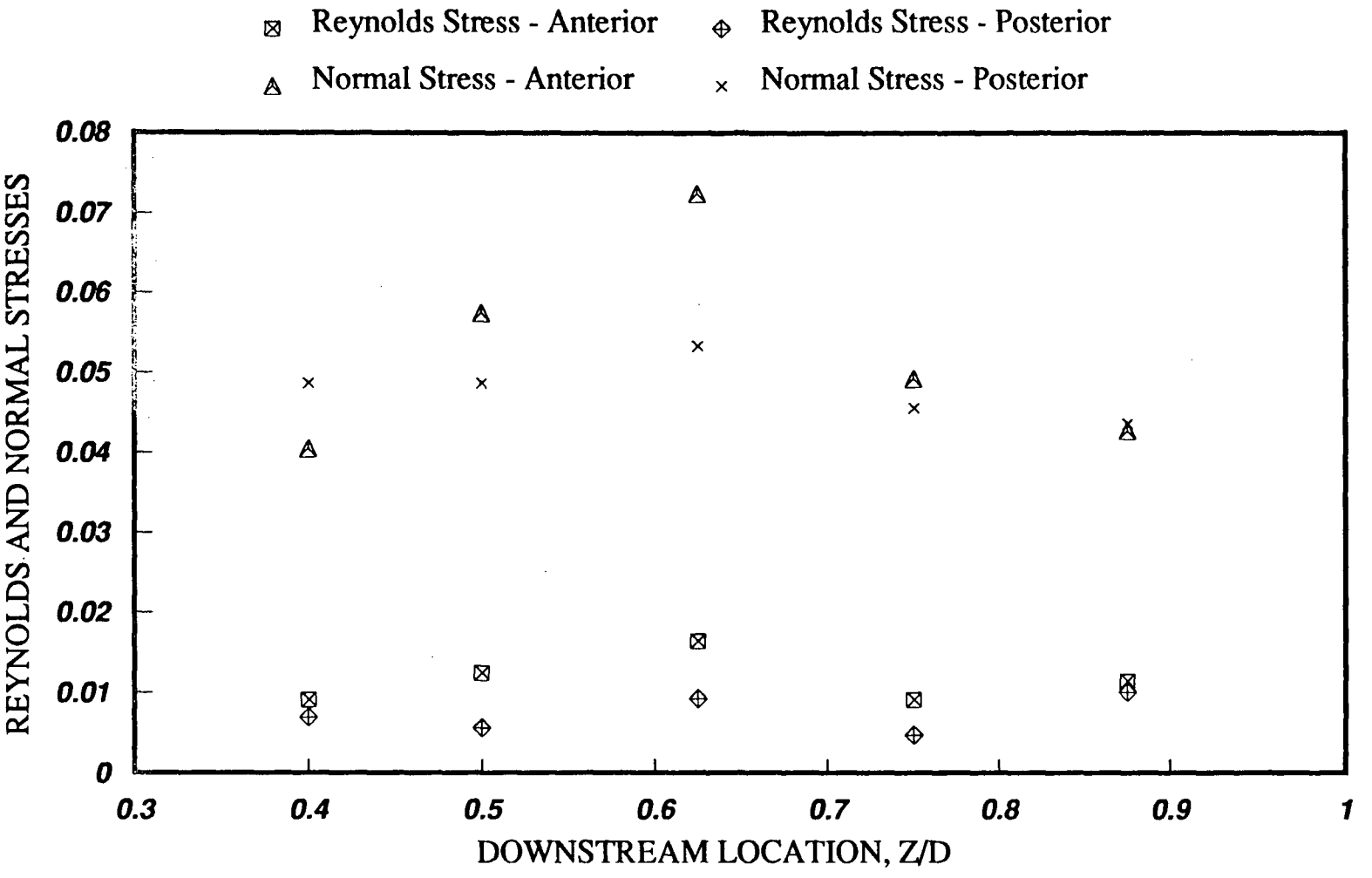

Figure 4-48 Variation of the nondimensional Reynolds and normal stresses at five downstream stations for the anterior and posterior orientations of the Bicer-Val prosthesis (27mm, Peak average stresses).

(i) Björk-Shiley c-c, inflow and outflow strut in line contact;

(ii) Björk-Shiley Monostrut, inflow strut in line contact and outflow strut in point contact with strut located in the middle of the minor orifice;

(iii) Bicer-Val, three point support mechanism with outflow strut located in the middle of the minor orifice.

Based on the results presented in the preceding sections, several observations can be made correlating locations of the highest stresses and the features of the valves themselves. At the outset, the obstruction of the strut structure and the discs disturb the flow fields significantly, creating high turbulent stresses. The turbulent intensity measurements showed high turbulent stresses occurred at locations that corresponded to high velocity gradients. This was usually confined to the edges of the jet-like flow fields that developed as a result of the geometry of the tilting disc. The larger the opening angle, the further downstream the peak values occurred. Furthermore, the highest stresses were experienced during the acceleration-phase, and the lowest stresses occurred during the deceleration stage. This could be attributed to the highly turbulent flow associated with opening of the disc.

The B-S c-c has the smallest opening angle of 60° among the three valves. This, combined with the two struts that protrude into the two orifices and obstruct part of the flow, caused two quite prominent jets to form, one from each orifice. As a result, high stresses were observed. The B-S mono valve opens a further ten degrees and the protruding outflow strut is replaced with a monostrut. Although two prominent jets continue to form as before, the larger opening angle combined with the new strut configuration appears to offer less of an obstruction to the flow, thus lowering the stresses. As previously mentioned, the Bicer valve has several features which

are quite different from the Björk-Shiley prostheses. The larger opening angle (75°) combined with an aerofoil shaped disc deflects the flow minimally creating a nearly laminar central flow with lower stress values.

The main objective in comparing the valve performance in anterior and posterior positions is to seek a preferential orientation based on stress analysis. A valve that creates unacceptable levels of stresses in one orientation may produce significantly lower levels in the another orientation (the B-S c-c being a good example). Therefore, a valve should not be deemed unacceptable or inferior in performance until different orientations have been explored. However, it is important to point out that the optimal orientation may vary for in vivo operation due to inherent limitations in simulating a living system. For example, a posterior orientation in some hearts adversely effects the opening of a tilting disc due to residual chordae tendineae[57].

Generally speaking though, the flow fields obtained with an anterior orientation appear to be more complex than those for the posterior orientation. In the anterior configuration, the flow through the major and minor orifices form two counter-rotating vortices inducing high turbulent structures particularly in the centre of the ventricle. In the posterior orientation, a single vortex is formed in early diastole which is further augmented by the dominant flow through the major orifice during mid-diastole. Here, the vortex appears to have minimal effect on the flow compared to the anterior orientation.

To help facilitate assessment and comparison of the stresses, both the peak and peak average values are used in the following figures. They compare stresses in the anterior orientation, the posterior orientation and finally individual stresses in both the orientations.

Nondimensional peak Reynolds and normal stresses for the three valves in the

anterior orientation at five locations within the ventricle are shown in Figure 4-49. The open symbols represent the normal stresses and the boxed symbols the Reynolds stress. The Björk-Shiley valves, with smaller opening angles than the Bicer valve, create higher stresses closer to the annulus. The 75° opening angle of the Bicer valve produces the highest stress further downstream (0.625D). In fact, the maximum normal stress and Reynolds stresses are associated with the Bicer valve. However, as emphasized previously, it is not enough to consider peak stresses by themselves. It is also important to look at the duration of their existence. Figure 4-50 shows the peak averages of the Reynolds and normal stresses. Now a different picture emerges. The Bicer valve no longer has the highest stresses thus suggesting that the maximum stresses last for a relatively short time. Note, the higher stress values are for the B-S c-c valve close to the annulus; however, further downstream they drop considerably to the range of the B-S mono and Bicer valves. In fact, all the three valves show significant drop in stresses far downstream.

Figure 4-51 shows the peak Reynolds and normal stresses for the posterior orientation. The Björk-Shiley valves again develop the highest peak stresses: normal stress at 0.625D for the B-S mono and the Reynolds stress at 0.75D for the B-S c-c. However, when averaged over the diastolic phase (Figure 4-52), the three valves show comparable performance with the Bicer valve perhaps having a slight edge. Notice essentially constant levels of stress at downstream locations as compared to the fluctuating stresses present with the anterior configuration. This is likely due to the formation of a single vortex instead of two.

Figures 4-53 through 4-56 compare stress levels for the three valves in both orientations. The boxed and open symbols represent the anterior and posterior orientations, respectively. Figure 4-53, representing the peak Reynolds stresses,

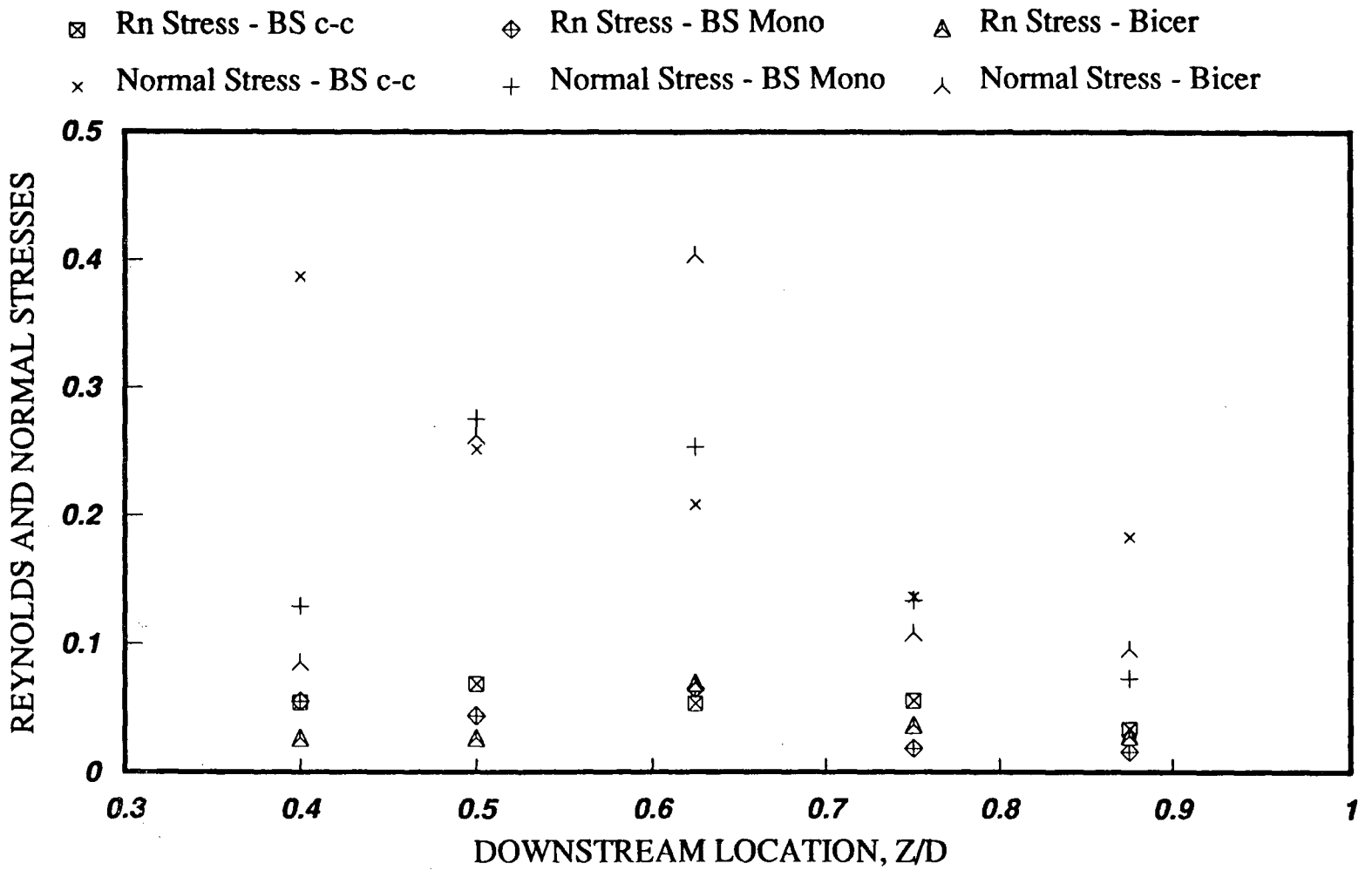

Figure 4-49 Variation of the peak nondimensional Reynolds and normal stresses at five downstream locations for the three tilting disc prostheses in the anterior orientation.

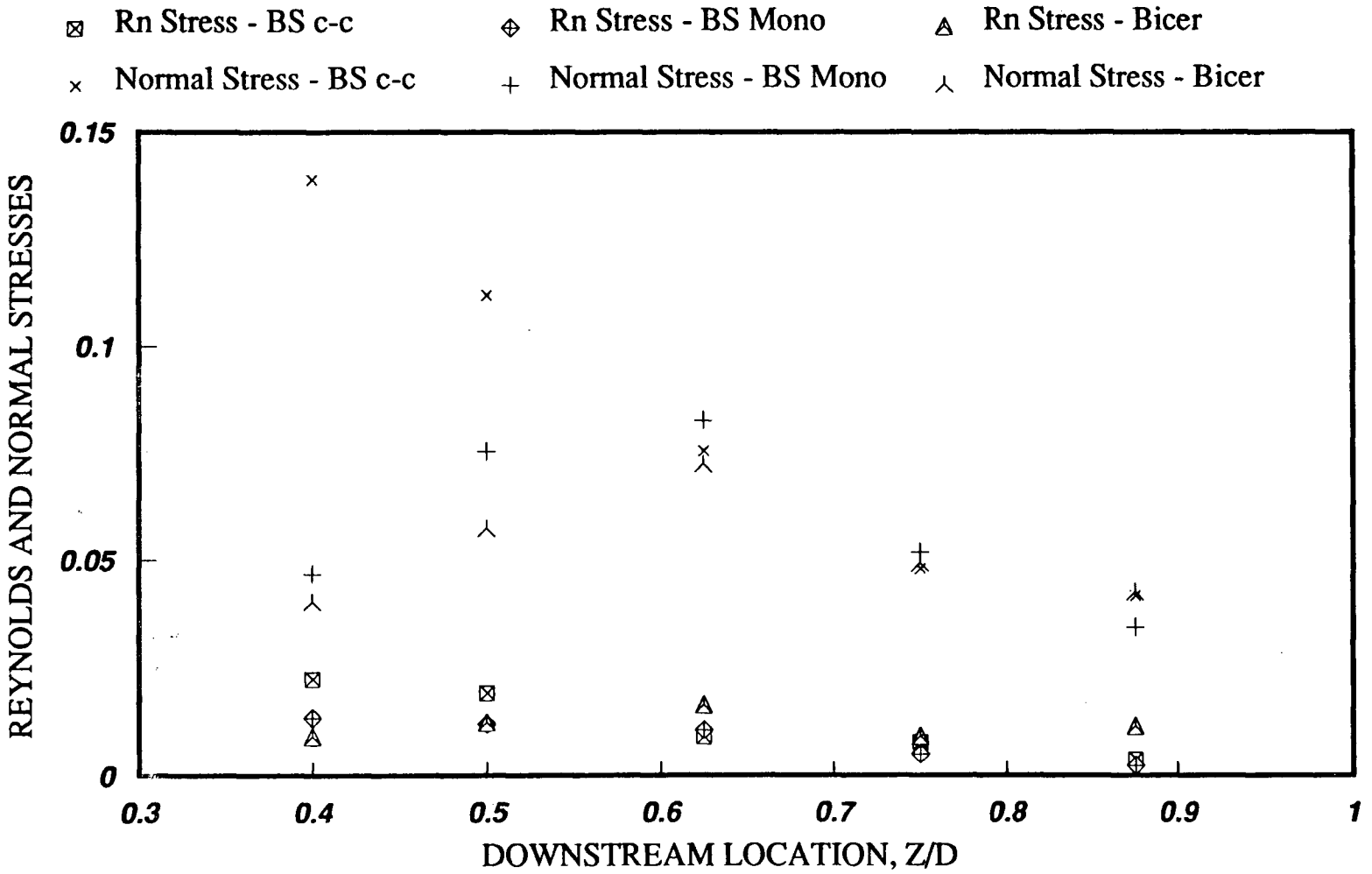

Figure 4-50 Variation of the peak average nondimensional Reynolds and normal stresses at five downstream locations for the three tilting disc prostheses in the anterior orientation.

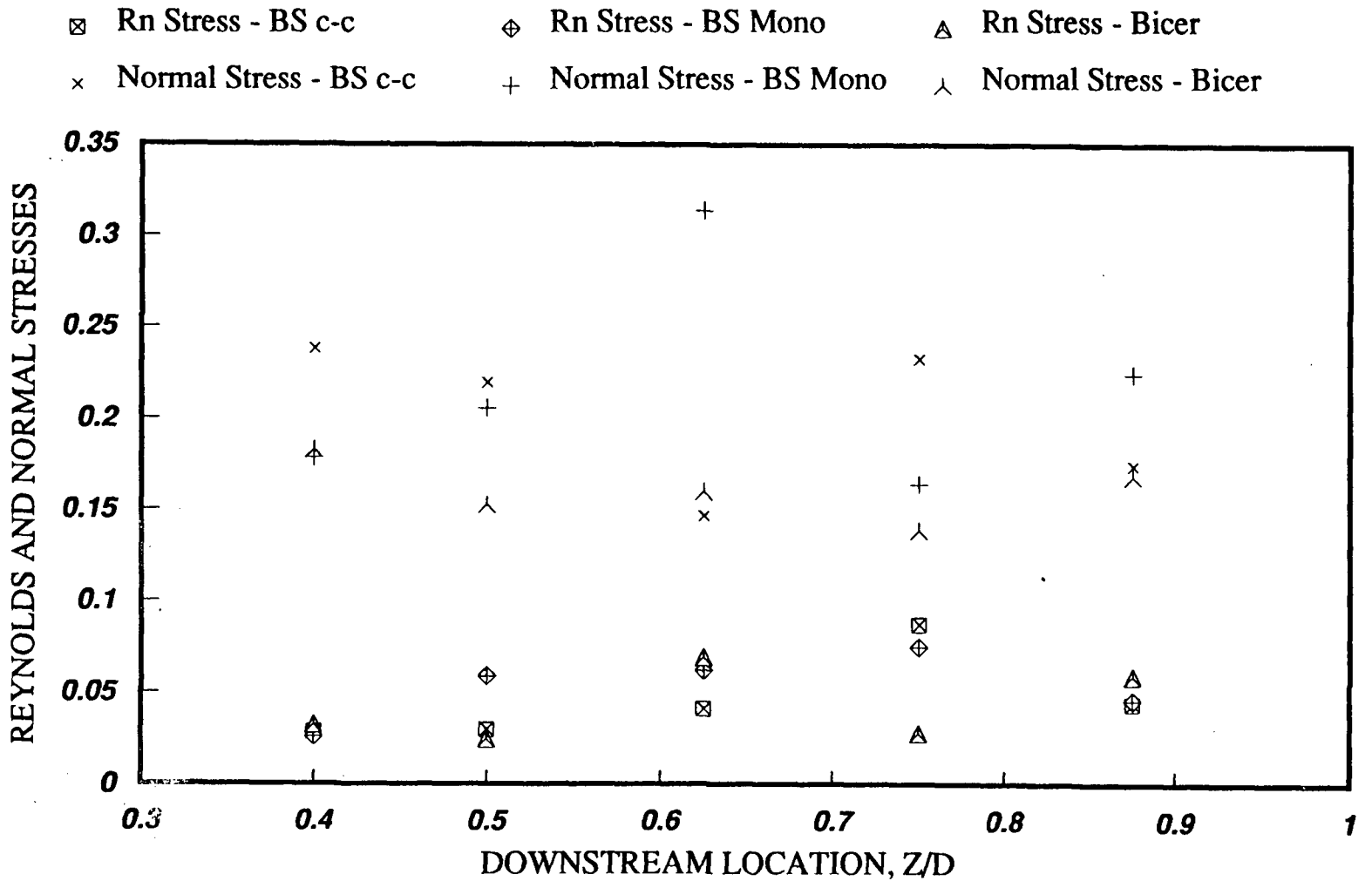

Figure 4-51 Variation of the peak nondimensional Reynolds and normal stresses at five downstream locations for the three tilting disc prostheses in the posterior orientation.

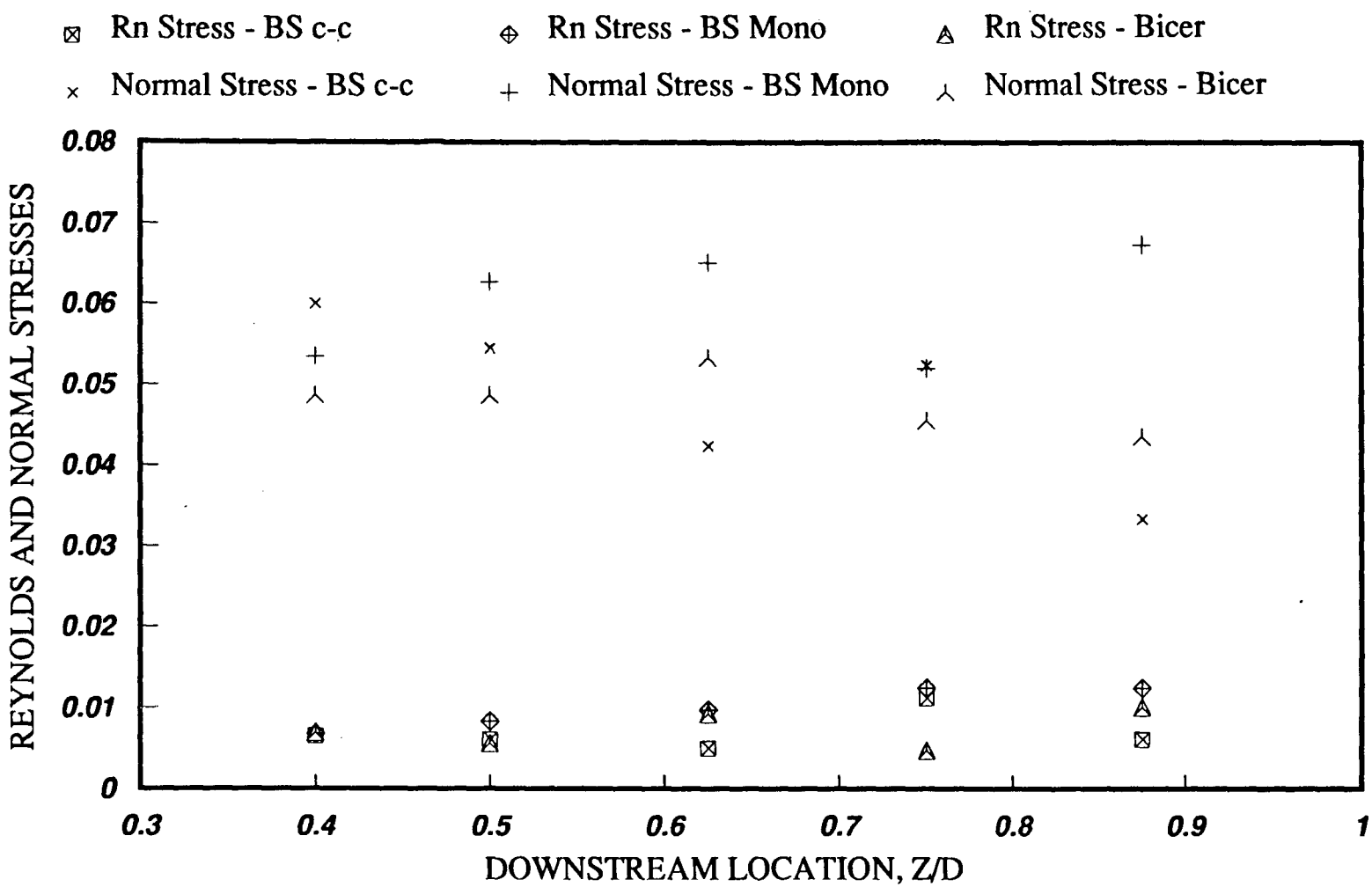

Figure 4-52 Variation of the peak average nondimensional Reynolds and normal stresses at five downstream locations for the three tilting disc prostheses in the posterior orientation.

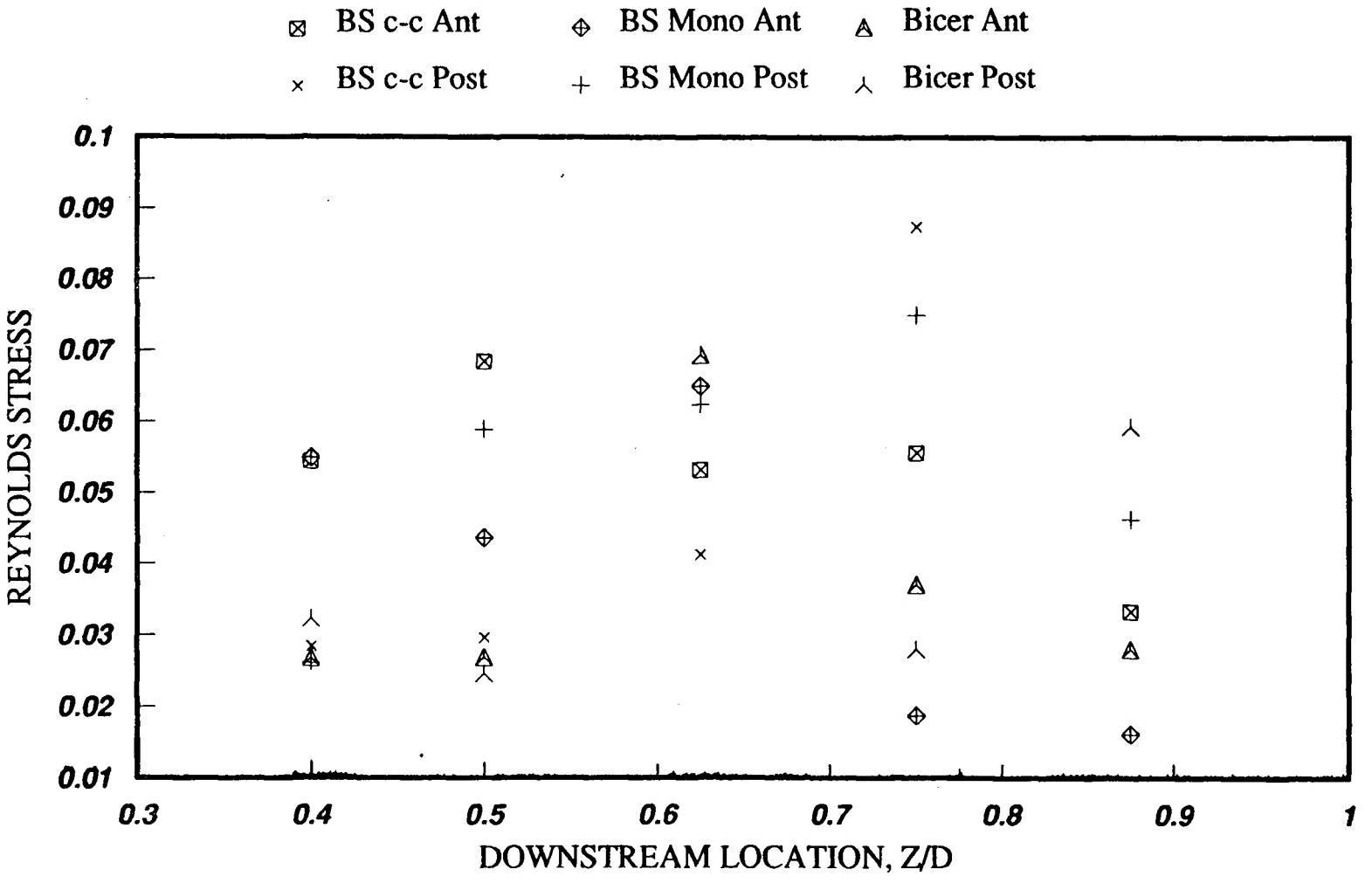

Figure 4-53 Variation of the peak nondimensional Reynolds stresses at five downstream locations for the three tilting disc prostheses in both orientations.

shows that close to the annulus, the anterior orientation creates the highest stress while the posterior orientation does the same further downstream. In fact, the posterior orientation resulted in the overall highest Reynolds stresses for all the three valves. However, Figure 4-54, showing the peak averages, gives a different picture. The highest values are now associated with the anterior orientation and occur close to the annulus. This suggests that the peak Reynolds stresses created in the anterior location are sustained for a longer period than those with the posterior orientation. Except for the two furthest measuring locations, the anterior orientations produced the highest Reynolds stress values. Even though the highest Reynolds stresses far downstream are associated with the posterior orientation, the levels are quite low compared to the anterior orientation values close to the annulus. Similar trends can be observed for the normal stresses especially for the peak average results. The peak normal stresses (Figure 4-55) are highest for the Bicer valve in the anterior orientation. As observed with the peak Reynolds stress data, the highest values close to the annulus are associated with the anterior orientation and those further downstream with the posterior configuration. This is also true for the peak average normal stresses (Figure 4-56). Thus, through this form of presentation of results, it becomes more clear that, considering stresses only, the posterior orientation is preferable.

Several observations can now be made with regard to valve orientation: (i) Although some of the highest stresses are associated with a posterior orientation, they are usually short-lived as seen in the peak average plots. (ii) The newer generation valves, in either orientation, clearly perform better, in terms of stresses, than the older one (represented by the B-S c-c) in the anterior orientation. This is not unexpected, as the newer valves were designed to combat some of the problems that arose with the older one. What is surprising is low level of the stresses (Reynolds

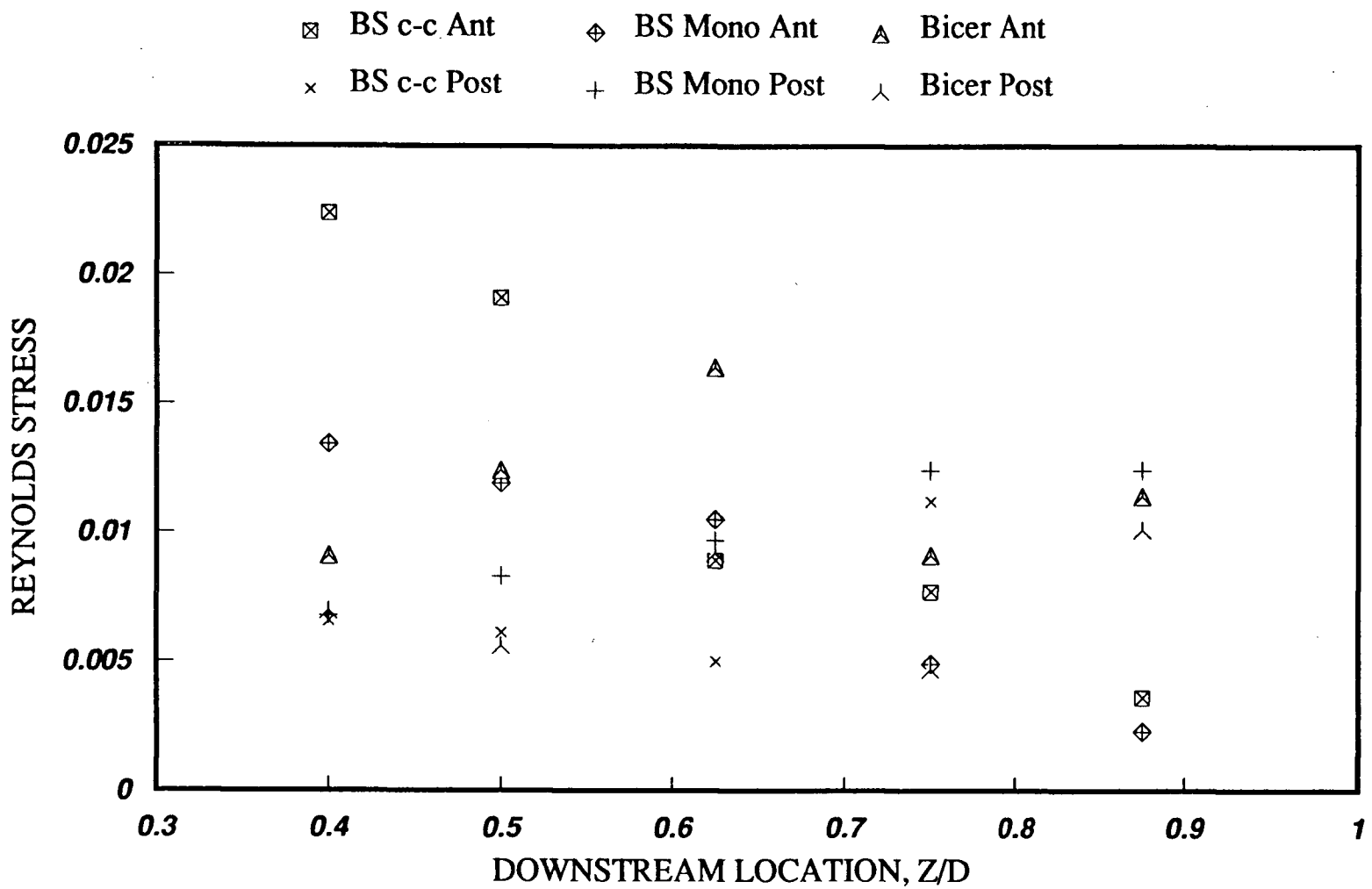

Figure 4-54 Variation of the peak average nondimensional Reynolds stresses at five downstream locations for the three tilting disc prostheses in both orientations.

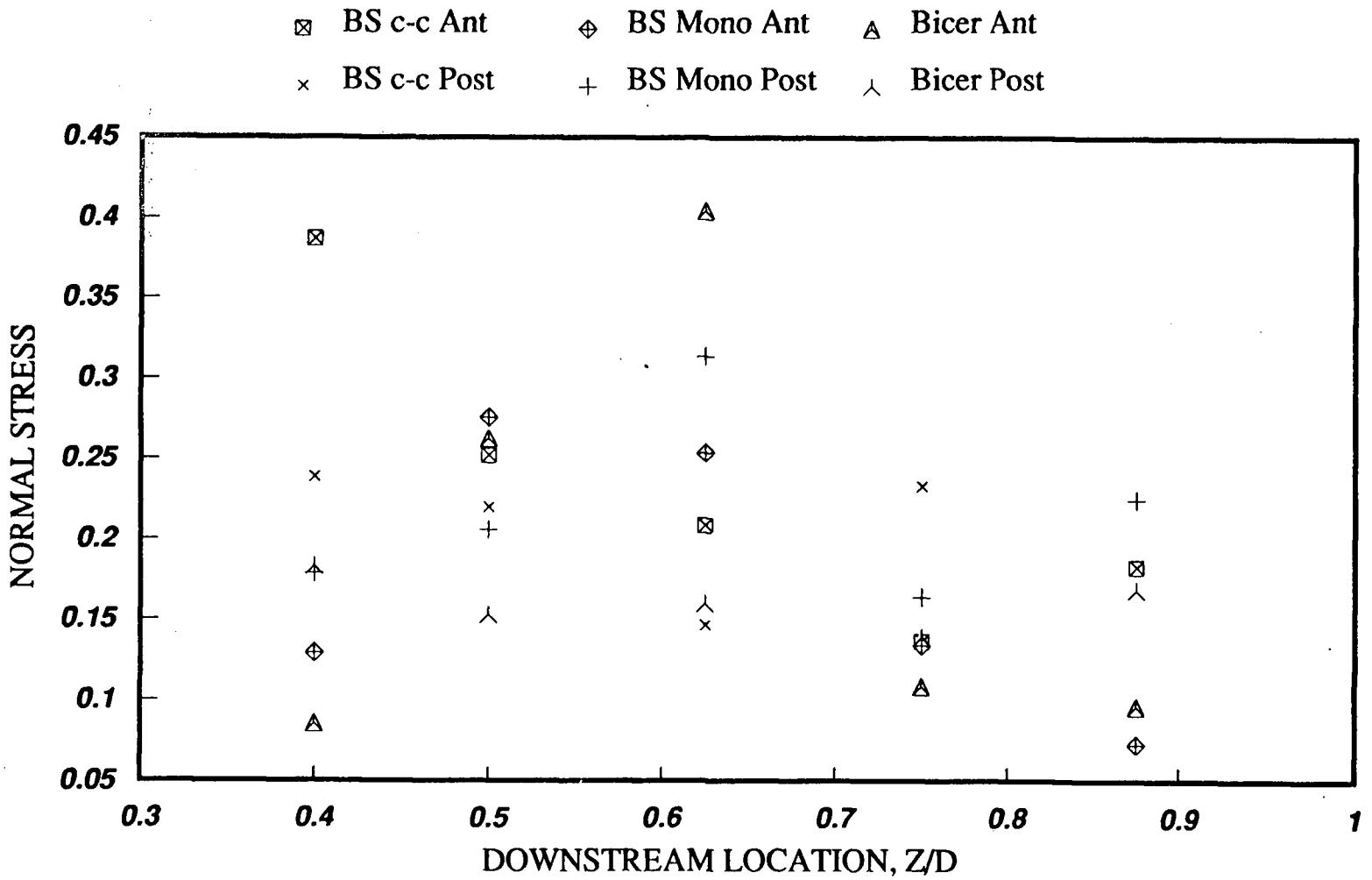

Figure 4-55 Variation of the peak nondimensional normal stresses at five downstream locations for the three tilting disc prostheses in both orientations.

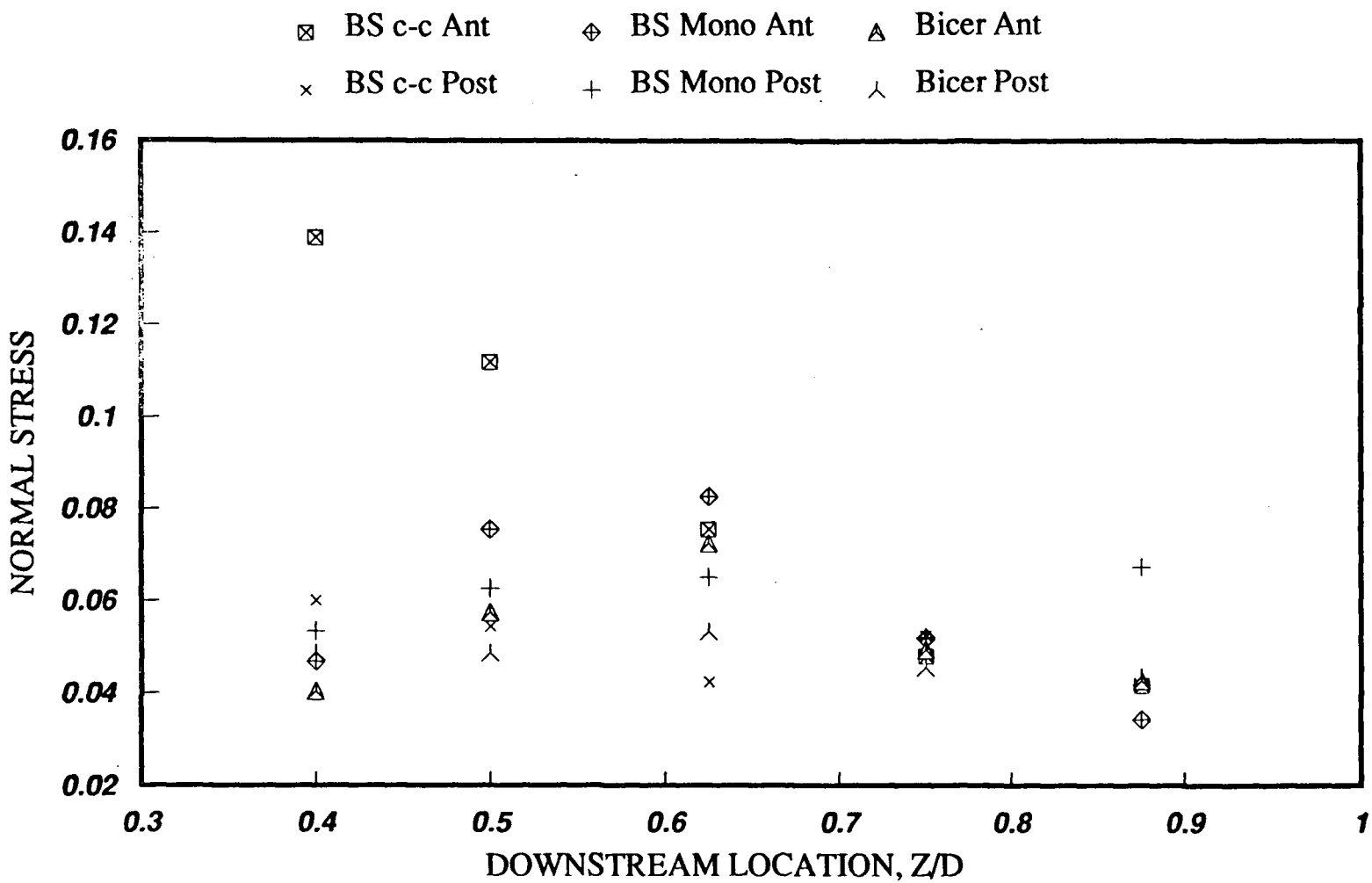

Figure 4-56 Variation of the peak average nondimensional normal stresses at five downstream locations for the three tilting disc prostheses in both orientations.

and normal) for the B-S c-c in the posterior orientation compared to the newer prostheses. (iii) In most cases, the posterior orientation produced lower stresses than the corresponding anterior configuration. (iv) Finally, although the anterior orientation resulted in high levels of stresses close to the annulus, in most cases their magnitudes diminish significantly further downstream. In the posterior orientation, while the stresses are not as high close to the annulus they remained high downstream.

Based on the above discussion, the preferred orientation for a tilting disc mechanical valve in the mitral position appears to be that with the major orifice towards the posterior wall (posterior orientation). It should be noted, however, that stress level is not the only consideration governing the implantation orientation for a valve. It has also been shown that a posterior orientation produces the lowest transvalvular pressure gradient and, in some instances, less regurgitation[57].

4.3 Biological Valves

Both the Hancock II and the Carpentier-Edwards supraannular prostheses represent recent modifications by Hancock and Edwards laboratories in an attempt to overcome problems that developed in the earlier models. The chosen Hancock II prosthesis is a size 27 and the Carpentier-Edwards supraannular prosthesis a size 29. This should not affect the results as all data are nondimensionalized.

4.3.1 Hancock II

Figure 4-57 shows the time history of four nondimensional fluid dynamic parameters at station 0.4D. The period covers from the mitral valve opening (T = 0 msec) to the closing (T = 420 msec). In early diastole (acceleration phase), the valve can

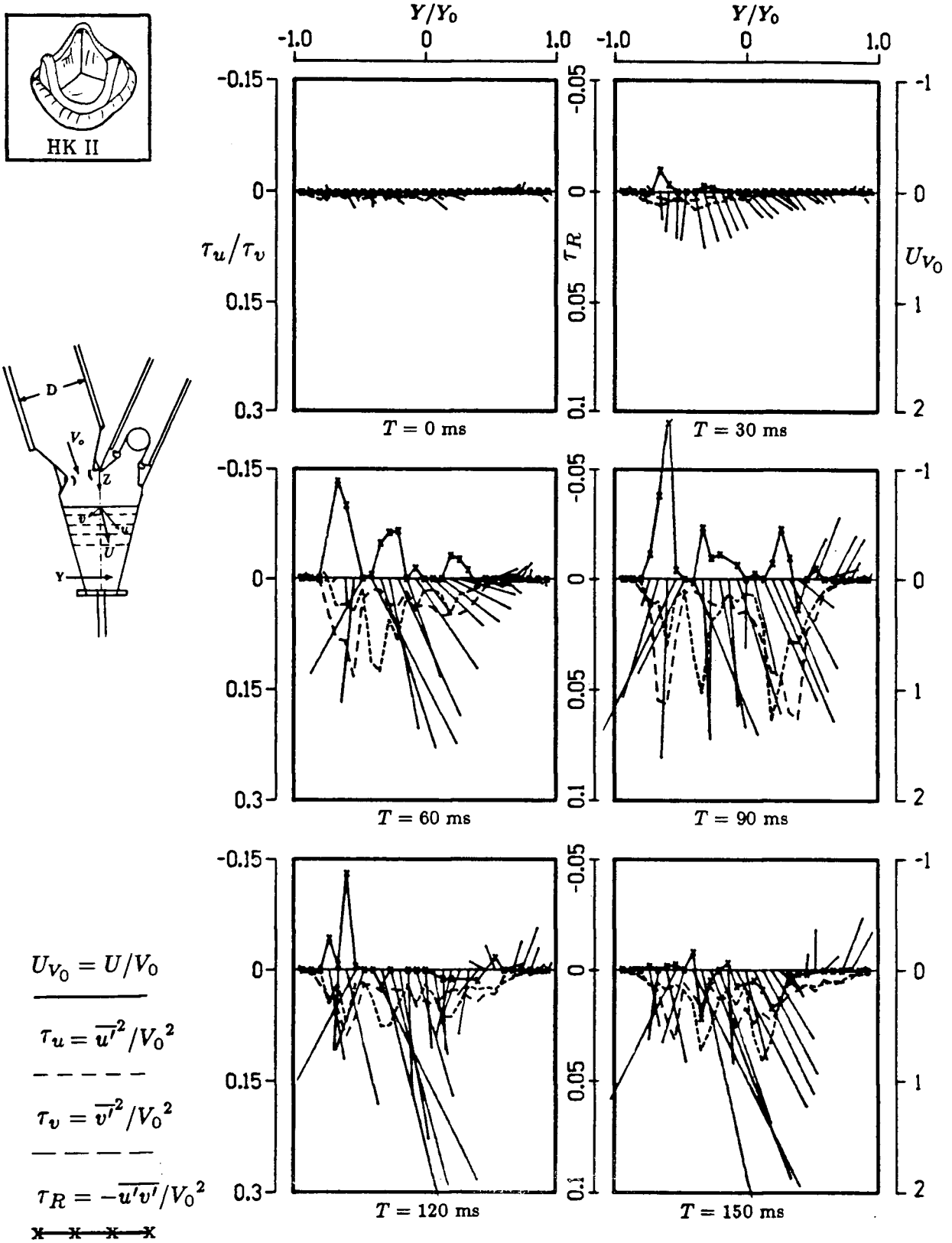

Figure 4-57 Time history of velocity and stress profiles for the Hancock II prosthesis at Z = 0.4D (0 - 150 ms).

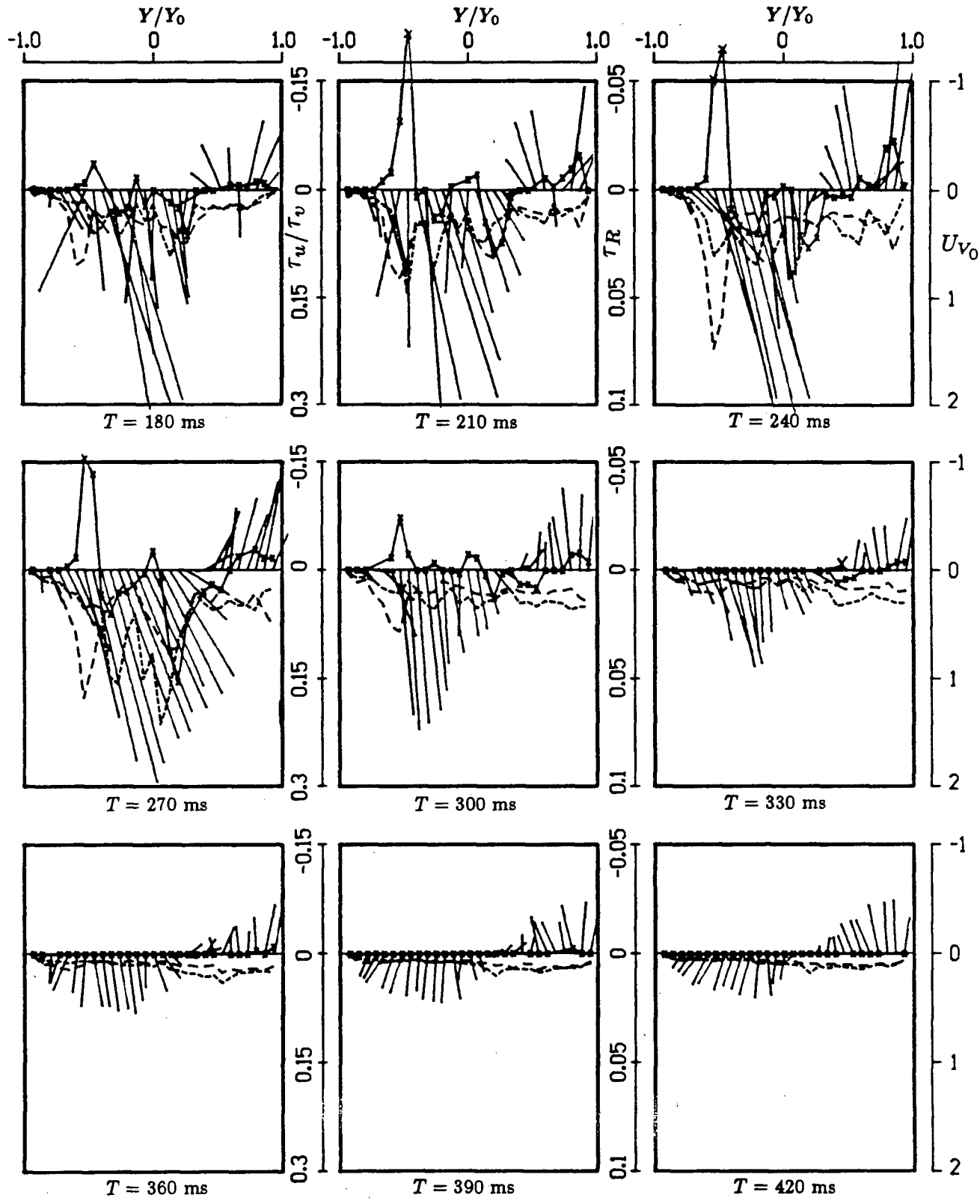

Figure 4-57 Time history of velocity and stress profiles for the Hancock II prosthesis at Z = 0.4D (180 - 420 ms).

be seen to open very rapidly creating a high velocity flow. The high velocity jet is produced by the narrow passage created when the valve opens. This jet causes a sudden increase in both the Reynolds and normal stresses. By mid-diastole (peak phase), a single vortex formation appears to develop. The stresses, however, remain elevated throughout this phase. It is not until the deceleration-phase (near the end of diastole), that the stresses are dramatically reduced.

Figure 4-58 shows spatial variation of the fluid parameters at the early stage of diastole (90 ms). The jet-like flow has reached the first two measuring locations resulting in an increase in stresses, particularly noticeable at the edges of the jet. Note, that the peak magnitudes of the stresses are considerably higher than those for the mechanical valves at the same instance in the diastolic phase. This could be attributed to the small orifice created by the valve leaflets as they open. As the flow continues to accelerate (Figure 4-59), the jet formation and resulting high stresses can be seen to travel downstream. Even at 0.875D, elevated stresses are detected. The peak Reynolds stress during this phase is 515 dynes/cm^2 located at 0.625D. The peak normal stress, also at 0.75D, registered a high of 1136 dynes/cm^2. Note, the separation of flow at the first three stations resembles the flow pattern detected with the tilting disc valves. This can possibly be attributed to the orientation and geometry of the valve. The frame of the tissue valve consists of three posts. For these experiments, one post is located posteriorly and the other two anteriorly. During the opening phase of the valve (before the valve leaflets have fully opened), the geometry of the valve aperture could deflect the flow in two directions leaving a small stagnant region as indicated in Figure 4-59. However, by the peak phase when the leaflets have fully opened (Figure 4-60), the flow has taken on the characteristics of a fully developed jet. Stresses continue to be the highest at the edges of the jet and are evident at the five measuring locations. The highest Reynolds stress was

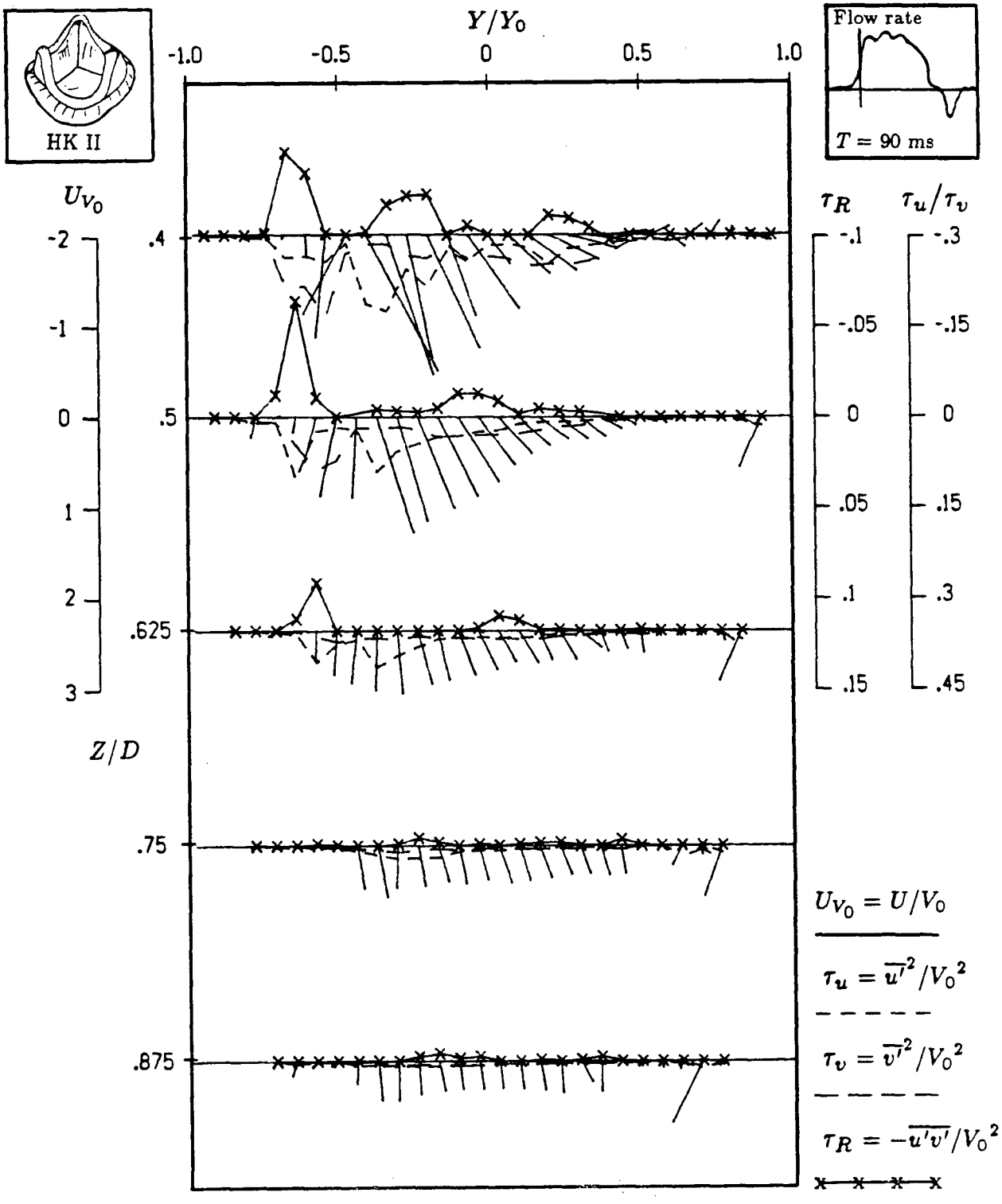

Figure 4-58 Variation of the nondimensional velocity, normal stresses, and the Reynolds stress at five downstream locations for the Hancock II prosthesis (27 mm, T = 90 ms).

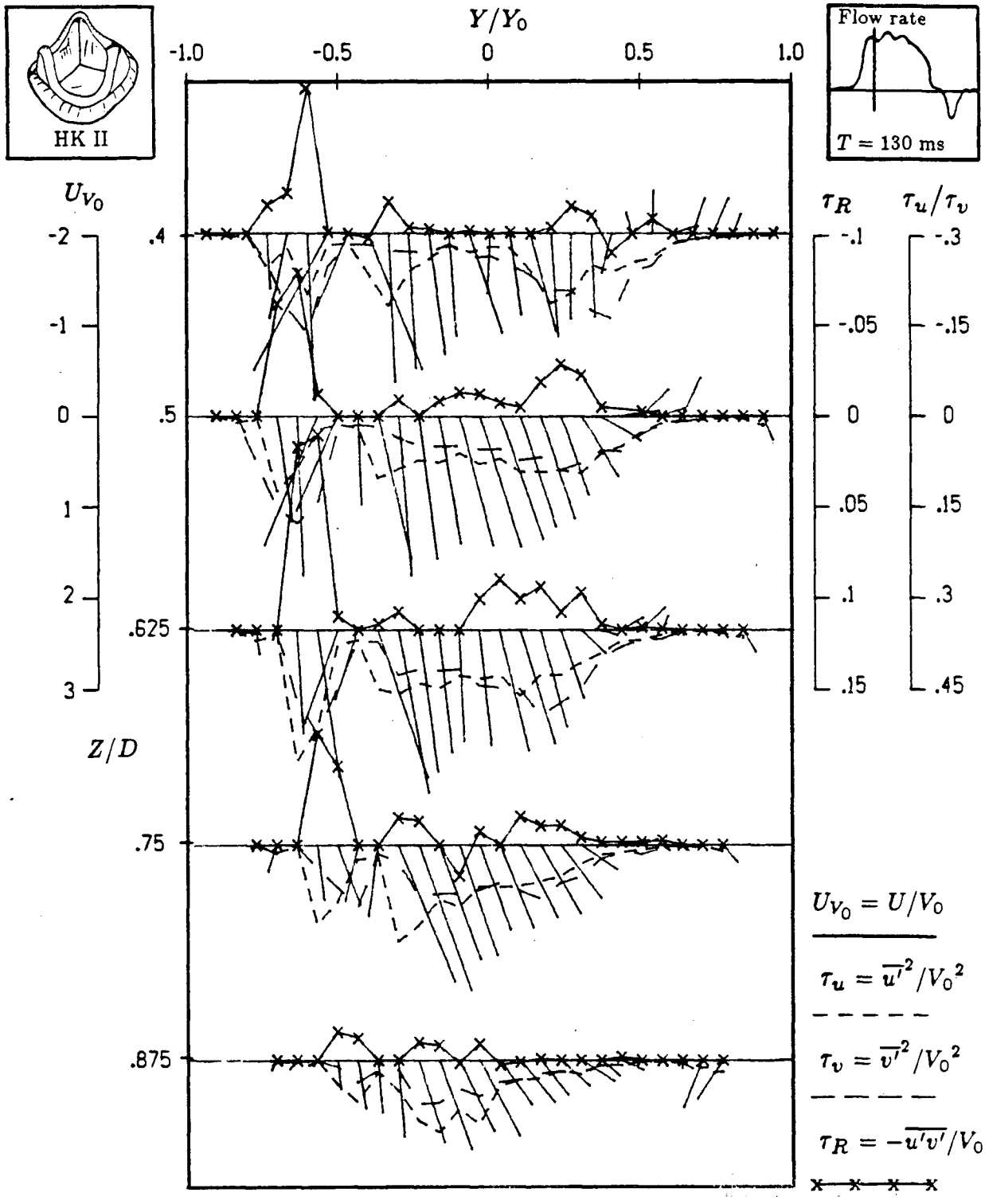

Figure 4-59 Variation of the nondimensional velocity, normal stresses, and the Reynolds stress at five downstream locations for the Hancock II prosthesis (27 mm, T = 130 ms).

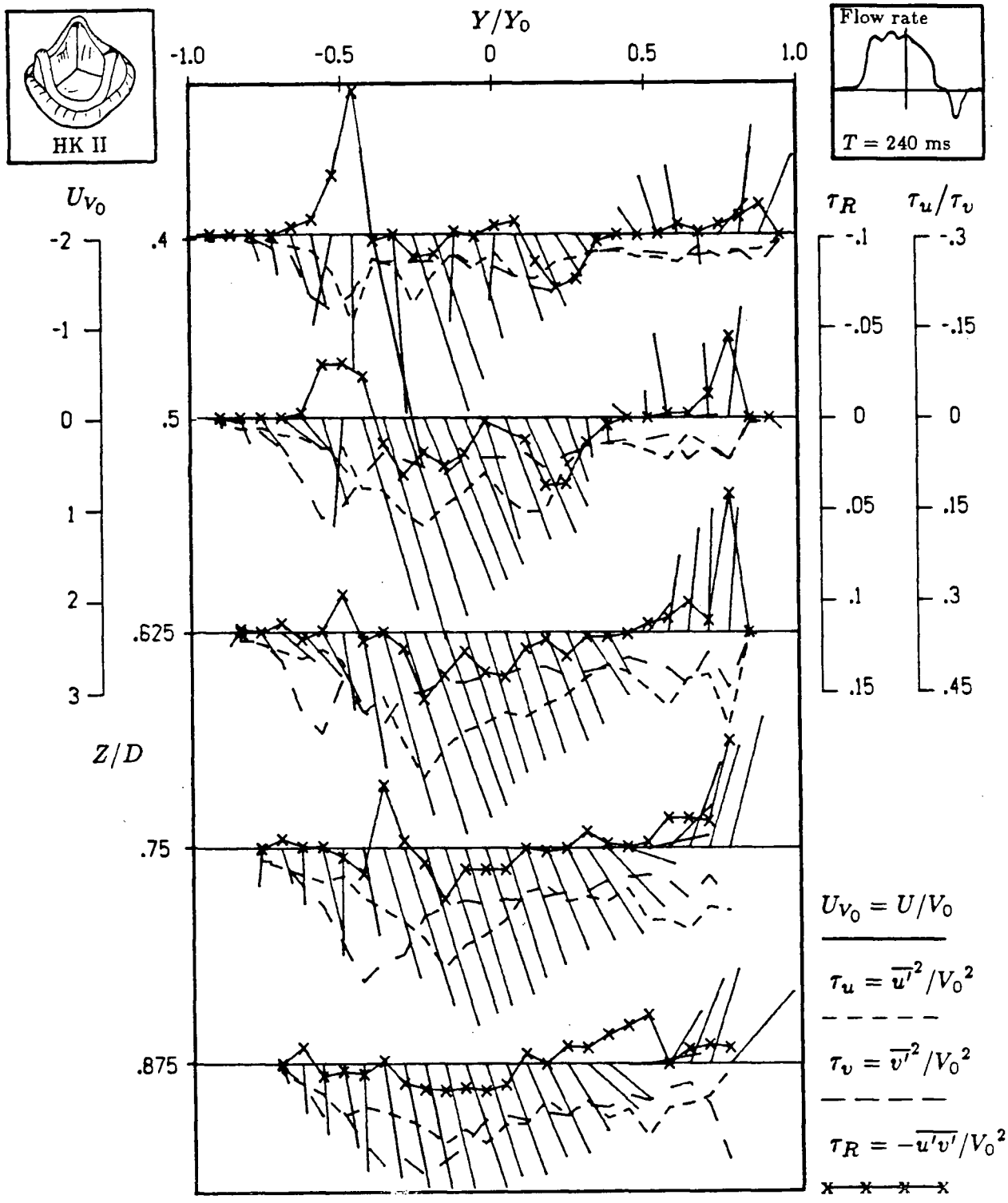

Figure 4-60 Variation of the nondimensional velocity, normal stresses, and the Reynolds stress at five downstream locations for the Hancock II prosthesis (27 mm, T = 240 ms).

441 dynes/cm^2 at 0.4D and the highest normal stress was 1436 dynes/cm^2 at 0.75D. Note, the Reynolds stress has decreased, but the normal stress has increased.

A significant decrease in velocity and stresses is observed during the deceleration phase (Figure 4-61). This appears to be a common denominator between the mechanical and tissue prostheses of this study.

Figures 4-62 and 4-63 show the Reynolds and normal stresses for the three phases of diastole (acceleration, peak and deceleration) in order to give a better understanding of the timing and duration of the stresses. Figure 4-62 shows the peak stresses. The Reynolds and normal stresses are dominant during the acceleration and peak phases, respectively. The highest values are far downstream, 0.625D for the Reynolds stress and 0.75D for the normal stresses. This is similar to the results found for the posterior configuration of the three tilting disc valves. This is not surprising as a single vortex circulation pattern is present for both. Figure 4-63 shows the peak averages. The results for the Reynolds stress show that, when averaged over the individual phases, the stresses during the acceleration and peak phases appear to be of the same magnitude. However, this is not the case for the normal stresses. The results here show that the normal stresses during the peak-phase are sustained considerably longer than those during the acceleration-phase. This differs from the tilting disc valves, where the acceleration-phase was always the most dominant. Also notice relatively low stress values during the deceleration-phase.

4.3.2 Carpentier-Edwards Supraannular

Figure 4-64 shows the time history at the station 0.4D. Similar to the Hancock II, the Carpentier-Edwards valve produces a high velocity jet-like flow soon after the

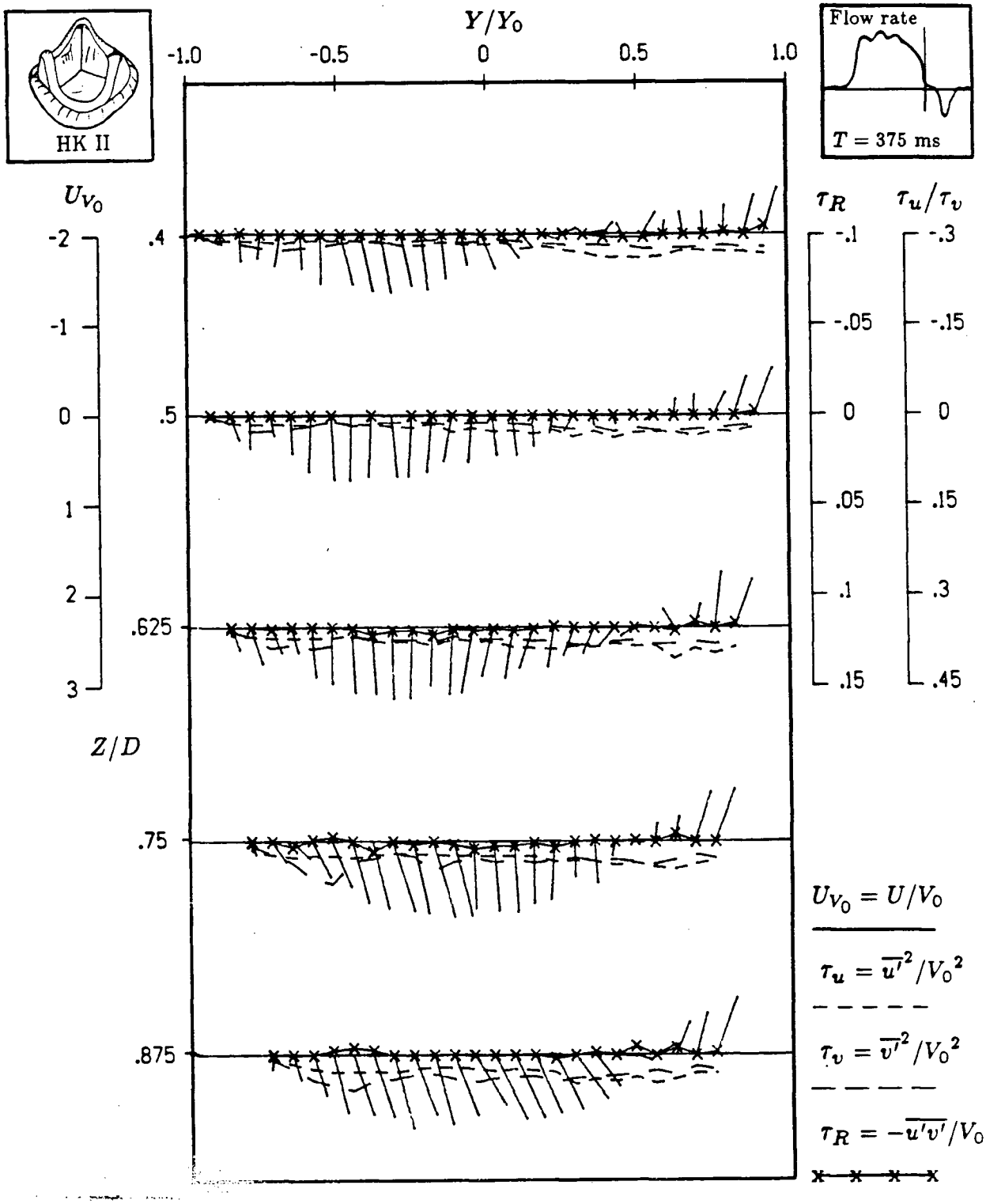

Figure 4-61 Variation of the nondimensional velocity, normal stresses, and the Reynolds stress at five downstream locations for the Hancock II prosthesis (27 mm, T = 375 ms).

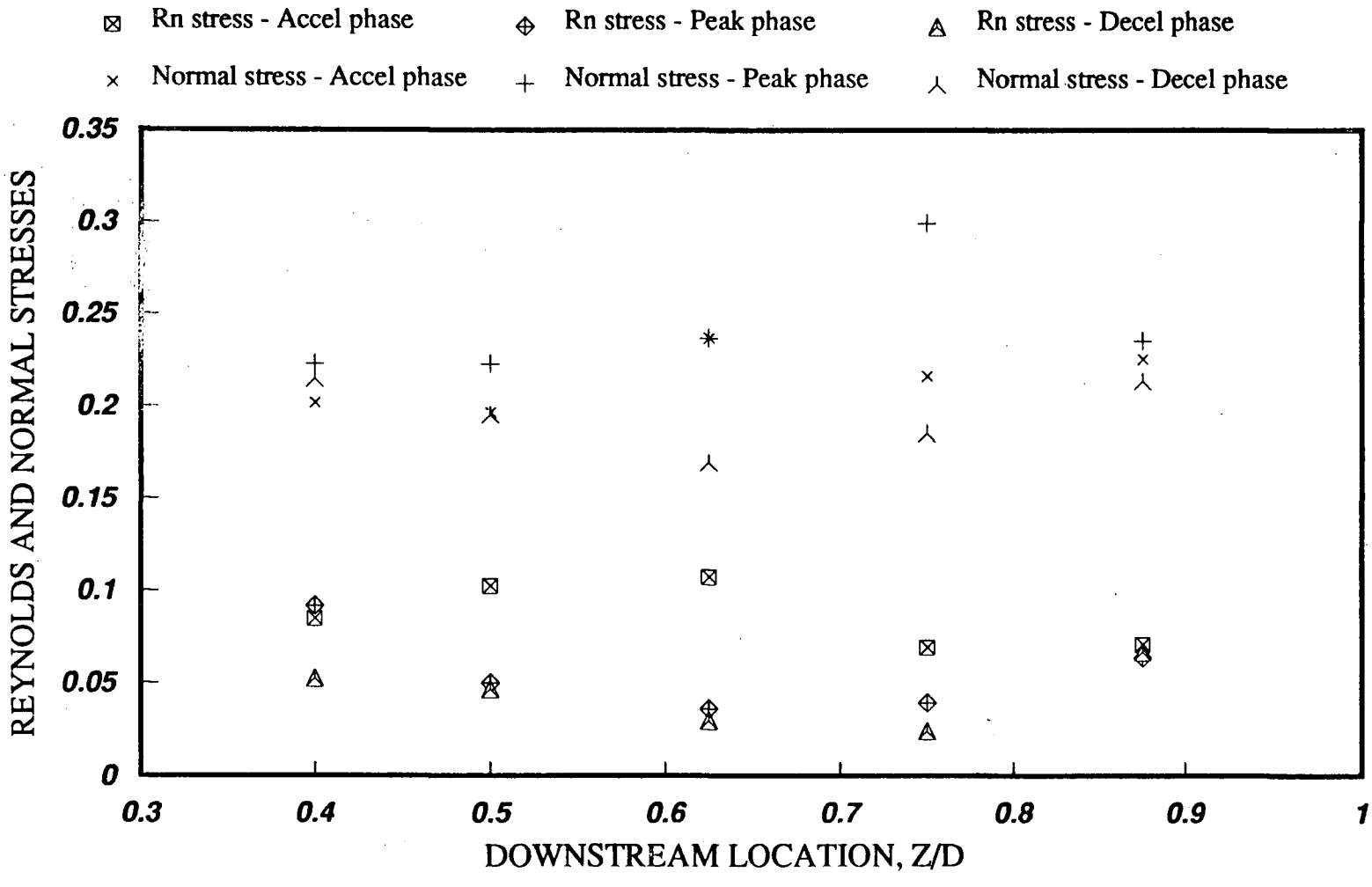

Figure 4-62 Variation of the nondimensional normal stresses and the Reynolds stress during the three phases of diastole at five downstream locations for the Hancock II prosthesis (27mm, Peak stresses).

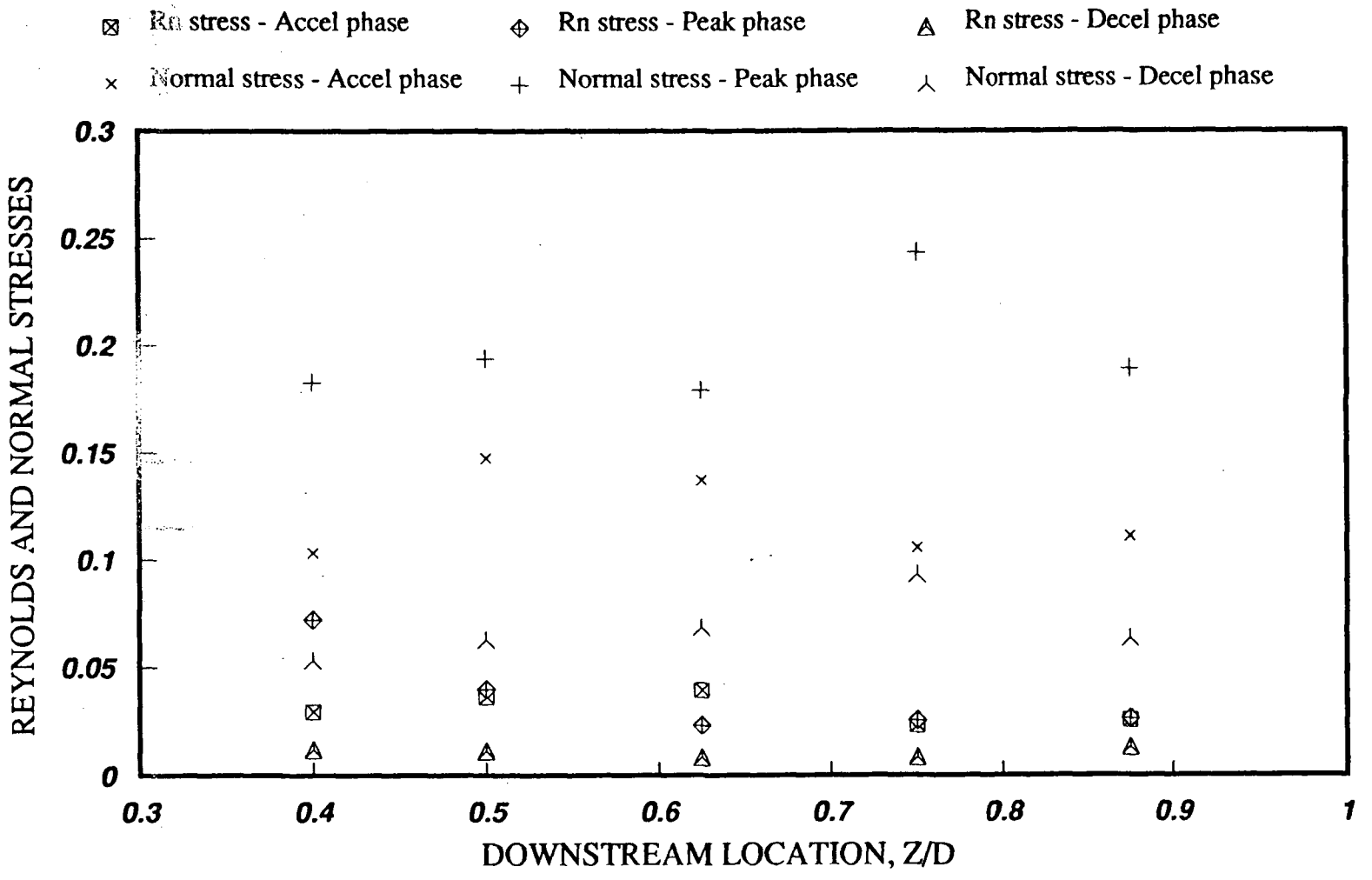

Figure 4-63 Variation of the nondimensional normal stresses and the Reynolds stress during the three phases of diastole at five downstream locations for the Hancock II prosthesis (27mm, Peak average stresses).

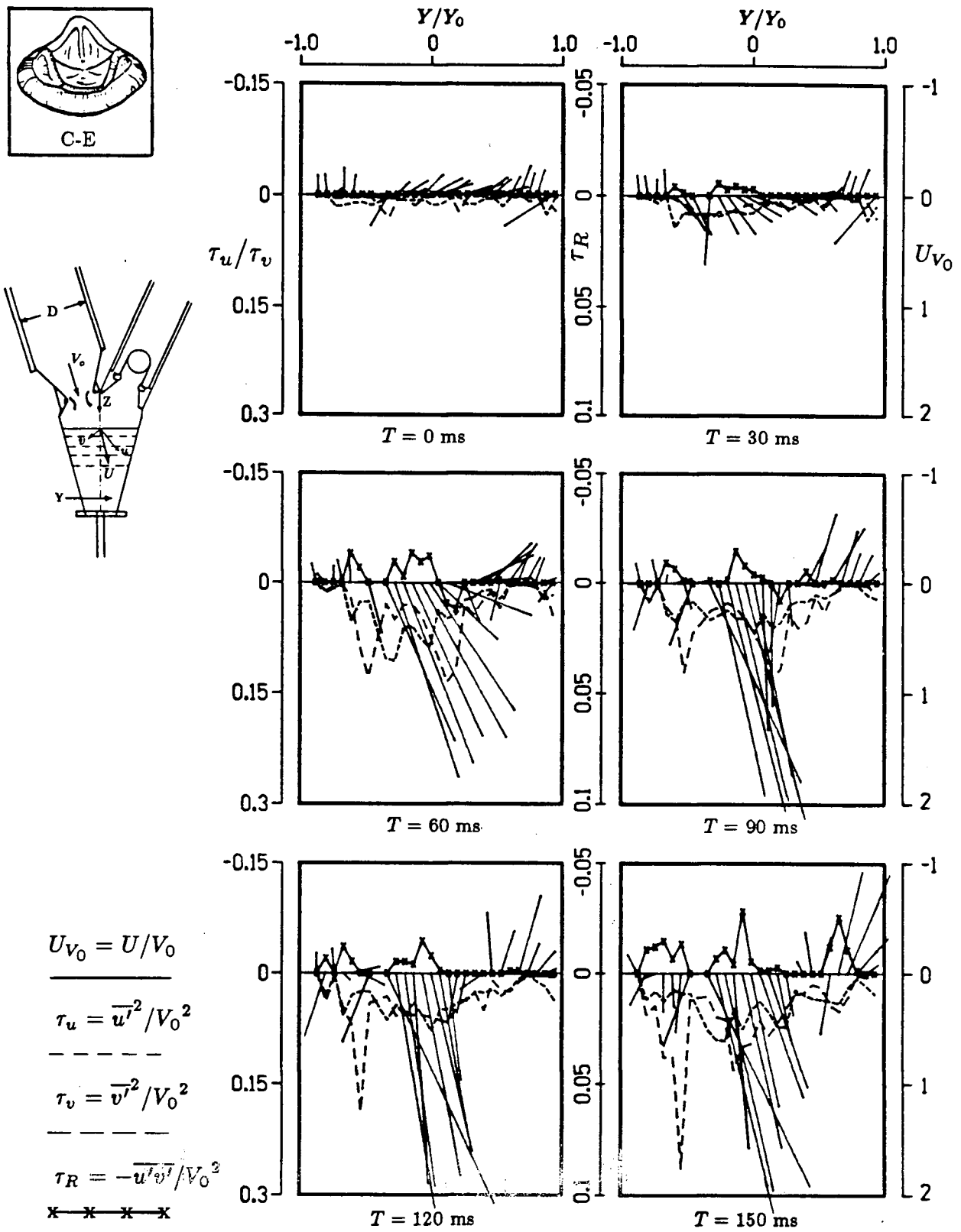

Figure 4-64 Time history of velocity and stress profiles for the Carpentier-Edwards Supraannular prosthesis at Z = 0.4D (0 - 150 ms).

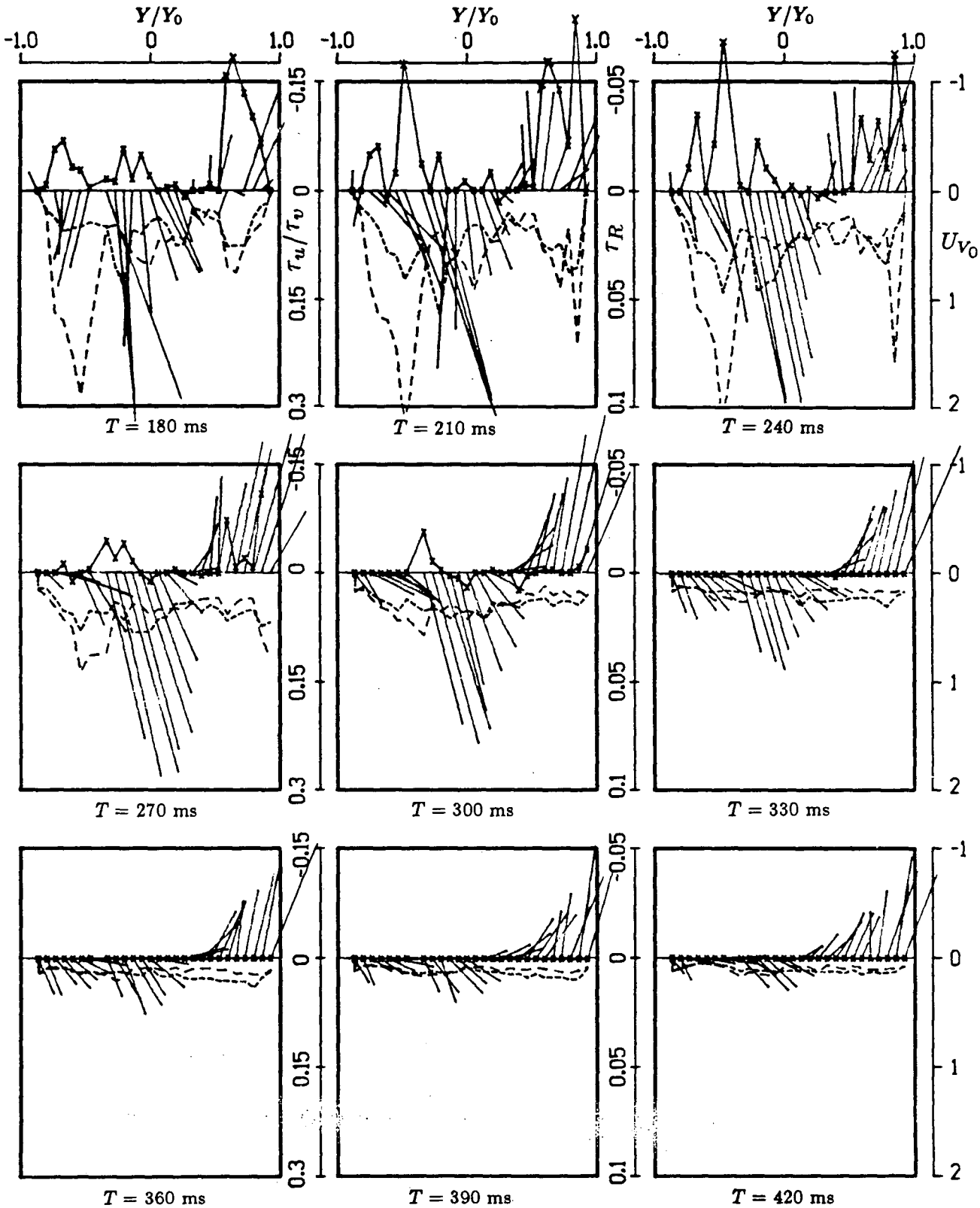

Figure 4-64 Time history of velocity and stress profiles for the Carpentier-Edwards Supraannular prosthesis at Z = 0.4D (180 - 420 ms).

opening. The jet continues to grow well into the peak-phase and is accompanied by high stresses particularly at the edges of the jet. However, as the flow decelerates, the stresses are reduced as observed with the mechanical valves.

To better appreciate the effects downstream of the valve, the following diagrams show the velocity and stresses for a cross section down the centerline of the ventricle.

Figure 4-65 shows the beginning of the diastole phase where the jet-like flow can be seen developing at the first two stations. As the flow is still partly disorganized (not fully formed), relatively high stresses are produced. As the acceleration phase continues (Figure 4-66), the high velocity flow field progresses downstream. Although the flow has become more organized, the stresses remain high. The highest Reynolds stress during this phase was 255 dynes/cm^2 (0.75D) and the highest normal stress was 764 dynes/cm^2 (0.5D). The effect on the flow field due to the geometry of the valve can be clearly observed in this plot. Unlike the natural mitral valve leaflets, which fold against the ventricle wall when open, the leaflets on the prosthetic valve are restricted from opening in a similar fashion by the three posts of the frame. Because of this, a narrow channel is created causing a narrow high velocity jet to form. This is particularly noticeable at the first two levels. Further downstream, the flow can be seen to diverge.

By the peak-phase (Figure 4-67), the flow has completely developed. However, instead of the stresses decreasing as is the case with the mechanical valves, the stresses increased. The peak Reynolds stress recorded was 280 dynes/cm^2 (0.5D) and the peak normal stress was 1345 dynes/cm^2.

A better break down of the timing and duration of the stresses is given in the following two figures. Figure 4-68 shows the peak Reynolds and normal stresses for the three phases. The maximum stresses appear to be of the same magnitude for

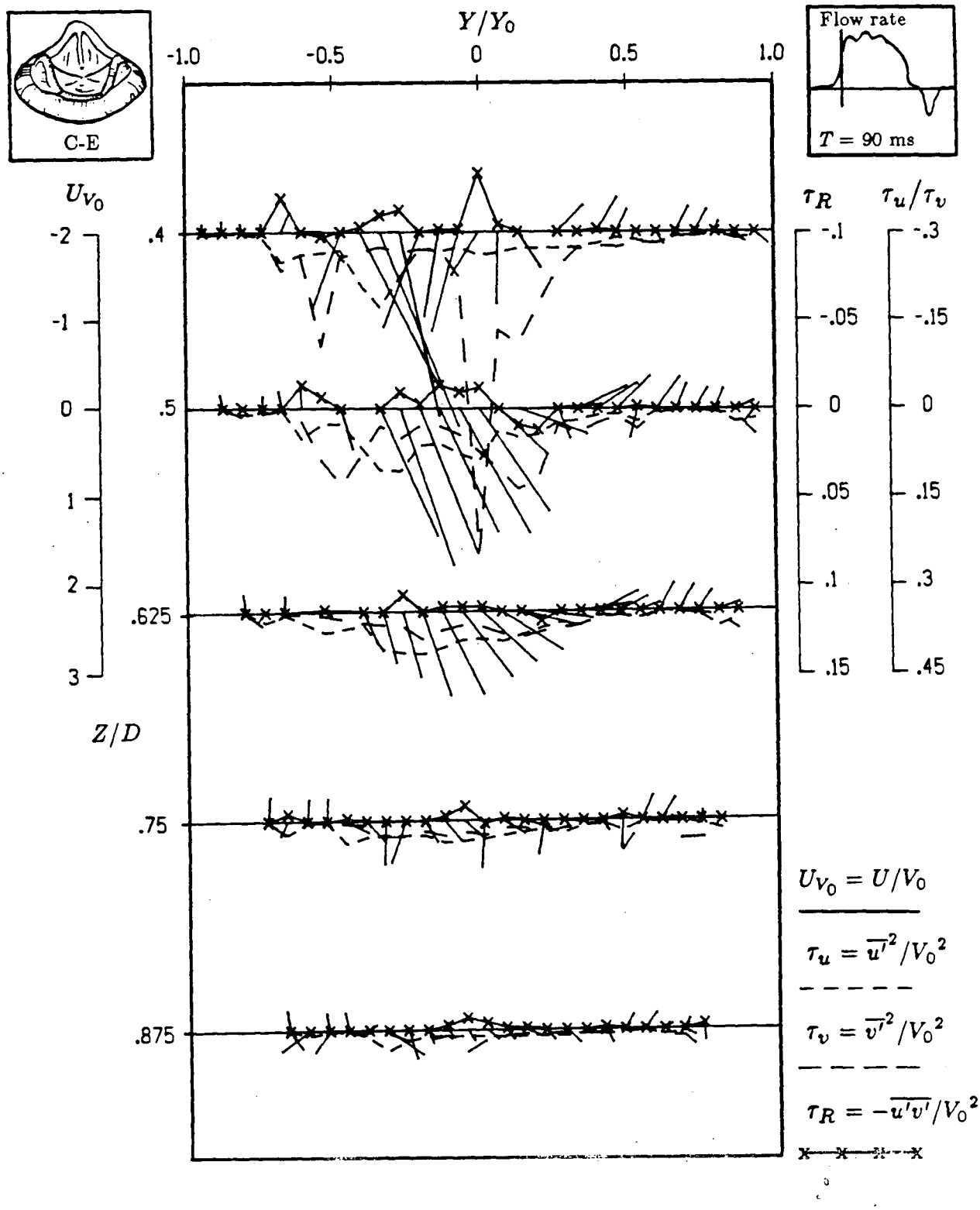

Figure 4-65 Variation of the nondimensional velocity, normal stresses, and the Reynolds stress at five downstream locations for the Carpentier-Edwards Supraannular prosthesis (29 mm, T = 90 ms).

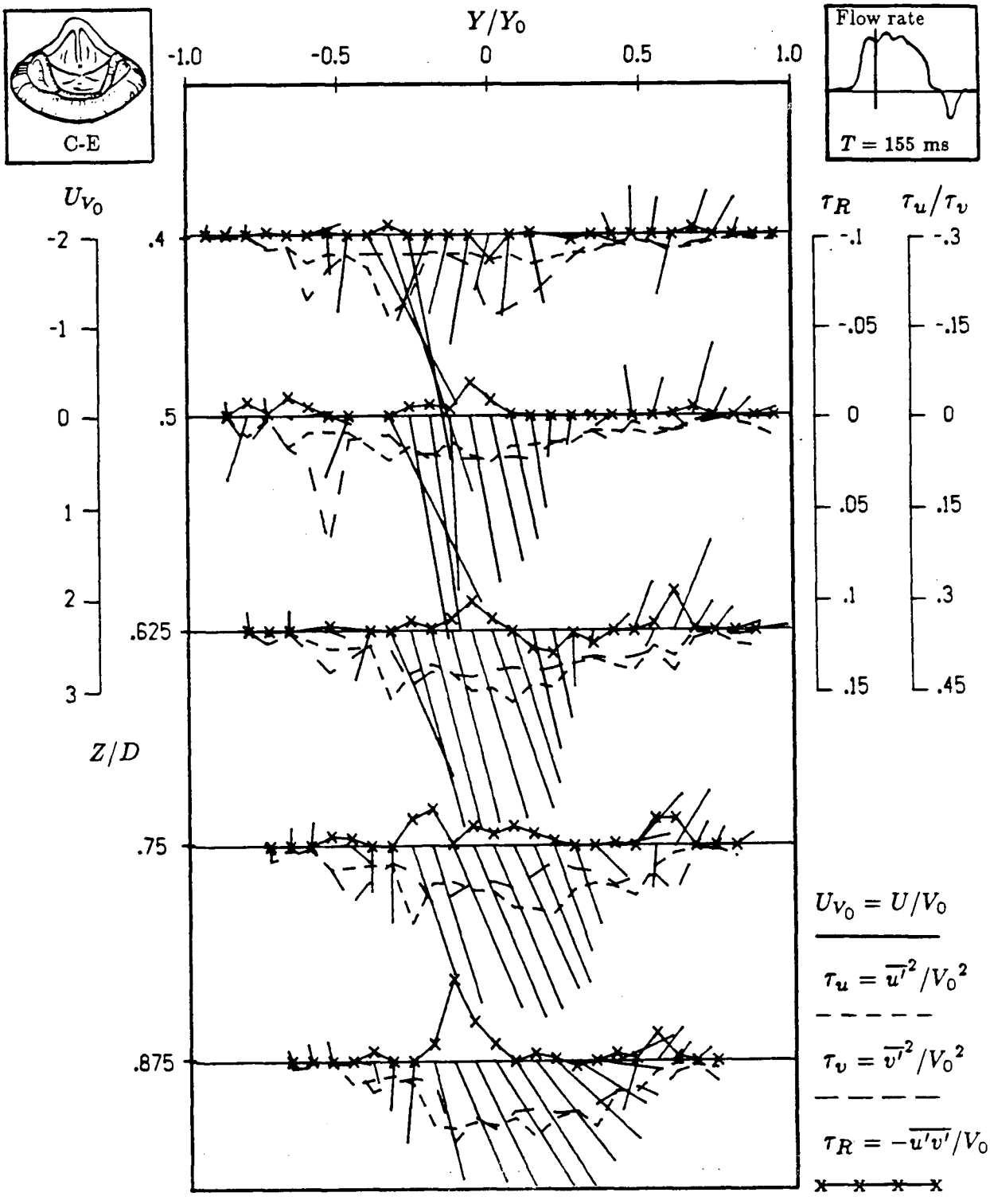

Figure 4-66 Variation of the nondimensional velocity, normal stresses, and the Reynolds stress at five downstream locations for the Carpentier-Edwards Supraannular prosthesis (29 mm, T = 155 ms).

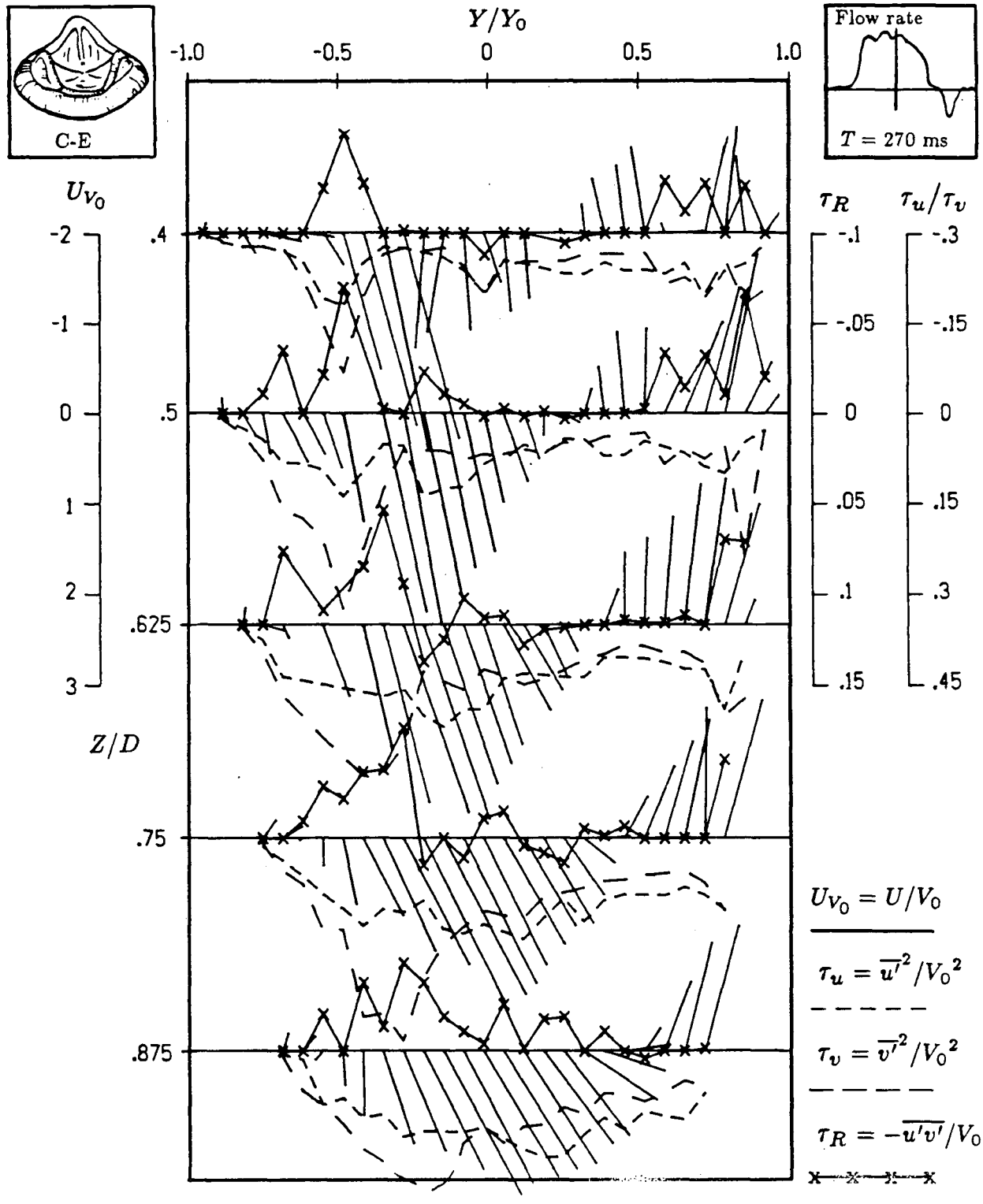

Figure 4-67 Variation of the nondimensional velocity, normal stresses, and the Reynolds stress at five downstream locations for the Carpentier-Edwards Supraannular prosthesis (29 mm, T = 270 ms).

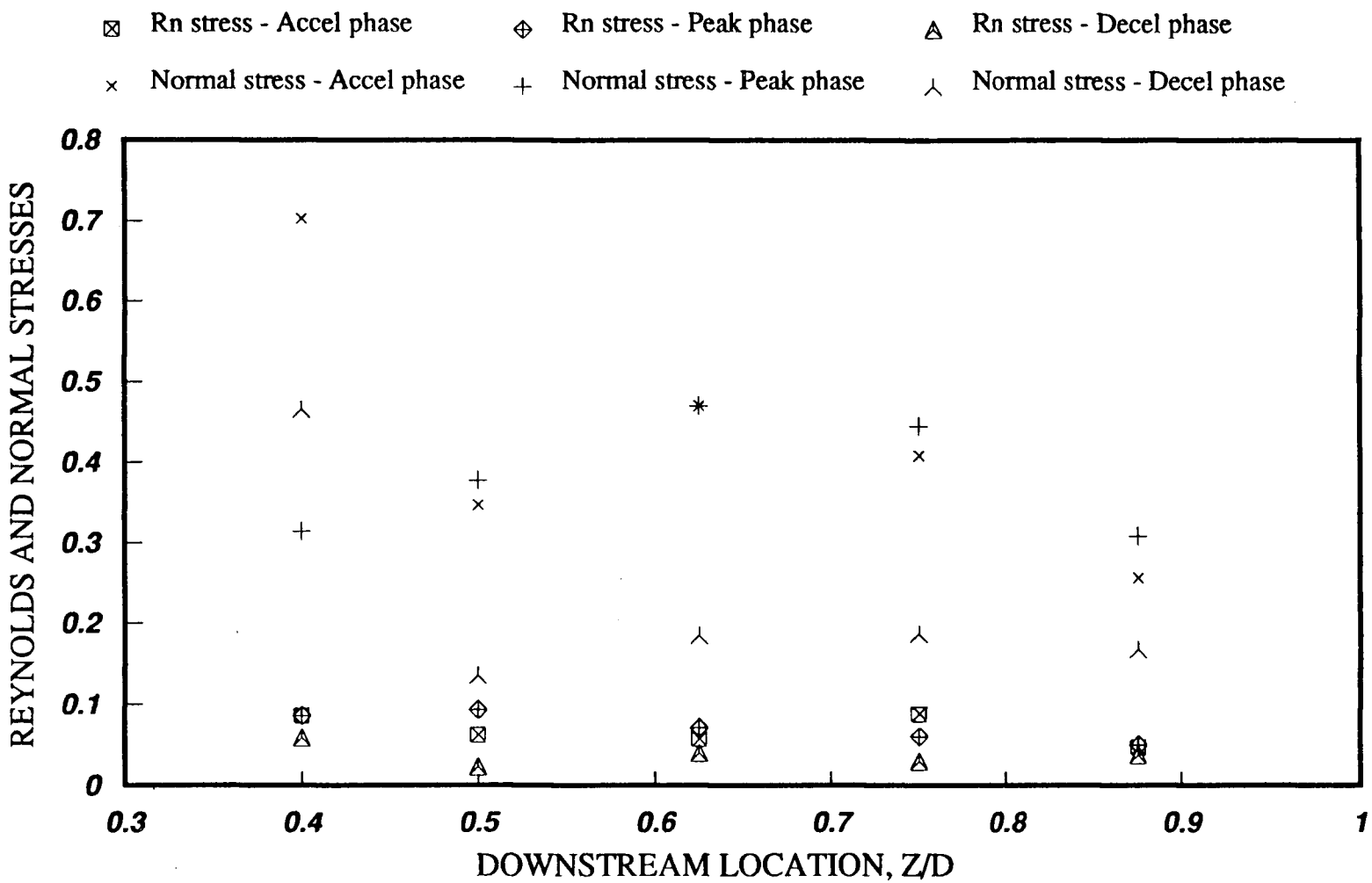

Figure 4-68 Variation of the nondimensional normal stresses and the Reynolds stress during the three phases of diastole at five downstream locations for the Carpentier-Edwards Supraannular prosthesis (29mm, Peak stresses).

the accelerating and peak-phases. However, when averaged over the diastolic phase (Figure 4-69), the stresses produced during the peak-phase last over a longer period than those during the acceleration phase. This is a completely opposite picture from the mechanical valves. However, as with the mechanical valve, the stresses during the deceleration phase are very low.

4.4 Summary of Comparative Performance (Biological prostheses)

Since the advent of the tissue prostheses, the main disadvantage, as opposed to the mechanical prostheses, has been their limited durability. Approaches to this problem have been the use of chemicals to retard the process of calcification, the redesign of stents (the frame upon which the leaflets are attached) and the development of new fixation methods for the attachment of the leaflets. The Hancock II and the Carpentier-Edwards supraannular prostheses represent two of the porcine tissue valves available on the market. Both are similar in design with slight variations in chemical treatment, fixation techniques and stent design.

Both the Hancock II and the Carpentier-Edwards supraannular valves produce a high velocity jet-like flow which forms a single vortex similar to that of the mechanical valves in a posterior orientation. This jet created high velocity gradients which led to high turbulent stresses usually confined to a region at the edge of the jet. These high turbulent stresses could damage the blood elements which in turn could lead to haemolysis or thromboembolism. Another concern are the possible regions of stagnation adjacent to the annulus which could lead to excess tissue overgrowth around the suture ring. The stagnant regions could form due to the obstruction offered by the valve to the circulation of the fluid, preventing the valve seat from being washed. This may depend on the height of the tissue valve stent. Tissue prostheses usually protrude further into the ventricle than most mechanical prostheses

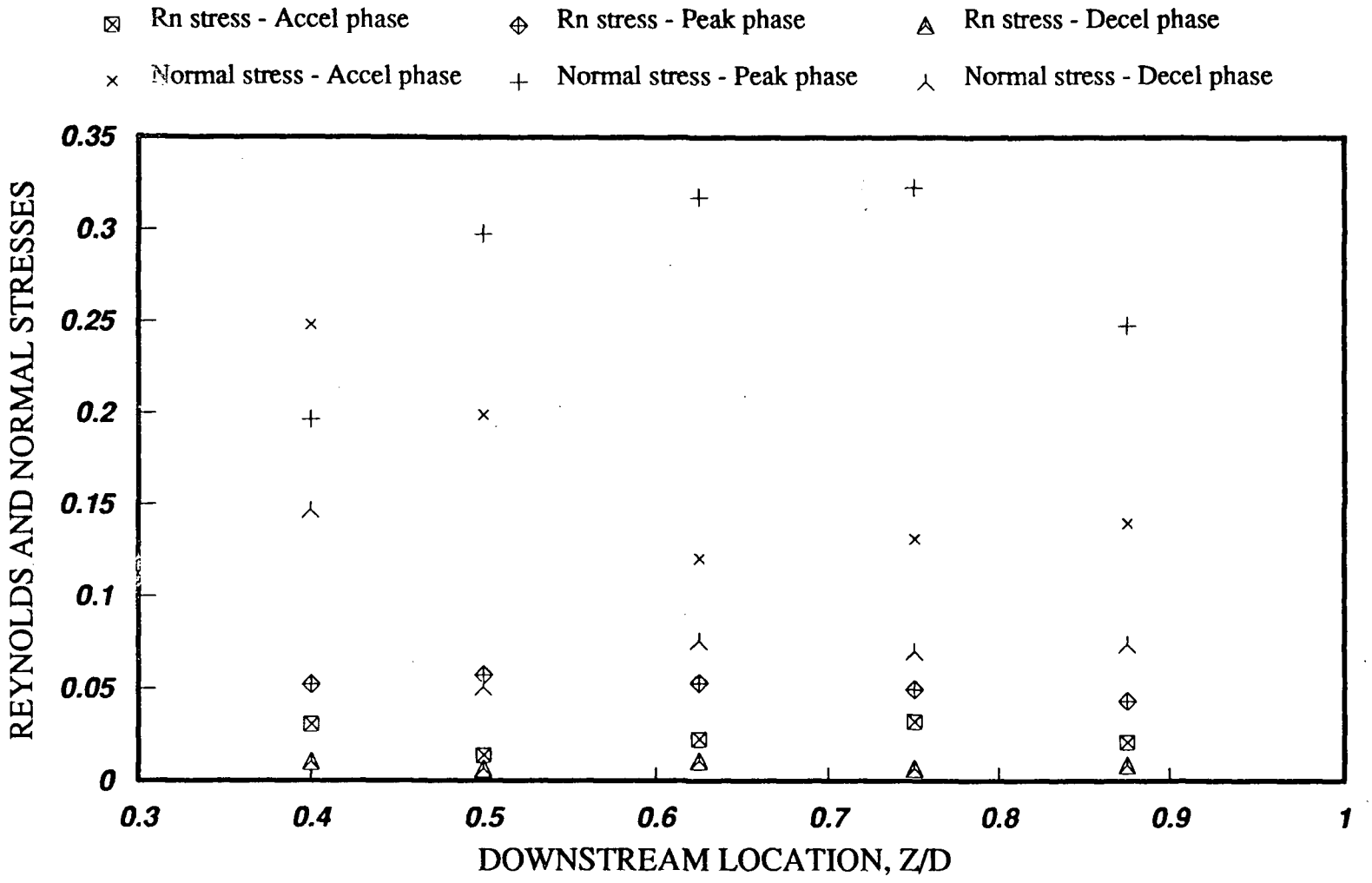

Figure 4-69 Variation of the nondimensional normal stresses and the Reynolds stress during the three phases of diastole at five downstream locations for the Carpentier-Edwards Supraannular prosthesis (29mm, Peak average stresses).

(tilting disc valves being a good example). Yoganathan[44]reported the presence of stagnation regions for the standard Hancock and Carpentier-Edwards valves which have a higher profile than these newer valves. However, due to restrictions in the present test facility, measurements could not be carried out close to the mitral valve thereby eliminating the chance to determine whether the lower profiles of the newer models provided better flow characteristics around the valve seat.

Figures 4-70 and 4-71 show a stress comparison between the two valves under study. Figure 4-70 shows the peak Reynolds and normal stresses for five downstream stations. The peak Reynolds stresses are of the same magnitude and show the highest value at 0.625D. The normal stresses, on the other hand, show the Carpentier-Edwards developing the highest values (by as much as 50% or more). However, when the stresses are averaged over the diastolic cycle (Figure 4-71), the normal stresses for the C-E valve are no longer dominant at all locations. In fact, the greatest difference between the stresses associated with the two valves is 15% at 0.4D. This would indicate that the peak normal stresses for the Hancock prosthesis are sustained for a longer time than those for the C-E prosthesis. However, the normal stresses are still higher for the C-E valve. The peak average Reynolds stresses give similar results as the peak values indicating that the Reynolds stresses for the two valves are of similar duration.

Despite the high turbulent stresses found in this study for the biological tissue valves, clinical studies on these valves to date show[21,22] that only mild amounts of haemolysis have been observed.

As a final note, the differences in results between the Hancock and Carpentier-Edwards valves may be attributed to possible biological changes in the leaflets. Due to the use of tissue in these valves, it was important to test the valves under

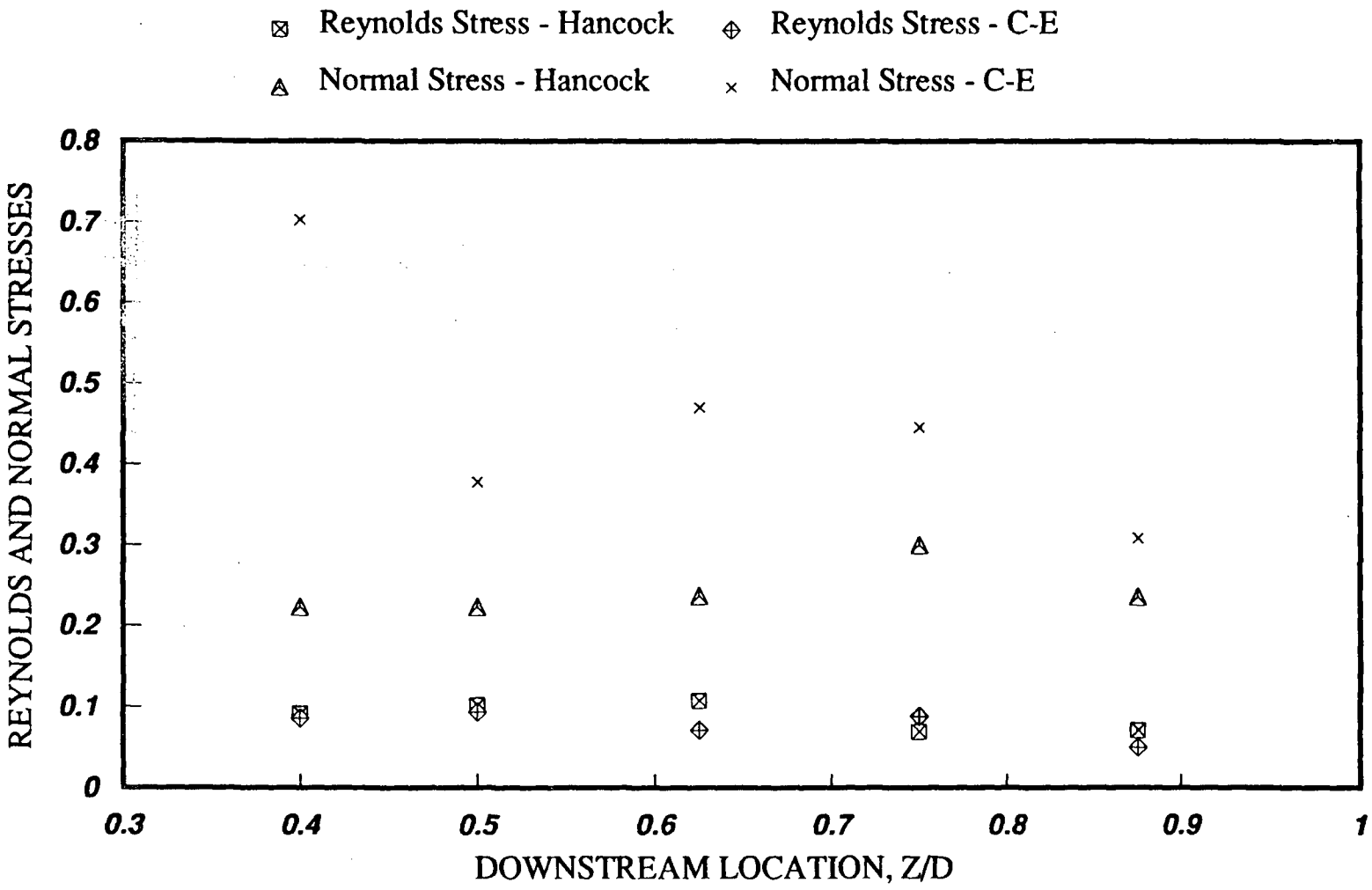

Figure 4-70 Variation of the peak nondimensional Reynolds and normal stresses at five downstream locations for the two tissue prostheses.

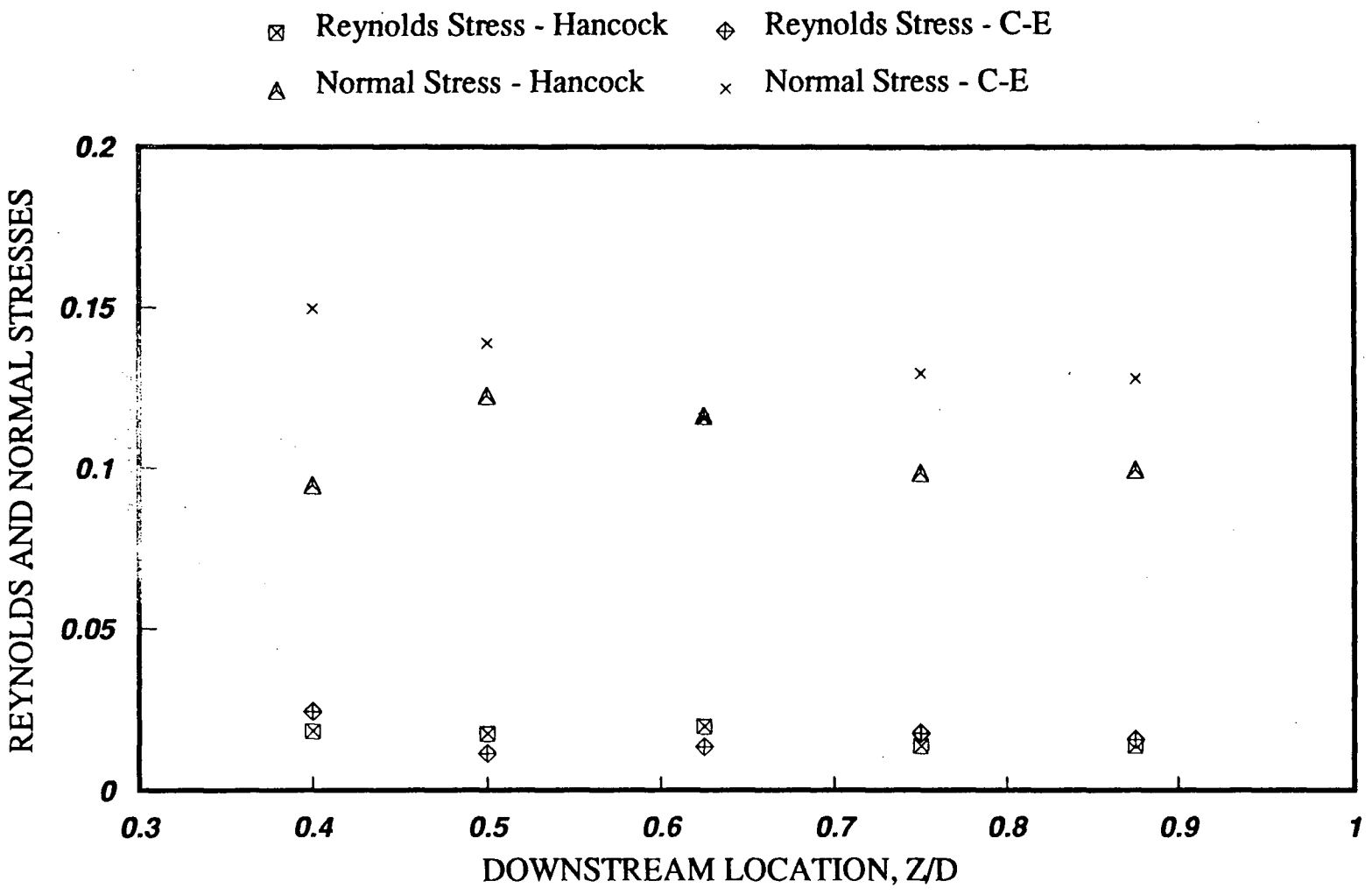

Figure 4-71 Variation of the peak average nondimensional Reynolds and normal stresses at five downstream locations for the two tissue prostheses.

controlled conditions. This involved using a saline solution for the test fluid and removing the valve if tests were not scheduled for several days. Due to the difficulty of maintaining a perfectly clean environment and the time consuming task of removing the valve from the test section, the Hancock II prosthesis may have suffered some biological changes in the leaflets. After tests were completed and the valve removed, it was observed that the leaflets had discoloured and thickened. Although both valves were isolated in the test section for approximately the same amount of time, only the Hancock II prosthesis underwent what appears to be a chemical change in the leaflets. This was evident by visual inspection only. The Carpentier-Edwards SAV prosthesis may have also undergone changes, however, they were not visually evident. Thorough tests would have to be conducted on both valves before any conclusions could be made. The fact that the Hancock prosthesis showed the better stress results, indicates that even if any physical metamorphosis did occur, it did not adversely effect the results.

4.5 Overall Performance of Prosthetic Valves

4.5.1 General Comments

The velocity profiles obtained with the heart valve prostheses indicate that the flow fields in the near vicinity of the valves are very complex. All the valves caused more obstruction to the flow than a normal natural valve. They produced jet-like flow fields in certain locations which depended on the geometry and orientation of the individual valve.

For the mechanical valves, the disc geometry, the disc opening angle and the valve orientation were factors that affected the flow fields and corresponding stress levels. The disc geometry appeared to effect the flow separation from the occluder.

For instance, the aerodynamic-shaped disc of the Bicer-Val valve minimized the flow separation. The opening angle, in addition to the disc geometry, also played an important role. The location of the jet usually varied as the disc opened (particularly with the anterior orientation). However, the full opening angle of the valve ultimately determined the location of the jet at the peak-phase. The larger the opening angle, the further downstream the jet was directed which in turn meant that the peak stresses were also located further away from the mitral orifice. The orientation of the valve may have played the most important role in reducing the stress level. In all the cases, the posterior configuration produced lower stress levels and, therefore, based on stress analysis, is the preferred orientation.

As the geometry for the two tissue valves were similar, it was expected that their flow fields would be similar. Both prostheses produced jet-like flows in the central part of the ventricle (similar to the posterior orientations for the tilting disc valves). The location of the jet generally was not affected by the opening and closing movement of the valve leaflets. The small orifice created by the opened leaflets was responsible for the high velocity gradients and subsequent high stresses.

4.5.2 Comparative Results

Figures 4-72 to 4-79 show the variation in Reynolds and normal stresses for all the mechanical and tissue prostheses. The first four diagrams present the results of the anterior orientation of the mechanical valves and both the tissue valves while the last four substitute the results for the anterior orientation with those for the posterior configuration. The boxed symbols represent the mechanical prostheses and the open symbols the tissue prostheses.

Figure 4-72 shows the peak Reynolds stresses for the mechanical valves in the

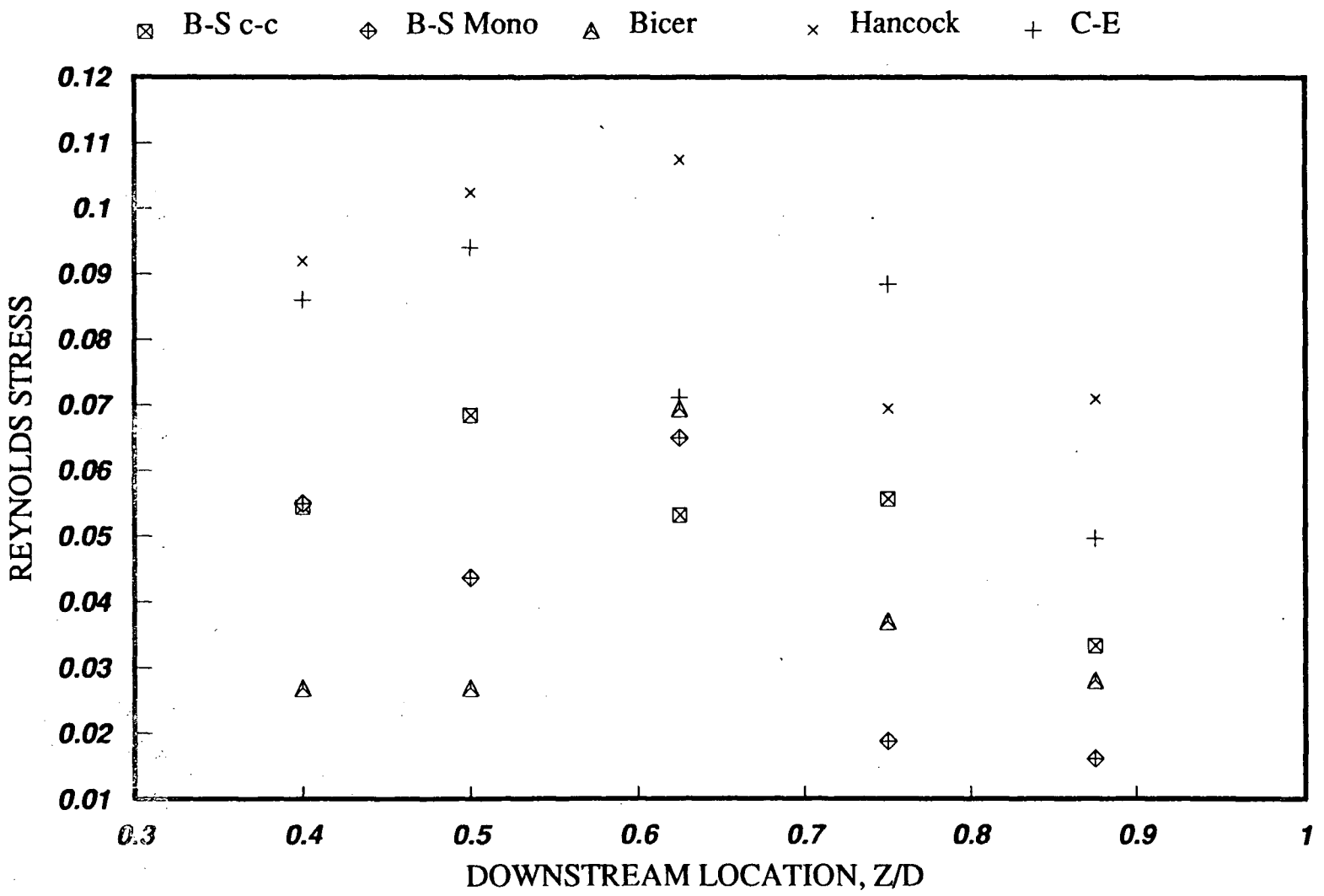

Figure 4-82 Variation of the peak Reynolds stresses at five downstream stations for the tissue prostheses and mechanical prostheses in the anterior orientation.

anterior orientation and the two tissue valves. The tissue valves show the highest stress values. However, when averaged over diastole (Figure 4-73), the Reynolds stresses associated with the tissue prostheses are not as dominant. The peak normal stresses (Figure 4-74) show the Hancock valve is comparable to the mechanical valves, but the C-E still has the highest stress levels. A similar trend can be seen when the normal stresses are averaged over the diastole (Figure 4-75).

Figure 4-76 compares the peak Reynolds stresses for the tissue prostheses and the mechanical prostheses in the posterior orientation. Again, the tissue valves have the highest values, dramatically so near the mitral orifice. The peak average results (Figure 4-77) show similar trends. The peak normal stress results (Figure 4-78), show similar trends as observed with the anterior orientation. The Hancock valve is comparable in performance to the mechanical valves, but the C-E valve shows exceptionally high normal stress values. This is further emphasized in the peak average diagram (Figure 4-79). The C-E valve continues to hold the highest normal stress values with the Hancock valve not far behind. These results clearly indicate that the stresses associated with the mechanical valves in the posterior configuration occur over short duration compared to those associated with the tissue prostheses.

Table 4-1 lists the peak stresses (highest values during the diastolic phase), the peak average stresses (highest values after averaging over the diastolic phase), and the average stresses (averaging over the diastolic phase and the cross-section). The results were taken down the centre line of the ventricle at five downstream stations as numerous tests showed that the flow and stress fields were highest in this area. The stress measurements show that the turbulent stresses produced by all the valves were high enough to possibly cause sublethal damage to the blood elements.

Since the measurements were taken at intervals of 2 mm, the measured maximum

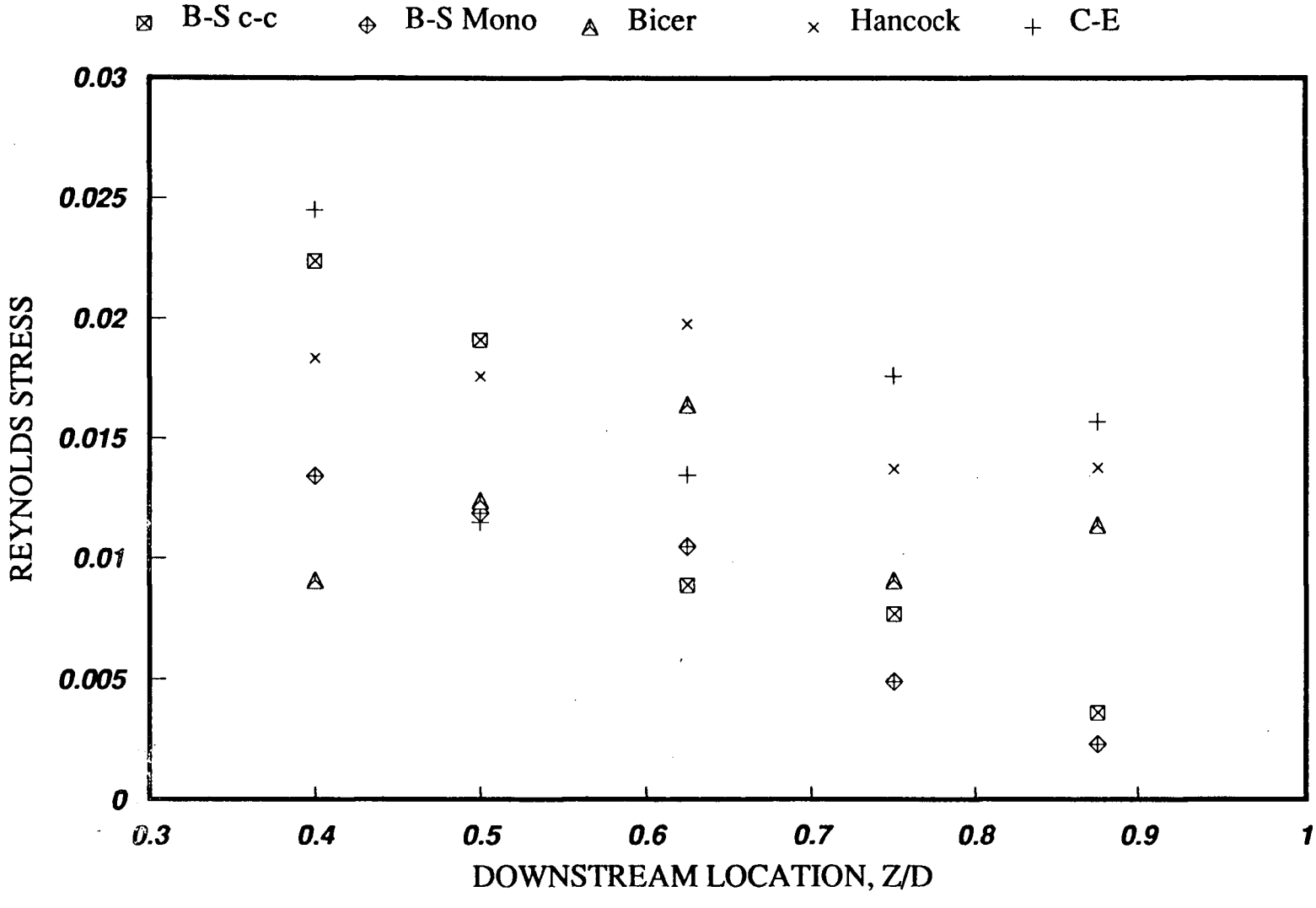

Figure 4-73 Variation of the peak average Reynolds stresses at five downstream stations for the tissue prostheses and mechanical prostheses in the anterior orientation.

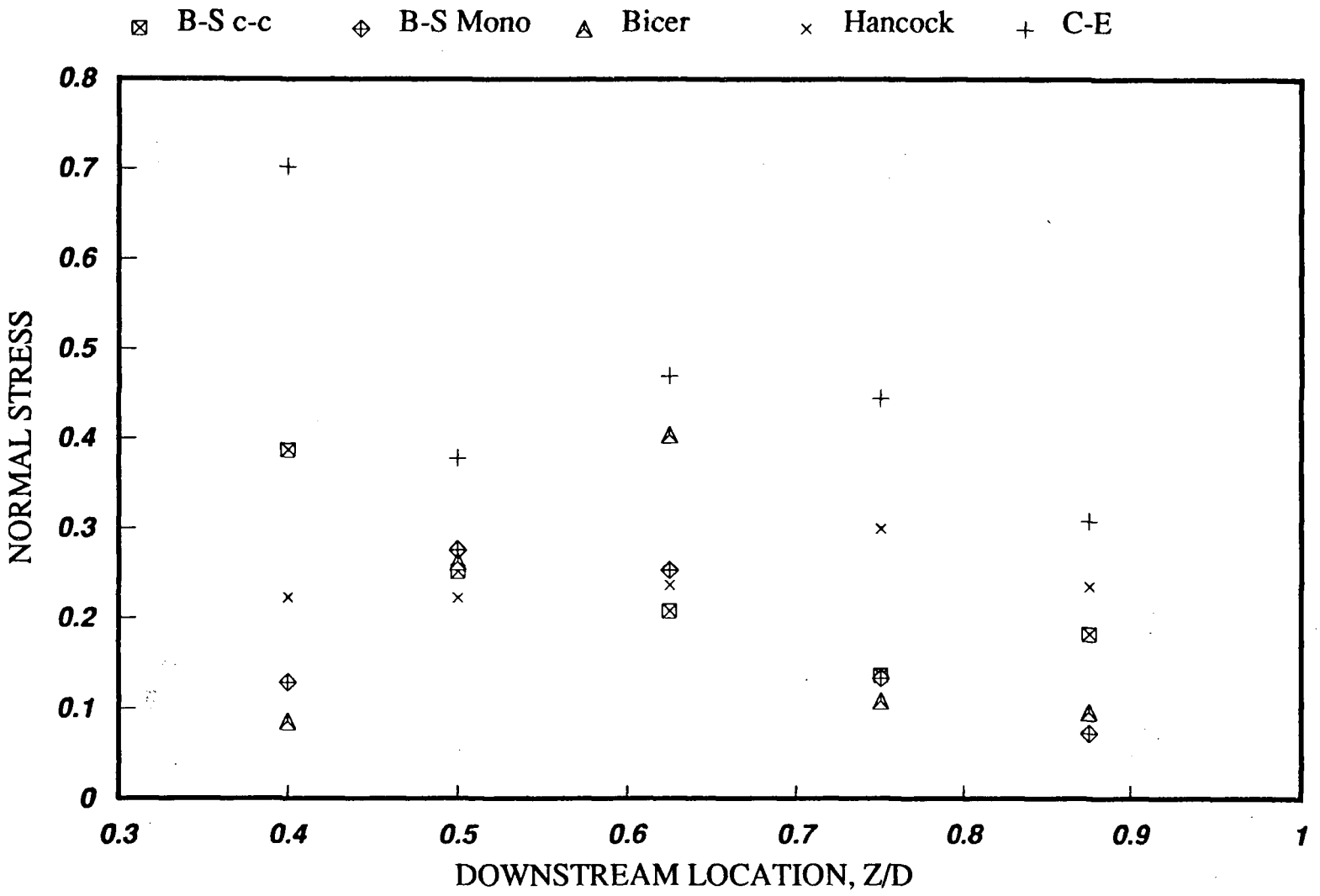

Figure 4-74 Variation of the peak normal stresses at five downstream stations for the tissue prostheses and mechanical prostheses in the anterior orientation.

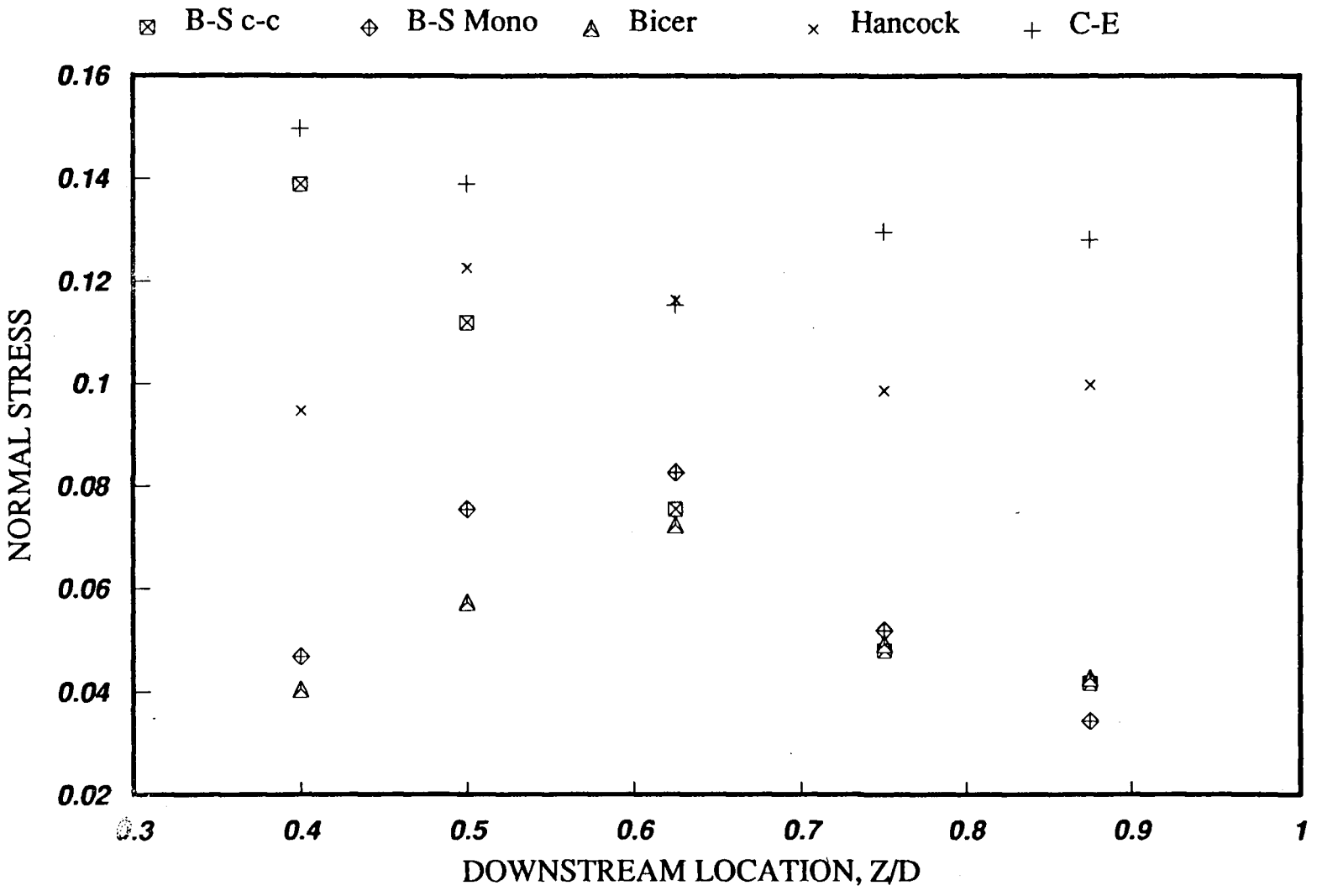

Figure 4-75 Variation of the peak normal stresses at five downstream stations for the tissue prostheses and mechanical prostheses in the anterior orientation.

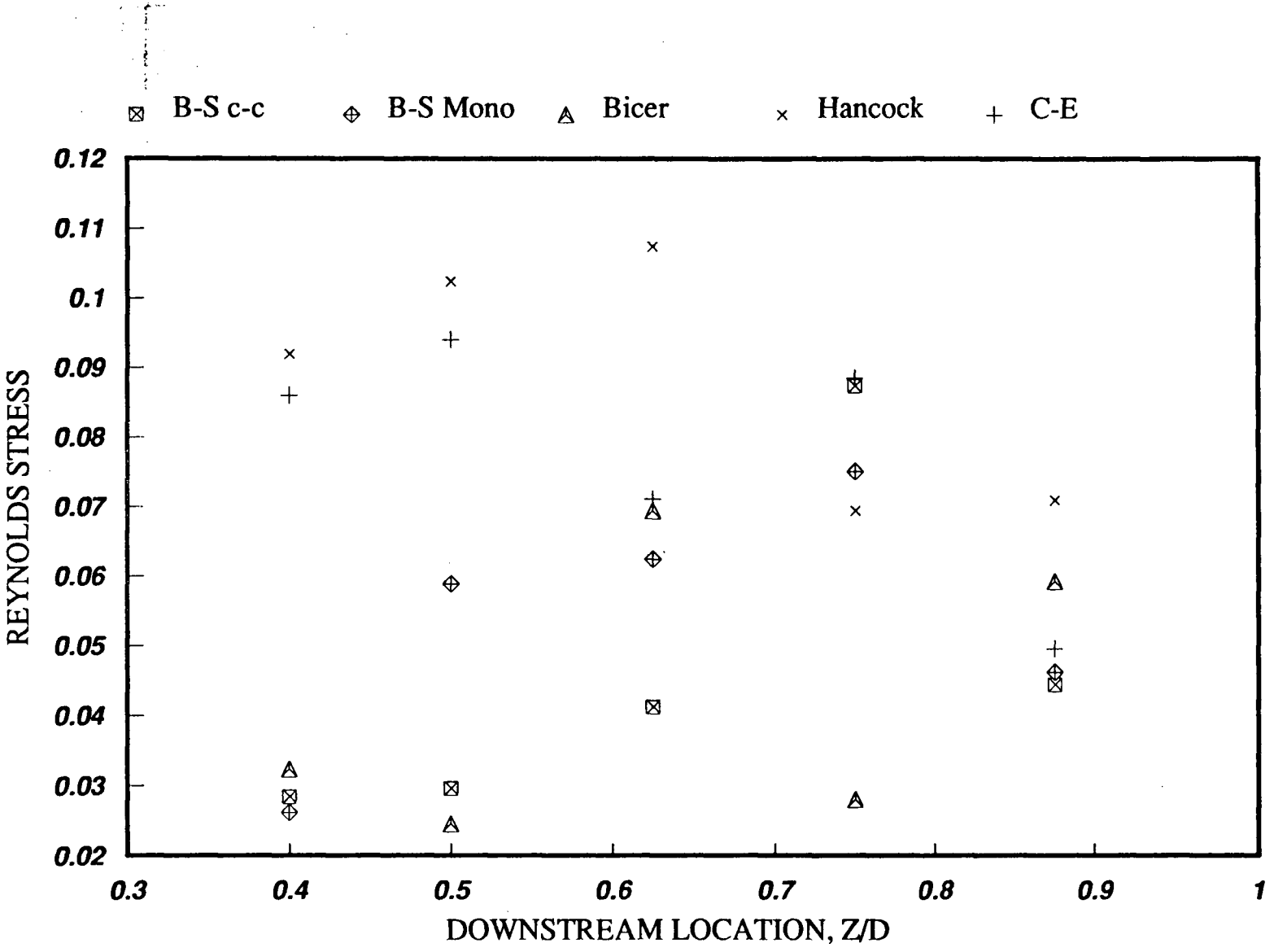

Figure 4-76 Variation of the peak Reynolds stresses at five downstream stations for the tissue prostheses and mechanical prostheses in the posterior orientation.

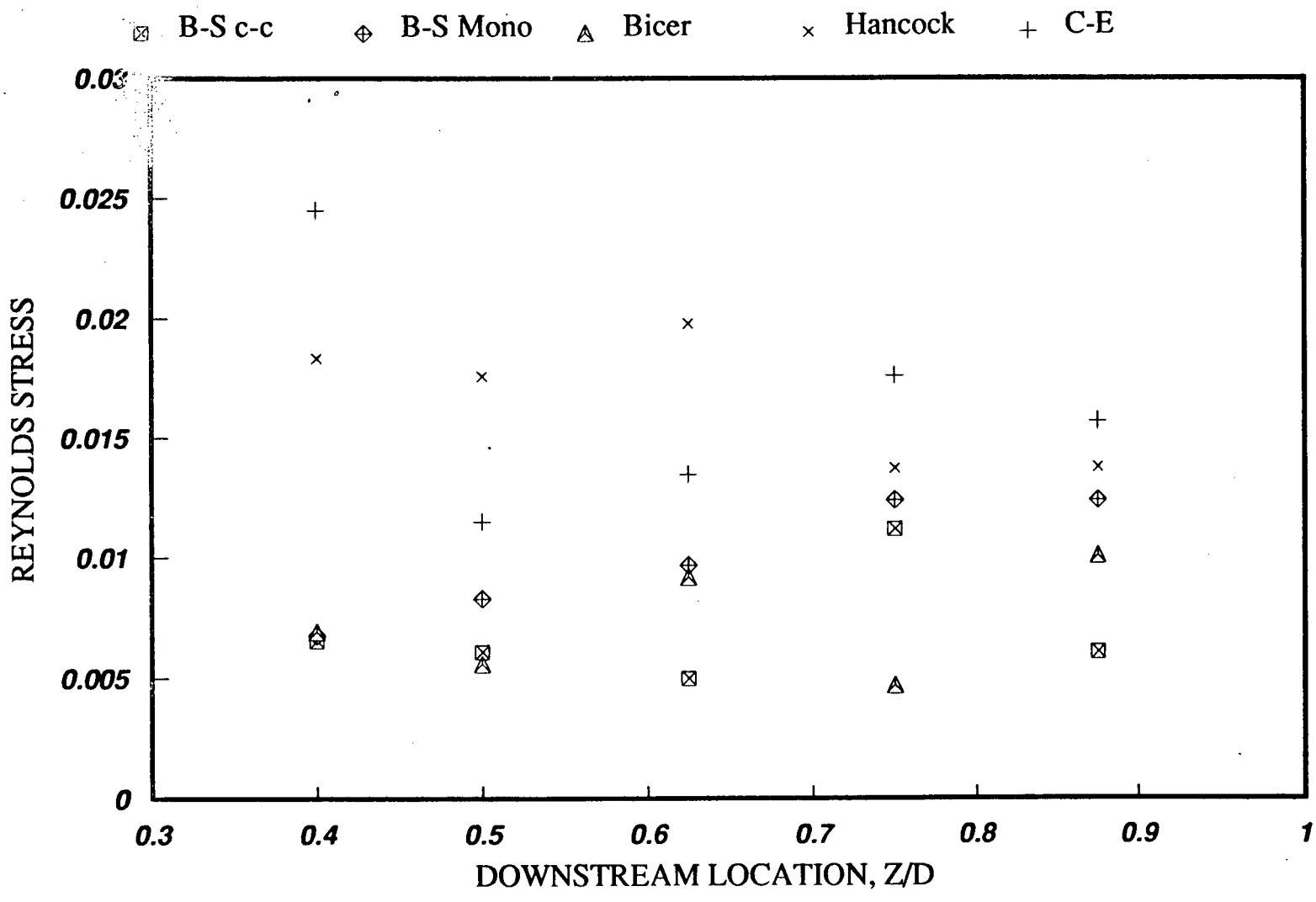

Figure 4-77 Variation of the peak average Reynolds stresses at five downstream stations for the tissue prostheses and mechanical prostheses in the posterior orientation.

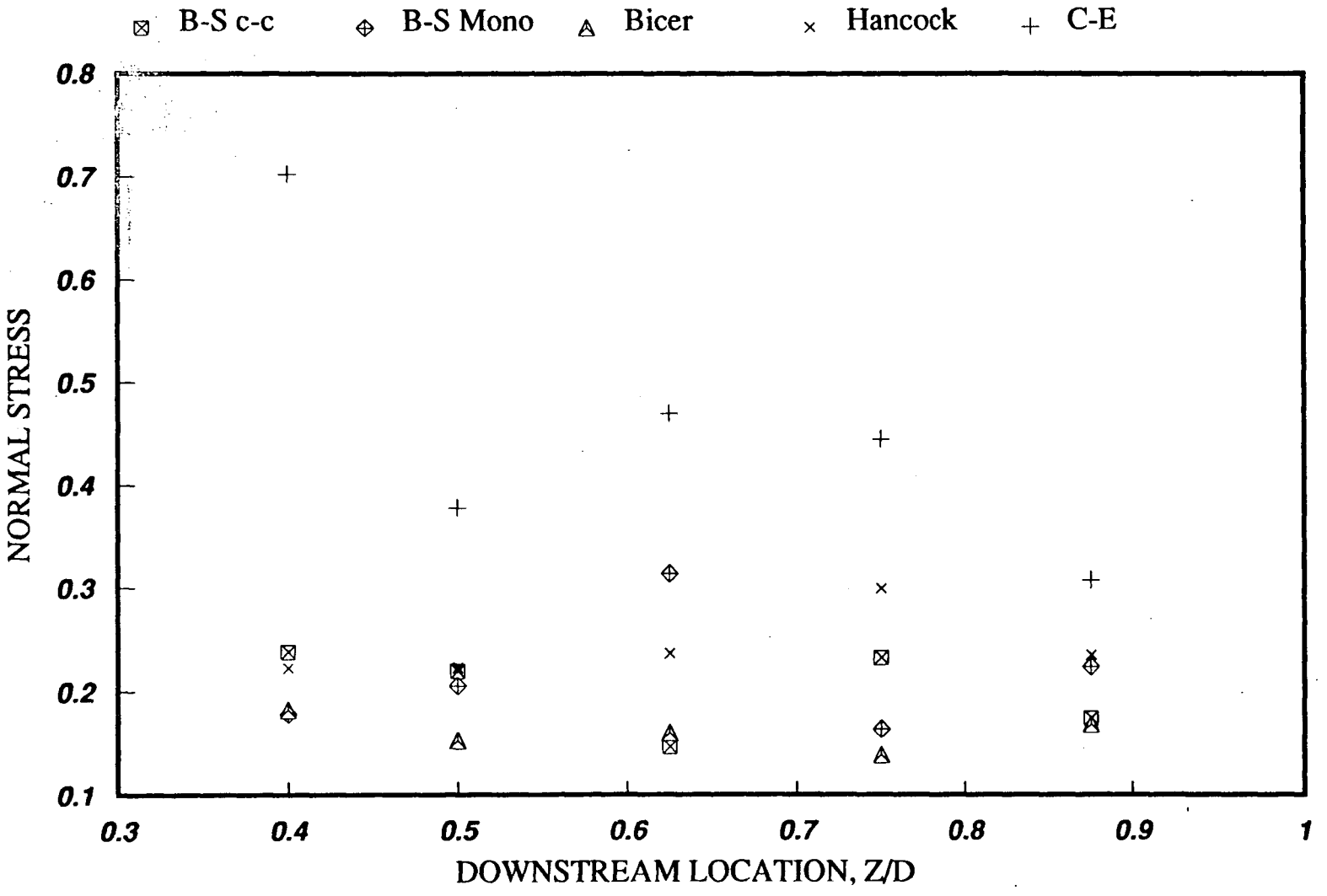

Figure 4-78 Variation of the peak normal stresses at five downstream stations for the tissue prostheses and mechanical prostheses in the posterior orientation.

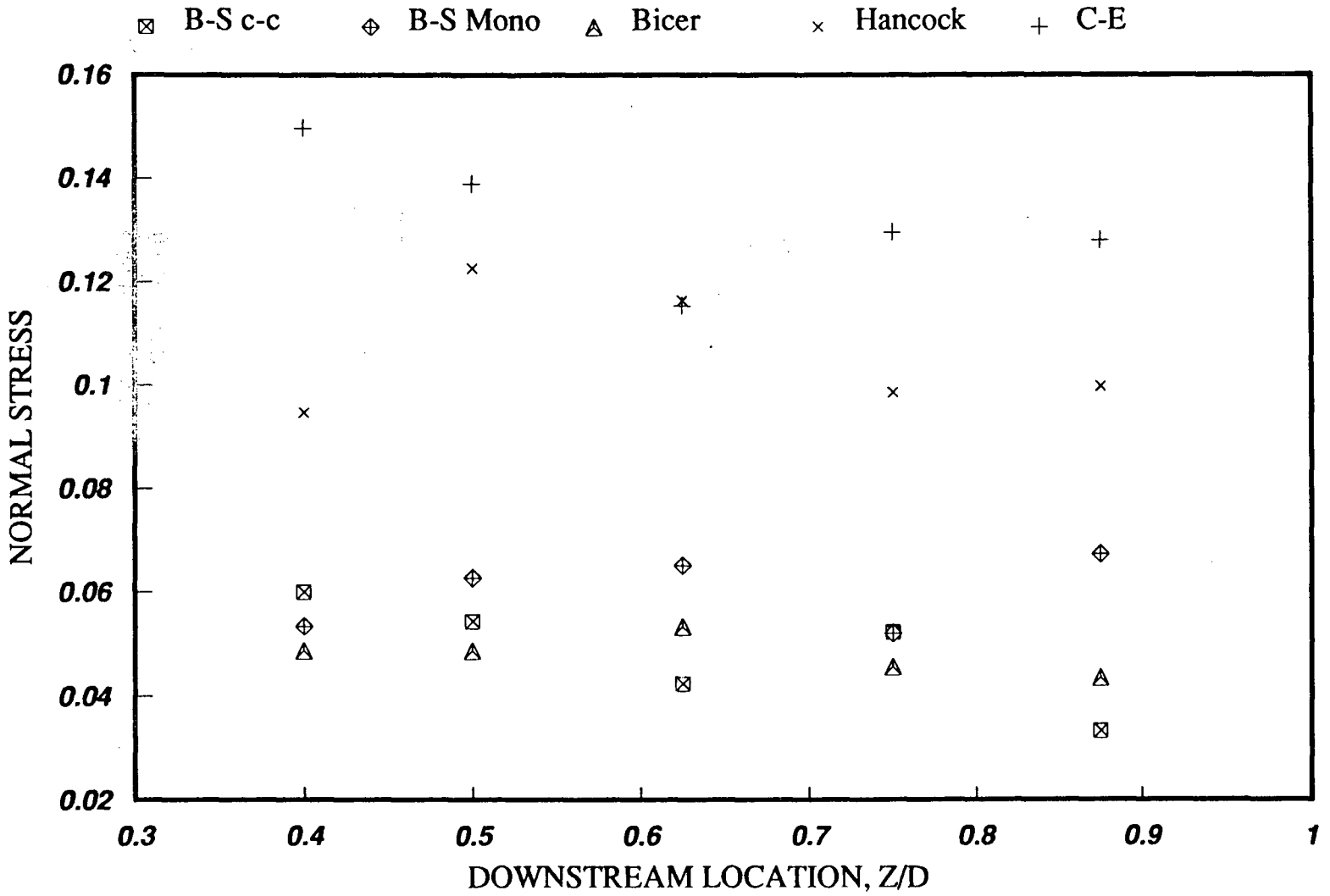

Figure 4-79 Variation of the peak normal stresses at five downstream stations for the tissue prostheses and mechanical prostheses in the posterior orientation.

Table 4-1 Peak, peak average and average stresses measured at five downstream locations for different valves.

Valve	Level	Reynolds			Normal		
		Peak	Max Avg	Avg	Peak	Max Avg	Avg
B-S C-C anterior	0.400	0.0544	0.0224	0.0053	0.3869	0.1389	0.0440
	0.500	0.0685	0.0191	0.0046	0.2518	0.1119	0.0440
	0.625	0.0532	0.0089	0.0033	0.2084	0.0755	0.0380
	0.750	0.0556	0.0077	0.0025	0.1366	0.0480	0.0303
	0.875	0.0333	0.0036	0.0017	0.1828	0.0417	0.0211
B-S C-C posterior	0.400	0.0284	0.0066	0.001	0.2384	0.0600	0.0235
	0.500	0.0296	0.0061	0.0012	0.2198	0.0544	0.0263
	0.625	0.0413	0.0050	0.0008	0.1467	0.0424	0.0247
	0.750	0.0874	0.0112	0.0019	0.2329	0.0523	0.0274
	0.875	0.0888	0.0101	0.0012	0.2132	0.0422	0.0123
B-S Mono anterior	0.400	0.0550	0.0134	0.0018	0.1291	0.0468	0.0242
	0.500	0.0437	0.0119	0.0025	0.2756	0.0755	0.0346
	0.625	0.0650	0.0105	0.0028	0.2536	0.0826	0.0343
	0.750	0.0188	0.0049	0.0010	0.1339	0.0519	0.0205
	0.875	0.0162	0.0023	0.0006	0.0728	0.0344	0.0135
B-S Mono posterior	0.400	0.0262	0.0068	0.0011	0.1786	0.0535	0.0252
	0.500	0.0589	0.0083	0.0021	0.2057	0.0628	0.0298
	0.625	0.0624	0.0097	0.0026	0.3141	0.0651	0.0304
	0.750	0.0750	0.0124	0.0035	0.1640	0.0520	0.0338
	0.875	0.0463	0.0124	0.0031	0.2245	0.0673	0.0278
Bicer anterior	0.400	0.0269	0.0091	0.0016	0.0853	0.0405	0.0228
	0.500	0.0269	0.0124	0.0023	0.2626	0.0575	0.0243
	0.625	0.0694	0.0164	0.0025	0.4043	0.0724	0.0252
	0.750	0.0370	0.0091	0.0023	0.1088	0.0493	0.0253
	0.875	0.0281	0.0114	0.0018	0.0960	0.0427	0.0158
Bicer posterior	0.400	0.0324	0.0069	0.0012	0.1828	0.0487	0.0235
	0.500	0.0246	0.0056	0.0014	0.1527	0.0487	0.0248
	0.625	0.0694	0.0092	0.0016	0.1599	0.0533	0.0243
	0.750	0.0281	0.0047	0.0015	0.1388	0.0456	0.0247
	0.875	0.0593	0.0101	0.0014	0.1686	0.0436	0.0239
Hancock II	0.400	0.0920	0.0183	0.0060	0.2229	0.0947	0.0381
	0.500	0.1024	0.0176	0.0072	0.2229	0.1226	0.0540
	0.625	0.1074	0.0198	0.0069	0.2369	0.1163	0.0573
	0.750	0.0694	0.0137	0.0068	0.2994	0.0985	0.0561
	0.875	0.0709	0.0138	0.0058	0.2354	0.0997	0.0547
C-E SAV	0.400	0.0861	0.0245	0.0032	0.2527	0.1497	0.0434
	0.500	0.0940	0.0115	0.0040	0.3779	0.1390	0.0582
	0.625	0.0711	0.0135	0.0063	0.4699	0.1154	0.0614
	0.750	0.0885	0.0176	0.0064	0.4449	0.1296	0.0684
	0.875	0.0496	0.0157	0.0056	0.3082	0.1280	0.0676

velocities, normal stresses and Reynolds stress are not necessarily the maximum values in the flow fields. For the velocity measurements, the results show that more than adequate data points were obtained to construct a continuous profile. However, at locations of high velocity gradients, the turbulent stresses experienced drastic changes over small distances and the locations where the maximum stress occurred could have been missed.

5. CONCLUSIONS AND RECOMMENDATIONS

5.1 Concluding Remarks

The primary objective of the research program has been to gain a better quantitative understanding of the velocity and turbulent stress fields in the immediate vicinity of three tilting disc mechanical prostheses and two biological tissue prostheses.

The use of a sophisticated and versatile cardiac simulator in conjunction with a two component 3-beam Laser Doppler Anemometer enabled the measurement of the velocities and the stresses, in particular the Reynolds stress, at any location in the ventricle. As numerous tests showed that the highest velocities and stresses were located down the centreline of the ventricle, only those results were presented in this study.

The results presented in this study are unique in their contribution in a number of ways. First, the test facility, being highly versatile, permitted both steady-state and pulsatile experiments. Second, as the geometry of the natural left ventricle is modelled by this facility, the results obtained here are applicable to mitral valves. To date, most results obtained in other facilities have only analyzed protheses in the aortic position, as the aorta is easily modelled using a cylindrical section of pipe. Third, the use of the three-beam Laser Doppler Anemometer permits the simultaneous measurement of two velocity components in the fluid stream. This, in turn, makes it possible to calculate the Reynolds stress. Until recently, other investigators have only used two-beam Laser Doppler Anemometers which permit the measurement of only one velocity component at any given moment. Finally, the effect of valve orientation on the the fluid flow characteristics of tilting-disc

mechanical valves was presented.

The results and insight gained during the testing and analyzing phases of this investigation can be summarized as follows:

(a) The manner in which the data are presented is important in order to obtain an accurate picture of the overall performance. For this reason, nondimensional presentation of results is essential. While this is common practice in the engineering field, it is relatively new in the medical sciences. Successful identification of proper nondimensional parameters can essentially achieve results that are independent of test facilities, flow velocities, size of models, etc.

(b) Studies of prosthetic heart valves should always be conducted under pulsatile flow conditions. Due to the time independence of steady state experiments, any results gleaned could be misleading. Steady state investigations are useful as a first indication of acceptability but conclusions on the valves performance should never be based on this alone.

(c) The results showed that all the valves studied created very disturbed flow fields which generated high turbulent stresses. The tissue prostheses generally had the highest stress levels.

(d) The general features of the flow field produced by the mechanical tilting disc valves in the posterior orientation are quite different from those in the anterior orientation. The anterior orientation gave rise to a very complex flow pattern consisting of a least two vortices which led to high turbulent stresses. The posterior orientation usually created a single vortex, decreasing the number of turbulent interactions and thus producing lower stress levels.

(e) In overall analysis, the newer generation tilting disc mechanical prostheses (Björk-Shiley monostrut and Bicer-Val) are superior to the older generation valve rep-

resented by the Björk-Shiley c-c.

The presentation, and thus the results, of the turbulent stresses and the velocities (under steady and pulsatile flow conditions) were different from those of most other investigators. This can mainly be attributed to different experimental procedures and test-stations. If more results were presented in a nondimensional form, as done here, comparisons between data would have more validity. However, the one common conclusion arrived at by all investigators is that the study of prosthetic heart valves should always be conducted under the pulsatile flow condition.

5.2 Recommendation for Future Work

The investigation of prosthetic heart valves is a challenging and complex problem. The investigation reported here only represents a small step along a long journey. In order to obtain further information on the fluid dynamic characteristics of different types of prosthetic valves, so that better prostheses may be designed, efforts in the following direction are suggested:

(a) In order to determine that adequate washing occurs around the valve, i.e. to insure that no stagnation regions are present, it is necessary to obtain results as close to the valve as possible. Due to obstruction of the test chamber, the present LDA system is restricted in its traverse close to the valve. For $Z < 0.4D$, one (or more) of the three laser beams is interrupted by the top of the chamber. A possible redesign of the chamber would allow measurements of fluid dynamic parameters closer to the valve.

(b) The results from this study clearly indicate the importance of the orientation on stress levels for tilting disc mechanical valves. Only two configurations were studied (anterior and posterior) with dramatic results. The two orientations,

180° apart, leave many other positions open to study. Although not covered in this thesis, different orientations for tissue prostheses should also be explored as the valves are asymmetric.

(c) Additional mechanical and biological tissue prostheses should be studied.

(d) Flow visualization studies should be conducted in the present facility to further assess formation of vortices within the ventricle and also to determine the amount of regurgitation associated with each valve, something not covered in the present study.

(e) A detailed fundamental study is needed to assess the level of stresses and their duration that would result in the serious problems of thromboembolism, red cell and platelet damage, etc. This problem has been debated among many different researchers[47-49]. This question is particularly important because as shown, many of the valves produced high peak stress values but when averaged over the cycle, the stresses appeared to be short-lived. Therefore, it would be necessary to know whether short-lived high stresses would lead to any serious problems of thromboembolism and haemolysis.

(f) Finally, fluid dynamic parameters represent only one set of criteria to evaluate performance of a prosthetic heart valve. Other parameters such as fatigue strength and tissue integrity should also be explored.

REFERENCES

[1] Wright, J.T.M., "Hydrodynamic Evaluation of Tissue Valves," *Tissue Heart Valves*, Butterworths, London, 1979, pp. 29–87.

[2] Davey, T.B., Kaufman, B., Smeloff, E.A., "Pulsatile Flow Studies of Prosthetic Heart Valves," *J Thorac Cardiovasc Surg*, Vol. 51, 1966, pp. 264–267.

[3] Harken, D.E., Soroff, H.S., Taylor, W.J., et al., "Partial and Complete Prostheses in Aortic Insufficiency," *J Thorac Cardiovasc Surg*, Vol. 4, 1960, p. 744.

[4] Starr, A., Edwards, M.L., "Mitral Replacement: The Shielded Ball Valve Prosthesis," *J Thorac Cardiovasc Surg*, Vol. 42, 1961, pp. 673–677.

[5] Starr, A., Edwards, M.L., "Mitral Replacement: A Clinical Experience with the Ball Valve Prosthesis," *Ann Surg*, Vol. 154, 1961, pp. 726–740.

[6] Herr, R., Starr, A., McCord, C.W., et al., "Special Problems Following Valve Replacement: Embolus, Leak, Infection, Red Cell Damage," *Ann Thorac Surg*, Vol. 1, 1965, pp. 403–410.

[7] Hufnagel, C.A., Harvey, W.P., Rabil, P.J., and McDermott, "Surgical Correction of Aortic Insufficiency," *Surgery*, Vol. 35, No. 5, May 1954, pp. 673–683.

[8] Carpentier, A., "From Xenograft Valve to Valvular Xenobioprosthesis," *Proceedings of the Symposium on Bioprosthetic Cardiac Valves*, Deutsches Herzzentrum Munich, 1979, pp. 1–16.

[9] Rothlin, M.E., Senning, A., "Fifteen Years Experience with Fascia Lata Aortic Valves and the Outlook of Modern Bioprosthesis," *Proceedings of the Symposium on Bioprosthetic Cardiac Valves*, Deutsches Herzzentrum Munich, 1979, pp. 173–178.

[10] Angell, W.W., "A Nine Year Experience with the Angell- Shiley Xenograft and a Comparative Literature Review of the Porcine Bioprosthesis Versus the Mechanical Prosthesis," *Proceedings of the Symposium on Bioprosthetic Cardiac Valves*, Deutsches Herzzentrum Munich, 1979, pp. 81–106.

[11] Cortina, J.M., Martinell, J., et al., "Comparative Clinical Results with Omni-

science, Medtronic Hall, and Björk-Shiley Convexo-concave Prostheses in Mitral Valve Replacement," *J Thorac Cardiovasc Surg*, Vol. 91, 1986, pp. 174--183.

[12] Lindblom, D., "Long-term Clinical Results After Mitral Valve Replacement with the Björk-Shiley Prosthesis," *J Thorac Cardiovasc Surg*, Vol. 95, 1988, pp. 321–333.

[13] Stewart, S., Cianciotta, D., et al., "The Lillehei-Kaster Aortic Valve Prosthesis," *J Thorac Cardiovasc Surg*, Vol. 95, 1988, pp. 1023–1030.

[14] Lindblom, D., "Long-term Clinical Results After Aortic Valve Replacement with the Björk-Shiley Prosthesis," *J Thorac Cardiovasc Surg*, Vol. 95, 1988, pp. 658–667.

[15] Aris, A., Padro, J., et al., "Clinical and Hemodynamic Results of Cardiac Valve Replacement with the Monostrut Björk-Shiley Prosthesis," *J Thorac Cardiovasc Surg*, Vol. 95, 1988, pp. 423–431.

[16] Thulin, L., Bain, W., et al., "Heart Valve Replacement with the Björk-Shiley Monostrut Valve: Early Results of a Multicenter Clinical Investigation," *Ann Thorac Surg*, Vol. 45, 1988, pp. 164–170.

[17] Björk, V., Lindblom, D., "The Monostrut Björk-Shiley Heart Valve," *J Am Coll Cardiol*, Vol. 6, 1985, pp. 1142-1148 .

[18] Kopf, G., Hammond, G., et al., "Long-term Performance of the St. Jude Medical Valve: Low Incidence of Thromboembolism and Hemorrhagic Complications with Modest Doses of Warfain," *Circulation*, Vol. 76 (Suppl III), 1987, pp. 132–136.

[19] Chaux, A., Matloff, J., et al., "Clinical Results with the St. Jude Medical Valve," *Heart Valve Replacement and Reconstruction*, Year Book Medical Publishers, Chicago, 1987, pp. 191-199.

[20] Ionescu, M.I., Tandon, A.P., et al., "Heart Valve Replacement with the Ionescu-Shiley Pericardial Xenograft," *J Thorac Cardiovasc Surg*, Vol. 73, 1977, pp. 31–42.

[21] Jamieson, W.R.E., Burr, L.H., et al., "Quality of Life Afforded by Porcine Bioprostheses Illustrated by the New-generation Carpentier-Edwards Porcine Bioprothesis," *Heart Valve Replacement: Current Status and Future Trends*, Futura Publishing Co. Inc., Mount Kisco, NY, 1987, pp. 225–243.

[22] Wright, J.T.M., Eberhardt, C.E., et al., "Hancock II - An Improved Valve," *Second International Symposium on Cardiac Bioprostheses*, Cardiothoracic Institute, National Heart Hospital, London, 1981, p. 425.

[23] Lindblom, D., Rodriguez, L., et al., "Mechanical Failure of the Björk-Shiley Valve," *J Thorac Cardiovasc Surg*, Vol. 97, 1989, pp. 95–97.

[24] Gonzalez-Lavin, L., McGrath, L., et al., "Strut Fracture and Other Events After Valve Replacement with the 60 Degree Convexoconcave Björk-Shiley Prosthesis," *Circulation*, Vol. 76 (Supp III), 1987, pp. 132- -137.

[25] Hacket, D., Fessatides, I., et al., "Ten Year Clinical Evaluation of Starr Edwards 2400 and 1260 Aortic Valve Prostheses," *Br Heart J*, Vol. 57, 1987, pp. 356–363.

[26] Myers, M.L., Lawrie, G., et al., "The St. Jude Valve Prosthesis: Analysis of the Clinical Results in 815 Implants and the Need for Systematic Anticoagulation," *JACC*, Vol. 13, 1989, pp. 57–62.

[27] Antunes, M., Wessels, A., et al., "Medtronic-Hall Valve Replacement in a Third World Population Group," *J Thorac Cardiovasc Surg*, Vol. 95, 1988, pp. 980–993.

[28] Miller, C., Oyer, P., et al., "Ten-year Clinical Experience in 1651 Patients with One Type of Tissue Valve," *Heart Valve Replacement and Reconstruction*, Year Book Medical Publishers, Chicago, 1987, pp. 175–89.

[29] Ionescu, M., "The Ionescu-Shiley Pericardial Xenograft Heart Valve," *Tissue Heart Valves*, Butterworths, London, 1979, pp. 201–252.

[30] Hammermeister, K., Henderson, W., et al., "Comparison of Outcome After Valve Replacement with a Bioprosthesis Versus a Mechanical Prosthesis: Initial 5 Year Results of a Randomized Trial," *JACC*, Vol. 10, No. 4, October 1987, pp. 719–732.

[31] Reice, I.J., Anderson, J.D., et al., "A New Porcine Bioprosthesis: In Vitro and In Vivo Evaluation," *Life Support Systems*, Vol. 3, 1985, pp. 207–227.

[32] Magilligan, D., Kemp, S., et al., "Asynchronous Primary Valve Failure in Patients with Porcine Bioprosthetic Aortic and Mitral Valves," *Circulation*, Vol. 76 (Supp. III), 1987, pp. 139–141.

[33] Zhur, X., Guo-Jiaqiang, et al., "Ten-year Experience with Pericardial Xenograft Valves," *J Thorac Cardiovasc Surg*, Vol. 95, 1985, pp. 572–576.

[34] Barratt-Boyes, B., "Long-term Follow-up of Patients Receiving a Freehand Antibiotic Sterilized Homograft Aortic Valve," *Heart Valve Replacement: Current Status and Future Trends*, Futura Publishing Co. Inc., Mount Kisco, N.Y., 1987, p. 225.

[35] Smeloff, E.A., Huntley, A.C., et al., "Comparative Study of Prosthetic Heart Valves," *J Thorac Cardiovasc Surg*, Vol. 52, 1966, pp. 841–848.

[36] Hasenkam, J.M., Westphal, D., et al., "3-D Visualization of Axial Velocity Profiles Downstream of 6 Different Mechanical Aortic Valve Prostheses Measured with a Hot-film Anemometer in a Steady State Flow Model," *J Biomechanics*, Vol. 20, 1987, pp. 353–364.

[37] Hasenkam, J.M., Westphal, D., et al., "In Vitro Stress Measurements in the Vicinity of 6 Mechanical Aortic Valves Using Hot-film Anemometry in a Steady Flow," *J Biomechanics*, Vol. 21, 1988, pp. 235–247.

[38] Reul, H., Giersiepen, M., Knott, E., "Laboratory Testing of Prosthetic Heart Valves," *Heart Valve Engineering*, Mechanical Engineering Publications Ltd., London, 1986, pp. 3–13.

[39] Bruss, K.H., Reul, H., Gilse, J., Knott, E., "Pressure Drop and Velocity Fields at Four Mechanical Heart Valve Prostheses: Björk-Shiley Standard, Björk-Shiley C-C, Hall-Kaster and St. Jude Medical," *Life Support Systems*, Vol. 1, 1983, pp. 3– 22.

[40] Woo, Y-R, Yoganathan, A.P, "An Instrument for the Measurement of In Vitro Velocity and Turbulent Shear Stress in the Immediate Vicinity of Prosthetic Heart Valves," *Life Support Systems*, Vol. 4, 1986, pp. 47–62.

[41] Yoganathan, A.P., "Cardiovascular Fluid Dynamics of Prosthetic Aortic Valves," Ph.D. Thesis, California Institute of Technology, CA, 1978.

[42] Yoganathan, A.P., Woo, Y-R, et al., "In Vitro Hemodynamic Characteristics of Tissue Bioprostheses in the Aortic Position," *J Thorac Cardiovasc Surg*, Vol. 92, 1986, pp. 198–209.

[43] Woo, Y-R, Yoganathan, A.P., et al., "In Vitro Pulsatile Flow Velocity and Turbulent Shear Stress Measurements in the Vicinity of Mechanical Aortic Heart Valve Prostheses," *Life Support Systems*, Vol. 3, 1985, pp. 4–32.

[44] Woo, Y-R, Williams, F., Yoganathan, A.P., "In Vitro Fluid Dynamic Characteristics of Aortic Bioprostheses: Old vs New," *Life Support Systems*, Vol. 4, 1986, pp. 63–85.

[45] Woo, Y-R, Yoganathan, A.P., et al., "In Vitro Pulsatile Flow Measurements in the Vicinity of Mechanical Heart Valves in the Mitral Flow Chamber," *Life Support Systems*, Vol. 4, 1986, pp. 115–139.

[46] Yoganathan, A.P., Sung, H-W, et al., "In Vitro Velocity and Turbulent Measurements in the Vicinity of 3 New Mechanical Aortic Heart Valve Prostheses," *J Thorac Cardiovasc Surg*, Vol. 95, 1988, pp. 929–939.

[47] Nevaril, C., Hellums, J., et al., "Physical Effects in Red Blood Cell Trauma," *Amer Inst Chem Eng J*, Vol. 15, 1969, p. 707.

[48] Hellums, J.D., Brown, C.H., "Blood Cell Damage by Mechanical Forces," *Cardiovascular Flow Dynamics*, University Press, Baltimore, MD, 1977, p. 799.

[49] Ramstack, J.M., Zuckerman, L., Mockros, L.F., "Shear Induced Activation of Platelets," *J Biomechanics*, Vol. 12, 1979, pp. 113–125.

[50] Walburn, F.J., Sabbah, H.N, Stein, P.D., "Turbulent Stresses in the Region of a Hancock Porcine Bioprosthetic Aortic Valve," *Transactions of the ASME*, Vol. 107, 1985, pp. 200- -205.

[51] Knott, E., Reul, H., et al., "In Vitro Comparison of Aortic Heart Valve Prostheses Part 1: Mechanical valves," *J Thorac Cardiovasc Surg*, Vol. 96, 1988, pp. 952–961.

[52] Hasenkam, J.M., Nygaard, H., et al., "Turbulent Stress Measurements Downstream of 6 Mechanical Aortic Valves in a Pulsatile Flow Model," *J Biomechanics*, Vol. 21, No. 8, 1988, pp. 631–645.

[53] Stein, P.D., Walburn, F.J., Sabbah, H.N, "Turbulent Stresses in the Region of Aortic and Pulmonary Valves," *Transactions of the ASME*, Vol. 104, 1982, pp. 238–244.

[54] Scotten, L.N., Walker, D.K., Brownlee, R.T., "The In Vitro Function of 19-mm Bioprosthetic Heart Valves in the Aortic Position," *Life Support Systems*, Vol. 5, 1987, pp. 145–153.

[55] Akutsu, T., "Hydrodynamic Performance of Mechanical Prosthetic Heart Valves," Ph.D. Thesis, University of British Columbia, 1985.

[56] Chandran, K.B., Schoephoerster, R., et al., "Effect of Prosthetic Mitral Valve Geometry and Orientation on Flow Dynamics in a Model Human Left Ventricle," *J Biomechanics*, Vol. 22, No. 1, 1989, pp. 51–65.

[57] Björk, V.O., "Optimal Orientation of the 60 and 70 Degree Björk-Shiley Tilting Disc Valves," *Scand J Thor Cardiovasc Surg*, Vol. 16, 1982, pp. 113–118.

[58] Richie, R.O, Lubock, P., "Fatigue Life Estimation Procedures for the Endurance of a Cardiac Valve Prosthesis: Stress-life and Damage-tolerant Analyses," *J Biomechanics*, Vol. 108, 1986, pp. 153–160.

[59] Lawford, P.V., Roberts, K., et al., "The In Vivo Durability of Bioprosthetic Heart Valves: Modes of Failure Observed in Explanted Valves," *Heart Valve Engineering*, Mechanical Engineering Publications Ltd., London, 1987, pp. 65–74.

[60] Dobrova, N.B., Lofis, N.A., et al., "Analysis of Causes for Wear and Breakdown of Elements in Artificial Cardiac Valves of the Disc Type," *Biomedical Engineering*, Vol. 2, 1987, pp. 8–12.

[61] Byadretdinova, M.A., Ivanova, R.G., et al., "Artificial Heart Valve Made of Co-Cr-W- Ni Alloy," *Biomedical Engineering*, Vol. 1, 1986, pp. 21–24.

[62] Fisher, J., Reece, I.J., et al., "Laboratory Assessment of the Design, Func-

tion, and Durability of Pericardial Bioprostheses," *Heart Valve Engineering*, Mechanical Engineering Publications Ltd., London, 1986, pp. 57–64.

[63] Rabago, G., Martinell, J., et al., "Comparison of Mechanical and Biological Prostheses," *Heart Valve Replacement: Current Status and Future Trends*, Futura Publishing Co. Ltd., Mount Kisco, N.Y., 1987, p. 245.

[64] Chandran, K.B., "Prosthetic Heart Valves," *Mechanical Engineering*, January 1986, pp. 53–58.

[65] Fernandez, J., "Surgical Aspects of Valve Implantation," *Guide to Prosthetic Cardiac Valves*, Springer-Verlag, New York, 1985, pp. 121–157.

[66] Bicer Medical Ltd., "Bicer-valve Cardiac Prostheses", Company brochure, Richmond, B.C., Canada.

APPENDIX I

Accuracy of Results

In the investigation of this nature, with very little available information, it is important to obtain data with the utmost care and assured repeatability so that it can serve as a reference for future work.

To achieve this, a set of experiments in a given series (i.e. tests for the Bicer-Val in the anterior orientation) were repeated, on average, four times.. Normally, repeated tests were conducted a few days apart to ensure validity of data under independently adjusted experimental conditions. In most cases, the repeated experiments showed similar trends. However, the tissue prostheses showed consistent discrepancies when tests were conducted a week or more apart. This can possibly be attributed to a break-down or metamorphosis occuring in the tissue leaflets due to contaminants in the saline solution.

To further insure repeatability, each measured quantity (i.e. velocity) was averaged over 20 cardiac cycles.

Accuracy of other parameters are as follow:

Traversing Mechanism:

X direction: 0.002 mm

Y direction: 0.005 mm

Z direction: 0.1 mm

LDA:

1Mhz Range

Bandwidth2 for a 0.59 kHz cutoff (Akutsu[55]determined that contribution of turbulence above 0.25 kHz was minimal)

Shift 400 kHz

Doppler Frequency 40 MHz

Data Aquisition Board: 12 bit for 0.4% accuracy

APPENDIX II

Nondimensionalization Factor: V_0

Steady-State Experiments:

Mechanical:	Anterior	Posterior
B-S c-c	56.2 cm/s	52.2 cm/s
B-S mono	56.1 cm/s	50.5 cm/s
Bicer	59.9 cm/s	52.7 cm/s

Biological:	
HK	64.6 cm/s
C-E	48.2 cm/s

Pulsatile Experiments:

Mechanical:	
B-S c-c	57.2 cm/s
B-S mono	55.6 cm/s
Bicer	58.8 cm/s